AD-A107 733 WASHINGTON STATE UNIV PULLMAN PICOSECOND LASER LAB F/G 20/5
NANOSECOND AND PICOSECOND SPECTROSCOPY AND KINETICS OF DYNAMIC --ETC(U)
OCT 81 M W WINDSOR DAAG29-76-G-0275
UNCLASSIFIED ARO-18081.11-C NL

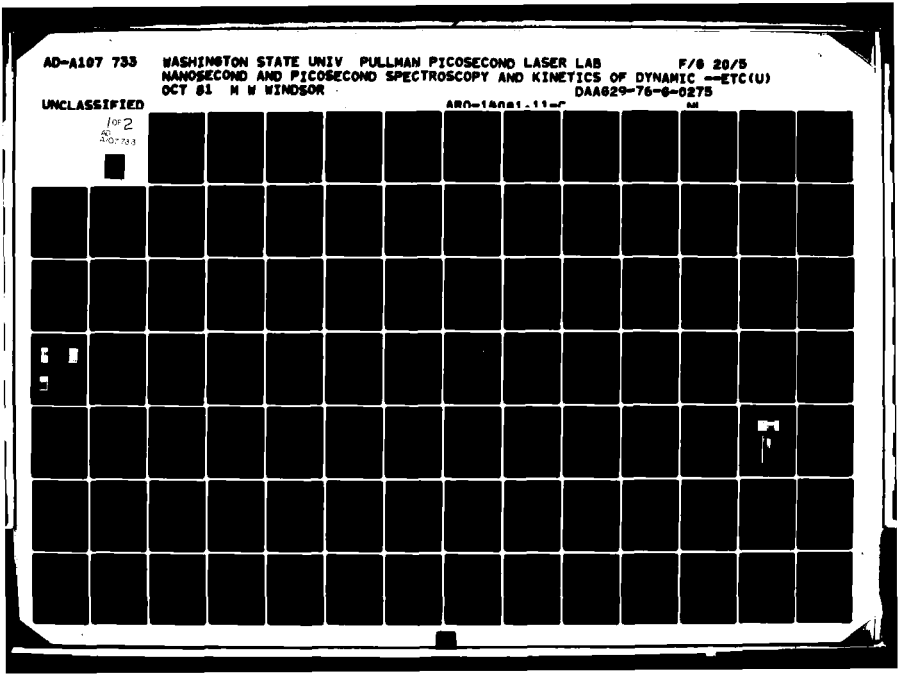

UNCLASSIFIED
SECURITY CLASSIFICATION OF THIS PAGE (When Data Entered)

REPORT DOCUMENTATION PAGE

READ INSTRUCTIONS BEFORE COMPLETING FORM

1. REPORT NUMBER	2. GOVT ACCESSION NO. AD-A107733 / 3. RECIPIENT'S CATALOG NUMBER
4. TITLE (and Subtitle) NANOSECOND AND PICOSECOND SPECTROSCOPY AND KINETICS OF DYNAMIC ABSORBING MATERIALS	5. TYPE OF REPORT & PERIOD COVERED FINAL: 6/76 - 6/81
	6. PERFORMING ORG. REPORT NUMBER
7. AUTHOR(s) MAURICE W. WINDSOR	8. CONTRACT OR GRANT NUMBER(s) DAAG29-76-G-0275
9. PERFORMING ORGANIZATION NAME AND ADDRESS Professor Maurice W. Windsor, Picosecond Laser Laboratory, Department of Chemistry, Washington State University, Pullman, WA 99164	10. PROGRAM ELEMENT, PROJECT, TASK AREA & WORK UNIT NUMBERS
11. CONTROLLING OFFICE NAME AND ADDRESS U.S. Army Research Office, Box 12211, Research Triangle Park, NC 27709	12. REPORT DATE October 8th, 1981
	13. NUMBER OF PAGES 172
14. MONITORING AGENCY NAME & ADDRESS(if different from Controlling Office)	15. SECURITY CLASS. (of this report) Unclassified
	15a. DECLASSIFICATION/DOWNGRADING SCHEDULE

16. DISTRIBUTION STATEMENT (of this Report)

Approved for Public Release, Distribution Unlimited.

17. DISTRIBUTION STATEMENT (of the abstract entered in Block 20, if different from Report)

18. SUPPLEMENTARY NOTES

THE VIEW, OPINIONS, AND/OR FINDINGS CONTAINED IN THIS REPORT ARE THOSE OF THE AUTHOR(S) AND SHOULD NOT BE CONSTRUED AS AN OFFICIAL DEPARTMENT OF THE ARMY POSITION, POLICY, OR DECISION, UNLESS SO DESIGNATED BY OTHER DOCUMENTATION.

19. KEY WORDS (Continue on reverse side if necessary and identify by block number)

Dynamic Absorbers, Dynamic Filters, Photochromism, Automated Picosecond Spectrometer, Laser-protective Materials, Nanosecond/Picosecond Spectroscopy and Kinetics, Photophysics/Photochemistry of Dyes, Porphyrins, Inorganic Complexes, Singlet-States, Triplet States, Radical Ions, Internal Conversion, Intersystem Crossing, Electron Transfer

20. ABSTRACT (Continue on reverse side if necessary and identify by block number)

There is an increasing need to provide protection for both personnel and electronic sensors against laser radiation in the visible and near infra-red regions. The proliferation of laser frequencies and the advent of tunable lasers combine to create a threat that static filters alone cannot combat. Dynamic filters that become highly absorbing only on exposure to the incident laser radiation would provide an attractive solution, especially if the dynamic absorption could be made to develop very rapidly and also be rapidly

DD FORM 1 JAN 73 1473 EDITION OF 1 NOV 65 IS OBSOLETE
S/N 0102-014-6601

UNCLASSIFIED
SECURITY CLASSIFICATION OF THIS PAGE (When Data Entered)

reversible after the laser pulse is over. This report describes research aimed at the further development of ultra-fast spectroscopic instrumentation constructed in the author's laboratory and its application to studying several phenomena capable of giving rise to dynamic absorption in selected classes of chemical compounds. These phenomena include the direct photoproduction on the picosecond time scale of absorbing transient species such as excited singlet states and excited triplet states of conjugated organic molecules and dyes, the production of radical ions of similar compounds via photoexcitation followed by fast electron transfer and the production of various excited states of inorganic complexes.

A low-cost automated, picosecond laser spectrometer based on a two-dimensional optical multichannel analyzer (OMA) interfaced to a home-assembled microcomputer has been developed. This instrument provides broad-band difference spectra of short-lived intermediates over a range of 300 nm in a few laser shots with excellent resolution in both absorbance (±0.025 optical density units) and wavelength (0.7 nm).

Several inorganic complexes of Cr(III) show promise as dynamic absorbers (ϵ ~10^4 $M^{-1}cm^{-1}$ in the excited state) in the 530 nm region. They respond in 10-25 ps and recover in the nanosecond time range.

Effects of intramolecular torsional motions and of the viscosity of the solvent medium on the excited state lifetime have been studied in a series of triphenylmethane dyes. These results offer possible ways of controlling the time response of dynamic filters in the picosecond to nanosecond time range.

Fast electron transfer has been studied as a way of producing highly absorbing radical ions in several porphyrins and micellar media have been investigated as a way of inhibiting the reverse electron transfer process, thus increasing the efficiency of production of the dynamically absorbing species.

A coherent laser upconversion technique for picosecond, time-resolved fluorescence emission studies with a synchronously pumped modelocked dye laser has been developed.

A comprehensive review of experimental techniques for chemical measurements in the picosecond time range has been prepared plus an historical review of the development of the flash photolysis technique from microsecond to picoseconds.

NANOSECOND AND PICOSECOND SPECTROSCOPY AND KINETICS OF DYNAMIC ABSORBING MATERIALS

FINAL REPORT

by

MAURICE W. WINDSOR

October 8th, 1981

U.S. ARMY RESEARCH OFFICE

Grant Number: DAAG29-76-G-0275

Picosecond Laser Laboratory
Department of Chemistry
Washington State University

FOREWORD

This report was prepared by Maurice W. Windsor, Professor of Chemistry and Chemical Physics, Washington State University. It describes research carried out under his direction from June 1976 to June 1981 in The Picosecond Laser Laboratory and supported by the U.S. Army Research Office under Grant Number DAAG29-76-G-0275.

CONTENTS

1. STATEMENT OF THE PROBLEM

Laser devices of various types are finding increasing military application. Consequently there has arisen a need to provide protection to both personnel and to electronic sensors against possible damage from exposure, either deliberate or accidental, to laser radiation. In the case of personnel, the greatest concern attaches to eye protection. Anti-laser devices that function in the region of the visible spectrum are therefore of greatest interest. In the case of electronic sensors, protection must, in addition, be provided in the ultraviolet and more especially in the infra-red.

Permanent filters that absorb radiation in predetermined regions of the spectrum can provide a certain measure of protection, particularly against lasers of known and non-variable wavelength. However, the proliferation of laser frequencies in recent years and the advent of tunable lasers combine to create a threat that static filters alone cannot combat. To illustrate this, consider the problem of providing eye protection over the entire visible region. A combination of several broadband static filters could be used to prevent damage, but at the cost of greatly impairing the individual's vision. A similar situation applies in the case of electronic sensors. Clearly a more sophisticated solution than the static filter must be developed.

Dynamic filters that become highly absorbing only on exposure to the threatening laser radiation would provide an ideal solution, especially if the dynamic absorption were also rapidly reversible. As a result of several basic and applied research efforts over the past fifteeen years, many classes of dynamic filter materials are now known. When their dynamic response occurs in the visible region, such materials are called "photochromic". Research on the development of reversible photochromic materials and their application to providing eye protection against the flash from nuclear weapons has been carried out by several investigators, including the present writer.[1] The

investigation of dynamic filter materials for laser protection has grown out of these early efforts to provide flash-blindness protection. Two small ($15K and $36K, respectively) research efforts under my direction, initially at TRW Systems[2] and more recently at Washington State University[3] showed that the approach seems to be theoretically feasible. While preliminary experiments have shown promise, dynamic effects adequate to provide significant protection have yet to be demonstrated.

It is harder to provide protection against laser than against nuclear weapons. In the case of nuclear devices, although eye-protection is needed throughout the entire visual region, ancillary wavelengths present in the nuclear flash (e.g., the ultra-violet) can be used to operate or trigger the protective device. In addition, because of the relatively slow rise time of the visible and thermal pulse, (milliseconds even for low-yield devices and much longer for larger weapons), resort must often be had to supplementary pumping of the photochromic device by means of an auxiliary flash lamp.[4] In the case of lasers, pulses of very short duration (10^{-7} to 10^{-12} sec) and very high power (10^{6} to 10^{12} watts) present the most severe threat. Such short, high-power pulses are often produced deliberately for specific applications, using techniques known as Q-switching and mode-locking. However, it is now recognized that many CW lasers and lasers designed for lower power, longer-pulse operation, may nevertheless become adventitiously mode-locked. Thus, protection against short-duration, high-power laser pulses must constantly be borne in mind.

In evaluating a prospective dynamic filter material, the properties that it is important to have knowledge of are:

1) the strength and spectral extent of excited state absorption.

2) the amount and spectral extent of ground-state bleaching.

3) the relaxation time of the excited state or states.

4) the pathway by which relaxation occurs if intermediate states are involved.

5) whether or not light is emitted when relaxation occurs.

6) quantum yield data where competing processes are involved, (or sufficient kinetic data that yields may be calculated).

In addition, it would be valuable to have enough such data and for enough representative compounds that correlations might be sought between excited state properties and molecular structure. If such generalizations could be found, they might then be used predictively for designing compounds that hopefully would turn out to have enhanced properties and improved behavior.

In addition to the search for suitable dynamic filter materials, there is also concern over the possible behavior of "permanent" filter materials when exposed to high-power laser radiation.[5] Possibly such filters may bleach when exposed to the very high optical intensities present transiently during exposure to a Q-switched or mode-locked laser pulse, thus losing their effectiveness. Such bleaching can occur when excitation by the laser pulse leads to the production of an excited state or states of the molecule that absorb less strongly than the ground state. Thus knowledge of the spectral extent and strength of absorption of excited states of molecular filter materials is of importance. It is also important to know the relaxation time of these excited states, i.e., how rapidly they revert to the ground state and whether or not light is emitted when this occurs. The more rapid the return to the ground state, the more "robust" the material will be toward bleaching, especially if the return is rapid in relation to the duration of the laser pulse. Conversely, slow return will mean that later portions of the laser pulse will encounter a lower absorbance than that met by earlier portions and some transmission may, therefore, occur.

To assess the effects of incident laser pulses on permanent filter materials and perhaps design improved materials, it is clear that the same kinds of information are needed as those already itemized for dynamic filter materials.

At present we do not have enough information on the properties of excited states of molecules from which to develop a theoretical understanding of their behavior when exposed to high-power, short-duration laser pulses. The data base of spectroscopic and kinetic measurements must be extended, especially for model compounds whose other properties are well understood. Correlations need to be sought between such data and the composition and structure of the molecules studied, in the hope that generalizations can be found that will be helpful in selecting or designing molecules for various dynamic filter applications.

The goal of the present research effort has been to further develop and refine the ultra-fast flash photolysis and spectroscopy technique developed in the author's laboratory[6] and apply it to obtaining nanosecond and picosecond spectroscopic and kinetic data on a variety of dynamic absorbing materials. Specific objectives envisaged in the original proposal were:

1. Improved efficiency of gathering and manipulating spectral and kinetic data, using a 2-dimensional optical multichannel analyzer (OMA) technique.
2. Improved sensitivity of measuring optical density changes and extension of the spectral range of monitoring.
3. Provision of excitation wavelengths additional to 1060 nm and 530 nm.
4. Employment of the improved instrumentation for spectroscopic and kinetic studies of the excited state behavior of various compounds thought to be promising for dynamic filter application.

5. An attempt to seek relationships between excited state properties and the chemical composition and structure of the molecules studied.

2. SUMMARY OF THE MOST IMPORTANT RESULTS

A detailed account of the research findings is given in the various publications listed in the following section (Section 3). We present a brief summary here keyed to these publications. To avoid confusion with the bibliography at the end of the report we identify these publications alphabetically.

2.1 Automated Picosecond Spectrometer with 2-d OMA Detection.

A low-cost system for converting a single-pulse picosecond laser spectrometer to an automated instrument has been successfully developed and tested (C and J). This system makes possible the acquisition, in less than an hour using only one or two dozen laser shots, broad-band absorption difference spectra of short-lived intermediates over a range of up to 300 nm with excellent resolution in both absorbance ($\pm$ 0.025 optical density units) and wavelength (0.7 nm). Lower resolution spectra, suitable for exploratory study of new compounds that are potentially dynamic absorbers, are obtained in a matter of minutes with only a few laser shots. The automated spectrometer employs a standard vidicon-optical multichannel analyzer (OMA) detector, operated in the 2-dimensional mode, for data acquisition, and this is then interfaced to a reliable home-assembled microcomputer. The latter can also be used for acquisition and analysis of data from other laboratory instruments.

2.2 Excitation Wavelength Flexibility

Additional flexibility in excitation wavelength in the region 530 nm to 650 nm has been obtained by stimulated Raman scattering of the Nd laser second harmonic pulse at 530 nm in suitable solvents (see D, Table 5.1). For example, we now routinely employ a 7 ps, 600 nm excitation pulse produced in a

5 cm cell of perdeuterocyclohexane. Conversion efficiency is in the range 10-20% compared to the 530 nm pump pulse.

Efforts to obtain shorter wavelength picosecond excitation pulses using a ruby laser system met with poor success (see Progress Report for 7/1/78 through 12/31/78). Mode-locked operation of the oscillator in the TEM_{00} mode was unreliable. Less than one shot in five gave a pulse train clean enough for single pulse selection. Multimode operation gave more reproducible pulse trains, but at the expense of a more divergent beam that could not be amplified significantly. The ruby laser was therefore converted to normal Q-switched operation and has subsequently been used profitably for measurements in the nanosecond time range. Attempts to generate the third and fourth harmonics (353 nm and 265 nm) of our Nd/glass laser following two stages of amplification were only partially successful. Although detectable amounts of energy could be generated at these wavelengths, conversion efficiencies were too low for application as excitation pulses for picosecond spectroscopy. It was not therefore possible to study some of the simple aromatic hydrocarbon systems, such as anthracene and coronene, that are potentially valuable for structural correlations. A Nd/YAG laser system operated in the TEM_{00} mode, or a synchronously pumped, mode-locked dye laser system with harmonic doubling appear now to be better approaches to extending picosecond spectroscopic studies to shorter excitation wavelengths.

2.3 Inorganic Complexes, Especially Cr(III), as Dynamic Absorbers.

Promising results relevant to the problem of finding dynamic absorbers to provide protection in the mid-visual range around 530 nm were obtained with a series of complexes of chromium(III) (see A, B and p. 260 of D). The species studied were trans-$Cr(en)_2(NCS)_2^+$; trans-$Cr(NH_3)_2(NCS)_4^-$; and $Cr(NCS)_6^{3-}$, all in fluid solution at room temperature. In their

ground states these ions absorb quite weakly ($\epsilon < 100\ M^{-1}\ cm^{-1}$) at 530 nm, but, in the doublet excited state, charge transfer transitions give rise to intense ($\epsilon \sim 10{,}000\ M^{-1}\ cm^{-1}$) and very broad ($\sim 8000\ cm^{-1}$) absorption centered near 540 nm. Our studies show that the doublet excited state is formed in 10-25 ps (this measurement is not instrument limited), dependent upon the species and the solvent (A), and persists for times in excess of 5 ns (B), the upper time limit of our system. Ohno and Kato have reported nanosecond lifetimes in fluid solutions increasing to milliseconds in rigid glasses at low temperatures or polymethylmethacrylate polymer at room temperature (7). In an earlier picosecond photographic study in our laboratory (8, see Fig. 1), the reduction in the intensity of the 530 nm pump pulse at 100 ps time delay compared to zero time delay is readily apparent. We recommend further studies of similar complexes.

2.4 Effects of Molecular Structure and Viscosity of the Medium on Relaxation of Excited States.

A continuing study of the electronic relaxation of the excited singlet state of triphenylmethane dyes, especially crystal violet (CV), as a function of solvent viscosity has provided valuable insights into the mechanisms by which excited states of large dye molecules are deactivated (F, H, M, N). Torsional motions of parts of the molecule in the excited state appear to play a crucial role in mediating electronic relaxation. Viscous damping by the solvent can hinder such motions, thereby lengthening the excited state lifetime. This result has important implications with regard to the formulation of dynamic filters because it could provide a means for controlling the time response of the system.

2.5 Laser Upconversion Technique for Picosecond Time-Resolved Fluorescence Studies

Closely related to and overlapping with the studies in 2.4 is the development of a laser upconversion technique for observing the excited state of CV and related molecules in emission, via upconversion of the fluorescence by coherent mixing with a component of the exciting laser pulse (H). This work was carried out during my sabbatical leave (1978-79) at The Royal Institution, London, England, using a synchronously pumped mode-locked dye laser system. The technique has high sensitivity, meaning that excited singlet states under conditions of very low fluorescence yield (<1%) can be studied, and also provides excellent time resolution (2-4 ps). Coupled with a picosecond tunable dye-laser system, it provides an excellent diagnostic tool for following time-dependent, spectral absorbance changes of dynamic filters down to the shortest times.

2.6 Radical Ions as Dynamic Absorbers and Electron Transfer Studies

Additional flexibility in providing very rapid changes in spectral absorbance in response to an incident laser pulse is provided by the recognition that electron transfer reactions can be exploited to generate new absorbing species in very short periods of time. In such systems, light absorption first produces an excited state of the donor (D) molecule, which then transfers an electron to another type of molecule called the acceptor (A). In the process two new chemical species are produced, the radical cation of the donor, D^+, and the radical anion of the acceptor, A^-. Electron transfer reactions are normally very rapid, taking place on the picosecond (10^{-12}sec) time scale. Thus if electron transfer takes place from the excited singlet state (S_1) of the donor that is directly produced by the initial act of light absorption, and if the donor and acceptor are in close proximity as in a molecular complex, the response time of the system can be extremely rapid. In

other cases, electron transfer occurs from the lowest triplet state (T_1) of the donor. In these cases, the response time will usually be in the nanosecond to microsecond time range, corresponding to the time for intersystem crossing from S_1 to T_1. In both cases (singlet donor and triplet donor) the response time may also be controlled by the time it takes for the donor and acceptor to meet each other (the encounter time) if both donor and acceptor are free molecules in fluid solution. This time could range from tens of picoseconds ($\sim 10^{-11}$sec) to microseconds depending upon the concentrations employed.

In the case of molecular excited states, the decay of the dynamic absorption will be first order, either radiatively by the emission of fluorescence or non-radiatively by internal conversion or more likely by both routes. The decay time can vary from picoseconds to as long as seconds where a spin-forbidden transition is involved, as for example when the excited state is a triplet-state of an aromatic molecule and a rigid medium is used. For radical ions, on the other hand, the decay entails a bimolecular encounter followed by a reverse electron transfer. In many cases the reverse electron transfer takes place extremely rapidly ($<10^{-11}$sec) before the radical ions have time to separate. For dynamic filter applications this is undesirable, because it means that the induced absorption does not persist long enough to provide a useful measure of protection against the incident laser pulse. In our research we are trying to find ways of inhibiting the reverse electron transfer process, while at the same time either not affecting or even perhaps speeding up the forward electron transfer reaction. Since nature has already accomplished this highly desirable state of affairs in photosynthetic reaction centers, there is much to be learned from studying these and related model pigment systems. A natural and synergistic overlap therefore occurs between

our research on dynamic absorbers and our studies of the primary charge separation process in photosynthesis. It is worth noting and emphasizing that porphyrins constitute a large and versatile class of molecules that are highly absorbing in the visible and near infra-red regions of the spectrum and which also possess a good measure of both thermal and photochemical stability.

Two publications (G,K) describe studies aimed at gaining an improved understanding of electron transfer reactions in micellar media. The structured environment provided by micelles (aggregates of detergent molecules) offers the possibility of controlling the rates of both the forward and reverse electron transfer reactions involved in the formation and decay of radical ions. One publication (L) describes a spectroscopic study of a series of porphyrin dimer complexes. The objective here is to better understand the photophysical and photochemical behavior of artificial systems that mimic closely in structure the very successful natural systems, many of which employ a chlorophyll dimer as the electron donor.

2.7 Invited Reviews of the Literature

The preparation of two comprehensive reviews (D and E) received partial support from this contract. The first (D) reviews the experimental techniques needed to make spectroscopic and kinetic measurements in the very short time range. The second (E) is narrower in scope and presents an historical and somewhat personal perspective on the development of the flash photolysis technique over the past three decades from the microsecond to the picosecond time range followed by a discussion of the primary charge separation process in photosynthesis. The latter survey was presented as an invited plenary lecture at a Royal Society Discussion on Ultra-Short Laser Pulses held at Carlton House, London, May 23-24, 1979.

3. PUBLICATIONS

A. PICOSECOND STUDIES OF EXCITED-STATE DECAY KINETICS IN CHROMIUM(III).
S. C. Pyke and M. W. Windsor, J. Am. Chem. Soc., 1978, 100, 6518-9.

B. PICOSECOND STUDIES OF TRANSITION METAL COMPLEXES.
P. Hoggard, A. D. Kirk, G. B. Porter, M. G. Rockley and M. W. Windsor, NBS Special Publication (U.S.), 1978, 526, 137-8.

C. A RELIABLE, INEXPENSIVE MICROPROCESSOR INTERFACE FOR THE OPTICAL MULTICHANNEL ANALYZER (OMA).
D. Holten, D. C. Cremers, S. C. Pyke, R. Selensky, S. S. Shah, D. W. Warner and M. W. Windsor, Rev. Sci. Instr., 1979, 50, 1653-1655.

D. MEASUREMENTS IN THE PICOSECOND AND SHORTER TIME RANGE.
S. C. Pyke and M. W. Windsor, Chapter 5, in "Chemical Experimentation Under Extreme Conditions, Volume 9 in The Techniques of Chemistry Series," Ed. B. W. Rossiter, John Wiley and Sons, Inc., New York, 1980, pp. 205-276.

E. PICOSECOND STUDIES OF PRIMARY CHARGE SEPARATION IN BACTERIAL PHOTOSYNTHESIS.
M. W. Windsor and D. Holten, Invited Plenary Lecture presented at the Royal Society Discussion Meeting on Ultra-Short Laser Pulses, London, May 23-24, 1979, Phil. Trans. Royal Soc. London, 1980, A298, 335-349.

F. A STUDY OF THE VISCOSITY DEPENDENT ELECTRONIC RELAXATION OF SOME TRIPHENYLMETHANE DYES USING PICOSECOND FLASH PHOTOLYSIS.
D. A. Cremers and M. W. Windsor, Chem. Phys. Letters, 1980, 71, 27.

G. ELECTRON TRANSFER FROM PHOTOEXCITED BACTERIOPHEOPHYTIN TO p-BENZOQUINONE IN CATIONIC MICELLES.
D. Holten, S. S. Shah and M. W. Windsor, presented at Second International Conference on Picosecond Phenomena, Cape Cod, Mass., June 18-20, 1980. Published in "Picosecond Phenomena II," Springer Series in Chemical Physics, Volume 14, Ed. R. Hochstrasser, W. Kaiser, and C. V. Shank, Springer-Verlag, New York, 1980, pp. 317-321.

H. PICOSECOND STUDIES OF ELECTRONIC RELAXATION IN TRIPHENYLMETHANE DYES BY FLUORESCENCE-UPCONVERSION.
G. S. Beddard, T. Doust and M. W. Windsor, presented at Second International Conference on Picosecond Phenomena, Cape Cod, Mass., June 18-20, 1980. Published in "Picosecond Phenomena II," Springer Series in Chemical Physics, Volume 14, Ed. R. Hochstrasser, W. Kaiser and C. V. Shank, Springer-Verlag, New York, 1980, pp. 167-170.

J. AUTOMATED PICOSECOND SPECTROSCOPY WITH A STANDARD TWO-DIMENSIONAL OPTICAL MULTICHANNEL ANALYZER AND AN INEXPENSIVE MICROPROCESSOR.
Dewey Holten and Maurice W. Windsor, Photobiochem. and Photobiophys., 1980, 1, 243-252.

K. MODELS FOR PHOTOSYNTHETIC CHARGE SEPARATION: EXCITED STATE ELECTRON TRANSFER REACTIONS OF BACTERIOPHEOPHYTIN IN MICELLES.
S. Sadiq Shah, Dewey Holten and Maurice W. Windsor, Photobiochem. and Photobiophys., 1980, 1, 361-373.

L. EXCITONIC INTERACTIONS IN COVALENTLY-LINKED PORPHYRIN DIMERS.
Ron Selensky, Dewey Holten, Maurice W. Windsor, John B. Paine, III, David Dolphin, Martin Gouterman, and John C. Thomas, Chemical Physics, 1981, 60, 33-46..

M. A KINETIC MODEL OF THE VISCOSITY-DEPENDENT ELECTRONIC RELAXATION OF TRIPHENYLMETHANE DYES.
David A. Cremers and Maurice W. Windsor, in preparation.

N. PICOSECOND FLASH PHOTOLYSIS: THE VISCOSITY-DEPENDENT RELAXATION OF SOME TRIPHENYLMETHANE DYES.
David A. Cremers, Ph.D., Thesis, Department of Physics, Washington State University, 1980.

4. PARTICIPATING SCIENTIFIC PERSONNEL

Professor Maurice W. Windsor, Principal Investigator

Dr. Dewey Holten, Postdoctoral Research Associate, 1976-1980

Dr. Stephen C. Pyke, Postdoctoral Research Associate, 1977-1980

David A. Cremers, Graduate Research Assistant, Ph.D., 1980

Andrew B. Nielsen, Graduate Research Assistant, M.S., 1978

Dewey W. Warner, Graduate Research Assistant, M.S., 1978

Ronald J. Selensky, Graduate Research Assistant, M.S., 1981

5. BIBLIOGRAPHY

1. W. R. Dawson and M. W. Windsor, "Triplet Materials Research and An Eye-Protective System," TRW Systems Final Report under USAF Contract AF 41(609)3201, June 1968, available from Clearinghouse for Federal Scientific and Technical Information (CFSTI), U.S. Dept. of Commerce, Springfield, VA. 22151. Also earlier reports available from CFSTI as ASTIC 026791 and AD-600-218P.
2. J. R. Novak, W. R. Dawson and M. W. Windsor, "Dynamic Filter Materials for 530 nm Radiation," TRW Systems Final Report under U.S. Army, Frankford Arsenal, Contract DAAA25-70-C0001, June 1970, available from DDC, Cameron Station, Alexandria, Va. 22314.
3. M. W. Windsor, "The Effects of Picosecond Laser Pulses on Dyes Employed for Laser Countermeasures," U.S. Army, Frankford Arsenal, Contract DAAA25-73-CO-208 with Washington State University, 1973-75.
4. W. R. Dawson and M. W. Windsor, "An Eye-Protective Panel Using Triplet State Photochromism," Applied Optics, 1969, 8, 1045.
5. J. J. Mikula, W. A. Thomas and F. D. Verderame, "Spectroscopy of Laser Radiation Absorbers in Liquid and Plastic Media," U.S. Army, Frankford Arsenal, Report R-1984, Nov. 1970. See recommendations on page 27.
6. D. Magde and M. W. Windsor, "Picosecond Flash Photolysis and Spectroscopy," Chem. Phys. Lett., 1974, 27, 31.
7. T. Ohno and S. Kato, Bull. Chem. Soc. Japan, 1970, 43, 8 and ibid., 1973, 46, 1602.
8. A. D. Kirk, P. E. Hoggard, G. B. Porter, M. G. Rockley and M. W. Windsor, "Picosecond Flash Photolysis and Spectroscopy: Transition Metal Coordination Compounds," Chem. Phys. Lett., 1976, 37, 199.

APPENDIX

COPIES OF PUBLICATIONS LISTED IN SECTION 3

[Reprinted from the Journal of the American Chemical Society, 100, 6518 (1978).]

Picosecond Studies of Excited-State Decay Kinetics in Chromium(III): *trans*-Diisothiocyanatobis(ethylenediamine)chromium(III), Reinecke's Salt, and Hexaisothiocyanatochromium(III) in H_2O and D_2O at Room Temperature

Sir:

The interest in excited-state relaxation in Cr(III) complexes stems from the debate over the identity of the photoactive state in Cr(III) photochemistry. Early work by Plane and Hunt[1] and Schläfer[2] suggested that the lowest doublet state was the primary intermediate responsible for photochemistry. Subsequently, Chen and Porter[3] established that at least some of the photoproduct in the photoaquation of *trans*-$Cr(NH_3)_2(NCS)_4^-$ must derive from sources other than the doublet. They suggested that the lowest quartet excited state was responsible. In addition, the lack of direct evidence for doublet photochemistry led them to suggest that all other photoproduct could be a consequence of thermally activated back intersystem crossing from the doublet to the quartet similar to the process of E-type delayed fluorescence. Since then, it has been demonstrated that some, if not all, of the photochemistry for several complexes derives from the lowest excited quartet state.[4] The quartet hypothesis is supported by the successful prediction of product stoichiometry by models based on the ligand field strength of the first coordination sphere. The first of the spectroscopic models was developed by Adamson.[5] Models have since been developed to rationalize Adamson's rules which use MO theory to account for changes in the σ and π character of the metal ligand bonds as a result of the change in electronic configuration in the lowest excited quartet state.[6] Even stereochemical changes have been rationalized.[7] The similarity in formal electronic configuration between the ground and doublet states (t_{2g}^3) and the negligible Stokes shift of the doublet phosphorescence has suggested that there was negligible difference in geometry between the two states and that bond rupture in the doublet was therefore no more likely than in the ground state.[8] However, this argument is weakened by the following considerations. Intensity progressions in the vibrational structure of the phosphorescence of $Cr(CN)_6^{3-}$ have been interpreted as evidence for considerable distortion arising from compression of the metal-ligand bonds in the doublet relative to the ground state.[9] In addition, configuration interaction ($t_{2g}^3 \rightleftharpoons t_{2g}^2 e_g$) could cause some increase in average bond lengths as the crystal field parameter ($10\,Dq$) decreases and the excited quartet-doublet energy gap shrinks.[10] Thus, doublet reactivity cannot, at present, be completely ruled out.

Excited-state kinetic and spectroscopic studies of Cr(III) complexes under photochemical conditions may contribute to the understanding of the mechanism of the photochemical reaction. Until recently, however, studies of the photophysics of excited states in Cr(III) have been limited to studies of ruby: observations of phosphorescence of complexes at low temperature; and to data obtained indirectly through studies of photochemistry, emission quenching or sensitization. Nanosecond pulsed laser studies of the decay of emission or excited state absorbance (ESA) in acidoammine complexes of Cr(III) may be helpful in assessing the role of the doublet state in photoreaction.[11-13] However, picosecond time resolution is needed to examine the role of the excited quartet state in Cr(III) photochemistry. Earlier studies in our laboratory, of picosecond excited-state relaxation in transition metal complexes, suggested that the excited quartet lifetime in Cr(III) complexes was too short to measure (<10 ps).[14] We have extended this work. Repeated studies of *trans*-$Cr(en)_2(NCS)_2^+$, *trans*-$Cr(NH_3)_2(NCS)_4^-$ and $Cr(NCS)_6^{3-}$ show that, while the rise time of transient absorbance is fast (11 ps $< \tau <$ 24 ps), it is within the time resolution of our picosecond flash system. We have also studied the influence of the medium on the rate of appearance of transient absorbance.

Excited-state spectroscopy and measurement of excited-state lifetimes were performed using the picosecond flash photolysis system described elsewhere.[15] Solutions were prepared in H_2O and D_2O at the start of each experiment. The counterions were K^+ and NH_4^+ in $Cr(NCS)_6^{3-}$ and *trans*-$Cr(NH_3)_2(NCS)_4^-$, respectively. The counterions were Cl^- and ClO_4^- in the case of *trans*-$Cr(en)_2(NCS)_2^+$, and the rise times of transient absorbance were equivalent in both media. Solutions of Cr(III) were typically 0.1 M, and a fresh solution was used for each flash. The transient spectra were identical with those observed in the earlier picosecond work[14] as well as those reported for the excited doublet state in low temperature glassy media.[16] Similar spectra were also observed in nanosecond room-temperature kinetic spectroscopy.[12,13] We have estimated the extinction coefficients of the excited-state transitions by comparison with the excited singlet transition in Rhodamine 6-G ($\epsilon(S_1) = 4.8 \times 10^4\ M^{-1}\ cm^{-1}$ at 450 nm[17]). The values all lie between 10^3 and $10^4\ M^{-1}\ cm^{-1}$ and agree

Table I. Rise Time of transient absorbance

complex	$\tau \times 10^{12}$, s	
	H_2O	D_2O
trans-$Cr(en)_2(NCS)_2^+$	16 ± 3 (4)[a]	24 ± 2 (2)
trans-$Cr(NH_3)_2(NCS)_4^-$	22 ± 2 (4)	11 ± 2 (3)
$Cr(NCS)_6^{3-}$	16 ± 2 (2)	12 ± 6 (2)

[a] The value in parentheses represents the number of measurements from which the standard deviation was calculated. In cases where an average is presented for only two measurements, the uncertainty reflects arbitrarily twice the difference between the two experimental values.

reasonably well with previously reported values.[12,16b] The rise times of excited-state absorbance (ESA) were independent of probe wavelength and are listed in Table I. By measuring the rate of appearance of excited singlet absorbance (S_1) in Rhodamine 6-G (6 ± 2(4) ps), we established that our measured rise times of transient absorbance observed for the Cr(III) complexes were within our experimental time resolution and also provided an independent measure of the width of our picosecond pulse. Rate plots were linear for 1 to 2 lifetimes and were not corrected for the influence of the pump pulse.

There are two notable features apparent in the data in Table I. First, there is very little change in the transient rise time from one complex to another. The transient has been assigned as the lowest doublet excited state on the basis of the close similarity in the lifetimes for the decay of ESA and the decay of phosphorescence intensity in *trans*-$Cr(NH_3)_2(NCS)_4^-$ at low temperature.[16b] If the rise in ESA reflects intersystem crossing (ISC) from the vibrationally equilibrated first excited quartet state to the doublet state, the lifetime might be expected to be dependent on the energy gap between the minima in the doublet and the excited quartet potential energy surfaces. The data show little or no dependence on 10 *Dq*, the value of which should reflect that gap. An alternative interpretation is consistent with evidence reported by Kane-Maguire et al.[18] that intersystem crossing may compete with vibrational equilibration in Cr(III) complexes. Since the energy of the lowest doublet is relatively insensitive to 10 *Dq*, the rise time may reflect a combination of intersystem crossing from the initially formed quartet state to the doublet state and relaxation within the doublet manifold from the vibrational level isoenergetic with the Franck–Condon state produced in the excited quartet at the energy of the laser pulse (1.88 μm^{-1} or 530 nm). The energy separation between the initially attained vibrational level in the doublet and the zeroth vibrational level would then be relatively independent of the nature of the complex. Consequently, the observed lifetime might not be sensitive to changes in 10 *Dq* if intersystem crossing were comparable with or faster than vibrational decay. A similar explanation was used recently to explain excited-state relaxation in *trans*-$Cr(NH_3)_2(NCS)_4^-$.[13] If this is the correct model, the observed lifetime might depend on the energy of the Franck–Condon state in the excited quartet manifold. Picosecond studies as a function of excitation wavelength would be helpful in examining this possibility.

Second, there is a modest but definite isotope effect. The expected effect of D_2O on the rate constant (a reduction) is observed, however, only in the case of *trans*-$Cr(en)_2(NCS)_2^+$. The reverse effect is observed in *trans*-$Cr(NH_3)_2(NCS)_4^-$ and perhaps in $Cr(NCS)_6^{3-}$, the rates in these cases being accelerated. Isotope exchange for coordinated ammine protons may be responsible for changes in the measured lifetimes, but still would be expected to lengthen quartet lifetimes in each complex regardless of whether the perturbarion was inner or outer sphere. However, the opposite effects on doublet risetimes may reflect a charge dependence similar to that reported in the photochemistry of *trans*-$Cr(en)_2NCSF^+$ and *trans*-$Cr(NH_3)_2(NCS)_4^-$,[19] and in photophysical studies of ESA decay on the nanosecond time scale for $Cr(NH_3)_5NCS^+$, *trans*-$Cr(NH_3)_2(NCS)_4^-$, and $Cr(NCS)_6^{3-}$.[12] Additional studies of the medium dependence of excited-state decay in Cr(III) complexes are underway.

In conclusion, we have shown that the rise time of excited-state absorbance is measurable and longer than the earlier estimate of <10 ps. We believe that the available evidence favors the doublet-state assignment for the observed ESA. However, the precise details of the relaxation mechanism from the initially excited quartet state to the doublet manifold remain to be unraveled.

Acknowledgment. The authors gratefully acknowledge discussions with Professors G. B. Porter and A. D. Kirk and also thank them for samples of [*trans*-$Cr(en)_2(NCS)_2$]ClO_4 and [*trans*-$Cr(en)_2(NCS)_2$]Cl. This work was supported by the U.S. Army Research Office under Grant DAAG 29-76-9-0275.

References and Notes

(1) R. A. Plane and J. P. Hunt, *J. Am. Chem. Soc.*, **79**, 3343 (1957).
(2) H. L. Schläfer, *J. Phys. Chem.*, **69**, 2201 (1965).
(3) S. Chen and G. B. Porter, *Chem. Phys. Lett.*, **6**, 41 (1970); see also G. B Porter, S. N. Chen, H. L. Schläfer, and H. Gausmann, *Theor. Chim. Acta*, **20**, 81 (1971).
(4) H. F. Wasgestian, *J. Phys. Chem.*, **76**, 1947 (1972); N. A. P. Kane-Maguire and C. H. Langford, *J. Am. Chem. Soc.*, **94**, 2125 (1972); C. H. Langford and L. Tipping, *Can. J. Chem.*, **50**, 887 (1972); R. Ballardini, G. Varani, H. F. Wasgestian, L. Moggi, and V. Balzani, *J. Phys. Chem.*, **77**, 2947 (1973).
(5) A. W. Adamson, *J. Phys. Chem.*, **71**, 798 (1967).
(6) J. I. Zink, *J. Am. Chem. Soc.*, **96**, 4464 (1974), and references therein; M Wrighton, H. B. Gray, and G. S. Hammond, *Mol. Photochem.*, **5**, 164 (1973); C. Furlani, *Theor. Chim. Acta*, **34**, 233 (1974); L. G. Vanquickenborne and A. Ceulemans, *J. Am. Chem. Soc.*, **99**, 2208 (1977).
(7) L. G. Vanquickenborne and A. Ceulemans, *J. Am. Chem. Soc.*, **100**, 475 (1978).
(8) V. Balzani and V. Carassiti, "Photochemistry of Coordination Compounds", Academic Press, New York, N.Y., 1970; A. D. Kirk, *Mol. Photochem.*, **5**, 127 (1973).
(9) C. D. Flint and P. Greenhough, *J. Chem. Soc., Faraday Trans. 2*, **70**, 815 (1974).
(10) J. C. Hempel and F. A. Matsen, *J. Phys. Chem.*, **73**, 2502 (1969).
(11) A. W. Adamson, C. Geosling, R. Pribush, and R. Wright, *Inorg. Chim. Acta*, **16**, L5 (1976); b) F. Castelli and L S. Forster, *J. Phys. Chem.*, **81**, 403 (1977).
(12) S. C. Pyke, M. Ogasawara, L. Kevan, and J. F. Endicott, *J. Phys. Chem.*, **82**, 302 (1978).
(13) A. R. Gutierrez and A. W. Adamson, *J. Phys. Chem.*, **82**, 902 (1978).
(14) A. D. Kirk, P. E. Hoggard, G. B. Porter, M. G. Rockley, and M. W. Windsor, *Chem. Phys. Lett.*, **37**, 199 (1976).
(15) D. Magde and M. W. Windsor, *Chem. Phys. Lett.*, **27**, 31 (1974).
(16) (a) R. A. Krause, I. Trabjerg and C. J. Ballahusen, *Chem. Phys. Lett.*, **3**, 297 (1969); (b) T. Ohno and S. Kato, *Bull. Chem. Soc. Jpn.*, **46**, 1602 (1973), and references therein.
(17) G. Dolan and C. R. Goldschmidt, *Chem. Phys. Lett.*, **39**, 320 (1976).
(18) N. A. P. Kane-Maguire, J. E. Phifer and C. G. Toney, *Inorg. Chem.*, **15**, 593 (1976).
(19) C. F. C. Wong and A. D. Kirk, *Can. J. Chem.*, **54**, 3794 (1976).

Stephen C. Pyke, Maurice W. Windsor*
Department of Chemistry, Washington State University
Pullman, Washington 99164

Received May 17, 1978

NBS Special Publication (US), 1978, 526, 137-8

PICOSECOND STUDIES OF TRANSITION METAL COMPLEXES

Patrick E. Hoggard, Alexander D. Kirk[1], Gerald B. Porter[2], Mark G. Rockley[3], and Maurice W. Windsor[4]

Department of Chemistry
Polytechnic Institute of New York
New York, NY

Lifetimes of excited electronic states of a number of transition metal complexes have been measured in solution at room temperature with picosecond time resolution [1][5]. Two experimentally distince lifetimes can be retrieved with this technique. The ground state bleaching (GSB) lifetime is that for the total repopulation of the ground state, measured by the regrowth in intensity of absorption bands, initially bleached because of depopulation by the pumping pulse. The excited state absorption (ESA) lifetime is that for depopulation of a particular excited state, measured by the decay of the electronic absorption spectrum from that state.

Both of these processes are observed only under somewhat special conditions, and in addition we have thus far been limited by the necessity that the sample absorb significantly at 530 nm, the double frequency of a Nd^{3+} laser. To observe GSB, the molar extinction coefficient at 530 nm must be higher than about 5000. A similar requirement applies to ESA - the extinction coefficient must be high, somewhere within the range of the instrumentation and the continuum pulse used for analysis. Additionally, observation is impossible if the excited state absorption is masked by the ground state absorption.

In spite of these restrictions, a number of transition metal complexes have been found for which we can observe GSB and/or ESA. A summary of some of these results is shown in the table.

In the case of the Fe(II) complexes, there are two absorption bands in the visible region, an intense band above 500 nm, representing a CTTL transition, and another much weaker band below 900 nm, assigned to a $^3T_{1g} \leftarrow {}^1A_{1g}$ ligand field transition. In addition, transitions from ^3CT and $^1T_{1g}$ states are probably masked by the spin allowed charge transfer band. An estimate of the radiative lifetime of the ^1CT state from the absorption spectrum plus the absence of observable luminescence allows us to rule out this state as too short-lived to contribute to the observed GSB lifetime. The 830 ps lifetime is consistent with estimates for the $^3T_{1g}$ lifetime, but could represent decay into the ground state from any of $^3T_{1g}$, $^1T_{1g}$, or ^1CT.

---

[1] Department of Chemistry, University of Victoria, B.C., Canada.

[2] Department of Chemistry, University of British Columbia.

[3] Department of Chemistry, Oklahoma State University.

[4] Department of Chemistry, Washington State University.

[5] Figures in brackets indicate the literature references at the end of this paper.

Chromium (III) complexes exhibit small extinction coefficients in general, so that GSB is not expected to be observed. Exited state absorption from the lowest ligand field states, $^4T_{2g}$ and ^2E_g would also be expected to exhibit small extinction coefficients within the manifold of ligand field states. Observation of ESA in the visible range is thus to be expected only with ligands which induce charge transfer states in the region of 30-40 kK above the ground state. Thiocyanate and acetylacetonate complexes exhibit the required CT bands, and ESA was observed for these complexes.

Table

Complex	Ground state bleaching	Excited state absorption	Type of transition
$[Fe(bipy)_3]^{2+}$	τ = 830 ps		
$[Fe(phen)_3]^{2+}$	Observed		
$[Ru(bipy)_2(CH_3OH)_2]^{2+}$	τ = 620 ps	$\lambda_{max} \leq$ 425 nm	probably intraligand
$[Cr(NH_3)_2(NCS_4)]^-$		λ_{max} ca 520 nm τ = 5 ns	Charge transfer M → L
$[Cr(acac)_3]$		λ_{max} ca 500 nm τ = 1.5 ns	Charge transfer M → L
$[Cr(NCS)_6]^{3-}$		λ_{max} ca 540 nm τ = 5 ns	Charge transfer M → L

Although the $^4T_{2g}$ state is reached by absorption, the ESA spectra of all 3 complexes match the ESA of the ^2E_g state measured at 77 K by Ohno and Kato [2]. Unless the ESA spectra of $^4T_{2g}$ and ^2E_g states are fortuitously the same, it appears that the $^4T_{2g}$ state undergoes intersystem crossing to the ^2E_g state in a time less than the duration of the pump pulse (*ca.* 5 ps).

References

[1] Kirk, A. D., Hoggard, P. E., Porter, G. B., Rockley, M. G., and Windsor, M. W., *Chem. Phys. Lett.* 37, 199 (1976).

[2] Ohno, T., and Kato, S., *Bull. Chem. Soc. Japan*, 43, 8 (1970).

Reliable, inexpensive microcomputer interface for the optical multichannel analyzer (OMA)

Dewey Holten, David A. Cremers, Stephen C. Pyke, Ronald Selensky, S. Sadiq Shah, Dewey W. Warner, and Maurice W. Windsor

Department of Chemistry, Washington State University, Pullman, Washington 99164

(Received 5 April 1979; accepted for publication 26 August 1979)

A microprocessor system and interface for the optical multichannel analyzer (OMA) is described. The interface hardware and software are very simple and easy to implement. The microcomputer is used in conjunction with the OMA in the 2-d (two-dimensional) mode as the data acquisition, analysis and storage system for a 8-ps-resolution transient absorption spectrometer. However, the microcomputer and interface hardware and software are of general use in any application where rapid transfer, processing and storage of spectroscopic information from the OMA are required.

Recent rapid advances in microprocessor technology make laboratory data acquisition and analysis systems based on the microprocessor a powerful yet inexpensive alternative to interfacing instrumentation with minicomputers. The purpose of this article is to describe how a simple inexpensive microcomputer was interfaced to a Princeton Applier Research (PAR) Optical Multichannel Analyzed (OMA). A block diagram of the experimental apparatus is shown in Fig. 1. We have chosen to describe this particular interface because of our specific experience and because the OMA and related rapid scan photodetection systems based on vidicon detectors and diode arrays are used for an increasing variety of tasks from Raman spectroscopy to quality

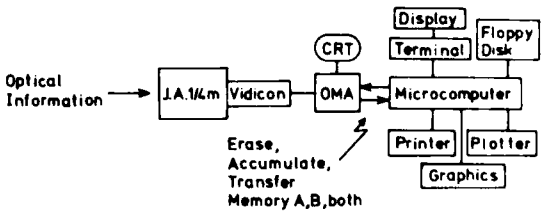

FIG. 1. Block diagram of the overall data acquisition, storage and analysis system of the picosecond absorption spectrometer. The monitoring pulse from the laser apparatus contains sample ground and excited state absorption information. This is dispersed by the monochromator and detected by the vidicon coupled to an optical multichannel analyzer (OMA). Spectral information from the OMA is processed by the computer to yield a transient absorption spectrum for a single laser shot, displayed and then stored on a floppy disk.

 0034-6748/79/121653-03$00.60

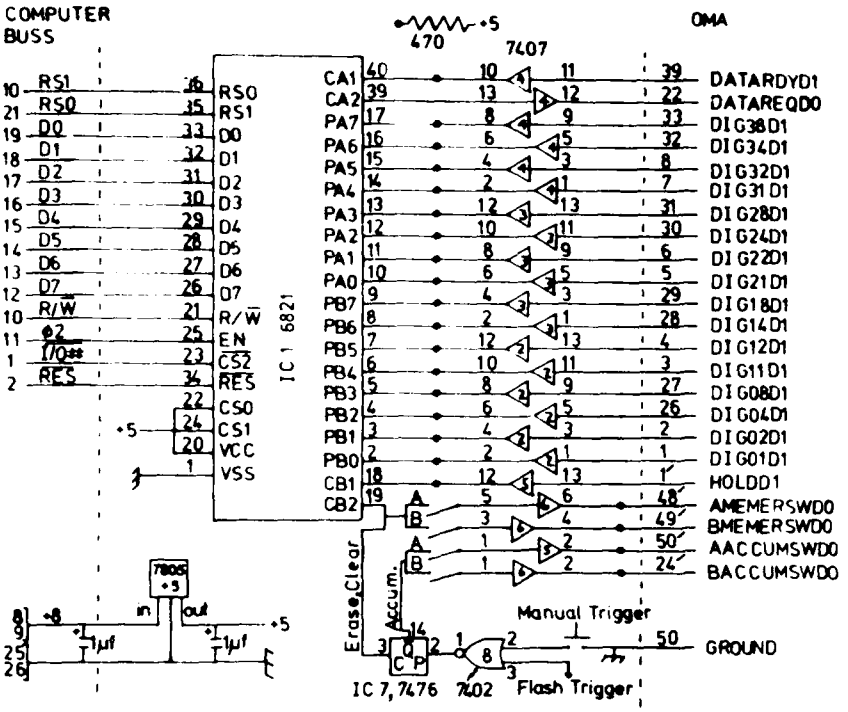

FIG. 2. Schematic of the OMA microcomputer interface circuitry for data transfer and associated handshake signals. The 6821 PIA chip is wired via register selects RS0 and RS1 to operate as a 16-bit port at computer I/O port 6. The 7407 open collector drivers (ICs 2–6) are located in a box at the OMA output connector and are powered from the 7805 voltage regulator. The 470-Ω pull-up resistors are located on the port 6 interface board. The primed numbers at the OMA refer to the remote program connector, unprimed numbers refer to the digital output connector. Note not shown in this figure is a 74121 IC between the CB2 pin and the A and B memory erase switches, configured as a one-shot to provide a low pulse of 1-ms duration necessary for complete erasure.

control in the manufacture of paints[1–4] but few microprocessor interfaces have been described.[5] This article describes a working OMA interface and is a starting point for those with interest in other related microprocessor applications.

The important advantages of our approach are as follows:

(a) The entire microcomputer system, including 28K static RAM memory, 4K programmable EPROM, terminal, printer, plotter, A/D and D/A converters, and 8-in. floppy disk drive with 350 Kbytes per disk, and software can be purchased for under $4000.

(b) The actual OMA interface requires about $20 in integrated circuit chips (ICs) and can be wired in only a couple of hours and is completely compatible with existing I/O signals available at the OMA console rear panel.

(c) Software requirements to drive the interface are minimal.

(d) General applicability of the hardware and software for use in applications where rapid transfer, storage and analysis of spectroscopic information from the OMA is required.

(e) Our OMA consists of the 1205B vidicon detector and the standard 1205A console. Thus the present interface gives this widely used OMA many of the features of the more expensive OMA2 (1215) recently introduced.

A Jarrel–Ash 0.25-m monochromator (without exit slit) is used to disperse the input signal onto the photocathode of the vidicon. The OMA converts the intensity of the signal at any particular wavelength to current by sweeping the photocathode with an electron beam. The current versus time signal is divided into 500 channels, with each channel corresponding to successive vertical sweeps of the photocathode. The signal is digitized and can be stored in either of two OMA memories. Each of the memory words contains 21 bits of intensity information including five places for magnitude (each comprising 4 BCD bits) plus a sign bit. We use only four places of accuracy (16 bits) and ignore the sign bit since all values are positive. Any one of the 500 words per memory can be displayed on the front panel and is also available at the digital output connector on the back panel for access by a computer interface. The data for each channel are in parallel form. Channels can be selected using a cursor button located on the front panel or by the computer via the digital output connector. Similarly, one can reset the cursor to channel zero or select either OMA memory A or B for output with push button or computer control.[6]

The microcomputer mainframe is a SWTPC 6800 (Southwest Technical Products Corporation, San Antonio, TX) with eight slots along the 50-pin bus for the microprocessing unit (MPU) and memory boards and eight slots along a reduced 30-pin bus for I/O cards. The Motorola 6800 MPU in our system is run at 890 KHz. The 28K of static (21L02) memory comprises the central memory, along with 4K of EPROM containing disk I/O and some data-crunching routines. Six of the I/O ports are alloted to interfaces for the SWTPC CT-64 terminal display, the SWTPC PR-40 dot-matrix printer, D/A converter, A/D converter, Houston Instruments HIPLOT digital plotter, and 8-in. floppy disk drive (model FD-8, Midwest Scientific Instruments, Olathe, KS). Port 6 along with an unused half of port 4 are used for the OMA interface described below. Each parallel interface consists of one Motorola 6821 peripheral interface adap-

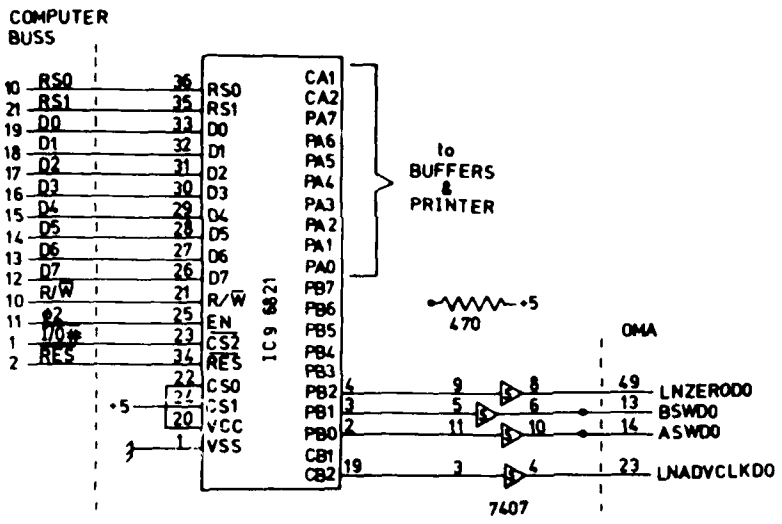

FIG. 3. Schematic of the OMA memory address and control circuitry making use of the B side of a PIA at computer I/O port 4. The A side of port 4 is dedicated to the PR-40 printer. Power is derived from the computer via an on board voltage regulator as in Fig. 2.

tor (PIA) chip and buffer/drivers for the I/O lines. The PIA has two essentially equivalent I/O sections each consisting of eight data lines and two control lines. The direction of flow on each data line and the response of the peripheral control lines are all under software control.[7] Each half also has an internal 8-bit control register and an 8-bit output (data) register, treated as memory locations to be read from or written into by the MPU. This gives the computer memory-mapped I/O. The PIA address lines RS0 and RS1 can be wired so that the addresses for the two 8-bit output locations alternate with those of the control locations or are sequential to each other. In the latter configuration the PIA can be used as a 16-bit port, the transmitted or received data being sent to or received from the PIA via one of the MPU's 16-bit registers with a single instruction. The present design uses this approach for the port 6 PIA (Fig. 2).

The OMA control and data signals are routed to the simple interface logic at the microcomputer I/O ports 6 and 4 as shown in Figs. 2 and 3, respectively. The total cost of the complete interface is under $20. The lines for each data bit are connected in ascending order to the data inputs of the peripheral interface adaptor (PIA) chip at computer I/O port 6 (Fig. 2) via 7407 open collector drivers IC's 2-6 and 470-Ω pull-up resistors. The data transfer proceeds as follows (Fig. 2). PIA control CB2 is set low by a software command. This erases either or both OMA memories depending on the positions of the SPST switches, and clears flip flop IC7, setting its $\bar{Q}$ output high so that the OMA is in the nonaccumulation mode.

When the experiment is initiated, a trigger pulse from a flashlamp light detection circuit in the main laser cavity applies a logic low to NOR gate IC8 and onto the set input of IC7. This toggles its $\bar{Q}$ out low, forcing the OMA accumulation line(s) low and allowing accumulation into the selected OMA memories for the preset number of accumulation cycles. Upon completion of this accumulation, the OMA HOLDD1[8] line goes high, indicating to the computer via the PIA CA1 control input that the experimental data is stored in the OMA memories and that data transfer from the OMA to the computer can now take place.

The transfer of 500 (channels) 16-bit data words is controlled by software through handshake between the PIA CA1 and CA2 lines and the OMA data ready and data request lines. The microprocessor cycle time for transferring data is about 30 μs for each channel as determined by the MPU clock frequency and the controlling software. During the transfer, selection of the appropriate OMA memory, resetting the cursor to channel zero, and sequentially addressing each of the OMA memory locations in order to transfer its stored data is controlled by one-half of a PIA at microcomputer port 4. This circuitry is shown in Fig. 3. The 6800 machine code for initiating the experiment and controlling data transfer from the OMA memories to the computer central memory is very simple and requires less than 200 bytes of memory.[9]

This work was supported by the Office of Naval Research, by the US Army Research Office under DAAG29-76-9-0275, and by NSF grants PCM75-23504 and PCM79-02911.

[1] R. B. Srivastava, M. W. Schuyler, L. R. Dosser, E. J. Purcell, and G. H. Atkinson, Chem. Phys. Lett. **56**, 595 (1978).
[2] M. A. El-Sayed and J. Terner, Biophys. J. **20**, 369 (1977).
[3] G. E. Busch and P. M. Rentzepis, Science, **194**, 276 (1976).
[4] S. I. Greene, R. M. Hochstrasser, R. B. Weisman, and W. A. Eaton, Proc. Natl. Acad. Sci. **75**, 5255 (1978).
[5] M. Castagne, J. Gasiot, and J. P. Fillard, J. Phys. E. **11**, 345 (1978).
[6] Optical Multichannel Analyzer Manual, Princeton Applied Research Corporation.
[7] Motorola M6800 Microprocessor Applications Manual, Motorola Semiconductor Products, Inc., 1975.
[8] Derived from the OMA timing board and transported to the remote program connector pin 1, replacing the unused +5-V output previously at pin 1. The HOLDD1 signal indicates that all accumulation cycles are complete (see Ref. 6).
[9] The complete machine language program for driving the interface and more details on the flashlamp trigger circuitry and alignment of the 2-d OMA are available upon request.

Chapter V

CHEMICAL MEASUREMENTS IN THE PICOSECOND AND SHORTER TIME RANGE

Stephen C. Pyke and Maurice W. Windsor

Offprints from
"CHEMICAL EXPERIMENTATION UNDER EXTREME CONDITIONS"
TECHNIQUES OF CHEMISTRY, VOL. IX
Edited by Arnold Weissberger and Bryant Rossiter
Published by John Wiley and Sons, Inc.

1 INTRODUCTION AND BACKGROUND

Why should we be interested in making chemical observations on a time scale as short as picoseconds (10^{-12} sec)? The first response that comes to mind is, "Because it is possible," reminiscent of the well-known replies to the questions, "Why should we climb Mt. Everest?" "Why should we go to the moon?" On reflection, we find this initial response a bit too hasty and unguarded. Many things are now possible that one might not want to do. It is possible for us to wipe out most, if not all, life on earth. It is possible to construct a building one mile tall. It is possible to recombine lengths of DNA to make genetic messages that have never before existed and that might prove a godsend to those suffering from genetic diseases such as diabetes and sickle cell anemia. Few (we would wish none) would want to implement the first possibility. The economic sense of the second is open to serious question—the first hundred floors of such a structure might be entirely consumed by elevator shafts and duct work for ventilation and other services. As to the third, a controversy is now raging as to whether the putative benefits of recombinant DNA research are worth the risk of possibly creating new viruses against which man might have no natural defenses. It is clear then that we should ask further questions before deciding to go ahead and do something just because it is possible, questions such as, "Does it make sense?" "Is it dangerous?" "Is the expected return likely to be worth the effort?" "Could we achieve the same results in some other way?" Let's examine some of these questions in relation to the matter of making chemical measurements in the picosecond and shorter time range.

First, does it make sense? To examine this question, we need to ask what chemical and physical molecular processes take place on the picosecond time scale. We note from the time scale shown in Fig. 5.1 that the average encounter time between gas molecules at 1 atm pressure at ordinary temperatures is about 100 psec; that proton and electron transfer reactions characteristically occur in times ranging from 100 psec to much less than 1 psec. There is recent evidence that the primary electron transfer

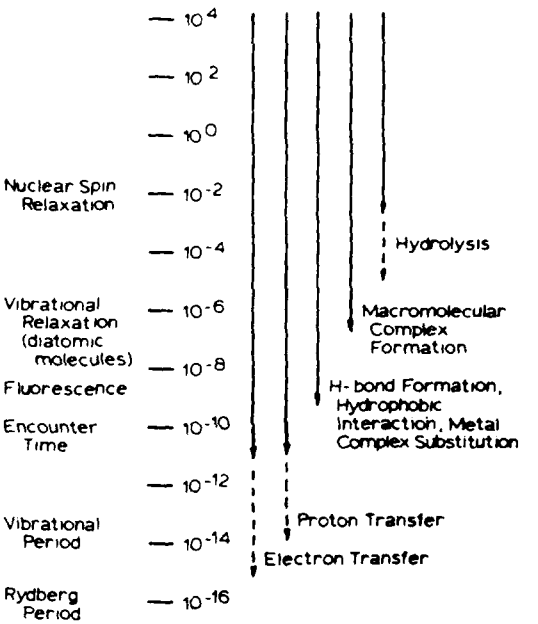

Fig. 5.1. Time scale of chemistry.

step in photosynthesis is a picosecond process. The periods of molecular vibrations lie in the range of 10^{-14} to 10^{-12} sec. Bond rupture and dissociation can occur on the same time scale, and so too can various kinds of isomerization. Internal conversion between states of the same multiplicity is thought to take place in a few picoseconds, as shown by the lifetimes of certain dyes used for laser modelocking. It appears that intersystem crossing between the lowest excited singlet state S_1 and the triplet manifold can also occur in picoseconds in favorable cases such as aromatic ketones. Intersystem crossing in inorganic systems is also fairly fast ($\sim 10^{11}$ sec $^{-1}$). Thus there seems to be plenty of incentive to attempt chemical (and physical) observations on the picosecond time scale. How about still shorter times? Should we try to extend observations to the femtosecond region (10^{-15} sec)? The picosecond–femtosecond time range could prove fruitful with regard to information on reactions involving proton or electron transfer. Photodissociation of hemoglobin–carbon monoxide complexes has recently been reported to occur in less than 0.5 psec using subpicosecond pulses from a passively mode-locked dye laser. Owing to the uncertainty principle, the information we gather becomes

spectroscopically (energetically) less and less precise as the time of observation gets shorter and shorter. Eventually, at about 1 fsec (10^{-15} sec) chemistry must come to an end. What a strange statement that is, and yet it must be so because of the dictates of the uncertainty principle. If the time of observation is no greater than 10^{-15} sec, then the corresponding uncertainty in energy from the relation $\Delta E \cdot \Delta t \geq h$ or $\Delta \nu \cdot \Delta t \geq 1$ turns out to be 30,000 cm^{-1} or about 90 kcal/mole. This figure is of the same order as the energies of chemical bonds. Thus the chemical identity of the species we are hoping to study will become indeterminate as we approach the femtosecond barrier. This same barrier poses no problem to the nuclear physicist, because an uncertainty of 90 kcal/mole or ~ 4 eV is still negligible compared to the binding energies of nuclear particles.

In summary then, it appears that the nanosecond-to-picosecond region is very important from the point of view of primary processes in chemical reactions, and this time range embraces many kinds of elementary chemical steps. This conclusion has been amply substantiated by many experimental studies over the past few years. We are just beginning to probe the subpicosecond range experimentally. Useful information on reactions involving photodissociation and on primary processes involving electron or proton transfer will probably be gained over the next five years as experimental techniques are further refined for subpicosecond studies.

Finally, let us deal briefly with the other questions we have posed. Could we get the same information another way? Certainly there are other ways of getting picosecond information. Studies of spectral line broadening can give kinetic information in the picosecond and subpicosecond ranges. However, the information obtained is less specific than that obtainable using picosecond absorption spectroscopy, and the systems that can be studied are more limited. Last, is it dangerous? We can see no special danger in picosecond laser studies, although eye protection is a concern when working with high-power pulsed lasers. Picosecond laser-induced thermonuclear fusion has already been demonstrated, and laser triggering of hydrogen bombs is therefore likely to be possible. But the attendant increase in danger is very small compared to the large potential return from controlled fusion as a new source of energy. It seems likely also that picosecond studies will be crucial in unraveling the complex processes that Nature uses to capture solar energy in photosynthesis. Armed with a detailed knowledge of these processes, we may be able to go one better than Nature and develop artificial photosynthetic systems for making fuels such as methanol and hydrogen or for converting sunlight directly into electricity.

Most reviews of picosecond spectroscopy and kinetics have discussed experimental technique only briefly and then only with reference to

specific applications and from the point of view of the specialist. The purpose of this review is to present a discussion of techniques to chemists not particularly well versed in laser physics and who might be interested in using picosecond techniques in their research. We have tried to identify and describe instrumental features that are particularly important in the development of dependable sources of single picosecond pulses. Finally we decided to stress a verbal rather than a mathematical discussion of the more complex subjects, including theory of mode-locked pulse production, sum and difference frequency generation, and correlation methods used in pulsewidth measurement. However, to assist those who wish to pursue these subjects further, we have provided references that cover each of these topics in greater depth. In addition, these resource materials provide alternative points of view, so that the reader can opt for a discussion that suits his or her particular background.

Our survey of the literature covers papers published through mid-1977. For the sake of simplicity, the formal charge of 3+ on Nd has been omitted from the text. For Nd:glass, the host is silicate glass unless otherwise noted (phosphate glass is becoming more widely used). Finally, Nd:YAG refers to Nd in a crystalline host (yttrium–aluminum–garnet).

2 INSTRUMENTAL TECHNIQUES

This section emphasizes the techniques used in generating and characterizing picosecond pulses as well as the ways picosecond pulses can be used to study the spectroscopy and decay kinetics of short-lived transient species.

We first describe some of the aspects of modelocking, single pulse selection, pulsewidth limitations, ways to change the wavelength of the pulses, and pulsewidth measurement, all of which we have found important in developing a dependable picosecond laser system. We originally had planned to include commercial information and guidelines for those committed to buying or building a picosecond laser system. However any information that we might have included soon would have been out of date. *Laser Focus* magazine publishes a comprehensive listing of manufacturers in their annual *Buyers' Guide*, which is the best resource for current information regarding commercially available laser systems, subsystems, and components. There are one or two additional points that are worth mentioning. Commercially available mode-locked laser systems are generally more expensive than normal laser systems, whereas the modelocking often requires little more than putting a modelocking dye cell in the cavity and adjusting the dye concentration and pump energy for the shortest pulses (see the section on pulsewidth measurements). The more

elaborate vibration-isolated honeycomb tables are generally not required. However some sort of rigid platform is advisable if one or more beams are to be focused onto a target after traveling more than a few feet. Otherwise frequent realignment of the system may be required. Finally, it is generally cheaper to purchase items such as Pockels cells, Nd and ruby rods, and doubling crystals directly from the manufacturer. They can be incorporated into an existing system with a little extra effort.

The section on fluorescence lifetime measurements outlines the methods used to characterize emission decay and spectra on the picosecond time scale. The section on production of tunable picosecond and subpicosecond pulses using dye lasers reviews the fairly recent development of mode-locked CW dye lasers and their use and application in measurements where subpicosecond resolution is required.

Production and Characterization of Picosecond Laser Pulses

Modelocking

The key to producing picosecond laser pulses lies in modelocking the laser cavity. Both active and passive techniques have been used, and a number of reviews are available for the reader who desires more detail [1–8]. Active modelocking involves the use of either an electro-optic or acousto-optic modulator which modulates the amplitude or the frequency of the radiation inside the laser cavity. The modulation frequency is tuned to the frequency separation between the modes of the cavity, $\omega = c/2L$, where L is the cavity length and c is the velocity of light. Many modes of the cavity are spanned by the emission profile of the gain medium ($\sim 10^4$ for a 1-m Nd:glass oscillator, $\sim 10^3$ for ruby), and consequently the energy stored in the radiation field inside the cavity will build up preferentially in these modes. As this occurs, the radiation field can be formulated as a single pulse, in time, traveling back and forth in the cavity with a width approximately equal to the inverse of the bandwidth of the gain medium, $\Delta\tau = 1/\Delta\nu$ (see section on pulsewidth limitations). At the output mirror, which is only partially reflecting, part of the pulse escapes the cavity, and the total output appears as a train of pulses, with each pulse separated by the time required for the pulse inside the cavity to make one complete round trip, $2L/c$. The pulse train will continue until the medium no longer provides gain. The action of the modelocker is to ensure that all the cavity modes oscillate in phase. In the frequency domain, the following description can be used. The mode of highest gain will appear first, and the modulation of its frequency will progressively introduce *in phase* other cavity modes that lie within the gain curve. Transformation of this assembly of inphase frequencies to the time domain (see later) gives a pulse of very short duration. The more cavity modes that are locked in phase, the shorter the resultant pulse. This is why a medium with a broad bandwidth gain curve, such as a laser dye, can give shorter pulses than say a ruby or Nd:glass laser.

While acousto-optic modulators were first used in active modelocking, electro-optic modulators were found to be much more dependable. With the application of saturable dyes and passive modelocking, the production of picosecond pulses by active modelocking has virtually disappeared for pulsed lasers, although active modelocking is still employed for CW ion and dye lasers.

Passive modelocking is accomplished by placing a saturable absorber in the cavity. Theoretical and numerical treatments for the development of picosecond pulses are available [9–11] and are beyond the scope of this review. As lasing begins, picosecond- and subpicosecond-duration spikes with a random phase relationship exist simultaneously inside the cavity. These spikes are part of the noise spectrum of the emitting medium and arise because the emission by excited states is a statistical process. If a bleachable dye solution is placed inside the cavity, only those spikes with sufficient intensity will bleach the solution and penetrate the dye cell, and only these spikes will gain intensity on passing through the gain medium. If the dye absorbance is chosen properly and the laser operated at or very near threshold, ideally only one pulse should gain intensity. Figure 5.2 shows how the dye selects a pulse and shrinks the pulsewidth on successive passes. The dye absorbs the first part of the pulse before saturation, and if the recovery time of the dye is short compared with the pulsewidth the trailing low-intensity portion of the pulse is also absorbed. Several dyes have been used in passive modelocking. Eastman Kodak dyes No. 9860 and No. 9740 and the nickel dithiene bis(4-dimethylaminodithiobenzyl)nickel(II) (BDN) [12] have been used to modelock the Nd:glass oscillator [56, 134], whereas the polymethine dyes 1,1′-diethyl-2,2′-dicarbocyanine iodide (DDI) and 1,1′-diethyl-4,4′-carbocyanine iodide (cryptocyanine) have been successfully employed to modelock the ruby laser. The polymethine dye 3,3′-diethyloxadicarbocyanine iodide (DODCI) has been used to modelock the rhodamine 6G (R-6G) and rhodamine B flashlamp-pumped dye lasers, and DODCI has been employed to modelock CW dye lasers as well [13]. Double modelocking (using one laser dye to modelock a second in a single cavity) has also been accomplished. Because of the high gain, saturation of the gain medium also plays an important role in pulse shortening in dye lasers. Modelocking in CW ion and dye lasers is discussed in more detail later.

The size and the location of the dye cell in the cavity have been important considerations. Bradley and co-workers have maintained that the shortest pulses are obtained when the dye cell is thin (30 to 100 μ)

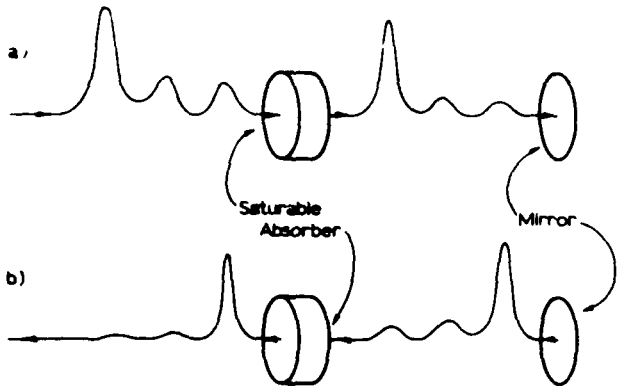

Fig. 5.2. Effect of a saturable absorber on spikes of different intensity. Since the transmittance of the dye varies as the square of the intensity, the largest spikes will be absorbed less strongly than the weaker ones. The leading edge of each pulse will lose more intensity than the center for the same reason, and if the recovery time of the dye is short compared with the pulsewidth, a similar loss will occur for the trailing edge of the pulse. The dye concentration and the flashlamps are adjusted so that the gain-to-loss ratio is greater than unity for only the most intense spike. (a) poles propagating left to right; (b) poles propagating right to left.

and when the dye is in contact with one of the cavity mirrors [14]. Figure 5.3 outlines this type of cavity configuration. While this arrangement may reduce the pulsewidth somewhat, its primary advantage may be convenience. Since the dye volume is small, a flowing cell is advisable to avoid breakdown of the dye, and a large reservoir of dye solution can be employed. In the alternative arrangement, a dye cuvette with relatively small volume (~10 ml) and 10 mm path length is used, and the dye solution must be changed regularly. When the dye cell is removed and replaced, a slight alteration of the cavity characteristics is inevitable. The cavity retuning required is minimal but can be avoided by using the

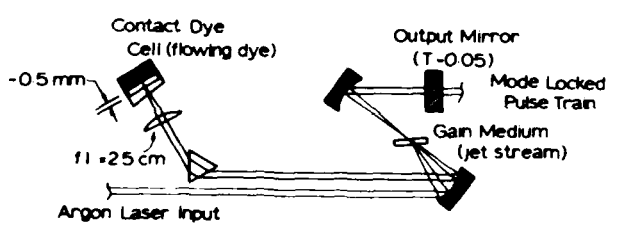

Fig. 5.3. Schematic of mode-locked CW dye laser showing the contact dye cell [85].

optically contacted flowing dye cell. Yu and Alfano [15] maintained that satellite pulses cannot be excluded from the pulse train unless an optically contacted dye cell is used, and Garmire and Yariv [16] pointed out that a nonoptically contacted dye cuvette may sometimes lead to the formation of subcavities. These can produce secondary pulse trains separated from the primary train by $2L'/c$, where L' is the distance between the dye cuvette and one of the cavity mirrors. This problem can be avoided with an optically contacted dye cell but need not preclude the use of the cheaper dye cuvette in passive modelocking, as long as subcavities are avoided by careful placement and orientation of the cell.

Although passive modelocking has proved to be the simplest way to produce picosecond pulse trains in Nd:glass and ruby laser systems, repeatable performance is a much more sensitive function of cavity stability, flashlamp intensity, and rod temperature for ruby than for Nd:glass systems. Quality of the ruby rod is also important. Cavity configuration seems to have little effect in producing mode-locked pulse trains in that modelocking in ruby has been achieved with concentric cavities and plano–plano cavities. Confocal cavities are not advised, however, because mirror damage is much more likely.

Single Pulse Selection

While the entire pulse train from a modelocked laser has often been used as a source of excitation, complications often ensue. For Nd:glass lasers, the pulsewidth increases from the beginning to the end of the train by 20 to 30%. For flashlamp-pumped dye lasers, on the other hand, the opposite is true, because of gain saturation. Figure 5.4 illustrates the effect of a greater number of cavity round trips in the flashlamp-pumped dye laser [17]. Consequently, when the entire pulse train is used for measuring transient phenomena, true lifetimes will be convoluted with an average pulsewidth, and power levels will be averaged over the whole train. Thus both lifetimes and pulse intensity will be difficult to determine

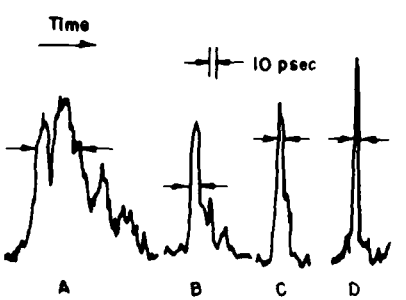

Fig. 5.4. Microdensitometer traces of streak camera records showing progressive shortening of the output pulse from a rhodamine 6G dye laser as a function of the number of cavity round trips: (*A*) seven cavity round trips; (*B*) 20 round trips; (*C*) 28 round trips; and (*D*) 45 round trips into the pulse train. Full widths at half-maximum are indicated by arrows [17].

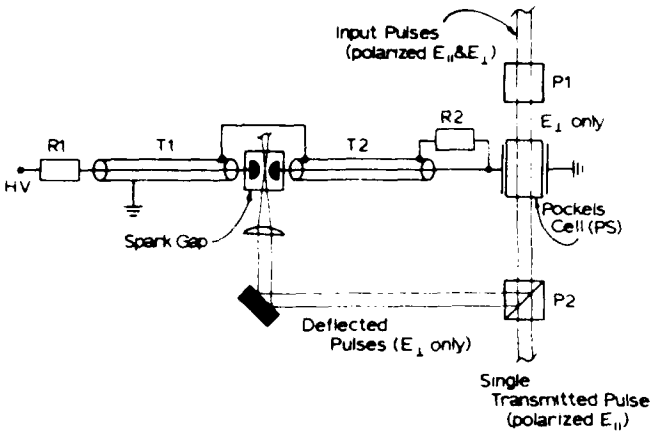

Fig. 5.5. Schematic of a single-pulse selector using an optically triggered spark gap and Pockels cell.

precisely. Other complications that can occur are saturation of the ground-state transition; absorption of a second photon by long-lived transients ($\tau > 2L/c$) produced by the first part of the pulse train; stimulated emission; and excited-state annihilation occurring only at high powers where excited-state concentration is high. For these reasons, it is generally more convenient to select out a single pulse to excite the system under study. Intracavity pulse selectors were used initially, but extracavity methods were developed to avoid component damage from the high power densities inside the cavity. Figure 5.5 is a diagram of a popular pulse selector utilizing a Pockels cell and optically triggered spark gap. The laser rod is cut so that the ends are at Brewster's angle, and the dye cuvette is also situated so that its windows are at Brewster's angle with respect to the cavity mirrors. Thus the output radiation is polarized predominantly normal ($E_\perp$) to the plane of the diagram. The pulse train is then passed through a Glan–Foucault prism (a Glan polarizer with an air gap between the prism components) which eliminates the remaining light polarized in the plane ($E_\parallel$) of the diagram, and through a Pockels cell which is oriented so that, when relaxed, it passes only $E_\perp$ polarized light. A second Glan-Foucault prism passes only light with $E_\perp$ polarization and reflects the first part of the pulse train (with $E_\perp$ polarization) into a pressurized spark gap with quartz windows. As the height of successive pulses grows, one pulse finally triggers the spark gap, and a high-voltage pulse is applied to the Pockels cell for a short time. The high voltage induces a birefringence, and the next picosecond optical pulse to reach

the Pockels cell has its polarization rotated by 90° and is then able to pass through the second Glan–Foucault prism. A more detailed description of the electro-optic effect can be found in Ref. 18.

The timing of this optical trigger, which is critical to the successful selection of one picosecond pulse, is controlled by simple RC time constants of a circuit as outlined in Fig. 5.5. The threshold pulse causes the spark gap to break down, and the high voltage begins to affect the Pockels cell in a time determined by the length of cable T2 between the spark gap and the Pockels cell and the speed of a signal in RG-8/u cable (~0.6 the speed of light). The cable length is adjusted so that the half-wave voltage applied to the Pockels cell is synchronized with the arrival of the next optical pulse. The total time that the Pockels cell feels the high voltage is determined by the length of cable between the resistance box R1 and the spark gap. The cable length T1 is usually adjusted to provide a window ~5 nsec in duration. The duty cycle of the Pockels cell (time required before another pulse can be selected) is determined by the RC time constant of the resistance $R1$ and the cable capacitance from R1 to the spark gap, and since $R1 \cong 10^8\ \Omega$, $RC \sim 80$ msec. The pulse trains are typically less than a few milliseconds in duration. Consequently only one pulse in each train is capable of activating the Pockels cell. A detailed description of a similar pulse selection method using a Kerr cell was presented by von der Linde, Bernecker, and Laubereau [19]. High-voltage pulse power supplies with very low jitter are now available and are begining to replace spark gap-activated Pockels cells. These power supplies can be triggered by photodiodes and will deliver a triangular HV pulse with a width, peak voltage, and delay relative to the trigger pulse which can be changed to permit pulse selection from different points in the train. In the case of spark gaps, this can be accomplished by adjusting the electrode separation, the nature of the filling gas (usually N_2), or (most easily) the gas pressure. With a spark gap, the pulsewidth is adjusted by using different lengths of cable T1.

Pulsewidth Limitations

The theoretical limit of the minimum pulsewidth is related to the bandwidth of the emission profile by a Fourier transform:

$$F(\omega) = \frac{1}{\sqrt{2\pi}} \int_{-\infty}^{\infty} f(t)\, e^{i\omega t}\, dt$$

The symmetry inherent in the Fourier transform yields

$$f(t) = \frac{1}{\sqrt{2\pi}} \int_{-\infty}^{\infty} F(\omega)\, e^{-i\omega t}\, d\omega$$

and results in the following constraint: $\Delta\nu \cdot \Delta t \geq 1$, where $\Delta\omega = 2\pi\,\Delta\nu$. Since the emission bandwidth of the lasing medium $\Delta\nu \approx 100$ cm^{-1} for Nd:glass, the theoretical minimum pulsewidth is ≈ 0.3 psec. For ruby the bandwidth is smaller, $\Delta\nu \approx 10$ cm^{-1}, because of the crystalline host, and $\Delta t \geq 3$ psec. For Nd:YAG, $\Delta\nu \approx 1$ cm^{-1}, and $\Delta t \approx 30$ psec. Subpicosecond pulses have been obtained from dye lasers whose bandwidth is 10 to 100 cm^{-1}; and for ruby, dye, and Nd:YAG lasers nearly transform-limited pulsewidths have been achieved. However modelocked Nd:glass lasers, which have been used most frequently in the study of picosecond physical and chemical processes, have rarely produced transform-limited pulses.

For all passively mode-locked solid-state laser systems, the relaxation time of the modelocking dye, τ_r, must be fast compared with the reciprocal of the gain width of the lasing medium in order to achieve transform-limited pulsewidths ($\tau_r < 1/\Delta\nu$). The situation in which $\tau_r > 1/\Delta\nu$ leads to longer than transform-limited pulsewidths [20, 21]. This is clearly the case for Nd:glass lasers, where $1/\Delta\nu \approx 0.3$ psec. A short dye relaxation time is necessary in order that the weaker photon noise be eliminated by the saturation behavior of the dye both before and after the intensity maximum as shown in Fig. 5.2. When $\tau_r > 1/\Delta\nu$, the result is a skewed pulse shape due to the inability of the absorber to recover fast enough to attenuate photon noise following the peak of the pulse. Self-focusing and resulting self-phase modulation (SPM) at high power densities leads to nonlinear dispersion and contributes to temporal broadening of the pulse. In addition, spectral narrowing of the gain width of the Nd:glass laser occurs in the initial linear growth region of amplification. The reason for this is that the modes nearest the emission maximum will store energy at a faster rate than those modes on the wings of the emission band. This reduces the effective bandwidth of the medium near the lasing threshold and results in an increase in the effective pulsewidth. Von der Linde and Rodgers [22] have used an intracavity Fabry–Perot etalon to reduce the rate of spectral narrowing in the linear amplification regime of an Nd:glass laser by tuning the etalon so that the transmission minimum coincides with the gain maximum. This gives those modes in the wings of the gain width more of a chance to grow before threshold is reached. Dye lasers, on the other hand, produce nearly transform-limited pulsewidths because of gain saturation. With each cavity round trip the nonlinear absorption of the modelocking dye attenuates the leading edge of the pulse, but it is the gain saturation of the lasing dye that leads to reduced gain for the trailing edge of the pulse [23], the bulk of the excited state population being exhausted by the earlier portions of the pulse. In addition, pulsewidths are shortened somewhat by nonlinear optical elements such as doubling crystals and Kerr cells which discriminate against the lower power levels at the beginning and end of each picosecond pulse. Finally, the dye cell thickness and position described above in the section on modelocking has been found to be important in the reduction of pulsewidths in passively mode-locked lasers [14].

Harmonics and Wavelength Tuning in Solid-State Lasers

The high powers of typical picosecond pulses from mode-locked solid-state lasers ($\geq 10^8$ W) permit the utilization of nonlinear optical and spectroscopic properties, notably sum and difference frequency generation and stimulated Raman scattering (SRS) to alter the fundamental lasing frequency.

Sum and difference frequency generation (SFG and DFG) are processes that occur in materials with high nonlinear susceptibility or that respond to the applied optical electric field of high-power laser pulses with a change in the polarization, which is dependent on the square (or higher powers) of the applied field. Polarization corresponds to the induced distortion of the equilibrium distribution of electrons around the nuclei. Formally known as three- and four-wave mixing, the theoretical description of SFG and DFG is beyond the scope of this review and is well described in a monograph by Zernike and Midwinter [24] and a review by Yariv and Pearson [25]. Second harmonic generation (SHG) is the most common form of sum frequency generation (SFG), and nonlinear materials and their use in SHG are listed in Zernike and Midwinter [24]. The most frequently used materials are those of the crystallographic point group $\bar{4}2m$: KH_2PO_4 (KDP), $(NH_4)H_2PO_4$ (ADP), and their deuterated analogs abbreviated KD*P and AD*P, respectively. The main advantages are their high efficiency (up to 70 to 80% is attainable, but 10 to 20% is more usual), high damage threshold, relatively low cost, and the availability of large optical-quality crystals. Their disadvantage is that they are all hygroscopic. The most general application of SFG involves the input of two different frequencies, and the materials used in SHG are also used in this application. KDP and ADP have thresholds for UV absorbance below 200 nm [26] and therefore can be used where the sum frequency occurs at a wavelength longer than about 200 nm. However phase matching in the near UV is more difficult, since differences in group velocity limit the use of KDP or ADP very near the absorption threshold. Group velocity dispersion refers to the different speeds of the input and output frequencies within the crystal. This can lead to a breakdown of the precise phase-matching conditions required for efficient SFG and generally leads to a broadened output pulsewidth. Where the peak power is sufficiently high, group velocity dispersion can be minimized, at the cost of some efficiency, by using crystals with a short path length.

Difference frequency generation (DFG) also requires two photons to

generate a third or in some circumstances requires three photons to produce a fourth, otherwise called three- and four-wave mixing. The theory is the same as that used to describe SHG and SFG, except the output photon frequency is the difference rather than the sum of the energies in two or three other photons. The same nonlinear media are generally also employed. One percent conversion efficiencies have been observed in two-photon generation of tunable IR pulses from a mode-locked Nd:glass laser and spontaneous parametric fluorescence in $LiNbO_3$ [27]. Picosecond pulses from Nd:glass lasers can also be mixed with pulses generated by stimulated Raman scattering (SRS) and self-phase modulation (SPM) to yield difference frequencies in the IR. Tunable IR output from 1.4 to 3.8 μm has been generated directly, in a cavity, by synchronously pumping (see section on production of tunable picosecond and subpicosecond pulses using dye lasers) a crystal of $LiIO_3$ with a mode-locked Nd:glass laser [28] with about 2% efficiency. Moore and Goldberg [29] mixed the output of a synchronously pumped dye laser with that of the mode-locked Nd:YAG laser in various nonlinear materials to generate SFG from 270 to 432 nm and DFG from 1.13 to 5.6 μm. Their conversion efficiency was about 2% for pulses from 1.1 to 2.3 μm, but conversion efficiency for longer wavelengths is not quoted.

Stimulated Raman scattering (SRS) in liquids has also been an efficient way of changing the frequency of a high-power picosecond laser pulse. By capitalizing on the coherent nature of the SRS process [30], one can shift the pulse frequency by an amount corresponding to the energy of a Raman-active vibrational mode of the medium while maintaining low divergence and narrow bandwidth in the converted beam. Table 5.1 outlines some of the frequency shifts that can be obtained using SRS.

Production of picosecond pulses in the vacuum UV (197 nm) has been demonstrated in strontium vapor near 600 C [31] following earlier work of Kung et al. [32] and Hodgson et al. [33]. Very recently XUV frequencies down to as short as 38 nm have been obtained by high-order harmonic generation in rare gases, using up to the seventh harmonic of a Nd:YAG laser output at 266 nm as the pump frequency [34]. Streak cameras necessary to characterize picosecond pulses in the VUV and X-ray regions are also under development [35].

Pulsewidth Measurements

Along with the production of picosecond pulses came the problem of finding a way to measure the pulsewidths accurately. Photoelectric measurement is limited by the bandwidths of commercially available oscilloscopes. At the present time the fastest oscilloscope and amplifier combination available through Tektronix is the 7904 mainframe and the 7A19

Table 5.1 Table of SRS Shifted Wavelengths for Various Pump Frequencies [30]

	SRS Wavelength (nm)		
Solvent	*Nd (SH) at 530 nm*	*Ruby at 694 nm*	*Ruby (SH) at 347 nm*
Benzene	559	745	359
CS_2	550	729	355
Nitrobenzene	570	765	364
Chlorobenzene	560	745	359
Ethanol	627	870	386
Methanol	624	864	385
	628	872	386
Isopropanol	626	867	386
Acetone	627	871	386
1,1,1-Trichloroethane	628	872	386
Calcite	562	750	360
Water	648	912	394

amplifier, which together provide an 800-psec risetime with a sensitivity of 10 mV/cm. With direct access to the CRT, using a 7A21N plug-in, a bandwidth of 1 GHz and a risetime of 350 psec can be attained, but sensitivity is reduced to 5 V cm. Oscilloscopes with bandwidths up to 5 GHz have been manufactured but are not readily available, and at these frequencies the writing speed becomes a limiting factor. Sampling scopes have better time resolution (25 psec for a Tektronix S 4 sampling head); however, high repetition rates and reproducible signals are required. Sampling scopes can be applied to measure fluorescence decay but are still too slow to resolve pulsewidths generated in most mode-locked lasers. Even the fastest oscilloscope and photodiode combination lacks the resolution to measure picosecond pulses. Consequently the so-called correlation methods were developed to measure indirectly the widths of picosecond pulses.

Correlation methods have been extensively reviewed by Ippen and Shank [36] and Bradley and New [37] and will be discussed only briefly. The popular nonlinear correlation methods involve the superposition of one pulse with itself (autocorrelation) or another pulse in a nonlinear optical medium where a property such as second harmonic generation (SHG) or two-photon fluorescence (TPF), which is dependent on the square of the input power, can be observed. Figure 5.6 represents a zero-background technique developed by Weber [38] to measure the amount of second harmonic produced when pulses were split by a par-

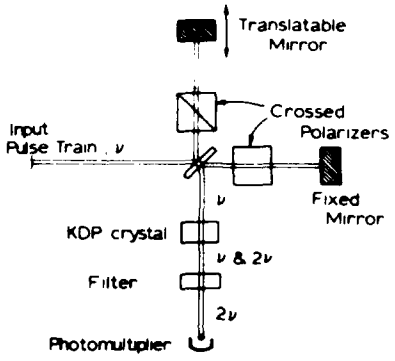

Fig. 5.6. Schematic of correlation technique developed by Weber [38] to measure picosecond pulsewidths. Orthogonal pulse polarization permits type II phase matching in KDP and the elimination of background signal due to SHG from only one pulse (orthogonal polarization is required in type II phase matching).

tially reflecting mirror, passed through polarizers to produce orthogonal polarizations in the two beams, and later recombined and passed through a crystal of KDP. The intensity of the second harmonic is recorded, the relative position of the two pulses is altered by moving a mirror, and the laser is fired again. Clearly SHG will be at a maximum when the two pulses overlap in the crystal and there is zero phase shift. The pulse profile is then plotted against mirror position X, and the width ΔX is related to the pulse duration by the speed of light ($\Delta t = \Delta X/c$). A similar technique using the second harmonic reflection produced at the surface of a nonlinear crystal (GaAs) was introduced by Armstrong [39] and used more recently by Tomov [40]. Weber's method has been successfully applied in measuring pulsewidths from mode-locked CW dye lasers, because the pulse trains are continuous and the signal-to-noise ratio is improved owing to signal averaging. Figure 5.7 illustrates the approach taken by Ippen and Shank. When pulsed lasers are used, the primary weakness of SHG, in both KDP and reflections from GaAs, was that many laser shots were required to construct a picture of the pulse profile, and the profiles represented the time average of all the pulses in the train. These limitations were eliminated by the development of the two-photon fluorescence (TPF) technique [41] and the measurement of the widths of single pulses. Figure 5.8 illustrates this experiment. A single pulse is extracted from the train and split by a partially reflecting mirror and recombined in a medium transparent to the lasing wavelength, but it will simultaneously absorb two photons and exhibit a fluorescence with an intensity dependent on the square of the input power of the pulse. The fluorescence is photographed, and the pulsewidths are determined by measuring the size of the fluorescence image directly with a ruler or from microdensitometer traces. No information is available about the symmetry of the pulse, and data from the microdensitometer must be fit to an arbitrary pulse shape (usually Gaussian) to yield a value for the pulsewidth. In TPF a peak-to-background contrast ratio of 3:1 is a general feature of a good single-pulse measurement. The 4:1 ratio, calculated from the I^2 dependence of two-photon fluorescence, is not expected because the two pulses propagate in opposite directions and a correlation must involve an average of all possible relative phase angles. In fact, a 3:1 ratio is often not observed, and background may even approach the peak intensity for pulses from a poorly mode-locked laser. The pulse intensity

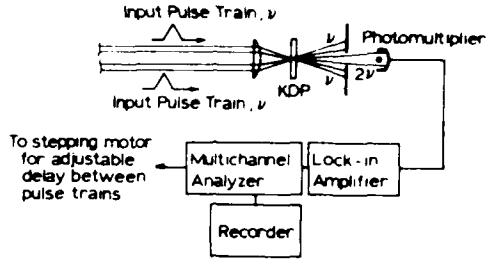

Fig. 5.7. Ippen and Shank's adaptation of Weber's technique for pulsewidth measurements of pulses from a mode-locked CW dye laser (*Laser Focus*, July 1977). Second harmonic output is at an angle to the fundamental frequency and eliminates the need for filters to separate ν from 2ν. One of the input pulse trains is chopped, and the lock-in amplifier provides synchronous detection of 2ν at the chopping frequency. This increases signal-to-noise ratio dramatically, and weak (second harmonic) signals are more easily measured.

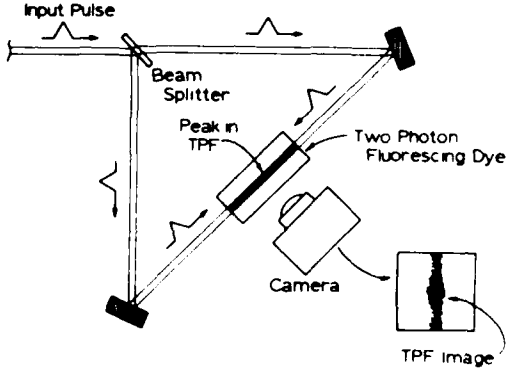

Fig. 5.8. Two-photon fluorescence (TPF) method. Pulsewidths are generally determined from a microdensitometer trace of the photographed fluorescence image.

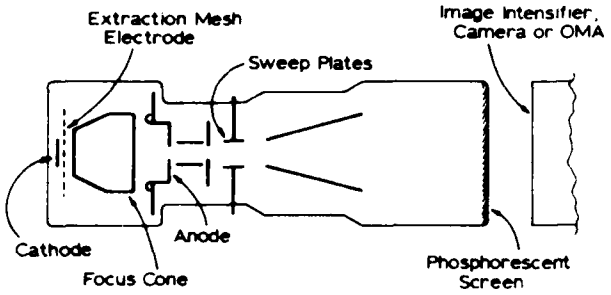

Fig. 5.9. Streak tube from an Imacon II streak camera (Hadland Photonics, Ltd.).

must be just intense enough to produce a readable track, otherwise TPF will occur with just half of the pulse with an efficiency approaching that when the pulses overlap. Rentzepis and Duguay [42] were able to reduce the background by producing a two-photon fluorescence from the superposition of the residual fundamental pulse at 1060 nm from an Nd:glass laser and the weaker second harmonic at 530 nm. Rentzepis et al. [43] measured the third-order correlation function by three-photon fluorescence (3PF), which gives a much higher value of contrast (10:1) and the additional advantage that the pulsewidths are independent of the assumed pulse shape.

The most direct method for measuring picosecond pulsewidths is electron-optical chronography. The instrumentation used is commonly known as a streak camera. It consists of an image tube, high-voltage pulse circuitry, and a data storage system. The streak camera was proposed for kinetic studies of short-lived emission by Zavoiskii and Fanchenko [44] but was limited to nanosecond resolution until the development of picosecond laser systems. However the ultimate resolution of the streak camera was shown to be limited only by the distribution of electron transit times in the image tube [44], and several streak cameras with resolutions of between 1 to 10 psec are now commercially available. Very simply, the streak camera can be thought of as the first stage in a common photomultiplier tube with minor modifications. Figure 5.9 shows the Imacon II streak tube (Hadland Photonics, Ltd.). The photoelectrons emitted from the photocathode are accelerated in an electric field generated by a very high potential on an extraction mesh electrode very close to the photocathode (~20 kV/cm). This effectively eliminates the spread in transit times due to the energy distribution of the photoelectrons. The photoelectrons are then focused to a beam, and the beam is deflected by a fast voltage ramp which streaks the photoelectrons across a phosphorescent

screen or an image intensifier. The final image is either photographed or recorded by an optical multichannel analyzer (OMA). The pulsewidths can then be related to the intensity profile of the streaked image on the phosphor and can be determined exactly by calibration. Calibration can be performed easily by reflecting a picosecond pulse from a glass slide or optically flat piece of glass or quartz of known thickness and then streaking the reflected pulses. The separation of the pulse image reflected off the first surface and that reflected off the second surface is then related to the distance between the surfaces and the speed of light in the medium.

Principles of Picosecond Measurement

In this section we classify picosecond measurement techniques according to the physical principles on which they are based. Then we give a detailed account of each type of experimental approach. New kinds of measurement techniques become possible in the picosecond-to-nanosecond time regime that are not practicable on a longer time scale. This is so because we are dealing with time intervals so short that even light can travel only fairly modest distances in the times involved. For example, light travels 1 ft, or 30 cm, in 1 nsec and only 0.03 cm in 1 psec. (These are in vacuo distances; in material media the velocity is reduced still further according to the refractive index of the medium.) Thus a new class of measurement techniques is opened up. These are based on using a short-duration monitoring pulse to take a snapshot of the fading trail of excited molecules that each picosecond excitation pulse leaves behind as it sails through the medium. Think of the wake of a ship and then imagine taking a snapshot. In front of the ship (picosecond pulse) the medium is as yet undisturbed. Immediately behind, the medium is maximally perturbed, and further down the wake, the disturbance progressively relaxes. In essence we have substituted distance for time; as we proceed back along the wake, we encounter regions that were excited progressively longer ago in time. We shall call such techniques optical wake techniques and discuss them in more detail later on. A number of variations exist, and we give several examples. If the excited molecules emit, time-resolved fluorescence studies can be made in the same manner.

Some measurement techniques used in longer time frames can be adapted for use in the picosecond regime provided certain instrumental advances can be made. The very successful technique of flash photolysis and spectroscopy can be extended to the picosecond time range, given the availability of broad-band continuum monitoring pulses of picosecond duration. Absorption spectra of transient species can be recorded photographically for exploratory work. Single-shot spectrophotometry can then be used to measure the optical density changes at a given wavelength and

time delay, using a Vidicon detector (similar to a TV camera) coupled to an optical multichannel analyzer (OMA). Repeating such measurements at many wavelengths allows the absorption spectrum of an intermediate to be built up at a given time delay. Alternatively a kinetic study can be made at a chosen wavelength by taking measurements at many different time intervals after excitation. It is worth noting that the detector in picosecond flash-photolysis studies is not required to provide time resolution but simply a measurement of intensity. Time resolution is provided by the known preset time delay between the excitation pulse and the monitoring pulse. A more detailed discussion of picosecond flash photolysis is given later.

If a detector that *can* provide picosecond time resolution is available, such as a fast streak camera, the decay of excited species can be monitored temporally after a single laser shot. Fluorescence decay studies have been made and lifetimes measured in this way. Absorption decay studies are also possible, given a suitable background-monitoring pulse, but none has been done to date using a streak camera.

We devoted a separate section below to fluorescence lifetime measurements. Measurements that use a continuous train of picosecond laser pulses and a signal-averaging detection technique have been most useful in extending time resolution into the subpicosecond time domain. A later section therefore discusses dye laser techniques and subpicosecond measurements.

Additional techniques have been used to measure subnanosecond lifetimes. For instance, in measurements of emission lifetimes, intensity-modulated excitation sources and phase-sensitive detection systems (lock-in amplifier) have been used [45]. Recently an inexpensive variation was proposed [46]. For species that do not emit, other methods that yield excited-state lifetimes include saturation spectroscopy [47] and other nonlinear techniques for studying coherent transients [48]. We do not discuss these methods further. Those desiring additional details should consult the references just given.

Picosecond Absorption Techniques

Picosecond absorption measurements have several advantages over emission measurements. First, excited states that do not emit can be studied. Since there are many more states that do not emit than states that do, this is an important benefit. For example, there are many states, such as $n\pi^*$ singlet states and triplet states and higher excited electronic levels, for which the quantum yield of radiative emission is extremely low ($< 10^{-3}$), either because the radiative rate is small or because the competing quenching processes are very fast ($> 10^{9}$ sec^{-1}). For such states excited-

state absorption (ESA) measurements are the only way to follow the time evolution and decay of their populations. Second, using absorption techniques one can study the kinetics of the bleaching of the ground state (GSB) and its subsequent repopulation (GSR). There is of course no alternative way of studying the time history of the ground state. Third, absorption studies are more amenable to quantitative measurements than are emission studies. The reason for this is that, in absorption studies, one can measure the attenuation of a monitoring beam of known intensity and cross section on passage through a known path length of sample. By contrast, quantitative emission studies require the collection of all photons emitted within a well-defined and known solid angle. (Concern is also necessary for possible polarization effects and resultant anisotropy in the spatial distribution of the emitted radiation.) To obtain quantum yields, intensity comparisons must be made with standard systems of known yield. In making such comparisons, allowance must be made for the lifetime of the emitting state. Either the emission must be integrated over a time several times longer than the exponential decay time or the lifetime must be measured and photons collected over a well-defined time interval.

Both for absorption and for emission studies, laser pulses greatly facilitate the making of quantitative measurements compared to the use of incoherent light sources. The energy of a laser pulse can be accurately measured either by actinometry or by a well-calibrated thermopile bolometer. Because of the spatial coherence of the laser output, it is then relatively easy to focus the collimated beam onto a well-defined cross section of the sample. If a sample of high optical density is used, essentially all of the energy of the laser pulse is absorbed in a short path length (1 or 2 mm or even 0.1 mm in special cases). If absorption is not complete, the fraction absorbed can be found by measuring the energy of the pulse after leaving the sample. Thus the number of photons absorbed and therefore the number of initially excited states produced in a given sample volume can be calculated. Knowing the extinction coefficient of the ground state, one can then readily calculate the extinction coefficient for the excited-state absorption from the observed change in optical density at a particular wavelength.

We now proceed to a detailed discussion of several types of picosecond absorption measurements. A useful recent review of picosecond techniques is given by Ippen and Shank [36].

Optical Wake Techniques

The earliest picosecond studies fall in this category [49]. On longer time scales, say a nanosecond or greater, the spatial extent of the light pulse greatly exceeds the length of the sample. This is illustrated in Fig. 5.10*a*.

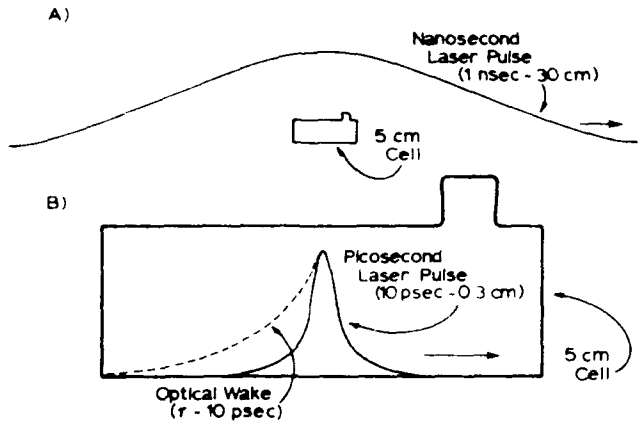

Fig. 5.10. Spatial extent of laser pulses relative to same size: (*A*) pulsewidth = 1 nsec, (*B*) pulsewidth = 10 psec.

For all intents and purposes, the medium is homogeneously illuminated and excited by the light pulse. To make a kinetic measurement, we must wait until the pulse has gone by and then send a weaker probe pulse through the sample at a known time later and measure its attenuation. This is what is done in flash photolysis. Alternatively we can use a CW probe beam and monitor its transmitted intensity continually using a detection system that provides time resolution, such as a photomultiplier and an oscilloscope. Usually we make such measurements at a chosen wavelength, and the technique is called kinetic spectrophotometry. The time resolution is limited by the falltime of the trailing edge of the pump pulse. Only events with relaxation times comparable to or longer than this time are amenable to measurement

Now let us examine the situation when a picosecond excitation pulse is used. Picosecond pulses are so limited in spatial extent that new monitoring techniques become possible. A 5-psec pulse is a little bullet of light less than 2 mm long. Thus we have the interesting situation that we can quite conveniently make the sample longer than the pumping pulse. As it passes through the sample medium, the pump pulse leaves behind a progressively decaying trail of excited molecules—an optical wake. (The situation is analogous to that present behind a shock wave in a shock tube experiment, but here the time scale is much faster because the perturbation is optic rather than acoustic.) The picosecond light pulse and its optical wake are shown in Fig. 5.10*b*. All we have to do is stand off to one side of the beam path and take a snapshot that freezes the pump pulse and

its attendant trail of excited molecules. For this to work the probe pulse must be as short as or shorter than the pump pulse, weak enough that it does not itself perturb the excited-state population and spatially homogeneous in intensity over the length of sample being monitored. We also need a detector. Several ingenious experimental arrangements based on the above principles have been developed.

In the earliest experiments by Rentzepis and co-workers [50], a 530-nm picosecond pulse was used to excite azulene in solution to an upper vibronic level of its first excited singlet state, S_1. The optical wake of excited S_1 molecules was then made visible by sending an interrogating 1060-nm picosecond pulse through the sample in the opposite direction. The energy of this pulse (9434 cm^{-1}) was sufficient to raise the S_1 excited molecules still higher, to S_2. Since azulene fluoresces from S_2 to S_0, the decaying population of S_1 molecules could be monitored by photographing the fluorescence so produced. The spatial decay of the fluorescence along the wake gave a time of about 7.5 psec for the vibrational relaxation of azulene in the third or fourth vibrational level of S_1 [50].

The above experimental technique is not readily extended to other molecules because it depends on a fortuitous matching between energy gaps in the azulene molecule and the laser frequencies and also upon the unusual circumstance that azulene fluoresces from its S_2 level. Another cause for concern is that the interrogating pulse itself must lose intensity as it proceeds down the wake, and allowance should somehow be made for this factor in extracting the relaxation time from the trace that records the decay of fluorescence intensity from S_2. This factor was not considered in these early experiments. Azulene is discussed further in the section on electronic relaxation.

A more versatile variation of the above technique, using a crossed-beam geometry, was described by Malley and Rentzepis [51]. The principle is shown in Fig. 5.11. A picosecond laser pulse is divided by a beam splitter. The stronger pulse (90%) traverses a rectangular (2 mm × 10 mm) sample cell. To eliminate inhomogeneity throughout the cross section of the weaker interrogating pulse, it is first spatially broadened by passage through a coarse (500 lines/in.) diffraction grating, called a Ronchi ruling, and is then caused to pass through the sample cell at right angles to the bleaching pulse. If the timing is right, the interrogating pulse catches the bleaching pulse within the cell and takes a snapshot, in the manner previously described, that includes a region of unexcited sample ahead of the bleaching pulse, the excited region occupied by the pulse, and the optical wake behind the pulse. The detector can be either a camera or a diode array (Vidicon or Reticon) coupled to a data storage device such as an OMA, minicomputer, or storage scope. In the reference cited, 1060-nm

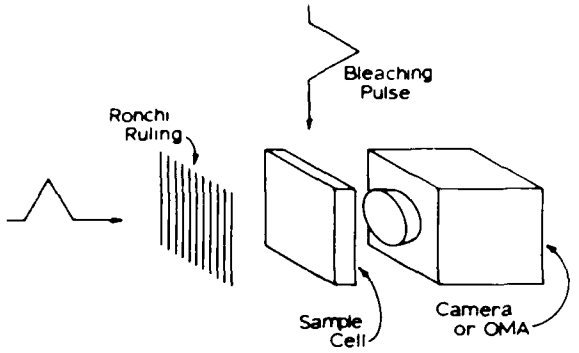

Fig. 5.11. Malley–Rentzepis crossed-beam technique [51]. The interrogating pulse is passed through a Ronchi ruling, about 1 m from the ruling, to smooth its cross-sectional intensity profile. In this way homogeneous illumination of the sample cell is accomplished. This assures reasonably accurate determination of decay kinetics from optical wake profiles.

pulses were used and a camera with Polaroid Type 413 film was the detector. The sample studied was the Kodak Q-switch/modelocking dye 9860. A value of 9 psec was found for the ground-state recovery time, in good agreement with earlier measurements. The result obtained on the photographic film is actually the convolution of the bleaching pulse, the monitoring pulse, and the recovery time of the dye; but, provided that the laser pulses are well characterized, the dye recovery time can be deduced. Time resolution is limited not only by the pulse durations but also by the thickness of the sample cell, since the bleaching pulse moves slightly during the time it takes for the interrogating pulse to pass through the cell. Thinner cells can be used, but then the sample concentration must be increased to ensure enough optical density to provide a detectable contrast ratio.

In the so-called echelon technique, if an interrogating laser pulse is passed through a stepped stack of glass plates, or *echelon*, as shown in Figs. 5.12 and 5.22 the pulse is dissected into a series of pulses equally spaced in time and distance by an interval determined by the delay, relative to air, introduced by the plate thickness. For a 1-mm-thick glass plate this delay is about 1.7 psec. The echelon technique, as originally developed by Topp, Rentzepis, and Jones [52], was first used in conjunction with an optically triggered CS$_2$ Kerr cell, or "light gate," to take time-resolved photographs of the stimulated emission from several laser dyes (see section on fluorescence lifetime measurements). For absorption studies, as illustrated in Fig. 5.12, the bleaching pulse and the series of

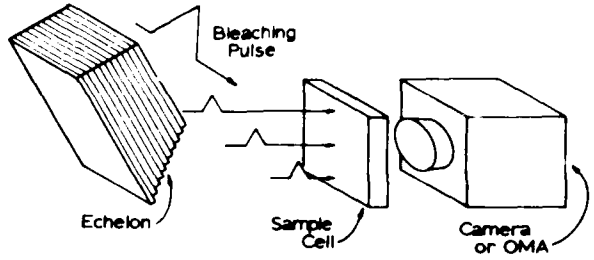

Fig. 5.12. Echelon technique developed by Topp, Rentzepis, and Jones [52]. If the bleaching pulse illuminates the sample uniformly, a microdensitometer trace of the photograph of the interrogating pulse will resemble a histogram of intensity bands reflecting decay of excited-state absorbance or return of ground-state absorbance. If a spectrograph is used, a photographic record will also include spectral information and allow the calculation of rate constants at several wavelengths.

monitoring pulses travel almost colinearly through the cell. After passing through the cell, the latter pulses are detected either on film or with the aid of a Vidicon/OMA combination as before. Because of the colinear relation of the excitation and measuring beams, the cell thickness limitation of the crossed beam technique is avoided. However, there is the disadvantage that each interrogating pulse monitors a different spatial region of the sample. Spatial uniformity of the bleaching pulse over the entire sample cross section that is being monitored is therefore required for quantitative work. Group dispersion effects must also be taken into account when several frequencies are used [53]. Such effects can be avoided by using a reflecting echelon, so that the interstep delay is provided simply by the longer optical path *in air* rather than by passage through an extra thickness of dispersive medium such as glass.

The echelon technique has been extensively used, especially by Rentzepis and co-workers. It has several advantages. It provides a kinetic record in a single laser shot; and, if a continuum monitoring pulse is used, a set of time-resolved spectra can be obtained in a single shot. This is very valuable, when we bear in mind the shot-to-shot lack of reproducibility of mode-locked lasers. It is also useful for extracting as much information as possible from a single experiment on a photolabile system, for example, rhodopsin. There is also a price to pay. It is important that both pump and probe pulse be spatially uniform in intensity over the cross section of the beam, since measurements at different time delays do not correspond to the same region of the sample. The jumps in time from segment to segment are discrete and several echelons are needed to cover adequately a time span of say 1 nsec. (However, Topp [54] has recently

described a technique that uses group dispersion in a series of three prisms to give a continuous time scan over about 85 psec.) In practice, echelons are most useful for the shorter end of the time range. For example, a stack of 20 glass plates each 2 mm thick would, if used in transmission, cover from 0 to 60 psec in 3-psec steps. If 3-mm plates were used and the echelon used in reflection, the interstep delay would be a 6-mm path in air, or about 20 psec, and a 20-step echelon would cover about 400 psec.

Picosecond Flash Photolysis

This is a direct extension to the picosecond region of the well-known microsecond technique of flash photolysis using rare-gas-filled flashlamps. A mode-locked laser provides the picosecond excitation pulse. The spectroscopic flash for monitoring purposes is a picosecond continuum pulse and can be obtained by focusing a portion of the laser pulse into a variety of optical media. A variable time delay between the two pulses is obtained by changing the difference in optical path length between the two beams. The apparatus developed by Magde and Windsor [55] is shown in Fig. 5.13. A mode-locked Nd:glass laser, with single pulse selection (SPS) and one stage of amplification, produces a 5- to 8-psec pulse of 15- to 20-mJ energy at 1060 nm. Single pulse selection is accomplished using an optically triggered spark gap and Pockels cell as described in detail in the section on single pulse selection. A pulse early in the pulse train is

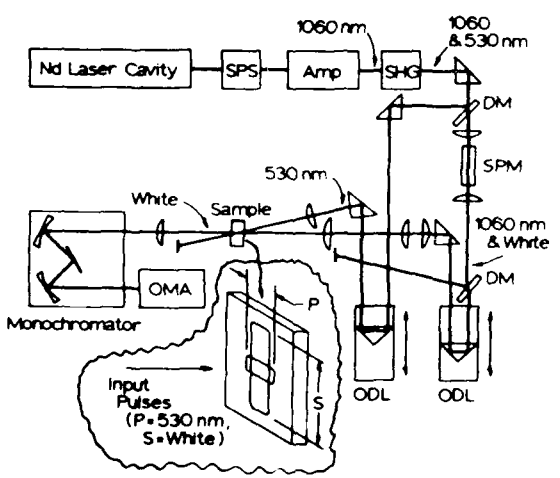

Fig. 5.13. Picosecond flash photolysis apparatus developed by Magde and Windsor (55). See text for detailed description.

selected for amplification because it has been shown that early pulses have a shorter duration than later pulses. Passage of the 1060-nm pulse through a suitably oriented crystal of potassium deuterium phosphate (KD*P, where the asterisk denotes deuteration) gives second harmonic generation (SHG) at 530 nm with a conversion efficiency of about 15%. The 530-nm and 1060-nm pulses are separated by a dichroic mirror that selectively reflects the 530-nm radiation while transmitting the 1060-nm pulse. After passage through an optical delay line (ODL), consisting of a rooftop prism mounted on an optical rail, the 530-nm pulse P (for photolytic) impinges on the sample, usually a 1- or 2-mm-thick cuvette. Any 530-nm light transmitted by the sample is intercepted by an optical stop. As a further precaution against scattered P light entering the spectrograph, it is arranged that the P beam make a slight angle (10°) with the monitoring beam S (for spectroscopic), as shown in Fig. 5.13.

The key to the technique of picosecond flash photolysis is the picosecond continuum pulse. In our experiments this is obtained by focusing the residual 1060-nm radiation into a 10-cm-long cell containing carbon tetrachloride (CCl_4). Self-focusing and filamentation occur, and a small fraction (~0.1%) of the incident beam is converted into a broad continuum. The generation of this continuum may involve several nonlinear effects, but for brevity we shall term the process SPM, for self-phase modulation. The continuum retains both the short pulse duration and much of the spatial collimation of the pumping pulse. Thus, to all intents and purposes, we have a white light laser. (Later in this section we provide a more detailed discussion of old and new work on continuum generation, specifically the SPM continuum.) Another dichroic beam splitter separates the essentially undiminished 1060-nm pulse from the continuum. The 1060-nm pulse can be used for sample excitation or can be blocked, as in Fig. 5.13. The continuum S passes through a variable optical delay line and arrives at the sample at a predetermined time relative to the P pulse. By adjusting the two ODLs we can vary the time interval between S and P between zero and about 4 nsec. Kinks in the optical rails make registration of the two beams at the sample plane unreliable for delays in excess of 4 nsec, though with better rails there is no reason why longer delays should not be used. Probably about 10 nsec is a practical limit. Negative delays (i.e., S arrives before P) are also readily obtainable. These are useful in providing a record of the sample prior to excitation for control purposes and correspond to "infinite delay" shots in conventional flash photolysis.

Let us now discuss the manner in which optical density changes induced in the sample by the P pulse are measured. The inset at bottom center of Fig. 5.13 shows the cross-section geometry of the two beams at

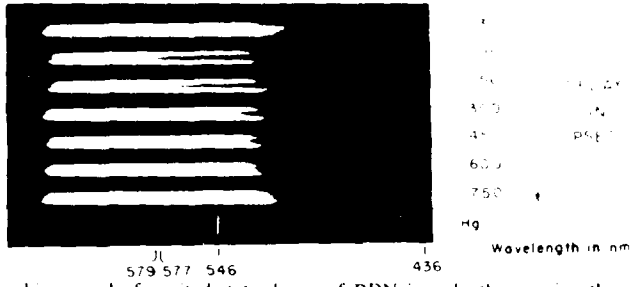

Fig. 5.14. Photographic record of excited-state decay of BDN in iodoethane using the Magde–Windsor technique [56]. The film plate is moved and the delay time between excitation pulse and monitoring pulse is changed between exposures. The dark central portion of each image is due to absorbance of the continuum by the excited state.

the sample. The detail of the geometry in this region is very important. The key point is that the probe beam is elongated along its vertical axis by means of a cylindrical lens so that it samples simultaneously the excited volume in the center and unexcited *reference* volumes both above and below the excited region. The cross section of the excited volume can be adjusted in the range 1 mm to about 5 mm by means of a lens. The entire area is then imaged at about 1:3 demagnification onto the slit of a spectrograph and, ultimately, onto either photographic film or a vidicon detector. By having a reference spectrum both above and below a purported transient spectrum, we greatly reduce the risk of misinterpreting random fluctuations in the intensity of the continuum as genuine transient effects.

The photographic method is all but essential for exploratory survey work on a previously uncharacterized system. It provides wide spectral coverage in a single shot and the time history of whatever transient changes are present can be seen at a glance on a single film or plate by taking a short sequence of shots at different time delays. This is demonstrated in Fig. 5.14 through 5.16. Figure 5.14 shows the decay of transient excited-state absorption (ESA) in the region 430-600 nm for the laser modelocking dye bis(4-dimethylaminodithiobenzyl)nickel(II) (BDN) over the time range of 0 to 750 psec [56]. Figure 5.15 shows similar picosecond flash-photolysis results for octaethylporphinatotin(IV) dichloride [(OEP) $SnCl_2$] [57]. The value of the wide spectral coverage provided by the photographic record is particularly evident here. The photograph clearly shows two regions of ESA: a short-lived transient with a main absorption peak at ~450 nm and absorption extensity to longer wavelengths, and a much longer-lived absorption in the blue with a peak at about 430 nm. Additional studies using the Vidicon enable these two transient absorptions to be spectrally characterized and attributed, respectively, to the

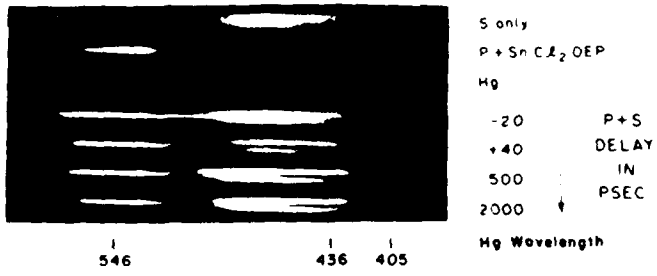

Fig. 5.15. Photographic record of excited state decay of [(OEP) $SnCl_2$] in 1,2-dichloroethane showing both S_1 and T_1 absorption as studied by Magde et al. [57]. The persistent excited-state absorbance due to the T_1 state is particularly evident in the 500- and 2000-psec exposures.

excited singlet S_1 state and the triplet T_1 state of the porphyrin. The photograph is very helpful in choosing suitable wavelengths for subsequent quantitative kinetic measurements.

Figure 5.16 shows a much more complicated photographic record for the molecule 3,3′-diethyloxadicarbocyanine iodide (DODCI) [55]. In the region from about 440 to 510 nm, excited-state absorption (ESA) with a lifetime of about 1 nsec can be seen. In this experiment the 530-nm excitation beam was focused to a cross section of about 1 mm, so the ESA appears as a narrow, dark band. Bleaching of the ground-state absorption in the 560- to 590-nm region is also readily seen and is especially apparent on the 20-psec exposure as a narrow, white central band that corresponds to enhanced transmission of the probe beam caused by the laser excitation

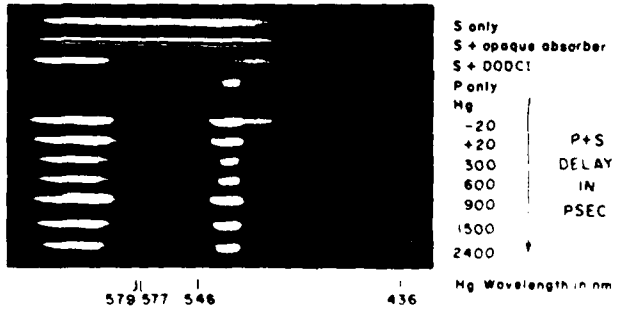

Fig. 5.16. Photographic record of excited state decay of DODCI in ethanol as studied by Magde and Windsor [55]. Bleaching of ground state absorbance can be seen between 560 and 590 nm as a light central band in the shorter time exposures.

pulse. By suitable selection of wavelength, kinetic studies may be made of either ESA or ground-state repopulation (GSR). When interpreting picosecond photographic spectra, allowance must be made for "chirping" of the probe pulse—a slight dispersion in the arrival time of the various colors at the sample due to the relatively long path through dispersive media. This amounts to 16 psec between 430 and 650 nm, the blue end of the spectrum being delayed with respect to the red, and is easily accounted for in interpreting results. Of course, when kinetic measurements are subsequently made using the Vidicon OMA, only a narrow band of wavelengths is monitored, and chirping is negligible.

It will be clear from the above discussion that, although the photographic method is of great value for survey work, it is not the most convenient method for determining precise kinetic data. Therefore once the photographic spectra reveal the best wavelengths to monitor, we replace the camera with a slit and use photoelectric detection—normally a Princeton Applied Research (PAR) 1205B Vidicon tube coupled to a 500-channel optical multichannel analyzer (OMA). We then monitor only a single narrow band of wavelengths, using the OMA to obtain an intensity profile along the length of the slit as shown in Fig. 5.13. This is exactly equivalent to a densitometer trace taken vertically across the photographic spectrogram. The natural logarithm of the ratio of the measured intensity in the reference regions (averaged over the above and below portions) to that in the central excited region gives the optical density change (ΔOD) due to the transient absorption (or bleaching). Usually four or five shots are taken at a given wavelength and time delay, in order to obtain an average value plus the standard deviation. Repeated measurements at the same wavelength and different time delays provide a plot such as that shown in Fig. 5.17, from which the decay kinetics can be determined. By keeping the time delay constant and changing the wavelength, we can obtain the difference spectrum at a given time delay. In most cases, because of spectral overlap of the ground-state and excited-state absorption regions and because, at the laser powers used, significant depletion of the ground state is common, the spectrum obtained must be considered a "difference spectrum" that represents the sum of the changes caused by ground-state depletion and production of the excited state. A typical difference spectrum for a photosynthetic system is shown in Fig. 5.18. By detailed studies it is usually possible to find wavelengths at which kinetic studies of one species can be made without interference by optical changes due to another species [58].

The advantages of picosecond flash photolysis over the echelon technique are (1) less severe constraints on the spatial uniformity of the continuum and (2) the provision of continuously variable delay times over

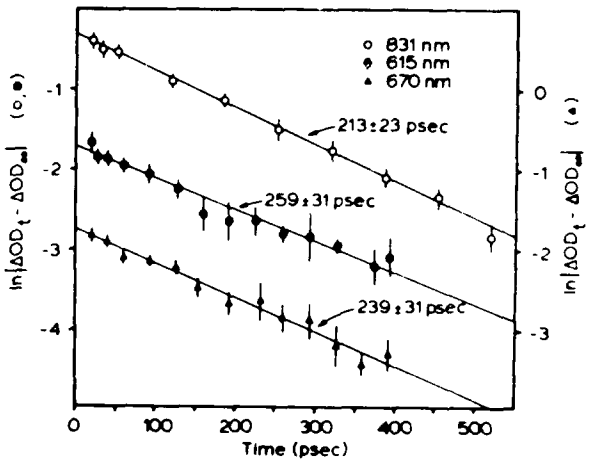

Fig. 5.17. Kinetics of one of the electron transfer steps in bacterial photosynthesis measured at three different wavelengths in reaction centers isolated from the photosynthetic bacterium *viridis*. Figure 5.18 shows the spectra of the states before and after this step. From Holten et al. [196].

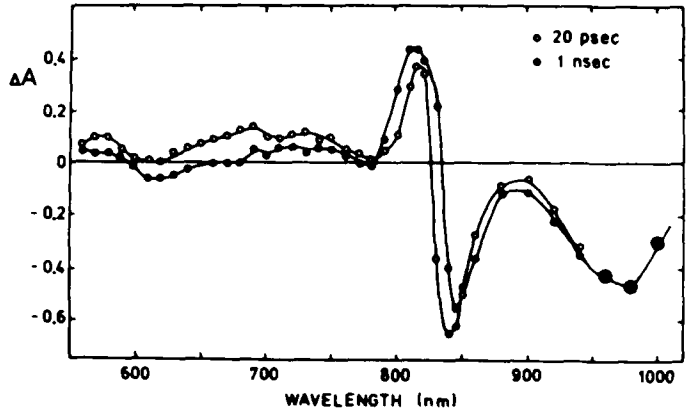

Fig. 5.18. Absorbance changes at room temperature for reaction centers of *Rhodopseudomonas viridis*, measured after time delays of 20 psec (open circles) and 1 nsec (closed circles). The change in the difference spectrum between the two time delays reflects the transfer of an electron from a molecule of bacteriopheophytin to ubiquinone. The kinetics of this process are shown in Fig. 5.17. From Holten et al. [196].

the range 3 psec to 4 nsec instead of the discontinuous jumps in time delay over a limited temporal range given by the echelon. The main disadvantage of picosecond flash photolysis is that each shot gives a measurement at only one wavelength and one time delay, necessitating a laborious series of shots to obtain either a complete spectral or complete kinetic record. This deficiency could be removed by the use of a minicomputer to retrieve data in two-dimensional fashion (optical density versus wavelength) from the vidicon surface in a single shot, an objective that we are actively pursuing at the present time.

Picosecond continua can be generated by focusing high-power picosecond laser pulses into a variety of optical media. Alfano and Shapiro [59] first described the use of picosecond continua for spectroscopic studies, although earlier papers from several groups had discussed the mechanisms by which the continuum is generated. The details of the mechanism are beyond the scope of this review and, in any case, are still not thoroughly understood. Some groups have called the process *self-phase modulation* (SPM), and we have used this as a convenient label in our own work. Others have described the mechanism as a four-photon parametric process. It seems likely that several coherent nonlinear effects combine to produce the continuum. We are concerned here with its use as a spectroscopic tool, so we provide some practical information on the generation and use of the SPM continuum without delving deeply into the mechanisms by which it is formed.

In their early work, Alfano and Shapiro [60] used samples of quartz and BK-7 glass up to 20 cm long and samples of NaCl and calcite. Using 530-nm excitation they produced continua that stretched to 300 nm in some cases. More recently Yu et al. [61] have described spectral broadening due to SPM of a 1060-nm pulse in KBr; and Ippen, Shank, and Gustafson [62] have observed SPM in CS_2-filled optical fibers 1 and 2 m long. To generate the continuum the laser pulse is focused with a short focal-length lens (5 to 10 cm) into the front portion of the sample. Self-focusing occurs and optical filaments are formed. The continuum is generated within these filaments, which remain tightly focused throughout the length of the rod and produce well-defined bright spots at the exit end. Because of this filamentation, it is wise to use a diffusing element, such as a piece of ground glass, between the SPM cell and the sample cell in order to average the beam spatially. The energy threshold for the SPM continuum is quite sharp. If a particular laser shot is a little below par, then no continuum will be observed. Also the efficiency depends on the interaction length in the generating medium. Although continua can be produced in 1- or 2-cm path lengths, it is much better to use longer optical paths up

to about 10 cm. In our own experiments we were able to generate useful SPM continua in many liquids (e.g., water, ethanol, hexane, benzene) using either 530-nm or 1060-nm excitation. We found empirically that carbon tetrachloride (CCl_4), gave especially good results. For CCl_4 in a 10-cm cell, 1060-nm-generated continua stretched all the way down to about 430 nm in the visible. Using 530-nm pumping allows the continuum to be extended to about 300 nm. The big advantage of using liquids as the generating medium is that optical damage, if it occurs, is self-healing. With quartz and glass rods, on the other hand, it is not uncommon to find optical damage, in the form of small fractures a few millimeters inside the front surface, after a few laser shots. Quite recently Mataga and Nakashima [63] have found that polyphosphoric acid is a particularly favorable medium for generating picosecond continua.

Transient Grating Method

Recently Phillon, Kuizenga, and Siegman [64] presented an alternative to the basic pump and probe method discussed above. The basic principles that underlie their technique are not new, and the reader is referred to Ref. 64 for a list of previous work. The fundamentals were developed along with the development of holography and have been applied by Phillon et al. to measure transient absorbance and bleaching in the picosecond time domain. Simply stated, two pulses of the same frequency are crossed in an absorbing medium. The interference pattern at the intersection of the two beams produces a spatial modulation of intensity within the sample. This fringe pattern resembles the rulings on a plane grating, because of the coherence of the two pulses, and it produces an image (spatial modulation of the excited-state population) which persists with a lifetime equal to that of the ESA or GSB. Figure 5.19 illustrates their experimental arrangement. A probe pulse is passed through the transient grating, and its intensity is detected at the diffraction angle θ determined by the relation

$$\lambda = D \sin \theta$$

where λ is both the pump and probe wavelength and D is the fringe spacing of the interference pattern. As time progresses, the grating will relax by decay of the excited-state population or the orientational anisotropy produced in the solution. Thus the kinetics of the underlying process can be followed by delaying the probe pulse with respect to the pump pulse. The principal advantage of this technique over the normal pump and probe techniques is in measuring small absorbance values. In the normal methods, for small absorbance changes, the difference between

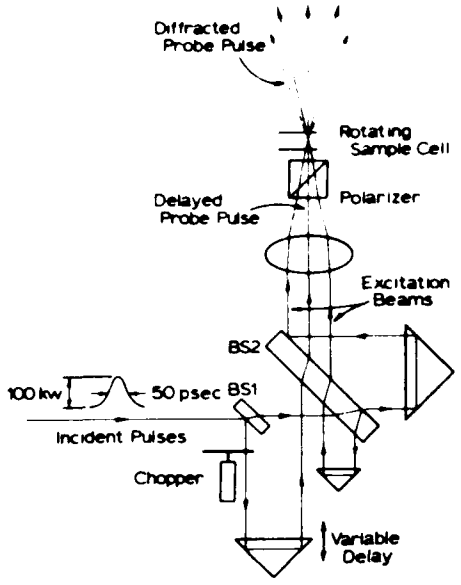

Fig. 5.19. Schematic of the method used to measure transient kinetics by the decay of a grating (interference pattern) produced when two coherent pulses cross in a sample cell. The interference pattern is a spatial modulation in the ratio of ground state to excited state and persists with a lifetime dependent on excited-state relaxation or decay of induced orientational anisotropy. Phillon et al. [64].

two nearly equal probe signals must be determined, whereas in the grating method a small signal is detected against a zero background. The uncertainty in absorbance values is therefore greatly reduced. In addition, the use of a Nd:YAG laser or mode-locked CW dye laser to generate a continuous train of picosecond pulses permits the use of signal-averaging techniques. In a subsequent report, Siegman [65] has proposed the use of a moving grating produced by two CW beams while one of the beams is tuned smoothly through a frequency range close to the other beam. A sample calculation showed that lifetimes of ~100 psec could be measured with input powers of ~1 W. He further suggested that a pair of mode-locked CW dye lasers with peak pulse powers of ~10^3 W could provide a means of resolving subpicosecond lifetimes. The double-mode-locked dye laser systems described in a subsequent section are excellent candidates for an experimental test of this method.

Fluorescence Lifetime Measurements

Ultrafast Optical Shutters

Fluorescence lifetime measurements on the picosecond time scale were made possible by the suggestion, in 1956 [66], and the observation, in 1964 [67, 68], that a birefringence could be induced in liquids by the intense electric fields associated with high-power laser pulses. Duguay and coworkers were the first to incorporate an optical Kerr cell in the measurement of picosecond fluorescence lifetimes [69, 70]. Typically a 1060-nm pulse is used to "gate" the Kerr cell, which contains carbon disulfide (CS_2) or some other appropriate liquid placed between crossed polarizers. Figure 5.20 illustrates the use of their design in picosecond fluorescence lifetime measurements. The high electric field of the gating pulse induces a birefringence in the liquid, which can be expressed as a convolution of the intensity profile of the gating pulse and the exponential decay of the induced orientational anisotropy of the solvent. Thus birefringence is proportional to $\Delta n(t)$, the difference in the refractive index of the solvent molecules in directions parallel and perpendicular to the electric field polarization of the gating pulse. If the lifetime for rotational relaxation is much shorter than the gating pulsewidth, the following expression for $\Delta n(t)$ results:

$$\Delta n(t) = \frac{1}{2} n_{2B} E^2(t)$$

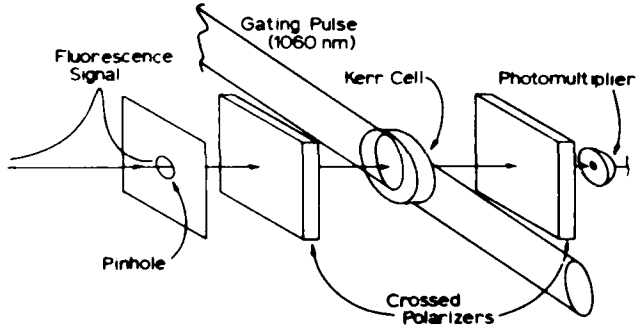

Fig. 5.20. Kerr shutter used in measuring fluorescence lifetimes. The photomultiplier detects the signal that passes through the Kerr cell coincident with the gating pulse. Delaying the arrival of the gating pulse allows the intensity of the fluorescence signal to be measured and plotted vs. the delay time. The resolution of the Kerr shutter is a function of the width of the gating pulse (~5 psec). Consequently this method works best when lifetimes are ≥ 50 psec. From Duguay et al. [69, 70].

where n_{2R} is defined as the optical Kerr constant and $E^2(t)$ is the square of the optical electric field amplitude associated with the gating pulse. Consequently the optical Kerr cell, when placed between crossed polarizers, acts as a shutter similar to the Pockels cell, rotating the polarization of the fluorescence pulse only while the medium is influenced by the optical electric field of the gating pulse. Using the formalism attributed to Fresnel, linearly polarized light can be considered as composed of two phase-matched, right- and left-hand circularly polarized beams. The activated optical Kerr cell will affect the speed of the two circularly polarized components differently and cause a differential phase lag

$$\Delta\phi(t) = \frac{\pi L n_{2R} E^2(t)}{\lambda}$$

where L is the path length of the cell and λ is the wavelength of the transmitted light. The differential phase lag determines the degree of rotation of the linearly polarized composite and the transmission of the Kerr shutter according to the expression

$$T(t) \propto \sin \frac{\Delta\phi(t)}{2}$$

Transmission is clearly a maximum when $\Delta\phi(t) = \pi$.

In principle, the aperture time of the Kerr cell can be shorter than the pump pulsewidth, since the optical Kerr effect is a nonlinear process that discriminates against the lower power in the wings of the pulse. Carbon disulfide is the preferred medium for Kerr cells because of its large optical Kerr coefficient n_{2R} and short orientational relaxation time, $\tau \sim 2$ psec [71]. The ratio of gated to ungated transmission, which is a measure of efficiency, is typically $\sim 10^3$. If the Kerr cell is gated at different times during the decay of fluorescence, only a small increment (~ 10 psec) of the emission intensity is imaged onto a photodiode or photomultiplier. The response of a photodiode is generally much slower than the speed of the shutter, but the peak in the output is directly proportional to the intensity of the incident signal. By plotting the peak voltage V_p versus the delay between the gating and fluorescence pulses, we can determine the fluorescence decay lifetime easily. Later designs permitted kinetic and spectral information to be recorded in one laser shot. Malley and Rentzepis have used a cross-beam geometry to make time-resolved measurements of stimulated emission and stimulated Raman scattering [72]. The 1060-nm gating pulse travels across a 1-mm-thick cell, and the intensity profile transmitted through the cell is recorded photographically. The intensity profile is related to the time dependence of the signal and the speed of the gating pulse as it travels across the optical Kerr cell. If a spectrometer is

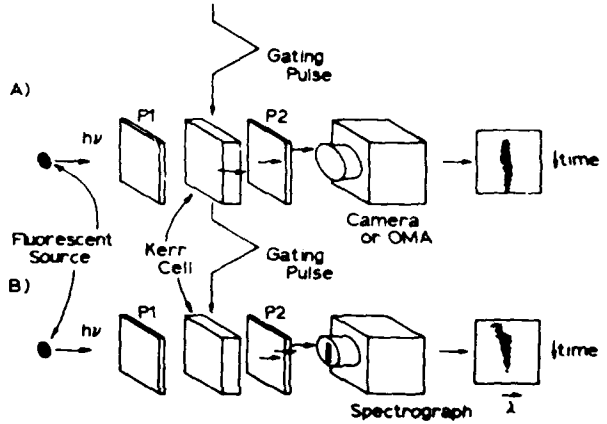

Fig. 5.21. Kerr shutter used to measure short fluorescence lifetimes (≤ 50 psec) in a single pulse: (*A*) kinetic data are obtained from OMA output from a microdensitometer trace of the photographic image; (*B*) kinetic and spectral data are both available in this design; P_1 and P_2 are crossed polarizers. From Malley and Rentzepis [72].

placed in front of the photographic film, a time-resolved emission spectrum is easily recorded (see Fig. 5.21). Topp et al. [52] used a colinear gating pulse in combination with an echelon to increase the transmission of the Kerr cell and the sensitivity of the technique (see Fig. 5.22).

A shutter that uses the high power of a picosecond pulse to saturate the absorbance of a dye was investigated by Mourou et al. [73]. They found that the extinction ratio and aperture time of this type of shutter were comparable to those of the Kerr shutter. The primary difference between the two systems was the wavelength discrimination. The Kerr shutter works at all wavelengths where the medium does not absorb light (CS_2 transmits all visible wavelengths), while the saturable absorber has a narrow bandpass (typically 20 nm or the width of the bleached absorption band). Filters must be used to prevent light from being transmitted where the dye absorbance is low.

Busch et al. [74] developed a shutter that provided an aperture time comparable to that of the Kerr shutter and the shutter that uses saturable absorbance. They called this shutter a picosecond-gated optical amplifier (PGOA). They were able to amplify the image intensity as well as gate the transmission by using the saturable absorber 3,3′-diethyloxadicarbocyanine iodide (DODCI). The amplification was a result of superradiance at the emission wavelength of DODCI caused by the light scattered from a dilute milk solution in a sample cell. The ungated transmission

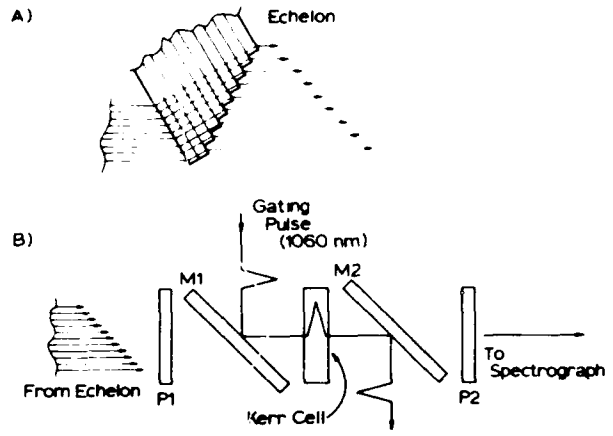

Fig. 5.22. (*A*) Detail of transmitting echelon. (*B*) Kerr shutter incorporating a colinear gating pulse and fluorescence signal. From Magde and Windsor [55].

was only $\sim 10^{-2}$, but the gated transmission was $\sim 10^{2}$, giving an overall efficiency tenfold better than either the Kerr shutter or the saturable absorber system proposed by Mourou. The limitation is that the bandpass is narrow, in this case being limited by the emission profile of the dye. Filters are again required to eliminate transmission where the dye does not absorb.

The Kerr shutter is useful in studies of emission lifetime and linear dispersion of the refractive index (chirp), as well as in studies of nonlinear optical properties such as continuum formation described in the section on picosecond flash photolysis. The Kerr shutter is also useful at the high repetition rates characteristic of picosecond pulses from mode-locked CW dye lasers (71).

Streak Cameras

The direct measurement of fast fluorescence lifetimes followed the development of streak cameras with picosecond resolution and obviated the use of fast shutters for this purpose. Gating is not necessary, resolution is improved, and the data for one lifetime can be obtained in a single pulse. A typical instrumental setup for picosecond emission studies using a streak camera is shown schematically in Fig. 5.23. A 530-nm pulse is split by BS1 into a reference beam and a sample beam. The sample beam is optically delayed using a rooftop prism arrangement and subsequently excites the sample. The sample fluorescence is collected and detected by a streak camera. The reference pulse also goes to the streak camera but,

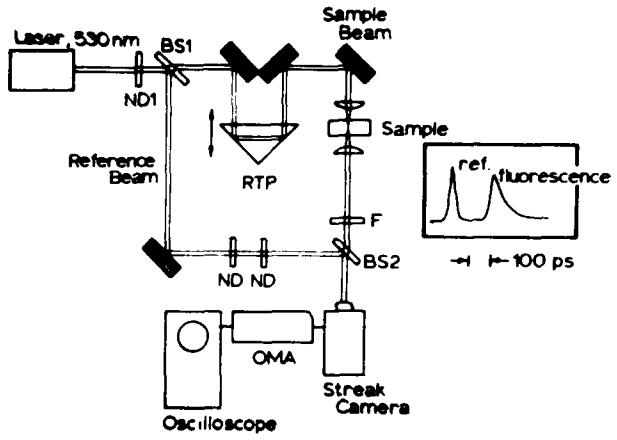

Fig. 5.23. Streak camera technique for measurement of fluorescence lifetimes. BS refers to beam splitters while ND refers to neutral density filters.

because of the shorter path traversed, arrives before the fluorescence. Thus the OMA output is displayed on a storage-type oscilloscope, as shown in Fig. 5.23. First there is a reference pulse that monitors the shape and duration of the laser excitation pulse, and then there is a pulse that shows the decay of fluorescence of the sample. Excitation intensity can be varied by changing ND1. Relative quantum yields can be obtained by integrating the fluorescence decay using the OMA and measuring the energy of the excitation pulse.

Production of Tunable Picosecond and Subpicosecond Pulses Using Dye Lasers

The development of mode-locked dye lasers has occurred along two separate and distinct paths. One approach uses pulsed excitation in which flashlamps or mode-locked pulse trains from neodymium and ruby lasers are used as the pumping source. The other involves the use of a CW ion laser as the pump and has two major advantages. First, a continuous train of pulses with a repetition rate of $\leq 10^{8}$ allows the use of signal averaging detection systems; and second, the lower peak pulse power ($\leq 10^{3}$ W) avoids the nonlinear effects described in the section on single pulse selection.

Flashlamp-pumped dye lasers have been used to produce high-power picosecond pulses in pulse trains lasting only as long as the flashlamp provides gain, which is typically only a few microseconds. The passive

modelocking of flashlamp-pumped dye lasers mimics that of the solid-state lasers, with the exception that the pulsewidths are close to the transform limit and pulsewidths decrease toward the end of the train [17]. This is primarily due to gain saturation mentioned in the section on pulsewidth limitations and illustrated in Figure 5.4. The possibility of tunable subpicosecond pulses from mode-locked dye lasers has been the driving force behind their recent and rapid development. However the development of mode-locked, flashlamp-pumped dye lasers has been reviewed [75] and is not described further in this review.

Pulse trains from mode-locked ruby and neodymium laser systems also have produced picosecond pulses from dye lasers. Superradiant picosecond pulses from dye solutions excited by mode-locked pulse trains from both ruby and neodymium laser systems have been reported [72, 76, 77]. When the cavity length of the dye laser is made equal to the cavity length of the mode-locked pump laser, the dye laser is mode locked by periodic gain modulation. This has been described as synchronous pumping and has been reported for dyes pumped by the output of a mode-locked Nd:glass laser [78] and argon ion laser [79*a*, *b*].

Perhaps the most exciting recent development in the production of mode-locked pulse trains from dye lasers has been the successful production of subpicosecond pulses from CW dye lasers. Dienes et al. [80] reported the first example of a CW dye laser mode locked by an acousto-optic modulator and a 55-psec pulsewidth. Kuizenga [81] subsequently modelocked a CW dye laser using a phase modula' scheme and was able to generate 200-psec pulses. Passive modelo king of a CW dye laser and a 1.5-psec pulsewidth was first reported by Shank et al. [82]. O'Neill [83*a*] was later able to reproduce these results using a contacted dye cell for the modelocking dye DODCI. In addition, Letouzey and Sari [83*b*] reported a passively mode-locked R-6G laser.

Typically 2 W from one or several lines of the CW argon ion laser was used to produce mode-locked pulse trains at repetition rates of 10^5 to 10^8 Hz with peak powers from 10^2 to 10^3 W. Figure 5.24 describes a multiple-mirror, folded dye laser cavity where the gain medium (R-6G) and saturable absorber (DODCI) are exposed to the pump beam in two free jet streams. The use of free jets avoids possible damage to the windows of optical cuvettes in the focal region and removes several optical interfaces from the laser cavity. Figure 5.3 shows a similar CW system, except that a dye cell is used for the modelocking dye. In both, flow configuration is required since the high average power of the CW laser compared with most pulsed systems can decompose both dyes. The pulsewidths were measured by second harmonic generation, using a modification of the zero-background method described by Weber and

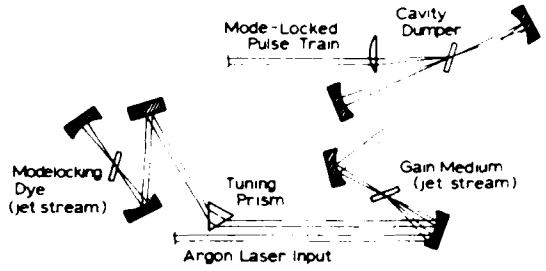

Fig. 5.24. Folded cavity configuration characteristic of the mode-locked CW dye laser systems developed by Ippen and Shank (*Laser Focus*, July 1977).

shown in Fig. 5.7. The high repetition rate and reproducible peak pulse powers made this method of pulsewidth measurement generally more convenient than when applied in measurements of mode-locked pulsed laser systems with lower repetition rates. The entire measurement takes only a few minutes, using the high repetition rates of mode-locked CW dye lasers. In early measurements the pulsewidths were obtained by fitting the experimental autocorrelation functions to either Gaussian or Lorentzian profiles, but recent theoretical treatments of modelocking under steady-state conditions using saturable absorbers predicted that the intensity profiles should show a sech^2 dependence on mirror displacement or time [11]. Later experimental results did indeed confirm that the main portion of the pulse profiles fit a sech^2 dependence.

Shank and Ippen [84] were also the first to report subpicosecond pulses. Using R-6G and DODCI in the same jet stream and dumping the cavity with an acousto-optic modulator, they were able to produce pulses of 4 kW peak power at a repetition rate of 10^5 Hz. The autocorrelation functions, however, were fit to Gaussian and Lorentzian profiles and yielded 0.7-psec and 0.5-psec pulsewidths, respectively. The pulsewidths would have been slightly smaller if the sech^2 profile were assumed. Using a mixture of two mode-locking dyes, DODCI and malachite green, to modelock R-6G and compressing the pulse using the method described by Treacy [85*a*], Ippen and Shank [85*b*] measured a 0.3-psec pulsewidth. Later, using an optically contacted flow dye cell for DODCI, Ruddock and Bradley [86] were able to produce 300-W transform limit pulses from R-6G (0.3 psec) which followed the sech^2 intensity dependence.

Ippen and Shank [87] were also able to obtain subpicosecond pulses by SHG in $LiIO_3$. The second-order power dependence of SHG discriminated against the lower powers in the wings of the pulses, and UV pulses at 307.5 nm were produced with 15% efficiency.

Synchronous pumping by a mode-locked argon ion laser was first reported by Shank and Ippen [79*a*]. The pulses from the actively mode-locked argon ion laser generated 125-psec pulses. Subsequently several groups have demonstrated 5- to 10-psec pulsewidths from dye lasers synchronously pumped by 100-psec pulses from mode-locked argon ion lasers [79*b*]. Although the pulsewidths are larger than those from a mode-locked CW dye laser, several dye lasers can be pumped simultaneously by the mode-locked output of the argon ion laser giving as many synchronized and independently tunable pulse trains. A sequential arrangement of mode-locked argon ion laser–dye laser–dye laser has been found to produce subpicosecond pulsewidths. Heritage and Jain [88] reported that with a 1.5-W mode-locked argon pump power, an average mode-locked output of about 250 mW at 570 nm was produced from the first dye laser (R-6G). The 55-psec pulses from the first dye laser were then used to synchronously pump a rhodamine B (R-B) dye laser to produce 0.8-psec pulses with average output of 20 mW between 609 and 620 nm. Further reduction of the R-6G pump pulsewidth failed to shorten the R-B pulsewidth any further. Double modelocking, where one laser dye is used to modelock a second, was recently predicted and confirmed experimentally [89]. The pulses exhibited a 3:1 intensity-to-background ratio, and the intensity profile fit the expected sech^2 *time* dependence. For R-6G and a CW argon pump power of 1.8 W, a stable pulsewidth of 0.68 psec was observed at 592 nm [89]. The R-6G output was modelocked by cresyl violet, which also produced mode-locked pulses of 1.1 psec at 635 nm. When the pump power was increased to 2.5 W, the R-6G pulses were shorter (~0.55 psec), and peak power was ~150 W at a repetition rate of $\sim 10^8$ Hz.

The advantages of mode-locked CW dye lasers are (1) the demonstrated long-term stability of the pulse trains and (2) data with good signal-to-noise ratio can be obtained by time averaging the observations over a large number of relatively low power pulses. The low power is especially useful in studies where ground-state populations would otherwise be severely depleted using higher-power pulses. For weakly absorbing systems, the lower-power pulses provide no advantage, and the high-power single pulses from mode-locked Nd:glass or ruby systems are preferred. A further restriction is that the continuum (see section on picosecond flash photolysis) is not produced at these low peak powers. A subpicosecond continuum has recently been generated by pulses from a mode-locked CW dye laser amplified 400 mW peak power [90], but until these amplified systems are put to use, the probe wavelength is constrained to be equal to or a harmonic of the pump wavelength. Synchronous pumping of two or more dye lasers and double modelocking with the attendant low jitter between pulse trains will relax this restriction and will likely approach the reliability and pulsewidths characteristic of the mode-locked CW dye laser systems.

3 APPLICATIONS

The emphasis on applications is secondary to that of the experimental techniques. However a few examples have been chosen to illustrate the diverse problems to which picosecond laser systems have been applied. Examples of the evolution of technique in the study of a single problem are also outlined.

Studies of Rotational Motion in Condensed Phase

Studies of rotational relaxation of small molecules have focused on the optical Kerr effect and have dealt with the relaxation of optically induced birefringence in CS_2, nitrobenzene, diiodomethane, and dichloroethane [69, 91]. Rotational relaxation of large dye molecules [92] has been studied by observing the time evolution of the anisotropic orientational distribution of ground-state molecules, produced by the selective absorption of a linearly polarized picosecond pump pulse by those molecules with transition moments oriented parallel to the polarization of the pump pulse (see Fig. 5.25). The decay of the induced dichroism was characterized by

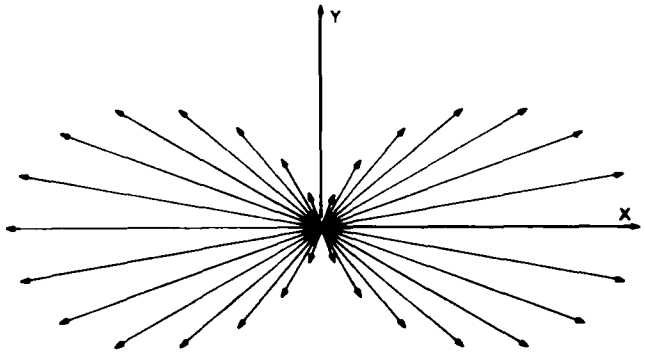

Fig. 5.25. Envelope of vectors reflecting the $\cos^2\theta$ distribution of ground-state moments remaining after absorption of a pulse linearly polarized in the *y*-direction (θ is the angle off the *y*-axis). The excitation pulse is traveling into the page along the *z*-axis. Molecules with transition moments perpendicular to *y* remain unexcited, whereas the ensemble of molecules with moments nearly parallel with *y* is maximally disturbed. The induced anisotropic distribution of moments will influence the relative transmission of the polarized light and will persist with a lifetime characteristic of excited-state decay or orientational redistribution

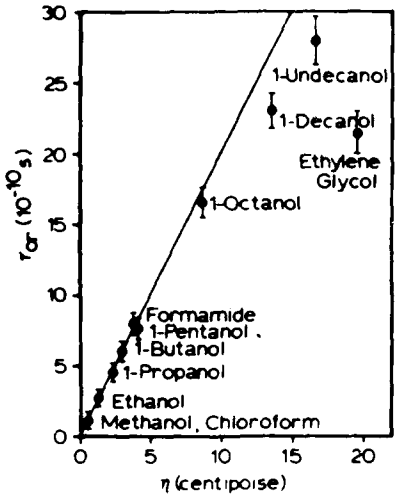

Fig. 5.26. Orientation relaxation times vs. solution viscosity for rhodamine 6G in different solvents. From Chuang and Eisenthal [93].

Eisenthal as the decay of the natural log of the ratio of intensities of transmitted probe beams parallel and perpendicular to the polarization of the pump pulse. The effect of solvent on rotation of rhodamine 6G (R-6G) was systematically studied by Chuang and Eisenthal [93] in an attempt to assess the effect of solute–solvent hydrogen bonding on rotational rates (see Fig. 5.26). They found that for the majority of solvents used, orientational relaxation times were linearly dependent on viscosity η, consistent with the Stokes–Einstein–Debye hydrodynamic model [94], in which the volume of the rotating molecule, V, is constant and the orientational relaxation time is $\tau = \eta V/kT$. This result was unexpected since it was thought that hydrogen bonding and solvent drag, in some solvents, would increase the effective volume of the solute molecule. The linear dependence was explained by assuming that the rupture and reforming of hydrogen bonds were both faster than orientational relaxation, thus reducing the effective drag of solvent hydrogen bonded to R-6G. The deviation from linearity for large alcohols was thought to be due to the breakdown of the solvent continuum approximation, since the solvent molecules are comparable in size to R-6G. The discrepancy in ethylene glycol was thought to exist because self-association is so strong in ethylene glycol that competition of hydrogen bonding to solute is negligible in comparison. By fluorescence depolarization measurements using a streak camera, Fleming et al. [95] were able to measure orientational relaxation times of eosin and rose bengal in methanol, ethanol, isopropanol, and water. They compared the observed orientational relaxation time with values calculated assuming spherical and ellipsoidal geometry. The values derived assuming ellipsoidal geometry were 0.3 to 0.6 times the measured value, whereas the calculated lifetimes based on a spherical geometry were 0.6 to 1.2 times the measured value. Based on the agreement with calculations assuming a spherical model, they concluded that solvent molecules fill out the planar shape of the solute molecule to a sphere (7 Å radius) and that the rotating species consists of both dye and hydrogen-bonded solvent. The apparent differences within the fluorescein group of dyes remain unresolved, but the authors suggest two reasons for the discrepancy between their results on eosin and rose bengal and previous studies on R-6G [93]. First, there is a charge difference between R-6G, a cation, and eosin and rose bengal, which are both dianions. Second, eosin and rose bengal presumably have more rigid structures than R-6G and can presumably sweep out a larger volume in rotation. In addition, Lessing and von Jena [96] reported that fluorescein 27, structurally similar to R-6G, eosin, and rose bengal, exhibits a lifetime for orientational relaxation of 8.5 ± 1 nsec in 1-decanol and 200 ± 50 psec in methanol, but decanol increases the apparent molecular volume $V = \pi kI\ \eta$ twofold over that expected from the molecular structure, again suggesting strong solute–solvent interaction. Finally, using their transient grating technique (see Fig. 5.19), Phillon et al. [64] reproduced some of the relaxation times of R-6G measured by Chuang and Eisenthal in low-viscosity solvents, supporting those authors' earlier contention that there is no rotational hindrance due to solvent hydrogen bonding to R-6G.

Both Fleming et al. [95] and Lessing and von Jena [96] have emphasized the necessity of separating decay kinetics of electronic relaxation from that for rotational relaxation, especially where both processes have comparable lifetimes. For instance, when rotational relaxation is slow compared with electronic relaxation, $\tau_{or} >> \tau_{el}$, the return to ground state will relax the orientational anisotropy. If $\tau_{or} << \tau_{el}$, orientational equilibrium will be established quickly, and decay of emission or transient absorbance will again reflect the electronic process. However, if $\tau_{or} \sim \tau_{el}$, orientational relaxation could be a large contribution to transient decay. In this case an independent experiment must be performed to separate the two processes. A simple way to perform lifetime measurements, independent of orientational effects, is to orient the pump beam polarization at an angle of 54.7° to the polarization of either the probe beam in transient absorbance measurements or emitted light in measurements of fluorescence lifetimes. This and other techniques for separating electronic and orientational contributions in transient decay are described in detail in Refs. 95 and 96.

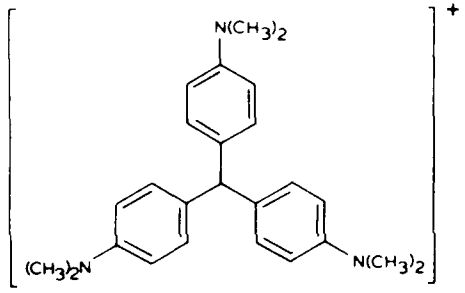

Fig. 5.27. Structure of the triphenylmethane dye crystal violet. Symmetry is D_3, with the phenyl groups at an angle to the molecular plane giving the molecule a propellerlike conformation. The structures of other triphenylmethane dyes are similar.

In addition to rotational motion of the entire molecule, internal motions of a molecule can be studied using picosecond pulses. For example, the triphenylmethane class of dyes in fluid solutions exhibits intense absorption [$\epsilon \sim 10^5$ l./(mole) (cm)] but only a slight degree of luminescence. Radiative emission is effectively quenched by fast nonradiative decay, which occurs in the picosecond regime [97]. However the fluorescence quantum yields of several triphenylmethane dyes have a marked dependence on solvent viscosity. In fluid media the yield is low (10^{-4}), whereas in rigid media it approaches a maximum of 0.35 [98]. This dependence has been interpreted in terms of the freedom of rotation of the phenyl rings about the central carbon–carbon bond axis shown in Fig. 5.27 [97–100]. Ring rotation in the excited molecule leads to a reduction in the energy gap between the ground- and excited-state potential energy surfaces with subsequent enhancement of rates of internal conversion. Increased solvent viscosity hinders ring rotation, allowing fluorescence to compete with the slower rates of internal conversion.

Early kinetic models viewed ring rotation as either a rotational diffusion process [100] or a driven rotation due to interactions between adjacent ring ortho hydrogens [98]. In order for the rotation to be driven, the difference in potential surface minima for the two states must be large as shown in Fig. 5.28*a*. However, molecular orbital calculations have indicated the difference in minima to be only a few degrees [101]. With the picosecond flash photolysis apparatus of Magde and Windsor [55], it has been possible to directly monitor the kinetics of ground- and excited-state populations of the triphenylmethane dye crystal violet shown in Fig. 5.27, which was excited at 530 nm by a 5- to 10-psec pulse. Kinetics of the

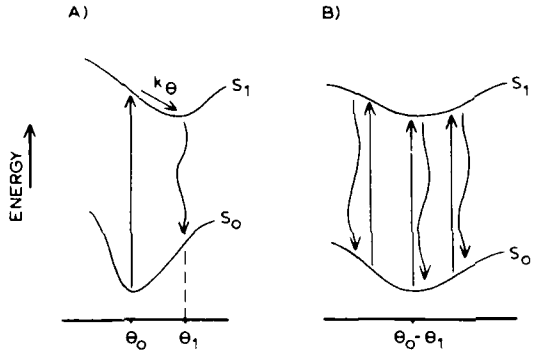

Fig. 5.28. (*A*) Driven rotation kinetic model requires the difference in ground- and excited-state potential energy minima to be large. The viscosity dependence of the ring rotation rate $k\theta$ accounts for the variation of the fluorescence quantum yield with viscosity. (*B*) Results of ground-state repopulation experiments can be explained by considering the potential surfaces to be shallow, with the excited-state surface somewhat shallower than that of the ground state. This results in excited molecules having distinct decay rates over a wide range of values. Observed viscosity dependence of kinetics results from ring rotation in low-viscosity solvents.

ground-state repopulation monitored at several wavelengths revealed nonexponential behavior in solvents having a wide range of viscosities (0.8 to 300 poises). The kinetics of ground-state repopulation also showed some wavelength dependence. As solvent viscosity is decreased, the return of ground-state absorption occurs more rapidly but the nonexponential character is retained. The existence of a purely driven rotation mechanism seems unlikely in view of the shape and temperature dependence of the kinetic curves.

The results of the ground-state repopulation measurements can be explained [102] by postulating that the ground- and excited-state potential surfaces are shallow so that thermal Boltzmann populations exist at angles "significantly different" from the minimum angle of each state. Excitation at 530 nm leads to a replica of the broad ground-state thermal distribution in the excited state. This produces an ensemble of excited molecules, each characterized by a distinct decay rate as shown in Fig. 5.28*b*. Molecules in the wings of the excited thermal population decay faster than those near the equilibrium angle because of the smaller energy gap at the larger angles. In very viscous media, ring rotation can be considered negligible on the time scale of ground-state repopulation. The decay curve then represents the sum of a large number of simple exponential decays, which agrees with our measurements. A decrease in

solvent viscosity allows phenyl ring rotation to angles where internal conversion occurs more quickly than at the excited-state minimum. However, in addition to ring rotation, other conformational changes, such as an increase in the central carbon–carbon bond lengths, may play key roles in describing radiationless transitions in these molecules.

Electron Localization

Ionization, γ-radiolysis and pulse radiolysis of glasses and crystals at low temperature have been used successfully to produce delocalized (quasi-free) electrons. Only with the developments of high-power mode-locked lasers and picosecond-pulse radiolysis techniques has the study of electron localization in polar liquids at room temperature been possible. Electron localization is the process by which an ionized or injected electron reaches equilibrium with the medium. With some nonpolar liquids (e.g., argon, krypton, and xenon), the quasi-free state is stable [103]. However in polar liquids, the quasi-free state is short lived, as evidenced by the rapid two-step evolution of the solvated electron spectrum, with an absorbance peak between 500 and 700 nm, from the initial absorbance spectrum with a peak in the infrared characteristic of the quasi-free electron [104]. The early attempts to measure the solvation rate in polar solvents using picosecond-pulse radiolysis [105] lacked the resolution, but a lower limit was determined, $k_s \geq 10^{11}$ s^{-1}. Somewhat later, Rentzepis et al. [106] photoionized an aqueous solution of $K_4Fe(CN)_6$ using the fourth harmonic (265 nm) of a single picosecond pulse from an Nd:glass laser system. They were able to observe the appearance of absorbance at 1060 nm, and reported a lifetime of 2 psec for the equilibration process. The same authors later used a continuum to probe for electron absorbance and were able to observe the blue shift in the spectrum as the solvent shell relaxed about the electron [107]. They observed a fast initial reaction, $\tau < 2$ psec, and revised their earlier estimate of ~2 psec to ~4 psec for complete electron localization. In this and previous papers they discussed this initial fast reaction in terms of an "intramolecular" nonradiative decay of a delocalized state of the electron, followed by solvent relaxation.

Using a stroboscopic pulse radiolysis system [108], Kenney-Wallace and Jonah [109] were able to observe the electron solvation process in six different linear alcohols and found that the relaxation times correlated well with the dielectric relaxation times of the solvent monomers. They observed an absorbance change, which occurred too quickly to measure, followed by a slower (~10 psec) change and suggested an alternative to the nonradiative process proposed by Rentzepis and co-workers. They argued that the quasi-free electrons became weakly trapped in preexisting

solvent clusters. Then these electrons equilibrated more slowly depending on the orientational relaxation time of solvent monomers. Their conclusions were supported by similar studies reported by Chase and Hunt [110]. Kenney-Wallace and Jonah then extended their studies to dilute alcohol–alkane solvent systems [111]. The relaxation time did not change significantly from 0.1 to 0.6 mole fraction of butanol in hexane, but the ratio of initial to final absorbance was lower than in neat butanol, consistent with the presence of fewer clusters to act as traps. The absorption spectra of solvated electrons were the same as in neat alcohol, which suggested that the electron states are the same in the mixtures and the neat liquid. No general agreement as to the precise nature of the process preceding solvent relaxation has been reached, and the dynamics of e^- localization remain a vibrant area of chemical research.

Solvent orientation certainly contributes to electron localization, but this could be a secondary process. There appears to be some relaxation which occurs much too fast to study with picosecond techniques currently available, with the possible exception of mode-locked CW dye lasers. Further mechanistic insight will require experiments using subpicosecond techniques.

Electronic Relaxation

For many years studies of electronic relaxation were limited to linewidth data and data that could be derived from measurements of emission yields and lifetimes at low temperature. More recently kinetic studies have been possible using nanosecond flash photolysis. However in many molecules, room temperature emission is very weak, implying that nonradiative relaxation occurs very rapidly. Mode-locked lasers and picosecond flash photolysis have played an important role in providing a means of observing nonradiative processes directly and assessing the degree to which they conform with theoretical models. There are many examples of the use of both pulse laser or subpicosecond CW techniques in the study of nonradiative relaxation. A few examples are discussed below in detail in order to illustrate the variety of ways picosecond techniques can be used in the study of electronic relaxation and the depth to which they have been applied in the study of some systems. Many other systems have been studied, and a summary is given in Table 5.2.

Azulene

Azulene was one of the earliest systems studied using mode-locked lasers. Fluorescence occurs from the second excited singlet state $\Phi_f(S_2) \approx 0.2$, with a lifetime $\tau_f(S_2) = 1.4$ nsec [112]. This yields a value of ~7 nsec for the natural radiative lifetime and of ~1.75 nsec for the nonradiative

Table 5.2 Picosecond Studies of Electronic Relaxation

Molecule	*Excitation Source*[a]	*Purpose*	*Ref.*[b]
Fluorescein	Nd:glass (SH)	Vibrational relaxation in S_1, $\tau(S_1)$	1
Eosin	Nd:glass (SH)	Vibrational relaxation in S_1, $\tau(S_1)$	1
Erythrosin	Nd:glass (SH)	Vibrational relaxation in S_1, $\tau(S_1)$	1
Naphthalene	Nd:glass (FH)	Relaxation from S_2 in gas phase	2
Anthracene	Ruby (SH)	S_1 and T_1 absorption spectra	3
Tetracene	Nd:glass (SH)	Energy relaxation in crystals	4
Tetracene	Nd:glass (SH)	Energy relaxation in crystals	5
Tetracene	Nd:YAG (SH)	Energy relaxation in crystals	6, 7
3,4-Benzpyrene	Ruby (SH)	Relaxation from S_2 in gas phase	8
Fluorenone	Ruby (SH)	Solvent dependence of $\tau(S_1)$	9
Anthrone	Ruby (SH)	Solvent dependence of $\tau(S_1)$	9
Xanthone	Nd:glass (TH)	$\tau(S_1)$ in benzene	10
Xanthione	Nd:glass (TH)	$\tau(S_1)$ and S_1 and T_1 absorption spectra	11
Benzophenone	Nd:glass (TH)	Energy transfer	12
Benzophenone	Nd:glass (TH)	Solvent dependence of $\tau(S_1)$	10
4-Phenylbenzophenone	Nd:glass (TH)	Solvent dependence of $\tau(S_1)$	10
Thionine	Nd:glass (SH)	Fluorescence quenching by Fe(II)	13
p-Dimethylaminobenzonitrile	Nd:glass (FH)	Solvent dependence of $\tau(S_1$ and $S_2)$	14
Quinoxaline	Nd:glass (TH)	S_1 and T_1 absorption spectra	10
s-Tetrazine	Nd:glass (SH)	psec photochemistry and $\tau(S_1)$	15

[a]SH = Second harmonic; TH = third harmonic; FH = fourth harmonic.

[b]References:

1. G. Porter, E. S. Reid, and C. J. Tredwell, *Chem. Phys. Lett.*, **29**, 469 (1974).
2. P. Wannier, P. M. Rentzepis, and J. Jortner, *Chem. Phys. Lett.*, **10**, 193 (1971).
3. N. Nakashima and N. Mataga, *Chem. Phys. Lett.*, **35**, 487 (1975).
4. T. L. Netzel and P. M. Rentzepis, *Chem. Phys. Lett.*, **29**, 337 (1974).
5. G. R. Fleming, D. P. Millar, G. C. Morris, J. M. Morris, and G. W. Robinson, *Aust. J. Chem.*, **30**, 2353 (1977).
6. A. J. Campillo, R. C. Hyer, S. L. Shapiro, and C. E. Swenberg, *Chem. Phys. Lett.*, **48**, 495 (1977).
7. F. Heisl, J. A. Miehre, B. Lipp, and M. Schott, *Chem. Phys. Lett.*, **43**, 534 (1976).
8. P. Wannier, P. M. Rentzepis, and J. Jortner, *Chem. Phys. Lett.*, **10**, 102 (1971).
9. T. Kobayashi and S. Nagakura, *Chem. Phys. Lett.*, **43**, 429 (1976).
10. R. H. Hochstrasser and A. C. Nelson, in *Lasers in Physical Chemistry and Biophysics*, J. Joussot-Dubien, Ed., Elsevier, Amsterdam, 1975, p. 305.
11. R. W. Anderson, R. H. Hochstrasser, and H. J. Pownall, *Chem. Phys. Lett.*, **43**, 224 (1976).
12. R. W. Anderson, R. M. Hochstrasser, H. Lutz, and G. W. Scott, *J. Chem. Phys.*, **61**, 2500 (1974).
13. M. D. Archer, M. I. C. Ferreira, G. Porter, and C. J. Tredwell, *Nouv. J. Chim.*, **1**, 9 (1977).
14. W. S. Struve and P. M. Rentzepis, *J. Chem. Phys.*, **60**, 1533 (1974).
15. R. M. Hochstrasser, D. S. King, and A. C. Nelson, *Chem. Phys. Lett.*, **42**, 8 (1976).

lifetime of S_2. The experimental nonradiative lifetime agreed reasonably well with the estimated (based on energy gaps and Franck–Condon factors) lifetime for S_2–S_1 internal conversion of 4 nsec and suggested that the large S_2–S_1 energy gap is responsible for the relatively long nonradiative lifetime and unusually high S_2 fluorescence quantum yield [112]. Of special interest has been the lifetime of S_1 and its unusually short nonradiative lifetime. The upper limit for the fluorescence yield, $\Phi_f(S_1) \sim 10^{-4}$, and the calculated radiative lifetime suggests a lifetime of ~1 psec for nonradiative decay from S_1. But an estimate based on energy gap and Franck–Condon factor leads to the same value for S_1–S_0 and S_2–S_1 nonradiative decay, ~4 nsec. Linewidth measurements by Hochstrasser and Li [113] suggested a lifetime of 2.6 psec. Linewidth narrowing on perdeuteration led the authors to conclude that the predominant relaxation pathway is internal conversion at low temperature.

Attempts to measure directly the lifetimes for relaxation of S_1 began in 1968 with the work of Rentzepis [50], who reported a 7-psec lifetime for the relaxation of vibrationally excited states in the conversion of S_1 to S_0. Subsequently Rentzepis and co-workers have measured relaxation from various excited vibrational levels within S_1 to S_0 [50, 114–117] using a mode-locked Nd:glass laser and obtained several values all of which were greater than 6 psec. Drent et al. [118] reported a value of 4 psec for $\tau(S_1)$ and an appreciable heavy-atom effect that suggested that intersystem crossing was an important decay pathway. Using a flashlamp-pumped dye laser, Wirth et al. [119] could not resolve a decay from S_1 and postulated a lifetime of $\tau < 1$ psec. Heritage and Penzkofer [120] recently measured the decay from vibrational levels 1600 and 3510 cm^{-1} above the S_1–S_0 origin. They found lifetimes of 1 and 2 psec respectively. Finally, using a mode-locked CW dye laser with subpicosecond resolution (see section on production of tunable picosecond and subpicosecond pulses using dye lasers), Ippen, Shank, and Woerner [121] were able to measure a lifetime of 1.9 ± 0.2 psec for the decay of S_1 from about 2000 cm^{-1} above the S_1–S_0 origin. They were unable to detect measurable differences in the S_1 lifetime in cyclohexane, benzene, and chloro- and bromobenzene. This led them to concur with the interpretation that S_1 relaxation occurs predominantly via internal conversion and not by intersystem crossing, as suggested by Drent et al. [118]. Eber et al. [122] reached the same conclusion from steady-state experiments on carbonyl compounds of azulene.

The lifetime of S_1 for azulene is almost certainly very short (~1 to 2 psec) and the reason why, as well as the discrepancy between the measured values, has yet to be resolved. However, where intensities of pump pulses vary from one laser system to another, nonlinear effects may

appear in experiments at high power (e.g., Nd:glass systems) that are absent in low-power systems (e.g., mode-locked CW dye lasers), and lifetimes may therefore be power dependent (see section on harmonics and wavelength tuning in solid-state lasers). For instance, Heritage and Penzkofer [120] were unable to eliminate S_2 fluorescence arising from absorption of two 530-nm photons for peak pulse powers from 2 to 200 mW/cm^2, thus casting doubt on the interpretations of the earlier experiments. A more critical evaluation of the possible influence of nonlinear processes on molecular properties is therefore desirable. In addition, the ability to resolve a 1- to 2-psec decay is clearly less when a 5- to 8-psec pulse from a Nd:glass laser is used than it would be for the 0.3-psec pulse from a mode-locked CW dye laser. This difference may be partially responsible for the variation in the reported S_1 lifetimes.

Acridine and Phenazine

Nitrogen heterocyclic compounds have been the subject of a number of photophysical studies because of their similarity to the analogous carbocyclic aromatic compounds [123, 124]. However, unlike the normal carbocyclic aromatics, the presence of nonbonding electrons in the nitrogen heterocyclic compounds can cause the transition energy and decay of $n\pi^*$ states to be quite solvent sensitive. For instance, while the polycyclic monoazines (quinoline, isoquinoline, and acridine) fluoresce in protic solvents, they are only weakly fluorescent in hydrocarbon solvents [123]. This dependence has been interpreted as a change in the lowest excited singlet state from $\pi\pi^*$ in protic solvents to $n\pi^*$ in hydrocarbons [125, 126]. To determine the nature of the lowest excited singlet and to characterize its relaxation pathways in hydrocarbon solvents, there have been two recent studies of the risetime of triplet–triplet (T–T) absorbance in acridine using picosecond flash photolysis [127, 128]. Hirata and Tanaka [127] used the doubled pulse (347 nm) of a mode-locked ruby laser to excite acridine in isooctane. The residual pulse at 694 nm was used to generate a picosecond continuum in CCl_4, and an echelon reflector was used to probe the growth of T–T absorbance at 430 nm as a function of time. Sundstrom et al. [128] used the third harmonic (353 nm) from a mode-locked Nd:glass laser, a continuum generated by residual 530- and 1060-nm pulses, and an echelon reflector in combination with an optical multichannel analyzer. They observed the growth of T–T absorbance in n-hexane at 430 nm. Hirata and Tanaka found triplet formation with a lifetime $\tau \sim 13$ psec, and Sundstrom et al. found $\tau \sim 17$ psec.

The $n\pi^*$ character of the lowest singlet was strongly suggested by a discrepancy between the experimental radiative lifetime τ_r and the value calculated for the lowest $\pi\pi^*$ based on the oscillator strength of the

observed transition. The calculated value was τ 10 ^{6} sec, but the experimental value ($\tau_f = \tau/\Phi_f$) was much too large, $\tau_f > 10^{-6}$ sec, using as an upper limit $\Phi_f \leq 10^{-3}$. The proposal of level inversion to explain the solvent effect [125, 126] appears justified. There is however disagreement as to the mechanism for relaxation from S_1. Hirata and Tanaka assume the singlet lifetime is limited solely by the rate of intersystem crossing, whereas Sundstrom et al. have presented evidence to suggest that the rate of internal conversion and intersystem crossing may be equally important.

In a subsequent paper Hirata and Tanaka [129] have reported details of the growth of T–T absorbance of 9,10-diazaanthracene (phenazine) in isooctane and methanol. The main difference is that the solvent effect on the S_1 lifetime is not significant. Using the mode-locked ruby laser and the same techniques, they found τ 20 psec in methanol and 14 psec in isooctane. This was explained in terms of the much larger $^1\pi\pi^* - {}^1n\pi^*$ splitting in phenazine than in acridine and consequently no inversion of states. They conclude that intersystem crossing is the predominant relaxation pathway because phenazine and other diazine molecules phosphoresce, and they explain the fast rate, in spite of a large S_1–T_1 energy gap, as due to effective spin-orbit coupling resulting from one-center integrals on nitrogen. The observation of the recovery of ground-state absorbance (GSR) could eliminate conjecture if the extent of GSR is measured during the S_1 lifetime.

Benzophenone and Nitronaphthalenes

Intersystem crossing in benzophenone was first observed by Rentzepis in a study of the growth of triplet–triplet (T–T) absorbance [130]. The purpose was to characterize relaxation in the small molecule limit [131] where intersystem crossing, from S_1, occurs to a relatively sparse density of vibrational levels within the triplet manifold. Nitzan et al. [131] found that intersystem crossing was consistent with the small molecule limit in that T–T growth was faster when excitation occurred near the S_1–S_0 origin, τ 5 psec, than when excited to a level (2000 cm $^{-1}$) higher in energy, τ 25 psec. Hochstrasser et al. [132] found a solvent dependence on the growth of T–T absorbance in benzophenone and concluded that more data were necessary to generate a framework for comparative solvent studies of ultrafast processes in condensed phase, but they interpreted the difference in S_1 lifetime between ethanol and benzene as involving a change in relative spacing of $n\pi^*$ and $\pi\pi^*$ singlet states.

Anderson et al. [133] proposed that intersystem crossing may be competing with vibrational relaxation in the S_1 manifold and that solvents may preferentially assist vibrational relaxation in benzophenone. In addition, solvent effects on T–T growth in 1- and 2-nitronaphthalenes are not easily

Table 5.3 Mean Lifetimes for T–T Growth Following 354-nm Excitation

Compound	*Solvent*	τ (psec)
1-Nitronaphthalene	Ethanol	8 · 2
1-Nitronaphthalene	Benzene	12 · 2
2-Nitronaphthalene	Ethanol	22 · 2
2-Nitronaphthalene	Benzene	10 · 2

accounted for by a simple change in S_1–S_2 energy spacing [133]. For instance, the authors observed a subtle, yet apparently significant, difference in the effect of ethanol and benzene on the rate of T–T growth for the compounds listed in Table 5.3. They suggested various causes for the solvent dependence including changes in the internal conversion and intersystem crossing rate constants as well as solvent-assisted vibrational relaxation.

Inorganic Systems

One of the earliest studies of electronic relaxation in inorganic systems was that of Magde, Bushaw, and Windsor [56] on bis(4-dimethylaminodithiobenzil)nickel(II) (BDN). This compound is useful as a Q-switch and modelocking dye for the Nd:glass laser [12, 134]. Electron-donating and heavy-atom solvents were found to increase both the decay rate of excited-state absorbance (ESA) and the rate of recovery of ground-state absorbance (GSR) by as much as fortyfold relative to benzene. The heavy-atom effect on ESA and GSR lifetimes is summarized in Table 5.4, and the single observed decay is consistent with an intersystem crossing process. However extensive ligand contribution to the nature of the excited states involved made unambiguous interpretation of decay pathways difficult.

Picosecond flash photolysis and spectroscopic techniques have also been applied in our laboratory to the study of a series of metalloporphy-

Table 5.4 Heavy-Atom Effect on ESA and GSR Lifetimes

Solvent	τ (*ESA*) nsec	τ (*GSR*) nsec
Benzene	9.0 · 3.0	9.0 · 1.0
1,2-Dichloroethane	3.6 · 0.6	3.6 · 0.5
1,2-Dibromoethane	2.6 · 0.5	3.4 · 0.4
Iodoethane	0.22 · 0.03	0.26 · 0.02

rins [57]. The photophysics of these systems has been well studied and is dominated by the π-electron system of the porphyrin macrocycle [135]. Magde et al. [57] were able to observe time-resolved spectra of S_1 and T_1 and measure the S_1 lifetime and the quantum yield of T_1 in octaethylporphinatotin(IV) dichloride [(OEP)$SnCl_2$] (see Fig. 5-15). From these data and a three-level kinetic scheme involving only S_0, S_1, and T_1, they calculated a triplet quantum yield of 0.8. Together with a fluorescence quantum yield of 0.007 [136], this indicated a quantum yield for internal conversion S_1–S_0 of about 0.19, a value intermediate between those obtained from flash photolysis [137] and flash calorimetry [138].

Electronic relaxation in coordination compounds, particularly those of Cr(III), has been studied in our laboratory by Kirk et al. [139]. The excited states are predominantly metal centered and well characterized by ligand field theory [140], and nonradiative relaxation has been of interest to those photochemists dealing with coordination compounds. In Cr(III), the lowest excited states are of quartet and doublet spin multiplicity. Photochemists studying Cr(III) have been especially interested in the lifetime of the lowest excited quartet, which is presumed to be the photoactive state [141]. Initial studies suggested that the lowest excited quartet decayed with a rate too fast to measure, $\tau < 10$ psec [139]. However recent work in our laboratory has established that the rise of doublet absorbance by intersystem crossing from the excited quartet in *trans*-$Cr(NH_3)_2(NCS)_4^-$ occurs in 24 psec in water [142]. In addition, for a series of thiocyanate complexes of Cr(III), there is a solvent dependence of the excited quartet lifetime, which appears to reflect the overall charge or symmetry of these ions in a manner that has yet to be determined.

Vibrational Relaxation

Experimental studies of picosecond vibrational relaxation of molecules, in the liquid state or in solution, have dealt with the relaxation of simple molecules within the ground electronic state and more complex dye molecules in both the ground and first excited singlet states. The earliest studies employed a mode-locked Nd:glass laser and a variation of the single-pulse and probe technique described in the section on picosecond absorption techniques. More recently, mode-locked CW dye laser systems have been used.

Laubereau et al. [143] were the first to apply picosecond laser pulses and detection to the study of vibrational relaxation in the ground state. They were able to measure two distinct vibrational lifetimes associated with the totally symmetrical CH_3 vibration in CH_3CCl_3 and ethanol, v_1. Molecules in the v_1 state were prepared via the Stokes shifted stimulated Raman scattering (SRS) of the picosecond pump pulse. Because SRS is an

efficient nonlinear process, a large fraction of the molecules in the beam are promoted to the v_1 state. In addition, the phase-matching conditions of this three-wave mixing process requires that the excited oscillators all be in phase (coherent) [144]. Such a system can be characterized by two measurable lifetimes: the decay of the excited population corresponds to one measured lifetime, whereas the decay of the *phase* relationship corresponds to a second lifetime. The dephasing time was measured by the decay of a coherent anti-Stokes Raman signal generated by a second delayed pulse at the same wavelength as the pump pulse. A precise phase relation must exist between all three waves in the SRS process, and the intensity of the *coherent* anti-Stokes Raman signal generated by the probe beam will decrease with delay as the molecules in v_1 no longer oscillate exactly in phase. Typically, dephasing times are as short as or shorter than the pump and probe pulsewidths and are difficult to determine precisely. Fischer and Laubereau [145] were able to describe dephasing times in terms of semiclassical collision theory and the interaction of vibrationally excited molecules with other nearby molecules.

The population of v_1 was monitored by observing the *incoherent* anti-Stokes Raman signal generated by the probe pulse, and a log plot of scattered intensity versus delay between the pump and probe pulses gave the lifetime of v_1. In their first paper, Laubereau et al. measured a population lifetime of 5 ± 1 psec for neat CH_3CCl_3 and 20 ± 5 psec for neat ethanol [143]. In later work Laubereau, Kirschner, and Kaiser [146] reported that the v_1 lifetime in CH_3CCl_3 was dependent on the square of the mole fraction of CH_3CCl_3 in CCl_4 solution, suggesting an intermolecular path contributing to vibrational relaxation. The decay appears to occur by way of fast energy transfer to the second harmonic of CH bending modes, since the rise and decay of an *incoherent* anti-Stokes Raman signal was observed at the CH bending frequency [146, 147]. The presence of CH bonds as well as the number of methyl groups were found to be influential in the vibrational relaxation in hydrocarbons. When a similar technique was used, the measured lifetimes varied from 11 to 60 psec [148]. Later work [147] on vibrational decay in ethanol, in which the v_1 state was pumped directly by an IR pulse derived from the pulse of a mode-locked Nd:glass laser and difference frequency generation in two $LiNbO_3$ crystals, showed an initial very fast decay of the scattering signal followed by a slower decay. The authors attributed the fast decay, $\tau \sim 2$ psec, to energy transfer to neighboring states with smaller scattering cross sections. These studies of relaxation in ethanol were performed in dilute solution at an ethanol concentration of 0.04 M in CCl_4, and the discrepancy between the slower decay, $\tau = 40 \pm 15$ psec, and the earlier reported lifetime of 20 psec was attributed to an intermolecular energy-transfer

pathway similar to that observed in CH_3CCl_3. Measurements of the decay of v_1 in CH_3I in CCl_4 solution revealed a lifetime $\tau \sim 2$ psec which showed no concentration dependence, as observed in ethanol and CH_3CCl_3, and suggested therefore that intramolecular vibrational relaxation was much faster in this molecule [147].

Vibrational relaxation of larger dye molecules has been studied in a number of laboratories and using a variety of experimental techniques. Ricard et al. [149] measured the rate of thermal equilibration in the first excited singlet states of R-6G and R-B in 10^{-4} M ethanol solutions by an analysis of the wavelength dependence of the risetime of stimulated emission. A single 6-psec pulse from a mode-locked Nd:glass laser was passed through a beam splitter, and one portion of the pulse was used to excite the dye while the remaining but equally intense probe portion was used to stimulate the emission of the excited dye as a function of the delay between the two pulses. Different pump and probe wavelengths were generated by stimulated Raman scattering followed by either phase-matched sum frequency generation or second harmonic generation in KDP. The rise of stimulated emission versus the time delay between pump and probe pulses revealed vibrational lifetimes within S_1 of 8 ± 3 psec for R-6G and ~ 2 psec for R-B. Mourou and Malley [150] measured lifetimes of R-6G, R-B, and erythrosin B, using an optical Kerr cell, to detect the delayed appearance of spontaneous fluorescence. Subsequently Ippen and Shank [151] used the frequency-doubled output (307 nm) of their subpicosecond mode-locked CW dye laser to repeat measurements of the gain risetime in R-6G and R-B and found a delay of less than 0.2 psec in methanol and glycerol solutions. Using two different methods, Penzkofer et al. [152] found viscosity-independent lifetimes for vibrational relaxation, following absorption only several hundred wavenumbers above the excited singlet minimum, for both R-6G and R-B of $0.5 \leq \tau \leq 1.0$ psec. The apparent sensitivity of these lifetimes to the experimental method has yet to be resolved and again may be a consequence of a nonlinear power dependence, especially since the yield of stimulated emission is proportional to the square of the pump pulse intensity.

Kaiser and Laubereau [153] reported a method for measuring the rate of vibrational relaxation in the ground state of coumarin 6. By exciting a solution of the dye in CCl_4 by a picosecond pulse at about 3000 cm^{-1} and probing at 530 nm, the emission intensity can be used to measure the amount of vibrational decay that has occurred as the pump and probe pulses are separated in time. The fluorescence threshold is very near the sum of the IR and visible pulses, and any decay of the vibrational states produced in the IR pulse will prevent the second photon from exciting the molecule to the S_1 state. They measured a fluorescence intensity which decayed with the lifetime of 1.3 ± 0.4 psec at room temperature.

Photochemistry

I_2

Recently there have been a number of picosecond studies of photolabile systems in which chemical reaction is an important excited-state relaxation pathway. The most notable has been the dissociation of I_2 in solution [154]. The disappearance (bleaching) of ground-state absorbance continued for ~ 10 psec following the decay of the 5-psec pump pulse at 530 nm. The longer risetime was interpreted as the collision-induced predissociation of some excited states of I_2 to yield two nonabsorbing I atoms. In CCl_4 and hexadecane, the orientational relaxation time of I_2 is faster than the rise in transmission and argues strongly against orientational relaxation as the cause for the ~ 10-psec risetime of probe transmission. The residual bleaching at 800 psec in hexadecane and CCl_4 was interpreted as a consequence of the escape of I atoms from the solvent cage; and because the fusion of I atoms from different solvent cages probably occurs in ~ 10 nsec [154], the decay kinetics of short-time bleaching and magnitude of the residual bleaching yields the rate and extent of geminate recombination. Yields of solvent-separated I atoms estimated from the bleaching of I_2 absorbance agree reasonably with the Noyes treatment of dissociation based on the continuum hydrodynamic properties of the solvents [155]. The lifetimes for geminate recombination are 70 and 140 psec in hexadecane and in CCl_4, respectively, and comparison with values for rates of geminate recombination, estimated using Noyes random walk model, shows the experimental values to be only slightly larger than expected [156]. Comparisons of yields for different excitation wavelengths should provide an additional test of the Noyes model, since shorter excitation wavelengths ($\lambda < 530$ nm) should result in a greater yield of solvent-separated I atoms.

Tetraphenylhydrazine

Anderson and Hochstrasser [157] studied the kinetics of photodissociation of tetraphenylhydrazine (TPH) in solution at room temperature. A transient absorbance was produced with a risetime less than the 353-nm 8-psec pump pulsewidth. The spectra at 6 psec and 1 nsec agreed favorably with that observed for radical pairs in the rigid glass [158] as well as that of the longer-lived (~ 1 μsec) free radicals [159]. The similarity of radical pair and free-radical spectra did not permit observation of the escape of the diphenylamine (DPA) radical products from the solvent cage, and the very fast absorbance risetime suggested only an upper limit on the lifetime

for the precursor excited singlet state, ~ 2 psec. The peculiar feature in the kinetics of these radicals is the apparent lack of any geminate recombination. The authors suggest that one of the radicals may have to be in an excited state for efficient recombination, a proposal supported by the formation of TPH from radical pairs under irradiation by red light [160]. An experiment using the second harmonic from a mode-locked ruby laser (347 nm) to pump the sample and the red fundamental (694 nm) to initiate recombination could be used to test this hypothesis. Delaying the fundamental relative to the 347-nm pump pulse allowed the rate of escape from the radical cage to be determined by the amount of photoinduced recombination as a function of the time delay between the pulses.

Tetramethyl-1,2-dioxetane

A mode-locked Nd phosphate glass laser with 10-psec pulse was used to study the photolysis of tetramethyl-1,2-dioxetane. In this study, Smith et al. [161] used a streak camera to detect the fluorescence of the acetone photoproduct *in* the S_1 excited state [162, 163] produced after excitation with the fourth harmonic at 264 nm. Deconvolution revealed that the fluorescence risetime was ~ 10 psec. This, coupled with the S_1 fluorescence decay (τ ~ 2 nsec), suggested that all acetone was produced only in the S_1 state during the pump pulse. Wavelength-dependent yields of S_1 acetone product [164] suggested to the authors that the process leading to S_1 acetone may be competing with vibrational equilibration and that equilibration followed by intersystem crossing leads to the same biradical intermediate and T_1 acetone product observed in the thermal decomposition of tetramethyl-1,2-dioxetane [164]. Here, as in the fusion of two DPA radicals, separation of radicals into acetone products is more efficient then radical recombination, given the near-unit quantum yield for acetone formation.

Photobiology

Almost all of the application of picosecond techniques to biology and biophysics has taken place in the past two or three years. Valuable new insights have been gained, and in some areas, notably photosynthesis, quite striking advances have been made. Picosecond spectroscopy, for the first time, enables us to take a look at the elementary steps that underlie the overall complexity of biological reactions. These primary processes, involving energy migration, bond rupture, molecular rearrangements, and charge transfer, all take place on a time scale from about 10^{-14} to 10^{-8} sec. Besides new data on photosynthesis, useful results have been obtained on visual pigments, hemoglobin complexes, and energy transfer in DNA. Recent reviews by Campillo and Shapiro [165] and Holten and Windsor [166] should be consulted for more detailed accounts of the application of picosecond techniques to biological systems. Here we attempt to do no more than summarize the new results and comment briefly on their significance.

The area that has received greatest emphasis to date is photosynthesis. This emphasis is undoubtedly appropriate since we are all dependent on photosynthesis both for our origin and for our continued survival. Picosecond fluorescence studies, in both green plants and photosynthetic bacteria, show that excitation energy migrates from the antenna or light-harvesting system (a structured pool or array of several hundred chlorophyll molecules that gather incident solar photons) to a specialized trap or reaction center (RC) in times that range from 10 psec to about 1 nsec, dependent upon species. Within the RC, the initial charge separation occurs in a time of about 200 psec, converting the electronic excitation and storing it as chemical potential [165, 166].

Picosecond techniques have been widely used to measure fluorescence lifetimes in photosynthetic systems [167]. Techniques employed include phase fluorometry [167], mode-locked CW laser methods with signal averaging [168], optical Kerr gate studies [169], and picosecond streak cameras [170–172]. Concern has been expressed about possible multiple-excitation effects when high-intensity ($> 10^{23}$ photons cm^{-2}) single picosecond pulses are used, leading to intensity dependence of quantum yield and lifetimes [173, 174] and in some cases to stimulated emission [175]. This has necessitated reinterpretation of some early measurements. However picosecond techniques can be valuable in measuring fluorescence lifetimes provided that care is taken in choosing the mode and intensity of excitation [172]. Techniques that avoid these difficulties are now available [36, 46, 176].

Green plants contain two photosystems, PSI and PSII, in close proximity; both absorb a photon, convert its energy to chemical potential, and cooperate in the later stages of photosynthesis. Photosynthetic bacteria contain only a single photosystem. Emission measurements on plant systems often show a biphasic decay with a fast component that decays in a few tens of picoseconds and a slower one that decays in a few hundred picoseconds. For example, Siebert and Alfano [169] studied chlorophyll *a* fluorescence in escarole chloroplasts and found maxima in the decay curves at 15 and 90 psec, with a dip at 50 psec. They interpreted these results as indicating fluorescence from both PSI and PSII, with respective decay times of 10 and 210 psec. Yu et al. [177] studied PSI- and PSII-enriched particles of spinach and found 60 ± 10 and 200 ± 20 psec components. Attempts to measure rates of energy migration from the antenna system to the reaction center have been made by studying the induction time for

the appearance of fluorescence after excitation by a short pulse. However interpretation of the results is clouded by the possibility of excited-state annihilation processes (singlet–singlet and singlet–triplet), especially at high light intensities [165, 172]. It is not yet known exactly how fast migration of excitation occurs within the antenna system or from the antenna to the reaction center, except that the time probably lies in the range of 10 psec to 1 nsec and depends upon the species. We do not even know whether such migration occurs via an exciton mechanism that involves many short hops (a few angstroms) between closely adjacent pigment molecules [178] or over somewhat large distances (10 Å) via a Förster mechanism [179]. Some very recent work [171] on photosynthetic bacteria supports a "lake" model, in which a single antenna system contains many different reaction centers any of which can receive the excitation. This is in contrast to the "puddle" model, in which independent photosynthetic units exist, each with its own reaction center and small antenna system. Given a "lake" model, it is easy to see why one would expect to observe a spectrum of trapping times. One would also expect an intensity dependence of quantum efficiency, since it takes several microseconds for an RC that has received excitation to convert it and become ready to receive again. Indeed it was by a study of such intensity dependence that the above conclusion was drawn [171].

Let us turn now to the energy conversion process that takes place within the RC. Much has been learned about this process recently from picosecond absorption studies on photosynthetic bacteria [166]. The majority of studies have been done on reaction centers of the bacterium *Rhodopseudomonas sphaeroides*, which has been well characterized as to its composition. These reactive centers contain four molecules of bacteriochlorophyll (BChl); two molecules of the magnesium-deficient analog bacteriopheophytin (BPh), one ubiquinone molecule (UQ); one nonheme iron atom, probably complexed to the UQ, and three different proteins in a 1:1:1 ratio and of molecular weight 28, 22, and 20 kdalton [180, 181]. Two of the BChl molecules form a special pair that absorbs maximally at 870 nm and is often called P870, or simply P. Receipt of excitation from the antenna system produces the excited singlet state BChl–*BChl. (In picosecond experiments on isolated reactive centers this state is excited directly or via very rapid (10 psec) energy transfer from a neighboring BPh that has absorbed a 530-nm laser pulse.) Picosecond spectral studies of transient intermediates [182–184], both in our own laboratory and in other laboratories, show that a special state, P^t, is formed in less than 10 psec and decays in about 200 psec with the concomitant appearance of absorption spectra characteristic of the oxidized donor BChl$^+$–BChl and the reduced "primary acceptor," X$^-$, where X is used to symbolize the

Fe–UQ complex. The net effect is that an electron is transferred from BChl–BChl to X in two stages, an initial very fast step (10 psec) and a second somewhat less fast step (200 psec). Much interest has focused on the identity of P^t, and it is now known to have the structure (BChl$^+$–BChl)BPh$^-$ [185, 186]. It appears that Nature has good reasons for making the first step so fast, namely, to prevent the excitation from "hopping" back out of the reactive center into the antenna pool [187]. It also appears, from very recent model system studies in our laboratory by Holten et al [187], that some quite subtle effects may be involved in slowing down dramatically the reverse electron transfer, thus protecting this first crucial step in capturing and using solar energy. There is also the possibility that the additional pigment molecules in the RC have a role in coupling a portion of the energy "losses" that accompany the electron transfer to structural changes that involve the membrane proteins [186]. In summary, we note that much insight has been gained into the details of the very early events in photosynthesis. However we still need to establish the role of the "extra" pigment molecules (two additional BChl and one additional BPh) and understand better the relationships between structure and function within the reactive center.

Turning now to studies of the visual pigment rhodopsin, we find that very few picosecond studies have been made, no doubt because its photolability necessitates a fresh sample for each experiment. The few studies that have been done [188, 189] have been supplemented by experiments on a closely related pigment, bacteriorhodopsin (bR), which occurs in the purple membrane of *Halobacterium halobium*, a bacterium that occurs in salt flats. Although bacteriorhodopsin does not function as a visual transducer but rather as a crude photosynthetic system that makes ATP, its early-time photochemistry parallels that of animal rhodopsin. Furthermore, it goes through a photochemical cycle in which the original form is regenerated within a few milliseconds—a considerable experimental advantage compared to animal rhodopsin [190]. The picosecond studies of bovine rhodopsin [188] and squid rhodopsin [189] show that formation of the first intermediate, called hypsorhodopsin, occurs in a time that cannot be distinguished from the rise of the excitation pulse (6 psec for Nd:glass in Ref. 188 and 20 psec for ruby in Ref. 189). Hypsorhodopsin can also be trapped at liquid helium temperatures [191]. Its formation probably involves a minor photochemically induced conformational change in the chromophore (11-cis retinal), probably around the 11th carbon atom, followed by a series of further changes that occur thermally and that can be resolved in low-temperature experiments. At physiological temperatures, conversion to the next intermediate, bathorhodopsin, occurs in about 55 psec [189] and conversion to the

subsequent one, lumirhodopsin, in about 30 nsec [188]. Similar changes occur in bacteriorhodopsin, but the initially excited singlet state can be resolved, and it appears to have a lifetime of about 15 psec [176, 192, 193].

Shank, Ippen, and Bersohn [194] have used subpicosecond pulses from a CW mode-locked dye laser to study the dissociation of oxygen and carbon monoxy complexes of hemoglobin, HbO_2 and HbCO. Hemoglobin has a much stronger absorption at 615 nm than its complexes have. Thus their dissociation can be studied by following the increases in absorbance at this wavelength. For HbCO a risetime of less than 0.5 psec is observed, and the absorption decays very little in the first microsecond after excitation [165]. It is concluded that the high quantum yield for photodissociation of HbCO is due to a fast rate of dissociation combined with a slow rate of recombination [194]. In the case of HbO_2 there is also a fast rise in absorbance at 615 nm, but it decays again in about 2.5 psec. Similar results are obtained when an experiment is done on deoxygenated hemoglobin samples. This result suggests that the increased absorbance for HbO_2, unlike HbCO, is due to a short-lived excited state that absorbs more strongly at 615 nm than does the ground state. The authors conclude that the low quantum yield for photodissociation of HbO_2 is due not to rapid recombination but rather to the relatively slow rate of dissociation from the excited state, which does not compete effectively with the very fast 2.5 psec nonradiative decay of the excited state.

Shapiro et al. [195] studied energy transfer in DNA–acridine orange complexes using picosecond techniques. They used a train of 265-nm 10-psec pulses to excite the sample and a streak camera to observe the fluorescence between 530 and 600 nm. The risetime was estimated to be < 20 psec. Since the polymer-to-dye ratio was 400 to 1, most of the excitation was absorbed by the DNA. All of the fluorescence, on the other hand, comes from acridine molecules excited by energy transfer from the DNA. A transfer distance of five to ten base pairs has been estimated from quantum yield measurements. If one takes the observed risetime of < 20 psec to be the time for excitation to transfer over this distance, the value obtained for the exciton diffusion coefficient is at least 1 (base pair)^2 per picosecond. For further details of the experiments on hemoglobin and on DNA, the review of Campillo and Shapiro [165] should be consulted.

ACKNOWLEDGMENTS

The authors gratefully acknowledge the comments of Dr. C. V. Shank on the section on subpicosecond pulses, Dr. Dewey Holten for reviewing the manuscript, and Dr. Stephen Rice for comments on electron localization. Special thanks are due to David Cremers for the description of his unpublished work given in the section on rotational motion in the condensed phase. The preparation of this review was supported in part by the U.S. Army Research Office under Grant DAAG 29-76-9-0275 and by the Office of Naval Research.

References

1. A. J. DeMaria, D. A. Stetser, and W. H. Glenn, Jr., *Science*, **156**, 1557 (1967).
2. R. C. Greenhow and A. J. Schmidt, in *Advances in Quantum Electronics*, Vol. 2, D. N. Goodwin, Ed., Academic Press, New York, 1974, p. 157.
3. D. J. Bradley, *Opt. Electron.*, **6**, 25 (1974).
4. M. M. Malley, in *Creation and Detection of the Excited State*, Vol. 2, W. R. Ware, Ed., Marcel Dekker, New York, 1974, p. 99.
5. P. W. Smith, M. A. Duguay, and E. P. Ippen, in *Progress in Quantum Electronics*, Vol. II, J. H. Sanders and S. Stenholm, Eds., Pergamon, Oxford, 1974, p. 107.
6. A. Laubereau and W. Kaiser, *Opt. Electron.*, **6**, 1 (1974).
7. G. E. Busch and P. M. Rentzepis, *Science*, **194**, 276 (1976).
8. D. J. Bradley, in *Ultrashort Light Pulses*, S. L. Shapiro, Ed., Springer-Verlag, New York, 1977, p. 18.
9. C. P. Ausschnitt, *IEEE J. Quantum Electron.*, **QE-13**, 321 (1977), and references therein.
10. D. J. Kuizenga and A. E. Siegman, *IEEE J. Quantum Electron.*, **QE-6**, 694, 709 (1970).
11. H. A. Haus, *J. Appl. Phys.*, **46**, 3049 (1975); *IEEE J. Quantum Electron.*, **QE-11**, 736 (1975); *Opt. Commun.*, **15**, 29 (1975).
12. K. H. Drexhage and U. T. Müller-Westerhoff, *IEEE J. Quantum Electron.*, **QE-8**, 759 (1972); K. H. Drexhage and G. A. Reynolds, *Opt. Commun.*, **10**, 18 (1974).
13. For a good review of the structure and properties of dyes used in lasers, see K. H. Drexhage, in *Dye Lasers*, F. P. Schäfer, Ed., Springer-Verlag, New York, 1973, p. 144.
14. D. J. Bradley, G. H. C. New, and S. J. Caughy, *Phys. Lett.*, **A30**, 78 (1969); *Opt. Commun.*, **2**, 41 (1970); D. J. Bradley and W. Sibbett, *Opt. Commun.* **9**, 17 (1973).
15. W. Yu and R. R. Alfano, *Opt. Electron.*, **6**, 243 (1974).
16. E. M. Garmire and A. Yariv, *IEEE J. Quantum Electron.*, **QE-3**, 222 (1967).
17. E. G. Arthurs, D. J. Bradley, and A. G. Roddie, *Appl. Phys. Lett.*, **23**, 88 (1973).
18. A. Yariv, *Quantum Electronics*, 2nd ed., Wiley, New York, 1975, p. 327.
19. D. von der Linde, O. Bernecker, and A. Laubereau, *Opt. Commun.*, **2**, 215 (1970).

20. E. G. Arthurs, D. J. Bradley, and T. J. Glynn, *Opt. Commun.*, **12**, 136 (1974).
21. H. Al-Obaidi, R. J. Dewhurst, D. Jacoby, G. A. Oldershaw, and S. A. Ramsden, *Opt. Commun.*, **14**, 219 (1975).
22. D. von der Linde and K. F. Rodgers, *Opt. Commun.*, **8**, 91 (1973).
23. E. G. Arthurs, D. J. Bradley, P. N. Puntambekar, I. S. Ruddock, and T. J. Glynn, *Opt. Commun.*, **12**, 360 (1974); G. H. C. New, *Opt. Commun.*, **6**, 188 (1972); G. H. C. New, *IEEE J. Quantum Electron.*, **QE-10**, 115 (1974); R. V. Ambartsumyare, N. G. Basov, V. S. Zuev, P. G. Kryukov, and V. S. Letokhov, *JETP Lett.*, **4**, 12 (1966).
24. F. Zernike and J. E. Midwinter, *Applied Nonlinear Optics*, Wiley, New York, 1973.
25. A. Yariv and J. E. Pearson, in *Progress in Quantum Electronics*, Vol. 1, J. H. Sanders and K. W. H. Stevens, Eds., Pergamon, Oxford, 1971, p. 1.
26. W. L. Smith, *Appl. Opt.*, **16**, 1798 (1977).
27. A. Laubereau, L. Greiter, and W. Kaiser, *Appl. Phys. Lett.*, **25**, 87 (1974).
28. R. B. Weisman and S. A. Rice, *Opt. Commun.*, **19**, 28 (1976).
29. C. A. Moore and L. S. Goldberg, *Opt. Commun.*, **16**, 21 (1976).
30. M. J. Colles, *Opt. Commun.*, **1**, 169 (1969).
31. T. R. Royt, C. H. Lee, and W. L. Faust, *Opt. Commun.*, **18**, 108 (1976).
32. A. H. Kung, J. F. Young, G. C. Bjorklund, and S. E. Harris, *Phys. Rev. Lett.*, **29**, 985 (1972).
33. R. T. Hodgson, P. P. Sorokin, and J. J. Wayne, *Phys. Rev. Lett.*, **32**, 343 (1974).
34. J. Reintjes, C. Y. She, R. C. Eckardt, N. E. Karangelen, R. A. Andrews, and R. C. Elton, *Appl. Phys. Lett.*, **30**, 480 (1977); C. Y. She and J. Reintjes, *ibid.*, **31**, 95 (1977), and references therein.
35. D. J. Bradley, A. G. Roddie, W. Sibbett, M. H. Key, M. J. Lamb, C. L. S. Lewis, and P. Sachsenmaier, *Opt. Commun.*, **15**, 231 (1975).
36. E. P. Ippen and C. V. Shank, in *Ultrashort Light Pulses*, S. L. Shapiro, Ed., Springer-Verlag, New York, 1977, p. 83.
37. D. J. Bradley and G. H. C. New, *Proc. IEEE*, **62**, 313 (1974).
38. H. P. Weber, *J. Appl. Phys.*, **38**, 2231 (1967); **39**, 6041 (1968).
39. J. A. Armstrong, *Appl. Phys. Lett.*, **10**, 16 (1967).
40. I. V. Tomov, *Opt. Commun.*, **10**, 154 (1974).
41. J. A. Giordmaine, P. M. Rentzepis, S. L. Shapiro, and K. W. Wecht, *Appl. Phys. Lett.*, **11**, 216 (1967).
42. P. M. Rentzepis and M. A. Duguay, *Appl. Phys. Lett.*, **11**, 218 (1967).
43. P. M. Rentzepis, C. J. Mitschele, and A. C. Saxman, *Appl. Phys. Lett.*, **17**, 122 (1970).
44. E. K. Zavoiskii and S. D. Fanchenko, *Sov. Phys. -Dokl.*, **1**, 285 (1956).
45. W. R. Ware, in *Creation and Detection of the Excited State*, Vol. 1, Part A, A. A. Lamola, Ed., Marcel Dekker, New York, 1971, p. 213.
46. Z. D. Popovic and E. R. Menzel, *Chem. Phys. Lett.*, **45**, 537 (1977).
47. A. Javan, V. S. Letokhov, M. S. Feld, and A. L. Schawlow, in *Fundamental and Applied Laser Physics*, M. S. Feld, A. Javan, and N. A. Kurnit, Eds., Wiley, New York, 1973.

48. E. Courtens, in *Laser Handbook*, Vol. 2, F. T. Arecchi and E. O. Schulz-DuBois, Eds., Elsevier, New York, 1972, p. 1259.
49. P. M. Rentzepis and W. S. Struve, in *International Reviews of Science, Physical Chemistry*, Series Two, Vol. 3, Spectroscopy, D. A. Ramsay, Ed., Butterworth, London/Boston, 1976, p. 263.
50. P. M. Rentzepis, *Chem. Phys. Lett.*, **2**, 117 (1968); *ibid.*, **3**, 717 (1969).
51. M. M. Malley and P. M. Rentzepis, *Chem. Phys. Lett.*, **3**, 534 (1969).
52. M. R. Topp, P. M. Rentzepis, and R. P. Jones, *Chem. Phys. Lett.*, **9**, 1 (1971).
53. M. R. Topp and G. C. Orner, *Chem. Phys. Lett.*, **32**, 407 (1975).
54. M. R. Topp, *Opt. Commun.*, **14**, 126 (1975).
55. D. Magde and M. W. Windsor, *Chem. Phys. Lett.*, **27**, 31 (1974).
56. D. Magde, B. A. Bushaw, and M. W. Windsor, *Chem. Phys. Lett.*, **28**, 263 (1974).
57. D. Magde, M. W. Windsor, D. Holten, and M. Gouterman, *Chem. Phys. Lett.*, **29**, 183 (1974).
58. M. G. Rockley, M. W. Windsor, R. J. Cogdell, and W. W. Parson, *Proc. Natl. Acad. Sci.*, **72**, 2251 (1975).
59. R. R. Alfano and S. L. Shapiro, *Chem. Phys. Lett.*, **8**, 631 (1971).
60. R. R. Alfano and S. L. Shapiro, *Phys. Rev. Lett.*, **24**, 584, 592, 1217 (1970).
61. W. Yu, R. R. Alfano, C. L. Sam, and R. J. Seymour, *Opt. Commun.*, **14**, 344 (1975).
62. E. P. Ippen, C. V. Shank, and T. K. Gustafson, *Appl. Phys. Lett.*, **24**, 190 (1974).
63. N. Mataga and N. Nakashima, *Spectrosc. Lett.*, **8**, 275 (1975).
64. D. W. Phillon, D. J. Kuizenga, and A. E. Siegman, *Appl. Phys. Lett.*, **27**, 85 (1975).
65. A. E. Siegman, *Appl. Phys. Lett.*, **30**, 21 (1977).
66. A. D. Buckingham, *Proc. Phys. Soc.*, **B69**, 344 (1956).
67. G. Mayer and F. Gires, *C. R. Acad. Sci. (Paris)*, **258**, 2039 (1964).
68. P. D. Maker, R. W. Terhune, and C. M. Savage, *Phys. Rev. Lett.*, **12**, 507 (1964).
69. M. A. Duguay and J. W. Hansen, *Appl. Phys. Lett.*, **15**, 192 (1969); *Opt. Commun.*, **1**, 254 (1969).
70. M. A. Duguay and A. T. Mattick, *Appl. Opt.*, **10**, 2162 (1971).
71. E. P. Ippen and C. V. Shank, *Appl. Phys. Lett.*, **26**, 92 (1975), and references therein.
72. M. M. Malley and P. M. Rentzepis, *Chem. Phys. Lett.*, **7**, 57 (1970).
73. G. Mourou, D. Drouin, and M. M. Denariez-Roberge, *Appl. Phys. Lett.*, **20**, 453 (1972).
74. G. E. Busch, K. S. Greve, G. L. Olson, R. P. Jones, and P. M. Rentzepis, *Appl. Phys. Lett.*, **27**, 450 (1975).
75. D. J. Bradley, in *Ultrashort Light Pulses*, S. L. Shapiro, Ed., Springer-Verlag, New York, 1977, p. 41.
76. M. E. Mack, *Appl. Phys. Lett.*, **15**, 166 (1969); C. Lin, T. K. Gustafson, and A. Dienes, *Opt. Commun.*, **8**, 210 (1973).

77. A. N. Rubinov, M. C. Richardson, K. Sala, and A. J. Alcock, *Appl. Phys. Lett.*, **27**, 358 (1975); B. Fan and T. K. Gustafson, *Appl. Phys. Lett.*, **28**, 202 (1976).
78. W. H. Glenn, M. J. Brienza, and A. J. DeMaria, *Appl. Phys. Lett.*, **12**, 54 (1968); B. H. Soffer and J. W. Linn, *J. Appl. Phys.*, **39**, 5859 (1968); T. R. Royt, W. L. Faust, L. S. Goldberg, and C. H. Lee, *Appl. Phys. Lett.*, **25**, 514 (1974); L. S. Goldberg and C. A. Moore, *Appl. Phys. Lett.*, **27**, 217 (1975); T. R. Royt and C. H. Lee, *Appl. Phys. Lett.*, **30**, 332 (1977).
79. (a) C. V. Shank and E. P. Ippen, in *Dye Lasers*, F. P. Schäfer, Ed., Springer-Verlag, New York, 1973, p. 137; (b) C. K. Chan and S. O. Sari, *Appl. Phys. Lett.*, **25**, 403 (1974); N. J. Frigo, T. Daly, and H. Mahr, *IEEE J. Quantum Electron.*, **QE-13**, 101 (1977); H. Mahr, *IEEE J. Quantum Electron.*, **QE-12**, 554 (1976); H. Mahr and M. D. Hirsch, *Opt. Commun.*, **13**, 96 (1975); R. K. Jain and J. P. Heritage, private communication.
80. A. Dienes, E. P. Ippen, and C. V. Shank, *Appl. Phys. Lett.*, **19**, 258 (1971).
81. D. J. Kuizenga, *Appl. Phys. Lett.*, **19**, 260 (1971).
82. (a) C. V. Shank, E. P. Ippen, and A. Dienes, *Digest of Tech. Papers, VII International Quantum Electronics Conf. Montreal, 1972*, IEEE, New York, 1972, p. 7; (b) E. P. Ippen, C. V. Shank, and A. Dienes, *Appl. Phys. Lett.*, **21**, 348 (1972).
83. (a) F. O'Neill, *Opt. Commun.*, **6**, 360 (1972); (b) J. P. Letellier and S. O. Sari, *Appl. Phys. Lett.*, **23**, 311 (1973).
84. C. V. Shank and E. P. Ippen, *Appl. Phys. Lett.*, **24**, 373 (1974).
85. (a) E. B. Treacy, *Phys. Lett.*, **28A**, 34 (1968); *Appl. Phys. Lett.*, **14**, 112 (1969); (b) E. P. Ippen and C. V. Shank, *Appl. Phys. Lett.*, **27**, 488 (1975).
86. I. S. Ruddock and D. J. Bradley, *Appl. Phys. Lett.*, **29**, 296 (1976).
87. E. P. Ippen and C. V. Shank, *Opt. Commun.*, **18**, 27 (1976).
88. J. P. Heritage and R. K. Jain, private communication.
89. Z. A. Yasa, *J. Appl. Phys.*, **46**, 4895 (1975); Z. A. Yasa and O. Teschke, *Appl. Phys. Lett.*, **27**, 446 (1975); Z. A. Yasa, A. Dienes, and J. R. Whinnery, *Appl. Phys. Lett.*, **30**, 24 (1977).
90. E. P. Ippen and C. V. Shank, private communication.
91. S. Kielich, in *Dielectric and Related Molecular Processes*, Vol. 1, Specialist Periodical Reports, The Chemical Society, London, 1972, p. 192.
92. For an outline of the theory regarding orientational relaxation, see K. B. Eisenthal, *Acc. Chem. Res.*, **8**, 118 (1975), and references therein; the theory behind the concept of photoselection was well described by Albrecht and may be useful to those who require additional background: A. C. Albrecht, *J. Mol. Spectrosc.*, **6**, 84 (1961).
93. T. J. Chuang and K. B. Eisenthal, *Chem. Phys. Lett.*, **11**, 368 (1971).
94. A. Einstein, *Ann. Phys.*, (Leipzig), **19**, 371 (1906); translated into English in *Investigations on the Theory of Brownian Movement*, Dover, New York, 1956, and P. Debye, *Polar Molecules*, Dover, London, 1929, p. 83.
95. G. R. Fleming, J. M. Morris, and G. W. Robinson, *Chem. Phys.*, **17**, 91 (1976).

96. H. E. Lessing and A. von Jena, *Chem. Phys. Lett.*, **42**, 213 (1976), and references therein.
97. D. Magde and M. W. Windsor, *Chem. Phys. Lett.*, **24**, 144 (1974).
98. T. Förster and G. Hoffman, *Z. Phys. Chem., Neue Folge* (Frankfurt), **75**, 63 (1971).
99. L. J. E. Hofer, R. J. Grabenstetter, and E. O. Wiig, *J. Am. Chem. Soc.*, **72**, 203 (1950).
100. G. Oster and Y. Nishijima, *J. Am. Chem. Soc.*, **78**, 1581 (1956).
101. B. Bushaw, Masters Thesis, Chemistry Department, Washington State University, 1976.
102. D. Cremers and M. W. Windsor, manuscript in preparation.
103. R. Olinger, U. Schindewolf, A. Gaathon, and J. Jortner, *Ber. Bunsenges. Phys. Chem.*, **75**, 690 (1971).
104. J. H. Baxendale and P. Wardman, *Nature*, **230**, 449 (1971); *J. Chem. Soc., Faraday Trans. I*, **69**, 584 (1973).
105. M. J. Bronskill, R. K. Wolff, and J. W. Hunt, *J. Chem. Phys.*, **53**, 4201 (1970).
106. P. M. Rentzepis, R. P. Jones, and J. Jortner, *Chem. Phys. Lett.*, **15**, 480 (1972).
107. P. M. Rentzepis, R. P. Jones, and J. Jortner, *J. Chem. Phys.*, **59**, 766 (1973).
108. C. D. Jonah, *Rev. Sci. Instrum.*, **46**, 62 (1975).
109. G. A. Kenney-Wallace and C. D. Jonah, *Chem. Phys. Lett.*, **39**, 596 (1976).
110. W. J. Chase and J. W. Hunt, *J. Phys. Chem.*, **79**, 2835 (1975).
111. G. A. Kenney-Wallace and C. D. Jonah, *Chem. Phys. Lett.*, **47**, 362 (1977).
112. J. B. Birks, *Photophysics of Aromatic Molecules*, Wiley, New York, 1970, pp. 166, 187.
113. R. M. Hochstrasser and T. Y. Li, *J. Mol. Spectrosc.*, **41**, 297 (1972).
114. P. M. Rentzepis, *Photochem. Photobiol.*, **8**, 579 (1968).
115. P. M. Rentzepis, *Science*, **169**, 239 (1970).
116. P. M. Rentzepis, J. Jortner, and R. P. Jones, *Chem. Phys. Lett.*, **4**, 599 (1970).
117. D. Huppert, J. Jortner, and P. M. Rentzepis, *J. Chem. Phys.*, **56**, 4826 (1972).
118. E. Drent, G. Makkes van der Deijl, and P. J. Zandstra, *Chem. Phys. Lett.*, **2**, 526 (1968).
119. P. Wirth, S. Schneider, and F. Dorr, *Chem. Phys. Lett.*, **42**, 482 (1976).
120. J. P. Heritage and A. Penzkofer, *Chem. Phys. Lett.*, **44**, 76 (1976).
121. E. P. Ippen, C. V. Shank, and R. L. Woerner, *Chem. Phys. Lett.*, **46**, 20 (1977).
122. G. Eber, S. Schneider, and F. Doerr, *J. Photochem.*, **7**, 91 (1977).
123. E. C. Lim, in *Excited States*, Vol. 3, E. C. Lim, Ed., Academic Press, New York, 1976, and references therein.
124. R. S. Becker, *Theory and Interpretation of Fluorescence and Phosphorescence*, Wiley, New York, 1969, and references therein.
125. M. A. El Sayed and M. Kasha, *Spectrochim. Acta*, **15**, 758 (1959).

126. V. L. Ermolaev and I. P. Kotlyar, *Opt. Spectrosc. USSR*, **9**, 183 (1960).
127. Y. Hirata and I. Tanaka, *Chem. Phys. Lett.*, **41**, 336 (1976).
128. V. Sundstrom, P. M. Rentzepis, and E. C. Lim, *J. Chem. Phys.*, **66**, 4287 (1977).
129. Y. Hirata and I. Tanaka, *Chem. Phys. Lett.*, **43**, 568 (1976).
130. P. M. Rentzepis, *Science*, **169**, 239 (1970).
131. A. Nitzan, J. Jortner, and P. M. Rentzepis, *Chem. Phys. Lett.*, **8**, 445 (1971).
132. R. M. Hochstrasser, H. Lutz, and G. W. Scott, *Chem. Phys. Lett.*, **24**, 162 (1974).
133. R. W. Anderson, Jr., R. M. Hochstrasser, H. Lutz, and G. W. Scott, *Chem. Phys. Lett.*, **28**, 153 (1974).
134. D. Magde, B. A. Bushaw, and M. W. Windsor, *IEEE J. Quantum Electron.*, **QE-10**, 394 (1974).
135. M. Gouterman, in *The Porphyrins*, D. Dolphin, Ed., Academic Press, New York, in press.
136. M. Gouterman, F. P. Schwarz, P. D. Smith, and D. Dolphin, *J. Chem. Phys.*, **59**, 676 (1973).
137. G. P. Gurinovich and B. M. Jagarov, in *Luminescence of Crystals, Molecules and Solutions*, F. Williams, Ed., Proc. Intern. Conf. Luminescence, Leningrad, Aug. 1972, Plenum, New York, 1973.
138. J. B. Callis, M. Gouterman, and J. D. S. Danielson, *Rev. Sci. Instrum.*, **40**, 1599 (1969).
139. A. D. Kirk, P. E. Hoggard, G. B. Porter, M. G. Rockley, and M. W. Windsor, *Chem. Phys. Lett.*, **37**, 199 (1976).
140. G. B. Porter, in *Concepts of Inorganic Photochemistry*, A. W. Adamson and P. D. Fleischauer, Eds., Wiley, New York, 1975, p. 37, and references therein.
141. F. V. Zinato, in *Concepts of Inorganic Photochemistry*, A. W. Adamson and P. D. Fleischauer, Eds., Wiley, New York, 1975, p. 143, and references therein.
142. S. C. Pyke, M. W. Windsor, G. B. Porter, and A. D. Kirk, 32nd Annual Northwest Regional Meeting of the American Chemical Society, Portland, Oregon, June 15–17, 1977, Abstract #156.
143. A. Laubereau, D. von der Linde, and W. Kaiser, *Phys. Rev. Lett.*, **28**, 1162 (1972).
144. A. Laubereau, *Chem. Phys. Lett.*, **27**, 600 (1974).
145. S. F. Fischer and A. Laubereau, *Chem. Phys. Lett.*, **35**, 6 (1975).
146. A. Laubereau, L. Kirschner, and W. Kaiser, *Opt. Commun.*, **9**, 182 (1973).
147. K. Spanner, A. Laubereau, and W. Kaiser, *Chem. Phys. Lett.*, **44**, 88 (1976).
148. P. R. Monson, S. Patumtevapibal, K. J. Kaufmann, and G. W. Robinson, *Chem. Phys. Lett.*, **28**, 312 (1974).
149. D. Ricard, W. H. Lowdermilk, and J. Ducuing, *Chem. Phys. Lett.*, **16**, 617 (1972).
150. G. Mourou and M. M. Malley, *Chem. Phys. Lett.*, **32**, 476 (1975).
151. E. P. Ippen and C. V. Shank, *Opt. Commun.*, **18**, 27 (1976).

152. A. Penzkofer, W. Falkenstein, and W. Kaiser, *Chem. Phys. Lett.*, **44**, 82 (1976).
153. W. Kaiser and A. Laubereau, in *Proceedings of the 2nd International Conference on Laser Spectroscopy, Megine, France*, S. Haroche, J. C. Pebay-Peyroula, T. W. Hänsch, and S. E. Harris, Eds., Springer-Verlag, Berlin, 1975, p. 380.
154. T. J. Chuang, G. W. Hoffman, and K. B. Eisenthal, *Chem. Phys. Lett.*, **25**, 201 (1974).
155. R. M. Noyes, *J. Chem. Phys.*, **22**, 1349 (1954); *J. Am. Chem. Soc.*, **78**, 5486 (1956).
156. R. M. Noyes, *Z. Elektrochem.*, **64**, 153 (1960).
157. R. W. Anderson, Jr., and R. M. Hochstrasser, *J. Phys. Chem.*, **80**, 2155 (1976).
158. D. A. Weirsma and J. Kommandeur, *Mol. Phys.*, **13**, 241 (1967).
159. T. Shida and A. Kira, *J. Phys. Chem.*, **73**, 4315 (1969).
160. D. A. Weirsma, J. H. Lichtenbelt, and J. Kommandeur, *J. Chem. Phys.*, **50**, 2794 (1969).
161. K. K. Smith, J. Y. Koo, G. B. Schuster, and K. J. Kaufmann, *Chem. Phys. Lett.*, **48**, 267 (1977).
162. N. J. Turro, P. Lechtken, A. Lyons, R. R. Hautala, E. Carnahan, and T. J. Katz, *J. Am. Chem. Soc.*, **95**, 2035 (1973).
163. P. Lechtken and N. J. Turro, *Angew. Chem. Int. Ed.*, **12**, 314 (1973).
164. N. J. Turro and P. Lechtken, *J. Am. Chem. Soc.*, **94**, 2886 (1972).
165. A. J. Campillo and S. L. Shapiro, in *Ultrashort Light Pulses*, S. L. Shapiro, Ed., Springer-Verlag, New York, 1977, p. 317.
166. D. Holten and M. W. Windsor, *Ann. Rev. Biophys. Bioeng.*, **7**, 189 (1978).
167. A. Yu. Borisov and M. D. Il'ina, *Biochim. Biophys. Acta*, **305**, 364 (1973).
168. H. Merkelo, J. H. Hammond, S. R. Hartman, and Z. I. Derzko, *J. Luminescence*, **1/2**, 502 (1970).
169. M. Seibert and R. R. Alfano, *Biophys. J.*, **14**, 269 (1974).
170. A. J. Campillo, R. C. Hyer, V. H. Kollman, S. L. Shapiro, and H. D. Sutphin, *Proc. Natl Acad. Sci. USA*, **74**, 1997 (1977).
171. A. J. Campillo, R. C. Hyer, T. Monger, W. W. Parson, and S. L. Shapiro, *Proc. Natl. Acad. Sci. USA*, **74**, 1997 (1977).
172. G. S. Beddard and G. Porter, *Biochim. Biophys. Acta*, **462**, 63 (1977).
173. A. J. Campillo, V. H. Kollman, and S. L. Shapiro, *Science*, **193**, 227 (1976).
174. D. Mauzerall, *J. Phys. Chem.*, **80**, 2306 (1976).
175. J. C. Hindman, R. Kugel, A. Svirmickas, and J. J. Katz, *Proc. Natl. Acad. Sci. USA*, **74**, 5 (1977).
176. M. D. Hirsch, M. A. Marcus, A. Lewis, H. Mahr, and N. Frigo, *Biophys. J.*, **16**, 1399 (1976).
177. W. Yu, P. P. Ho, R. R. Alfano, and M. Seibert, *Biochim. Biophys. Acta*, **387**, 159 (1975).
178. R. S. Knox, in *Bioenergetics of Photosynthesis*, R. Govindjee, Ed., Academic Press, New York, 1974.

179. G. F. W. Searle, J. Barber, L. Harris, G. Porter, and C. J. Tredwell, *Biochim. Biophys. Acta.*, **459**, 390 (1977).
180. R. K. Clayton, *Ann. Rev. Biophys. Bioeng.*, **2**, 131 (1973).
181. S. C. Straley, W. W. Parson, D. Mauzerall, and R. K. Clayton, *Biochim. Biophys. Acta*, **305**, 597 (1973).
182. K. J. Kaufmann, P. L. Dutton, T. L. Netzel, J. S. Leigh, and P. M. Rentzepis, *Science*, **188**, 1301 (1975).
183. W. W. Parson, R. K. Clayton, and R. J. Cogdell, *Biochim. Biophys. Acta*, **387**, 265 (1975).
184. M. G. Rockley, M. W. Windsor, R. J. Cogdell, and W. W. Parson, *Proc. Natl. Acad. Sci. USA*, **72**, 2251 (1975).
185. J. Fajer, D. C. Brune, M. S. Davis, A. Forman, and L. D. Spaulding, *Proc. Natl. Acad. Sci. USA*, **72**, 4956 (1975).
186. J. Fajer, M. S. Davis, D. C. Brune, L. D. Spaulding, D. C. Borg, and A. Forman, *Brookhaven Symp. Biol.*, **28**, 74 (1977).
187. D. Holten, M. W. Windsor, W. W. Parson, and M. Gouterman, *Photochem. Photobiol.*, in press.
188. G. E. Busch, M. L. Applebury, A. A. Lamola, and P. M. Rentzepis, *Proc. Natl. Acad. Sci. USA*, **69**, 2802 (1972).
189. T. Kobayashi, H. Ohtani, T. Yoshizawa, and S. Nagakura, paper presented at 26th IUPAC Conference, September 1977, Tokyo, Japan.
190. R. Lozier, R. Bogomolni, and W. Stoeckenius, *Biophys. J.*, **15**, 955 (1975).
191. T. Yoshizawa, in *Handbook of Sensory Physiology*, Vol. VIII/1, H. J. A. Dartnall, Ed., Springer-Verlag, New York, 1972, p. 146.
192. R. R. Alfano, W. Yu, R. Govindjee, B. Cecher, and T. G. Ebrey, *Biophys. J.*, **16**, 541 (1976).
193. K. J. Kaufmann, P. M. Rentzepis, W. Stoeckenius, and A. Lewis, *Biochem. Biophys. Res. Commun.*, **68**, 1109 (1976).
194. C. V. Shank, E. P. Ippen, and R. Bersohn, *Science*, **193**, 50 (1976).
195. S. L. Shapiro, A. J. Campillo, V. H. Kollman, and W. B. Goad, *Opt. Commun.*, **15**, 308 (1975).
196. D. Holten, M. W. Windsor, W. W. Parson and J. P. Thornber, *Biochim. Biophys. Acta*, **501**, 112 (1978).

Phil. Trans. R. Soc. Lond. A **298**, 335–349 (1980)
Printed in Great Britain

Picosecond studies of primary charge separation in bacterial photosynthesis

By M. W. Windsor and D. Holten
Department of Chemistry, Washington State University, Pullman, Washington 99164, *U.S.A.*

With the aid of light and two coupled photosystems containing chlorophyll, green plants remove electrons from water, releasing O_2, and convey them to CO_2, reducing it to simple sugars and thence to carbohydrate. Photosynthetic bacteria operate more simply, employing a single photosystem. They reduce CO_2 but require substrates more easily oxidized than water, e.g. sulphide and succinate. Bacterial reaction centres free of the bulk chlorophyll that performs the light-harvesting function can be isolated. The reaction centre is the site where the electronic energy of the photoexcited molecule is converted to chemical potential. Thus bacterial reaction centres are ideal subjects for studying the details of this process by kinetic spectroscopy. Picosecond laser studies show that an electron is removed from the primary donor (a chlorophyll dimer) in 4 ps or less and transferred in several stages to the ubiquinone acceptor in *ca.* 200 ps. Remarkably, reverse electron transfer is several orders of magnitude slower. The paper discusses how Nature may have accomplished this.

1. Introduction

During the past 5 years, with the aid of new spectroscopic techniques based on ultra-short laser pulses, it has become possible to study the details of the primary charge separation process in bacterial photosynthesis (see Holten & Windsor (1978) for a recent review). Spectroscopic and kinetic studies with picosecond laser pulses have shown that electron transfer from the primary donor (a 'special pair' of chlorophyll molecules) to the ubiquinone acceptor takes place in about 200 ps. Even so, the transfer does not occur in a single step. Two or more stages are involved and the very first step is found to be exceedingly fast (less than 10 ps and perhaps as little as 4 ps). These times are several orders of magnitude shorter than had previously been assumed. Still more remarkable is the observation that the reverse electron transfer is three or more orders of magnitude slower, leading to a quantum efficiency very close to 100% for the primary charge separation. It is an intriguing challenge to seek to understand how Nature has accomplished this. Comparison of the new picosecond data on reaction centres of photosynthetic bacteria with the results of similar studies of electron transfer in model systems involving molecular solutions of photosynthetic pigments and various electron acceptors *in vitro* has been helpful in this regard. The purpose of this paper is to review the experimental data and discuss possible theoretical models. Some background on the primary events of photosynthesis will be given, with a brief account of the experimental techniques developed in our laboratory for picosecond spectroscopic studies.

2. Picosecond flash photolysis and spectroscopy

This is a direct extension to the picosecond region of the well known microsecond technique of flash photolysis with rare-gas filled flashlamps (Norrish & Porter 1949; Porter 1950). A mode-locked laser provides the picosecond excitation pulse. The spectroscopic flash for monitoring

purposes is a picosecond continuum pulse obtained by focusing a portion of the laser pulse into a variety of optical media. A variable time delay (from a few picoseconds to several nanoseconds) between the two pulses is obtained by changing the difference in optical path length between the two beams. The apparatus developed by Magde & Windsor (1974) is shown in figure 1. A mode-locked Nd:glass laser, with single pulse selection (s.p.s.) and one stage of amplification, produces a 5–8 ps duration pulse of 15–20 mJ energy at 1060 nm. Single pulse selection is accomplished by using an optically triggered spark gap and Pockels cell. Passage of the 1060 nm pulse through a suitably orientated crystal of potassium deuterium phosphate gives second harmonic generation (s.h.g.) at 530 nm with a conversion efficiency of about 15%.

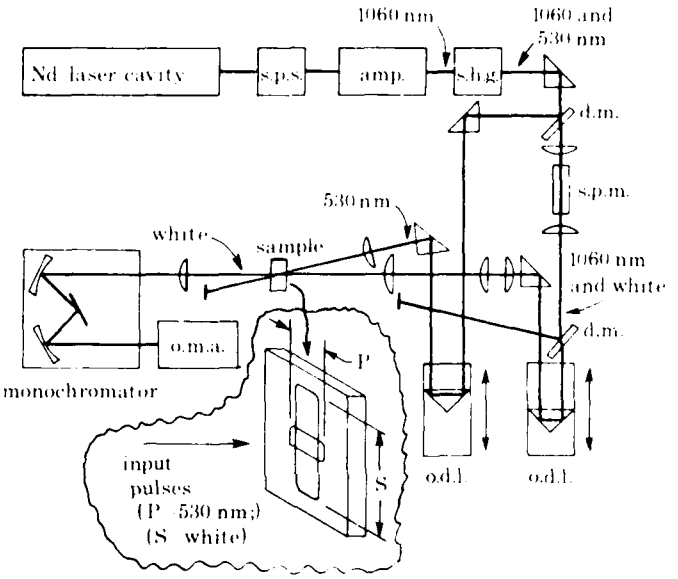

FIGURE 1. Diagram of apparatus for picosecond flash photolysis and spectroscopy.

The 530 and 1060 nm pulses are separated by a dichroic mirror that selectively reflects the 530 nm radiation while transmitting the 1060 nm pulse. After passage through an optical delay line (o.d.l.) consisting of a rooftop prism mounted on an optical rail, the 530 nm pulse (P for photolytic) impinges on the sample, usually a cuvette 1 or 2 mm thick. Any 530 nm light transmitted by the sample is intercepted by an optical stop. As a further precaution against scattered P light entering the spectrograph, it is arranged that the P beam makes a slight angle (10°) with the monitoring (S for spectroscopic) beam as in figure 1.

The key to the technique of picosecond flash photolysis is the picosecond continuum pulse. This is obtained by focusing the residual 1060 nm radiation into a cell 10 cm long containing carbon tetrachloride, CCl_4. Self-focusing and filamentation occur and a small fraction (*ca.* 0.1%) of the incident beam is converted into a broad continuum. The continuum retains both the short pulse duration and much of the spatial collimation of the pumping pulse. Thus, to all intents and purposes, we have a white-light laser. Another dichroic beam splitter separates the essentially undiminished 1060 nm pulse from the continuum. The 1060 nm pulse can be used for sample excitation or can be blocked, as in figure 1. The continuum (S) passes through a variable optical delay line and arrives at the sample at a predetermined time relative to the P

pulse. By adjusting the two o.d.ls the time interval between S and P can be varied between zero and about 9 ns. Negative delays (i.e. S arrives before P) are also readily obtainable. These are useful in providing a record of the sample before excitation for control purposes and correspond to 'infinite delay' shots in conventional flash photolysis.

Optical density changes induced in the sample by the P pulse are measured in the following way. The inset at bottom centre of figure 1 shows the cross-sectional geometry of the two beams at the sample. The details of the geometry in this region are very important. The key point is that the probe beam is elongated along its vertical axis by means of a cylindrical lens so that it samples simultaneously the excited volume in the centre and unexcited *reference* volumes both above and below the excited region. The cross section of the excited volume can be adjusted in the range 1 mm to about 5 mm by means of a lens. The entire area is then imaged at about 1:3 diminution on to the slit of a spectrograph and, ultimately, on to either photographic film or a vidicon detector coupled to an optical multichannel analyser (o.m.a.). The absorption spectrum of a transient intermediate then appears sandwiched between two reference spectra of the unexcited sample, as in figure 2*a*. By having a reference spectrum both above and below a purported transient spectrum, we greatly reduce the risk of misinterpreting random fluctuations in the intensity of the continuum as genuine transient effects. For comparison we provide in figure 2*b* the photographic record of the decay of triplet 1,2-benzanthracene in solution (Porter & Windsor 1958) taken by conventional flash photolysis in the microsecond-millisecond region. Taken together, these two figures show how in two decades, aided by the laser, the time resolution of flash photolysis has been extended by six decades from 10^{-6} to 10^{-12} s.

The photographic method is almost essential for exploratory survey work on a previously uncharacterized system. It provides wide spectral coverage in a single shot, and the time history of whatever transient changes are present can be seen at a glance on a single film or plate by taking a short sequence of shots at different time delays. This is demonstrated in figure 2*a*, which shows picosecond flash photolysis results for octaethylporphinatotin(IV) dichloride (OEP $SnCl_2$ Magde *et al.* 1974*b*). The value of the wide spectral coverage provided by the photographic record is particularly evident here. The photograph clearly shows two regions of excited state absorption, a short-lived transient with a main absorption peak at *ca.* 450 nm and absorption extending to longer wavelengths, and a much longer-lived absorption in the blue with a peak at about 430 nm. Additional studies with the vidicon enable these two transient absorptions to be spectrally characterized and attributed respectively to the excited singlet S_1 state and the triplet T_1 state of the porphyrin. Broad-band picosecond spectra such as these are very helpful in choosing suitable wavelengths for subsequent quantitative kinetic measurements.

Although the photographic method is of great value for survey work, it is not the most convenient method for determining precise kinetic data. Therefore, once the photographic spectra reveal the best wavelengths to monitor, we replace the camera with a slit and use photoelectric detection, normally a Princeton Applied Research (PAR) 1205B vidicon tube coupled to a 500-channel optical multichannel analyzer (o.m.a.). We then monitor only a single narrow band of wavelengths, using the (o.m.a.) to obtain an intensity profile along the length of the slit. This is exactly equivalent to a densitometer trace taken vertically across the photographic spectrogram. The natural logarithm of the ratio of the measured intensity in the reference regions (averaged over the portions above and below) to that in the central excited region gives the absorbance change (ΔA) due to the transient absorption (or bleaching). Usually four or five

shots are taken at a given wavelength and time delay to obtain an average value and the standard deviation. Repeated measurements at the same wavelength and different time delays provide a plot from which the decay kinetics can be determined. By keeping the time delay constant and changing the wavelength, the different spectra at a given time delay can be obtained. In most cases, because of spectral overlap of the ground state and excited state

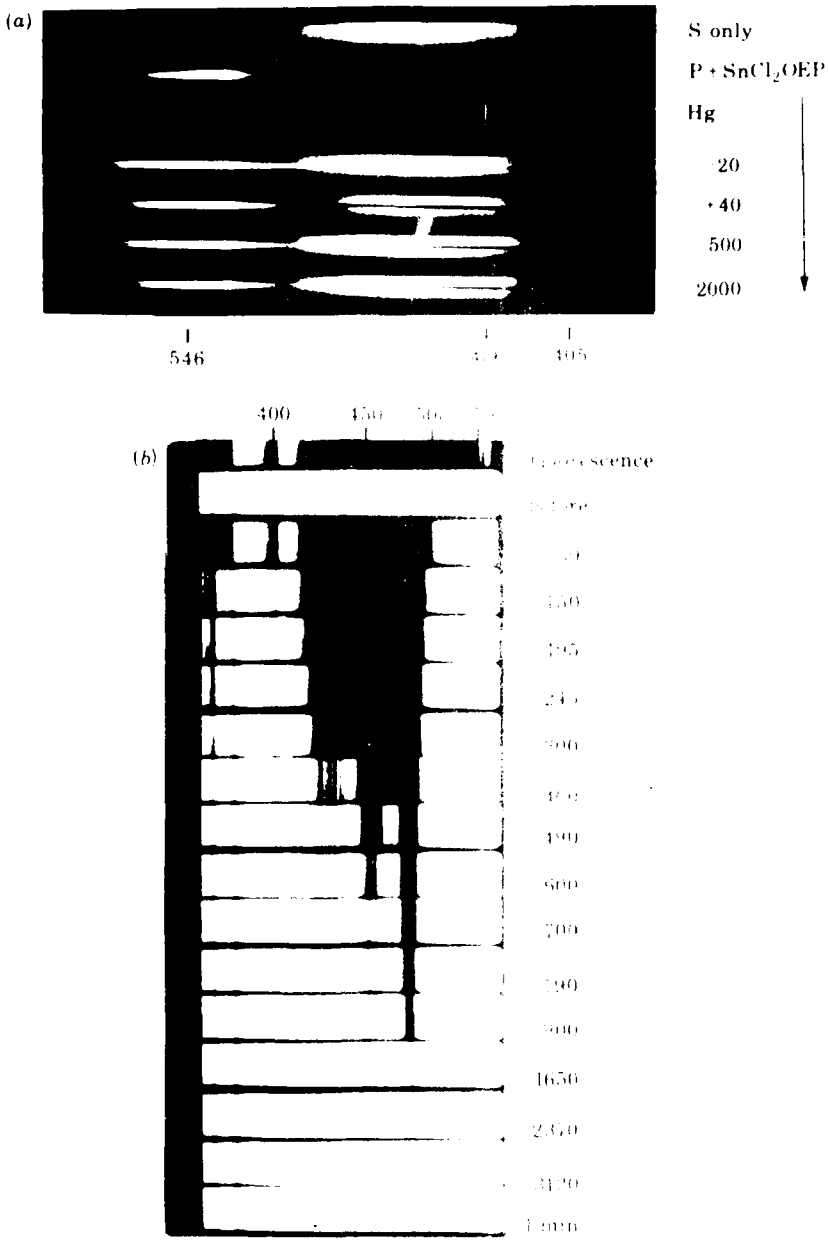

FIGURE 2. (*a*) Picosecond flash photolysis of tin dichlorooctaethyl porphyrin, showing decay of excited singlet absorption (short-lived) and triplet absorption (longer-lived). (*b*) Conventional flash photolysis of 1,2-benzanthracene in viscous paraffin solution showing decay of triplet absorption. Time scale in microseconds.

absorption regions and because, at the laser powers used, significant depletion of the ground state is common, the spectrum obtained must be considered a 'difference spectrum' that represents the sum of the changes caused by ground state depletion and production of the excited state. This is especially true of photosynthetic systems in which spectral overlap of the various constituents pigments and associated molecules is common. By detailed studies it is usually possible to find wavelengths at which kinetic studies of one species can be made without interference by optical changes due to another species (see Rockley *et al.* 1975).

Very recently, we have interfaced our picosecond flash photolysis apparatus to a dedicated microprocessor (Holten *et al.* 1979*a*; Holten & Windsor 1980). This makes it possible to obtain picosecond transient spectra over a spectral range of 300 nm with a single laser shot. It also provides the advantage of computer processing of the experimental data. All of the experimental results described in this paper, however, were obtained by the more laborious point-by-point technique.

3. Background on photosynthesis†

In green plants, sunlight is absorbed by an antenna or light-harvesting system comprising many hundreds of chlorophyll molecules complexed to protein and situated in a lipid bilayer membrane. The excitation energy of electronically excited chlorophyll is rapidly conveyed by non-radiative mechanisms in times that range from 10 ps to about 1 ns, dependent upon species, to a special chlorophyll complex that acts as a trap. This is situated in a reaction centre (RC) complexed to other pigments and protein and to an electron acceptor, normally a quinone. Within the RC, charge separation takes place, the special chlorophyll complex being oxidized to a cation while the acceptor receives an electron and is converted to an anion. In this manner the energy of solar photons, transferred from the antenna to the RC as electronic molecular excitation, is captured within the RC as chemical potential. In green plants two coupled photosystems, called PS1 and PS2, cooperate to produce a strong oxidant capable, via an as yet poorly understood series of reactions, of oxidizing water to molecular oxygen and a strong reductant capable of reducing CO_2 to simple sugars and eventually carbohydrate. Described in another way, we can say that photosynthesis removes electrons from H_2O, thus releasing O_2, pumps them uphill in redox potential with the aid of two boosts from solar photons and finally places them on CO_2, thus allowing it to pick up hydrogen ions and be converted to a simple sugar. On a scale of redox potential this is illustrated in figure 3*a*.

Photosynthetic bacteria, like green plants, also contain an antenna system that harvests incident photons and transfers the excitation to an RC, but, unlike plants, bacteria employ only a single photosystem which more closely resembles PS1 in plants (figure 3*b*). The primary oxidant has a potential of about +0.45 V. This is insufficient to oxidize water, and bacteria require more easily oxidizable substrates, e.g. sulphide, succinate or thiosulphate. The primary reductant, as in plants, is coupled to the synthesis of ATP and the reduction of CO_2. A further advantage of photosynthetic bacteria is that, by suitable detergent treatments, RC preparations free of antenna pigments can be obtained (Clayton 1973). The presence of a single photosystem and the availability of isolated reaction centres have made bacterial RCs the preferred choice of most investigators for detailed studies of the process of primary charge separation. The majority of studies have been made on RCs of two species, *Rhodospeudomonas sphaeroides* and *Rhodospeudomonas viridis*, although other species such as *R. rubrum*, *C. vinosum* and *C. minutissimum* have been

† See Holten & Windsor (1978) for a more detailed account.

used on occasion. Reaction centres of *R. sphaeroides* contain four molecules of bacteriochlorophyll (BChl), two of the magnesium-deficient analogue, bacteriophaeophytin (BPh), one ubiquinone (UQ), one non-haem iron atom and three different proteins in a 1:1:1 ratio and of relative molecular masses 20000, 22000 and 28000 (Clayton 1973). These components are packaged in a lipid bilayer membrane with the primary UQ situated at or near the membrane surface with ready access to the aqueous medium. An 'artist's conception' of a possible arrangement is shown in figure 4. Reaction centres of *R. viridis* contain a similar complement of pigments and proteins, but the chlorophyll absorption bands are shifted to longer wavelength. The major band is at 960 nm in *R. viridis* compared with 870 nm in *R. sphaeroides*. RCs of *R. viridis* also retain bound cytochrome *C*, whereas *R. sphaeroides* RCs lose their cytochromes during the preparation procedure. This is an advantage for certain picosecond experiments, as will be seen later.

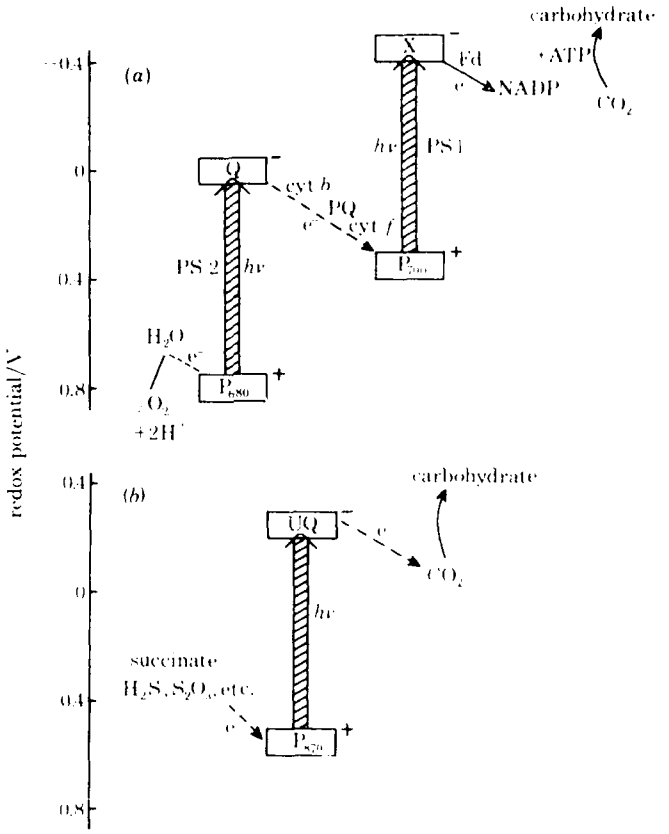

FIGURE 3. (*a*) Z-scheme for green plant photosynthesis; (*b*) similar scheme for bacterial photosynthesis.

4. PICOSECOND STUDIES OF ELECTRON TRANSFER IN BACTERIAL REACTION CENTRES

4.1. *Rhodopseudomonas sphaeroides*

In RCs of *R. sphaeroides*, the longest wavelength absorption peak lies at 870 nm. In recognition of this the unexcited state of the RC is often characterized as P_{870} or, more simply, P. The absorption spectrum also displays bands near 540 and 760 nm attributable to BPh and bands

near 600 and 800 nm attributable to BChl. The 870 nm band is strongly bleached upon illumination and a weaker absorption band characteristic of P^+ appears in the region of 1250 nm. This 1250 nm band can also be produced by oxidizing the RCs either chemically with, for example, potassium ferricyanide, or electrochemically. The 600 nm band bleaches to a lesser extent than the 870 nm band and the 800 nm band undergoes a slight blue shift to 798 nm. These changes, together with linear and circular dichroism measurements and e.s.r. studies, lead to the belief that two of the four BChl molecules form a closely coupled dimer or 'special pair' and that it is this species that, on oxidation, loses an electron to produce the primary oxidant P^+. The other two BChl molecules give rise to a component of the 800 nm band. The 540 nm band of BPh can be resolved at 77 K into two components at 532 and 544 nm, suggesting that the two PBh are situated in different environments (Clayton & Yamamoto 1976). See Holten & Windsor (1978) for a more detailed account.

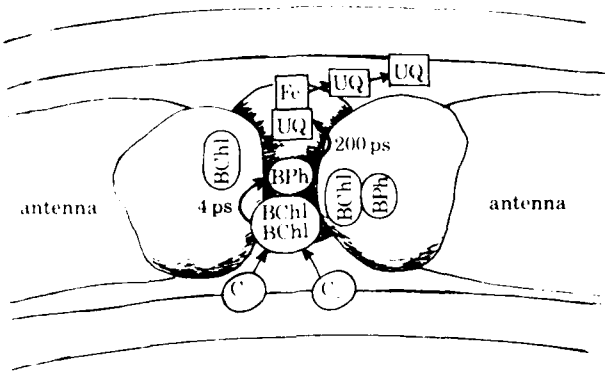

FIGURE 4. Artist's conception of bacterial reaction centre showing characteristic times of the early events in the primary charge separation.

The first attempts to observe transient intermediates in photosynthetic bacteria used RCs of *R. sphaeroides* poised at an artificially low redox potential by the presence of excess sodium dithionite (Parson *et al.* 1975). Lowering the redox potential in this manner, by reducing the UQ electron acceptor (often also denoted by X^-, would be expected to frustrate the transfer of an electron from any antecedent intermediate, thus increasing its lifetime. Indeed, with excitation by 20 ns laser flashes at 694 or 834 nm, the above authors observed the immediate (less than 20 ns) formation of a spectroscopic intermediate, which they called P^F, with an exponential decay time of about 15 ns. The quantum yield of formation of P^F is close to unity both at 295 K and at 15 K. As P^F decays, another intermediate, called P^B, appears which has a half-time of 6 μs at 295 K and 120 μs at 15 K. At 295 K its quantum yield of formation is low (0.1), but this value rises to unity at 15 K. The spectrum of P^B suggests that it is the triplet state of the BChl dimer. The processes described above are summarized in scheme (*b*) of figure 5. The other two schemes summarize the results of picosecond studies shortly to be described.

The rapid formation of P^F, and its accumulation in high yield when normal photochemistry is blocked, suggested that it might be an intermediate in the normal electron transfer reaction. But, then again, it might have been an artefact of the artificially reducing conditions used to facilitate its detection. To resolve this situation, studies of RCs under normal physiological conditions, i.e. with the acceptor X in its normal *unreduced* state, were needed. Picosecond laser

studies provided the improved time resolution, Independent results from two laboratories (Kaufmann *et al.* 1975; Rockley *et al.* 1975) showed that in RCs of *Rps. sphaeroides* under these conditions, P^F could be spectroscopically identified. It appeared essentially immediately (less than 10 ps) on excitation with an 8–10 ps laser pulse, and exhibited a lifetime of about 200 ps. Kinetic studies showed that an absorbance decrease at 610 nm characteristic of P^+ appeared with the same time constant as the disappearance of P^F. These results demonstrated that P^F was not an artefact of the conditions used in the earlier nanosecond experiments, but was indeed a direct intermediate in the electron transfer reaction that culminates in the oxidation of P_{870} and the reduction of the acceptor X. They also showed that both steps in the two-stage transfer of the electron were exceedingly and perhaps unexpectedly rapid.

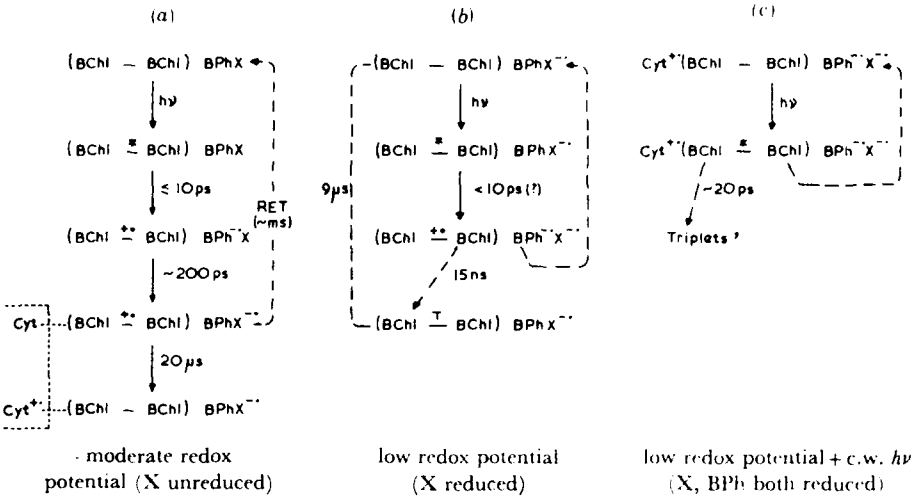

FIGURE 5. Scheme of early events in bacterial photosynthesis.

Attention now centred on the structural identity of the intermediate P^F. Rockley *et al.* (1975) compared their experimental spectrum with the sum of the absorbance changes that accompany the conversion of free BChl either to its cation radical, $BChl^{+\cdot}$ or its anion radical $BChl^{-\cdot}$. The calculated spectrum showed a fair measure of agreement, predicting the observed bleaching of bands near 380 and 600 nm and the appearance of new bands near 420, 500 and 650 nm, but did not predict the observed bleaching of the BPh bands. Such a procedure could be expected to give at best a rough approximation because it neglects interaction effects between the two molecules that form the biradical and also takes no account of the significant shift of the longest wavelength band of BChl from 770 nm in molecular solution to 870 nm in the RC. Nevertheless a surprising measure of agreement could be seen, as is shown in figure 6*a* and *b*. Subsequently Fajer *et al.* (1975) were able to obtain even better agreement by using a simulated spectrum composed of the sum of the absorbance changes that accompany chemical oxidation of RC (ΔP_{870}) and the reduction of BPh to $BPh^{-\cdot}$, which latter species had just been produced electrochemically and spectroscopically characterized in his laboratory. The comparison is shown in figure 6*c*. Further picosecond studies by Dutton *et al.* (1975) showed that the 1250 nm absorption band appeared promptly (less than 10 ps) upon excitation, rather than with the 200 ps risetime that would be characteristic of its formation from P^F. This led to the conclusion that the intermediate P^F must already contain the dimer cation radical P^+ as part of its structure, and lent

further support to the assignment of Fajer *et al.* Thus it is now believed that P^F has the structure $(BChl)_2^{+}\cdot BPh^{-}\cdot X$ and that the electron that takes up temporary residence on the BPh subsequently moves to X in a time of about 200 ps. These events are summarized in scheme (*a*) of figure 5.

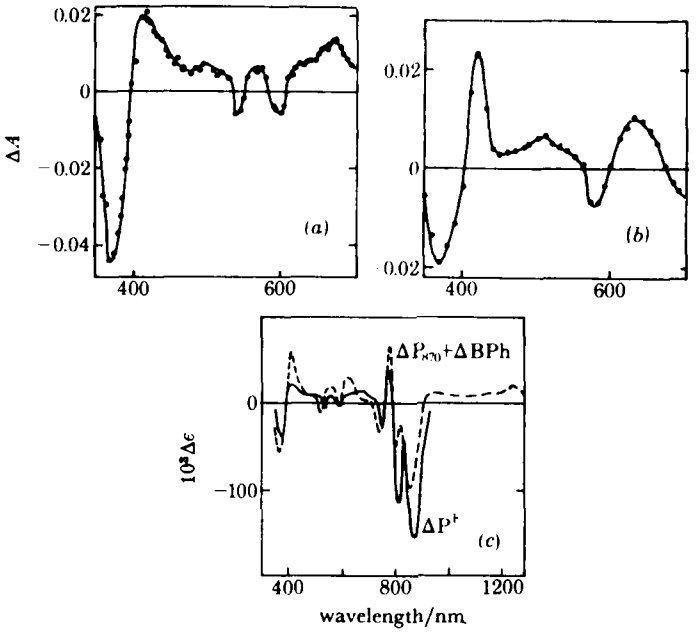

FIGURE 6. (*a*) Absorbance changes accompanying the photochemical formation of state P^F. (*b*) Sum of absorbance changes for $BChl^+$ and $BChl^-$ made electrochemically. (*c*) Comparison of laser-induced optical changes, ΔP^F, with sum of changes for ΔP_{870} plus ΔBPh^-.

Although much insight has been gained, the picture is still incomplete. Why has Nature placed a second BPh and two additional BChl molecules (the so-called P_{800} chlorophylls) in the RC? The low-temperature studies of BPh mentioned earlier suggest that only the longer-wavelength BPh is involved in the formation of P^F. Studies of *C. vinosum* (Tiede *et al.* 1976*a*), *R. viridis* (Tiede *et al.* 1976*b*) and *C. minutissimum* (Shuvalov & Klimov 1976) also support this conclusion. Perhaps the other two BChl molecules serve to 'solvate' one of the BPh molecules, as we have hinted in figure 4, thus facilitating the passage of an electron from $(BChl)_2$, or perhaps they help delocalize the transferred electron, thus hindering the back transfer. The first two of the above three studies cited also found partial bleaching at 800 and 595 nm, suggesting involvement of the P_{800} chlorophylls. It has also been suggested (Fajer *et al.* 1975) that the additional pigment molecules may have a role in coupling a part of the apparent energy losses that accompany the transfer of the electron to structural changes in the membrane that could, via Mitchell's chemiosmotic theory, be usefully harnessed to ATP production.

The identification of the acceptor X as ubiquinone (UQ) is supported by experiments by Kaufmann *et al.* (1976) showing that RCs depleted of UQ behave as though no acceptor is present. The state P^F lives for a time in excess of 1 ns. Addition of UQ restores the normal 200 ps kinetics.

4.2. *Rhodopseudomonas viridis*

Since the RC of *R. viridis* retains bound cytochromes, it offered the intriguing prospect of artificially prolonging the lifetime of the excited singlet state of the special pair P* that presumably must precede the first step in the charge separation. The rationale was to place RCs of *R. viridis* not only at low redox potential to keep X reduced but also under conditions of continual illumination to saturate electron transfer and maintain I (a complex involving BPh)

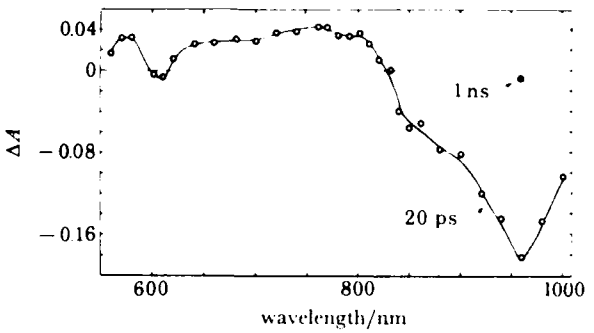

FIGURE 7. Difference spectrum accompanying formation of the excited singlet state, P*, of RCs of *R. viridis*.

also in the reduced state. The cytochromes would rereduce P^+ to P, leaving the system in the initial state, (BChl-BChl)-$BPh^{-\cdot}$ $X^{-\cdot}$, or more simply PI^-X^-, before picosecond excitation. Upon excitation, the reduced state of both I and X might be expected to frustrate electron transfer from P*, thus holding the system in the state $P^*I^-X^-$ for longer than usual. This scheme seems to have worked and we have observed, under these conditions, a spectroscopic intermediate that lives for about 20 ps (Holten *et al.* 1978*a*) (see figure 5*c*). At moderate redox potentials (figure 5*a*), corresponding to physiological conditions, the events observed closely parallel those found in *R. sphaeroides*. The P^F state is formed promptly and transfers an electron to X in about 230 ps. Netzel *et al.* (1977) found a prompt (less than 10 ps) rise of the 1310 nm band characteristic of P^+ in this species, in good agreement with our results. We also observe an additional step with 35 ps kinetics at 800–810 nm. At low redox potential (X reduced as in figure 5*b*), P^F lives for about 15 ns and decays, in part, to a longer-lived triplet state.

The difference spectrum corresponding to the conversion of P to P* under the 'super-reduced' conditions described above is shown in figure 7. The dominant feature is the bleaching of the 960 nm absorption band. Bleaching is present at 850 nm but drops to zero at 830 nm. The former band is characteristic of the special pair and the latter of the additional bacteriochlorophylls. These two bands are resolved in *R. viridis* but overlap in the 800 nm region in *R. sphaeroides*. These results support the conclusion that the primary donor in the RC is most likely the excited singlet state P* of a special pair of closely interacting BChl *b* molecules. However, interactions with the other two BChl *b* molecules are not excluded. E.s.r. and ENDOR studies (Fajer *et al.* 1977) suggest that the unpaired electron in P^+ is not shared equally by two identical molecules of BChl, as appears to be the case in *R. sphaeroides*. The spectral evidence also indicates that the intermediate acceptor I in *R. viridis* involves both BChl *b* and BPh *b* and that it is the BPh *b* component that is reduced when electron transfer from P* takes place.

4.3. *Additional studies on RCs*

We have attempted recently to elucidate further the early stages of the charge separation process with the aid of mode-locked continuous wave (c.w.) dye laser equipment capable of subpicosecond time resolution and with provision for monitoring over a wide range of wavelength with the use of a subpicosecond continuum (Holten *et al.* 1980*b*). These new results indicate that after excitation of RCs of *R. sphaeroides* at 610 nm (a wavelength absorbed predominantly by the primary donor $(BChl)_2$), an absorbance increase occurs at 672 nm (characteristic of P^F) with a risetime of 4 ps or less. Thus the electron must move from the excited state of the special pair P* to BPh within 4 ps. This value of the transfer time is consistent with the less than 10 ps result obtained in the single-pulse laser experiments. An opposing view is, however, presented by recent experiments of Shuvalov *et al.* (1978) on RCs of *R. rubrum*. Using a 25 ps pulse at 880 nm for excitation, they reported that bleaching occurs at 800 nm within 15 ps of excitation, whereas no prompt bleaching of the BPh bands is observed. The 800 nm bleaching recovers with a lifetime of 35 ± 5 ps and is accompanied by the formation of BPh^- as shown by bleaching at 748 nm. The state P^+BPh^- subsequently decays in 250 ± 50 ps. From these results the authors conclude that the electron 'appears to be extracted from P by BChl-800 which gives a radical anion, $BChl\text{-}800^{-\cdot}$. Transfer of the electron to BPh then occurs in a time of about 35 ps'. Our own studies, while not ruling out the participation of BChl-800 as an intermediary electron carrier, indicate that any such involvement must take place on a time scale not greater than 4 ps, since transfer to BPh to form the radical pair P^+BPh^- is essentially complete within this time. Further studies with the shorter (0.7 ps) pulses provided by the mode-locked dye laser and at additional excitation wavelengths, including 800 nm, would be helpful. It is also desirable that a comprehensive series of measurements be made on a single species of bacterium. Because of the flexibility of making measurements under normal, reduced and super-reduced conditions of the UQ acceptor, *R. viridis* is probably the best choice for such studies.

4.4. *Summary of results on RCs*

The finding of similar transient intermediates with similar kinetics in several species of bacteria suggests strongly that the composition and structure of the bacterial reaction centre have evolved to maximize the efficiency of the primary charge separation process. Those species that have been subjected to detailed study seem to parallel each other closely with regard to the composition of their RCs. We propose to assume that the component pigments and proteins in the various RCs each have a functional role to play in the process of charge separation. In defence of this we argue that it is unlikely that 'unnecessary baggage' would have survived more than a thousand million years of natural selection. Given this assumption, we believe that further insight into how the RC functions and how its functioning is related to its internal structure requires studies of electron transfer in a variety of model systems that seek either to mimic or omit various features present in the RC.

5. Picosecond studies of electron transfer in model systems

We have shown (Holten *et al.* 1976) that electron transfer from bacteriophaeophytin (BPh) to *p*-benzoquinone (Q) in molecular solution takes place predominantly via the triplet state of the donor. Figure 8 shows that in the presence of excess methyl iodide, which enhances inter-

system crossing i.s.c. in BPh by the heavy atom effect, the yield of the donor cation radical $BPh^{+\cdot}$ is greatly increased. Estimates of the half-cell potentials $BPh^{+\cdot}/BPh^{*}$ and $BPh^{+\cdot}/BPh^{T}$, the energy of the various collision complexes and the energy of the separated ions $BPh^{+\cdot}$ and $Q^{-\cdot}$ can be made (Gouterman & Holten 1977) and used to explain this observation (figure 9). In brief, we believe that both singlet and triplet charge transfer complexes $(BPh^{+\cdot}Q^{-\cdot})^{S}$ and $(BPh^{+\cdot}Q^{-\cdot})^{T}$ are formed from their respective collision complexes in less than 5 ps, but that the singlet complex suffers reverse charge transfer $(BPh^{+\cdot}Q^{-\cdot})^{S} \longrightarrow (BPh\ Q)$ in a time much shorter than that needed (*ca.* 230 ps) for the ion radicals to separate. The analogous process for the

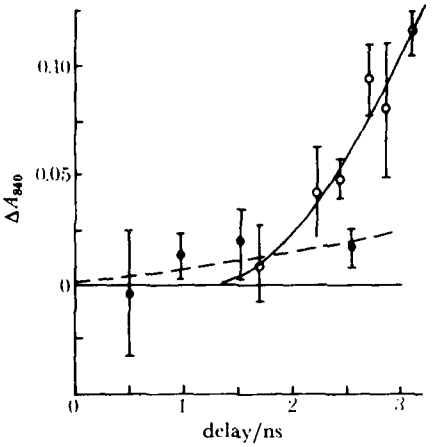

FIGURE 8. Enhancement of the yield of the cation radical $BPh^{+\cdot}$ by excess methyl iodide in the charge transfer *quenching of* BPh* by *p*-benzoquinone. ○, With 8 M MeI; ●, without MeI.

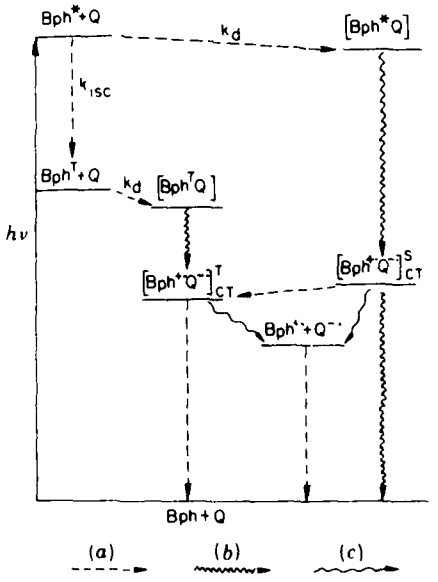

FIGURE 9. Proposed model for the bacteriophaeophytin (BPh), 40 mM *p*-benzoquinone (Q) and 8 M methyl iodide system, showing excited states and kinetic process. Here, k_d and k_{isc} are the rate constants for diffusion and intersystem crossing. The symbols S-CT and T-CT refer to singlet and triplet charge transfer complexes, respectively. (*a*) Processes slow because bimolecular or spin forbidden; (*b*) very fast spin allowed processes; (*c*) slower spin allowed processes.

triplet complex is spin forbidden so that, in the triplet case, ion separation competes favourably with quenching. Similar experiments in which benzoquinone is replaced by methyl viologen (MV^{2+}) or by *m*-dinitrobenzene (*m*-DNB) give results that support the above model. For both these systems, formation of the radical ions is energetically possible only from the excited singlet state BPh* and not from the triplet BPh^T. For *m*-DNB, BPh* is quenched but $BPh^{+\cdot}$ is not detectable. For MV^{2+} the quantum yield of $BPh^{+\cdot}$ is reduced to about 10%. Were it not for Coulombic repulsion assisting the separation of the radical ions $BPh^{+\cdot}$ and $MV^{+\cdot}$ in this case, the yield would doubtless be much lower.

6. Theoretical implications for charge separation in photosynthesis

If efficient charge separation in the molecular systems discussed above can occur only via the triplet state of the electron donor, how can efficient electron transfer in the photosynthetic system proceed via the excited singlet state of the primary donor? Furthermore, an important difference between RCs and molecular solutions is that in the former the donor and acceptor are constrained by their association with other pigment molecules, e.g. the P_{800} BChls and with protein. The radical ions are not free to move apart as they are in solution. This means that discrimination against reverse electron transfer from $BPh^{-\cdot}$ to $(BChl)_2^{+\cdot}$ must be even more effective in the RC. To account for the observed 100% quantum yield of the charge separation process, it must be assumed that this back reaction is about 100 times slower than the next forward step that transfers the electron from $BPh^{-\cdot}$ to UQ. Since the latter takes about 200 ps, the back electron transfer from $BPh^{-\cdot}$ in the RC must take 20 ns or longer. This reverse transfer is close to 10^4 times slower than the forward step (*ca.* 4 ps) from $(BChl)_2$ to BPh.

A possible explanation, based on our model system studies (Holten *et al.* 1978*b*, *c*) rests on the size of the molecule that functions as the initial electron acceptor. A comparatively small molecule, such as the benzoquinone used in our quenching studies of BPh in solution, would undergo a significant shape change on formation of the charge transfer complex BPh^+Q^-. Good Franck–Condon overlap of the vibrational wavefunctions between the singlet charge transfer state and the ground state facilitates fast internal conversion of the approximately 1 eV of electronic energy separating the two states into vibrational degrees of freedom (see figure 10). Thus the charge transfer complex formed from the excited singlet state of the electron donor is deactivated before separation of the charged radical ions can take place. The same situation would apply in the photosynthetic RC were it not that Nature has contrived to place a comparatively large molecule, BPh, as an intermediate electron acceptor between the primary donor and the eventual small molecule ubiquinone acceptor. X-ray crystallographic data on some porphyrins and recent resonance Raman measurements on BChl and BPh indicate that addition or removal of an electron from these comparatively large molecules causes only quite small changes in bond length and bond angles. The corresponding Franck–Condon factors are small (figure 10), and the back reaction is effectively inhibited. The second forward step takes the electron in about 200 ps from BPh to UQ. A significant shape change is expected for the conversion of UQ to UQ^-. However, although the Franck–Condon factors are favourable, the back conversion of $(BChl)_2{}^+BPh\ UQ^-$ to the $(BChl)_2BPh\ UQ$ ground state of the RC complex would involve the movement over a considerable distance of the electron back through the BPh to the $(BChl)_2$. Thus at this juncture physical separation of donor and acceptor supervenes to inhibit the back transfer.

The above model is speculative. Nevertheless it is valuable as a working hypothesis because it immediately suggests further experiments, the outcome of which may either disprove or modify the model. Of especial value would be studies of the quenching of BChl and synthetic BChl dimers in solution by acceptors of varying size. We plan to carry out such experiments when our instrumental developments make available suitable excitation wavelengths. An important step in this direction is the recent observation by Pellin *et al.* (1979) of a fast (less than 6 ps) high quantum yield electron transfer process in a model complex formed by covalently linking two molecules of pyrochlorophyll *a* with a primary alcohol derivative of phaeophytin *a*.

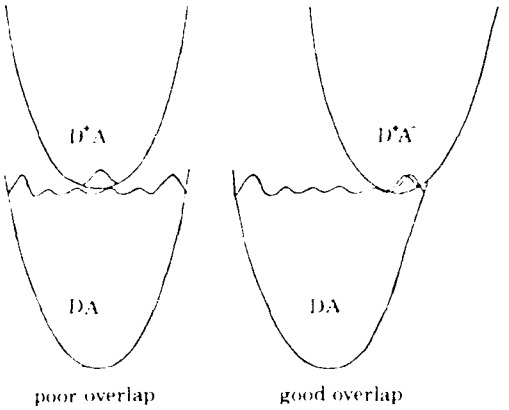

FIGURE 10. Franck Condon diagrams for small shape changes (poor overlap) and large shape changes (good overlap).

The above model does not account for the extremely high speed (*ca.* 4 ps) of the initial electron transfer step from $(BChl)_2$ to BPh. Favourable π-orbital overlap between the $(BChl)_2$ and one of the BPh, assisted by a preferred mutual orientation, perhaps induced by the proteins to which the pigments are complexed, may be responsible. It can be argued that the high speed of this step probably evolved as a means of preventing the excitation from 'hopping back' into the antenna system. Efficient trapping of antenna excitation by the reaction centres requires rapid transfer, but this must be backed up by very fast initial charge separation to prevent back transfer.

In conclusion, it appears that in the bacterial reaction centre Nature has evolved an extremely efficient device for converting the energy of molecular electronic excitation into chemical potential via a multi-stage process of charge separation. This process relies on a very fast initial step and the indirect transfer of an electron to a desired acceptor via one or more intermediate sites. Together, these allow the transfer of an electron from a bacteriochlorophyll dimer to a ubiquinone acceptor without the fast back reactions that greatly reduce the efficiency in corresponding *in vitro* systems.

The work described in this paper was supported in part by N.S.F. grant no. PCM 75-23504, by the Office of Naval Research and by the U.S. Army Research Office, Durham, under grant no. DAA G29-76-9-0275. M.W.W. is grateful to Sir George Porter for hospitality and facilities provided during his period of sabbatical leave at the Royal Institution, during which this paper was prepared.

REFERENCES (Windsor & Holten)

Clayton, R. K. 1973 *A. Rev. Biophys. Bioengng* **2** 131.

Clayton, R. K. & Yamamoto, T. 1976 *Photochem. Photobiol.* **24**, 67.

Dutton, P. L., Kaufmann, K. J., Chance, B. & Rentzepis, P. M. 1975 *FEBS Lett.* **60**, 275.

Fajer, J., Brune, D. C., Davis, M. A., Forman, A. & Spaulding, L. D. 1975 *Proc. natn. Acad. Sci. U.S.A.* **72**, 4956.

Fajer, J., Davis, M. S., Brune, D. S., Spaulding, L. D., Borg, D. C. & Forman, A. 1977 *Brookhaven Symp. Biol.* **28**, 74.

Gouterman, M. & Holten, D. 1977 *Photochem. Photobiol.* **25**, 85.

Holten, D., Cremers, D. A., Pyke, S. C., Selensky, R., Shah, S. S., Warner, D. W. & Windsor, M. W. 1979*a* *Rev. scient. Instrum.* **50**, 1653.

Holten, D., Gouterman, M., Parson, W. W. & Windsor, M. W. 1978*b* *Photochem. Photobiol.* **28**, 951.

Holten, D., Gouterman, M., Parson, W. W., Windsor, M. W. & Rockley, M. G. 1976 *Photochem. Photobiol.* **23**, 415.

Holten, D. & Windsor, M. W. 1978 *A. Rev. Biophys. Bioengng* **7**, 189.

Holten, D. & Windsor, M. W. 1980 *Photobiochem. Photobiophys.* (In the press.)

Holten, D., Windsor, M. W. & Parson, W. W. 1978*c* In *Picosecond phenomena* (ed. S. L. Shapiro, C. V. Shank & E. P. Ippen), p. 126. Berlin and New York: Springer-Verlag.

Holten, D., Windsor, M. W., Parson, W. W. & Thornber, J. P. 1978*a* *Biochim. biophys. Acta* **501**, 112.

Holten, D., Windsor, M. W., Shank, C. V., Migus, A., Schenk, C. C. & Parson, W. W. 1979*b* Unpublished work.

Kaufmann, K. J., Dutton, P. L., Netzel, T. L., Leigh, J. S. & Rentzepis, P. M. 1975 *Science, N.Y.* **188**, 1301.

Kaufmann, K. J., Petty, K. M., Dutton, P. L. & Rentzepis, P. M. 1976 *Biochem. biophys. Res. Commun.* **70**, 839.

Magde, D., Bushaw, B. A. & Windsor, M. W. 1974*a* *Chem. Phys. Lett.* **28**, 263.

Magde, D. & Windsor, M. W. 1974 *Chem. Phys. Lett.* **27**, 31.

Magde, D., Windsor, M. W., Holten, D. & Gouterman, G. 1974*b* *Chem. Phys. Lett.* **29**, 183.

Netzel, T. L., Rentzepis, P. M., Tiede, D. M., Prince, R. C. & Dutton, P. L. 1977 *Biochim. biophys. Acta* **460**, 467.

Norrish, R. G. W. & Porter, G. 1949 *Nature, Lond.* **164**, 658.

Parson, W. W., Clayton, R. K. & Cogdell, R. J. 1975 *Biochim. biophys. Acta* **387**, 265.

Parson, W. W. & Cogdell, R. J. 1975 *Biochim. biophys. Acta* **416**, 105.

Pellin, M. J., Kaufmann, K. J. & Wasielewski, M. R. 1979 *Nature, Lond.* **278**, 54.

Porter, G. 1950 *Proc. R. Soc. Lond.* A **200**, 284.

Porter, G. & Windsor, M. W. 1958 *Proc. R. Soc. Lond.* A **245**, 238.

Rockley, M. G., Windsor, M. W., Cogdell, R. J. & Parson, W. W. 1975 *Proc. natn. Acad. Sci. U.S.A.* **72**, 2251.

Shuvalov, V. A., Klevanik, A. V., Sharkov, A. V., Matveetz, Y. A. & Krukov, P. G. 1978 *FEBS Lett.* **91**, 135.

Shuvalov, V. A. & Klimov, V. V. 1976 *Biochim. biophys. Acta* **440**, 587.

Tiede, D. M., Prince, R. C. & Dutton, P. L. 1976*a* *Biochim. biophys. Acta* **449**, 447.

Tiede, D. M., Prince, R. C., Reed, G. H. & Dutton, P. L. 1976*b* *FEBS Lett.* **65**, 301.

A STUDY OF THE VISCOSITY-DEPENDENT ELECTRONIC RELAXATION OF SOME TRIPHENYLMETHANE DYES USING PICOSECOND FLASH PHOTOLYSIS

David A. CREMERS and Maurice W. WINDSOR
Department of Chemistry, Washington State University, Pullman, Washington 99164, USA

Received 29 October 1979

Time-resolved absorption measurements of ground-state recovery and excited-state absorption are reported for several triphenylmethane dyes in solutions of different viscosity. A kinetic model is proposed to explain the results of these and earlier measurements.

1. Introduction

The viscosity-dependent relaxation of photoexcited triphenylmethane (TPM) dyes (fig. 1) has been studied in several ways. Fluorescence quantum yield Q measurements [1–3] and direct kinetic measurements using picosecond spectroscopic techniques [4–8] indicate that increased solvent viscosity results in decreased rates of electronic relaxation. Förster and Hoffmann (FH) [1] proposed a model of this viscosity dependence which predicts the $Q \propto \eta^{2/3}$ relationship found in some measurements of Q [1,3,8]. According to this model, the photoexcited molecule undergoes a change in conformation to a new structure characterized by enhanced rates of non-radiative decay. The important conformational change is assumed to be synchronous rotation of the phenyl rings about the bond between the ring and central carbon atoms (see fig. 1). The rotation is driven by steric repulsion between adjacent ring orthohydrogen atoms and is hindered by viscous drag introduced by the solvent molecules. Increased viscosity slows the rate of ring rotation and lengthens the time interval between excitation and the achievement of those conformations that give rise to fast non-radiative decay. In solvents of low viscosity, these conformations are reached more rapidly and fluorescence is quenched by the faster radiationless paths of relaxation. Although the FH model predicts the observed $Q \propto \eta^{2/3}$ relationship, the time dependence of excited-state relaxation of $\exp(-at^3)$ also predicted by this model has not been observed.

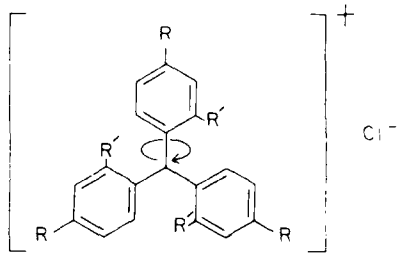

Fig. 1. The triphenylmethane dyes crystal violet CV (R = $N(CH_3)_2$, R' = H), ethyl violet EV [R = $N(C_2H_5)_2$, R' = H], parafuchsin PF (R = NH_2, R' = H), and the trimethyl crystal violet derivative TCV [R = $N(CH_3)_2$, R' = CH_3]. The arrow indicates the ring rotation specified by the Förster–Hoffmann model.

Magde and Windsor [4] measured the recovery of ground-state absorption of crystal violet (CV) following picosecond excitation. The data did not distinguish between several possible functional descriptions of the recovery. They concluded, however, that internal conversion is the dominant non-radiative mechanism. Ippen et al. [6] measured ground-state recovery (GSR) of malachite green and found it to be a single exponential for $\eta < 1$ poise. For $\eta > 1$ poise the recovery was described as a double exponential. Yu et al. [7] monitored malachite green fluorescence and found it to decay as a single exponential. Hirsch and Mahr [8] also

studied malachite green emission and characterized it as a double-exponential decay. The lifetimes of the faster decays of Hirsch and Mahr agree with the lifetimes of Yu et al. and the slower component of GSR measured by Ippen et al.

Despite the several studies referred to above, a description of the viscosity dependence has not yet been proposed which reconciles all the kinetic and quantum yield measurements. The role of viscosity in the picosecond relaxation kinetics of TPM dyes has been of interest to this laboratory for several years [4,5]. We present here a more detailed investigation of these viscosity effects.

2. Experimental

The dyes used in this study are shown in fig. 1. Crystal violet (Baker Chemical) used in the majority of experiments was purified via the leuco base. Ethyl violet (Eastman) and parafuchsin (Fridom Fluka) were purified by column chromatography since smaller amounts of these dyes were needed. The trimethyl derivative of CV was prepared and purified according to the literature [9]. All dyes were in the form of the chloride salt. Solvents of the desired viscosity were prepared by mixing deionized water, reagent-grade glycerol and glucose in various proportions. The viscosities of all dye solutions were directly measured. Unless otherwise specified, all measurements were made on 6×10^{-5} molar solutions at 25°C.

The picosecond flash photolysis apparatus used in this study is described elsewhere [10]. It is based upon a single-pulse-selected, mode-locked Nd : glass laser. A single amplified picosecond pulse at the laser fundamental (1060 nm) is 5–10 ps in duration and has an energy of about 15 mJ. Frequency doubling produces a 530 nm excitation (pump) pulse of about 2 mJ. The remaining 13 mJ of 1060 nm radiation is focused into a cell of CCl_4 to generate a spectrally broad (400–900 nm) picosecond probe pulse of weak intensity. The probe light transmitted by the sample is analyzed by a $\frac{3}{4}$ m Jarrell–Ash spectrometer and detected on an optical multichannel analyzer (Princeton Applied Research). The geometry of the pump and probe pulses at the sample [10] permits measurements of the difference in optical density (ΔOD) between excited and unexcited regions of the sample. Each laser firing produces a single measurement of ΔOD at a specific wavelength and delay.

The excitation and probing laser pulses were imaged onto a small volume of the dye solution contained within a 2 mm path length spectrometer cell. Following each laser firing, the contents of the cell were replaced by a fresh dye solution. The temperature of the sample region was carefully controlled to prevent fluctuations in viscosity due to thermal effects. This was especially critical for the more viscous solutions. The hygroscopic nature of glycerol made it necessary to shield the dye solutions from the atmosphere. The viscosity of the glycerol solutions is very sensitive to water contamination.

The intensities of the pump and probe pulses vary with each laser firing. Variations in probe intensity do not affect a measurement of ΔOD. Fluctuations in excitation power occur, and do cause changes in ΔOD, buth these are minimized by using sufficient power to saturate the sample. The effect of saturating the CV sample is shown in fig. 2. The changes in ΔOD due to variations in excitation power are small when 100% of the power is used. Each data point of a spectrum or kinetic curve in this study represents the average of usually six separate ΔOD measurements. The total length of the precision bars equals twice the standard deviation of the ΔOD values used to compute the average.

Experiments in which the relative polarizations of the excitation and probe pulses were adjusted either to accent or to mask the effects of molecular reorientation yielded similar results. Thus our measurements were apparently not affected by orientational relaxation of the entire molecule following photoexcitation.

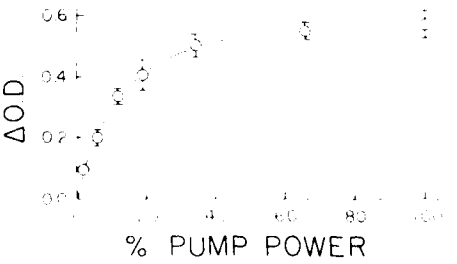

Fig. 2. Saturation curve for crystal violet (6×10^{-5} M in glycerol).

Undoubtedly this is a result of the high solvent viscosities we have used which cause overall rotational motions to be very much slower than the processes we have studied.

3. Results

Optical density difference spectra of CV over the range 380–900 nm at time delays of +20, +80 and +2730 ps are shown in fig. 3. To obtain data in the 380–450 nm region the picosecond apparatus was modified to permit generation of the probe pulse by the 530 nm excitation pulse. The continuum produced in this way has significantly greater intensity in the blue region than the 1060 nm generated continuum. The effects of dispersion in the arrival time of the probe pulse at the sample have not been removed from these spectra. Calculation and experience indicate that, over the spectral region considered here, the difference in arrival times between the red and blue probe light is, at most, 20 ps. Such dispersion has no effect on the kinetic data since these are taken within a narrowly defined wavelength band. The delays of +20, +80, and +2730 ps were established at 595 nm, the peak of CV absorption.

Three distinct regions are evident in the +20 and +80 ps spectra: (500–630 nm) ground-state bleaching; (380–500 nm) excited-state absorption (ESA), and (630–860 nm) stimulated emission. The presence of stimulated emission is indicated by apparent bleaching in a region of no ground-state absorption. In the 630–860 nm region the weak probe pulse is amplified in the excited region of the sample. Experiments in which stimulated emission was suppressed by filters in the probe beam before the sample, indicate that it has no effect upon the kinetics monitored at other wavelengths. This can be attributed to the weak intensity of the probe pulse.

In the event that a single type of excited molecule is produced by excitation, the spectra of fig. 3 can be used to find its spectrum, $\epsilon'(\lambda)$, at one of the delay times. The ΔOD produced in a sample of thickness l is

$$\Delta\mathrm{OD}(t, \lambda) = [\epsilon'(\lambda) - \epsilon_g(\lambda)]C'(t)l\,. \qquad (1)$$

Here $C'(t)$, $\epsilon'(\lambda)$ and $\epsilon_g(\lambda)$ are the concentration of the excited molecules, and the extinction coefficients of the excited- and ground-state molecules. If a wavelength $\bar{\lambda}$ exists for which $\epsilon_g \gg \epsilon'$, then at $\bar{\lambda}$,

$$\Delta\mathrm{OD}(t, \bar{\lambda}) \approx -\epsilon_g(\bar{\lambda})C'(t)l\,, \qquad (2)$$

which permits calculation of $C'(t)$. This value of $C'(t)$ can then be used in eq. (1) to find $\epsilon'(\lambda)$ since $\epsilon_g(\lambda)$ is known. We have applied this procedure at $\bar{\lambda}$ = 595 nm to the difference spectra to obtain $\epsilon'(\lambda)$ at +20 ps and +80 ps. Comparison of the excited-state spectra in fig. 4 indicates that over a time interval of 60 ps an increase of about 15% occurs in the blue absorption. Detailed measurements show that the excited-state extinction coefficient does increase with time in the region of 430 nm. This could be interpreted either as the formation of a small amount of triplet [4] or as an actual change in the value of $\epsilon'(\lambda)$ with time. In the

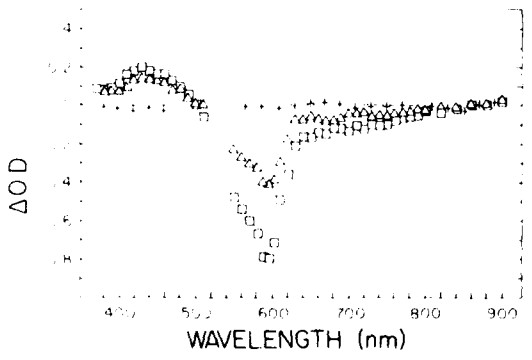

Fig. 3. Picosecond difference spectra of crystal violet in glycerol: (□) + 20 ps; (△) + 80 ps; (+) + 2730 ps.

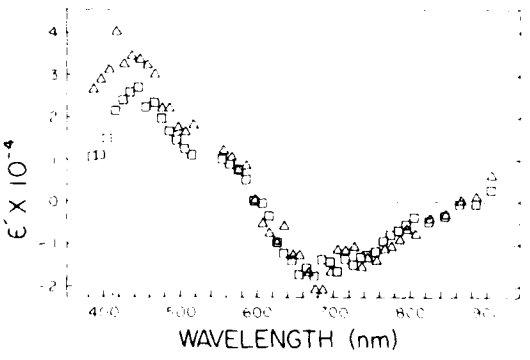

Fig. 4. Spectra of the excited state of crystal violet obtained by applying eqs. (1) and (2) to the difference spectra of fig. 3: (□) + 20 ps; (△) + 80 ps.

most viscous solutions ($\eta > 180$ poise), a small percentage of the excited dye molecules is converted to a long-lived species, possibly the triplet. This is shown by the residual ΔOD at 595 nm at a delay of 4.8 ns, which corresponds to about 10% of the initially excited population. In the least viscous solution ($\eta = 0.86$ poise) there is no evidence at any wavelength of the presence of the longlived species at 4.8 ns. The complete (within our experimental precision) decay of the absorption at 430 nm by 2.7 ns in glycerol (fig. 3) favors the interpretation that $\epsilon'(\lambda)$ increases with time.

The 5–10 ps pulses of our laser limit kinetic studies to solvents with viscosities in excess of 0.7 poise (i.e., relaxation times $\geq$30 ps). The viscosity dependence of ground-state repopulation (GSR) of CV was monitored at 564, 588 and 610 nm. The results of some measurements at 564 nm are presented in fig. 5. No significant differences were observed between GSR rates monitored at the three wavelengths. This is corroborated by the difference spectra of fig. 3 which show that the decay of bleaching proceeds uniformly over the 500–530 nm region. Ground-state recovery of CV in cyclohexanol (0.86 poise at 16°C) and of CV in a glycerol water solution of the same viscosity was similar. This supports the idea that viscosity, rather than another solvent property, is the controlling factor in the relaxation process. The agreement between the experiments of FH [1] and Brey et al. [3] in which viscosity was varied by changing solvent composition and by the application of high pressures, respectively, also supports this idea.

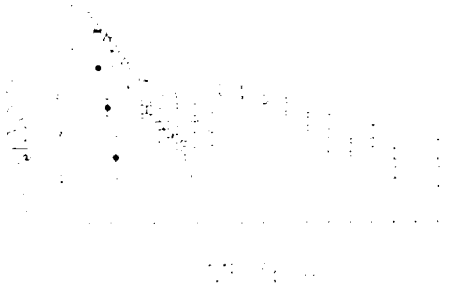

Fig. 5. Recovery of ground-state absorption in crystal violet. Solvents are: (○), 40% glucose/60% glycerol (η = 180 poise); (□), 20% glucose/80% glycerol (η = 40 poise); (△), glycerol (η = 8 poise); (●), 86.5% glycerol/13.5% H_2O (η = 0.8 poise). In both figs. 5 and 6 the residual optical density difference at 4.8 ns, ΔOD(∞), has been subtracted from measured ΔOD values to obtain the data shown here. The precison of the points without precision bars is less than or equal to the size of the point.

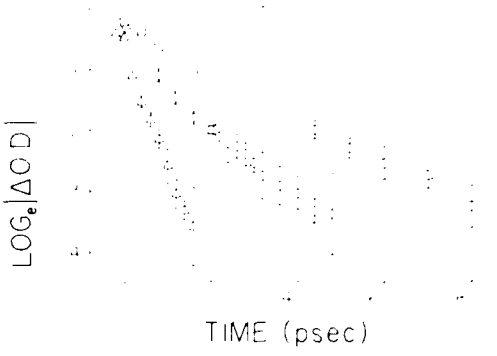

Fig. 6. Recovery of ground-state absorption in ethyl violet (▽), crystal violet (□), and parafuchsin (○).

The time dependence of crystal violet ESA was monitored at 430 nm. The decay curves were similar to those for GSR in solutions of corresponding viscosity. The time dependence of probe pulse amplification due to stimulated emission was observed at several wavelengths in the 630–860 nm region. If the reverse absorptive transition does not occur, this method can be used to monitor the excited-state population. These measurements gave relaxation rates similar to those obtained in the GSR studies.

The recovery of ground-state absorption following photoexcitation was also monitored in glycerol solutions of ethyl violet, parafuchsin, and the trimethyl crystal violet derivative. The results are in fig. 6. The GSR curves for crystal violet and the trimethyl compound were identical.

4. Discussion

The decay curves in fig. 6 support the idea that electronic relaxation of TPM dyes is affected by a conformation change hindered by viscous drag. The rates of relaxation decrease in the same order as the size of the phenyl ring para-substituent increases, i.e., PF, CV, EV. This suggests a direct connection between viscosity and rates of relaxation. However, the similarity of the GSR curves for TCV and CV appears to refute this suggestion. To investigate this we examined the structure of each

dye with space filling molecular models. The models indicate that the orthomethyls of TCV would not penetrate the surrounding solvent environment to the degree characteristic of the para-substituents. Hence the viscous drag introduced by the orthomethyls would not be as great as that due to large para-groups. It follows that their effect upon relaxation would not be as great as that due to large para-groups. It follows that their effect upon relaxation would not be as significant.

The GSR curves of figs. 5 and 6 indicate a complex relaxation mechanism. Ippen et al. [6] as well as Hirsch and Mahr [8] fitted similar curves to a double-exponential function. We have noticed, however, that a sum of many decaying exponentials

$$f = \sum_i N(0, k_i) \exp(-k_i t) \qquad (3)$$

can fit our GSR and ESA curves. Function f describes the decay of a collection of excited molecules grouped according to the decay rate k_i. The coefficient $N(0, k_i)$ is a constant and represents the number of molecules associated with rate k_i at time zero. If the $N(0, k_i)$ are equal and the distribution of decay rates between a minimum (k_1) and a maximum (k_2) value is uniform eq. (3) can be integrated to give

$$f \propto [\exp(-k_1 t) - \exp(-k_2 t)]\, t . \qquad (4)$$

Although this expression represents a sum of many equally weighted decaying exponentials it is possible, using physically reasonable values of k_1 and k_2, to duplicate a double-exponential function quite well.

A conformational analysis of TPM dyes [11] indicates they may represent a system described appropriately by eq. (3). The analysis shows (1) the ground-state potential surface is shallow with respect to asynchronous variation in the phenyl ring angles, and (2) the energy gap between the states S_0 and S_1 narrows with ring angle. Point (1) would permit a wide distribution of ground-state conformations. Point (2) would allow the decay rate k_i to vary with conformation, since rates of internal conversion are strongly dependent upon the $S_0 \rightarrow S_1$ energy gap. The quantum yield, kinetic, and conformational data suggest the following model of the viscosity dependence:

Photoexcitation leads to a replication of the ground-state conformation distribution in the excited state S_1. In high viscosity solvents the conformations are fixed and the decay of the excited-state population is described by eq. (3). Both fast (radiationless) and slow (luminescent) relaxation processes are important. As viscosity is reduced the possibility of a conformational change in the excited molecules prior to relaxation is increased. Excited molecules with decay rates near k_1 have a finite probability of acquiring a new conformation characteristic of the faster rates near k_2. This probability is related to the solvent viscosity. The observed increase in the excited-state extinction coefficient at 430 nm is consistent with a change in the molecular conformation of the excited state. Reduced viscosity then leads to a channeling of excited molecules into the faster nonradiative pathways of decay. Consequently the slower radiative processes are quenched.

The accumulated kinetic data can be understood in terms of this model. As viscosity is decreased only the fastest-decaying exponentials of eq. (3) remain important and in very fluid solutions eq. (3) may reduce to only a few exponential terms. This would explain the observation of Ippen et al. [6] that the description of GSR changes from a double exponential decay (or, as we suggest, a multiphasic decay) to a single exponential as viscosity is reduced. Luminescence is described by the slower (radiative) components of eq. (3). This explains why the faster component of luminescence noted by Hirsch and Mahr [8] agrees with the slower component of GSR measured by Ippen et al. On the other hand, the fast component of GSR is largely the result of radiationless decay of those molecules excited initially with large k_i values.

The above discussion shows that, on a semi-quantitative level, our model can describe the main features of electronic relaxation in triphenylmethane dyes. To test the model further, we have examined in some detail the effects of changing the angle between the phenyl rings and the molecular plane. In this study, based upon a conformational analysis that includes molecular orbital calculations as a function of ring angle, we used numerical methods to solve a modified Fokker–Planck differential equation. With this model we have been able to generate curves that show the same viscosity dependence as the experimental kinetic data. There is reason to believe that the model may also be able to account for the $Q \propto \eta^{2/3}$ relationship. A detailed account of this work is in preparation and will be presented elsewhere.

Acknowledgement

We thank Chris Kirmaier for the synthesis and purification of the trimethyl derivative of crystal violet. This work was supported in part by the Office of Naval Research and by the US Army Research Office (Durham).

References

[1] Th. Förster and G. Hoffmann, Z. Physik. Chem. NF 75 (1971) 63.
[2] C.J. Mastrangelo and H.W. Offen, Chem. Phys. Letters 46 (1977) 588.
[3] L.A. Brey, G.B. Schuster and H.G. Drickamer, J. Chem. Phys. 67 (1977) 2648.
[4] D. Magde and M.W. Windsor, Chem. Phys. Letters 24 (1974) 144.
[5] B.A. Bushaw, Ph.D. Thesis, Washington State University (1975).
[6] E.P. Ippen, C.V. Shank and A. Bergman, Chem. Phys. Letters 38 (1976) 611.
[7] W. Yu, F. Pellegrino, M. Grant and R.R. Alfano, J. Chem. Phys. 67 (1977) 588.
[8] M.D. Hirsch and H. Mahr, Chem. Phys. Letters 60 (1979) 299.
[9] C.C. Barker, M.H. Bride and A. Stamp, J. Chem. Soc. (1959) 3957.
[10] D. Magde and M.W. Windsor, Chem. Phys. Letters 27 (1974) 31.
[11] D.A. Cremers and M.W. Windsor, to be published.

Picosecond Phenomena II

Proceedings of the Second International Conference
on Picosecond Phenomena
Cape Cod, Massachusetts, USA
June 18-20, 1980

Editors
R. Hochstrasser W. Kaiser C.V. Shank

With 252 Figures

Springer-Verlag Berlin Heidelberg New York 1980

Electron Transfer from Photoexcited Bacteriopheophytin to p-Benzoquinone in Cationic Micelles

D. Holten[1], S. Sadiq Shah, and M.W. Windsor

Department of Chemistry, Washington State University,
Pullman, WA 99164, USA

Introduction

The primary energy storage reactions in photosynthesis are light-driven charge separation processes that take place within special pigment-protein complexes called reaction centers. In reaction centers isolated from photosynthetic bacteria, it appears that electron transfer occurs from the lowest excited singlet state (P*) of a bacteriochlorophyll dimer to a quinone by way of a molecule of bacteriopheophytin (BPh). Although the initial electron transfer from P* to BPh occurs within 4 ps of excitation by a short pulse of light (1), the reverse electron transfer step that returns the molecules to the ground state is more than 1000 times slower (2). This gives ample time for the electron to move from BPh^- to the quinone, which takes about 200 ps (3,4). Both of the forward electron transfer steps have quantum yields of 100%, even at cryogenic temperatures (2,5). Thus, within the bacterial reaction center light is converted to useful chemical potential via a highly efficient multistep charge separation process, initiated by an excited singlet state electron donor, in a time appreciably less than a nanosecond.

In homogeneous solution the situation is quite different. Although both the excited singlet and triplet states of BPh and chlorophyll (Chl) are effectively quenched by p-benzoquinone (BQ) and other electron acceptors in polar organic solvents, radical ions are detected only from the excited triplet state reaction [7-11]. The reason adduced is that reverse electron transfer within the intermediate triplet radical pairs to give the ground singlet state is spin-forbidden, giving the ions more time to diffuse apart [12]. It is not at present understood why the singlet pathway is so effective in the reaction center, whereas only the triplet route operates effectively in homogeneous solution, although several reasons for this difference in behavior have been considered. These include the effect of Franck-Condon factors on reverse electron transfer rates and the possibility that different orbitals may be involved in the forward and reverse electron transfer steps [12-14]. The possible importance of the microscopic environment in assisting charge separation and hindering reverse electron transfer in reaction centers has not explicitly been considered in these discussions. To explore its role, we have studied reactions of photoexcited BPh in aqueous micellar solutions with picosecond and slower spectroscopic techniques.

---

[1] Present address: Department of Chemistry, Washington University, St. Louis, MO 63130, USA

Surfactant (detergent) molecules possess a polar headgroup and a nonpolar hydrocarbon tail. These self-aggregate in aqueous solution to form colloidal complexes of high molecular weight, called micelles [15]. These are roughly spherical structures with a nonpolar inner core comprising the hydrocarbon tails and a charged surface region made up of the headgroups, called the Stern layer, surrounded by the counterions and the bulk aqueous phase. The micellar surface is positively charged (cationic) in the cetyltrimethylammonium bromide (CTAB) micelles. The hydrophobic interactions responsible for micellar stability are similar to those which stabilize biological membranes and globular proteins [15]. Micelles provide a means for imposing structure on the microscopic environment and for controlling the distance between the reactants.

Our purpose in undertaking the studies presented here was to find out if micelles could effect the rate of electron transfer between the reactants, the rate of reverse electron transfer within the radical pair state, and the recombination rate of separated ions. Previous studies in micelles of electron transfer from photosynthetic pigments and other porphyrins to various electron acceptors have had some success in this regard [16-18]. We chose to study BPh + BQ because the excited state photophysics and electron transfer behavior of BPh with this electron acceptor in homogeneous solution are well characterized [8,12-14]. By comparing results obtained in micelles, homogeneous solutions, and reaction centers, we hope to explore the effect of the environment on charge separation in a systematic way.

Experimental

The picosecond apparatus has been described previously [19]. For the present study, 8 ps 530 nm flashes were used to excite sample solutions of 40 μM BPh in 2 or 5 mm path cells. Microsecond flash photolysis studies made use of 200 ns 530 nm excitation flashes from a flashlamp-pumped coumarin-7 dye laser. The detection system had a response time of about 1 μs.

BPh was prepared as described previously [8]. Micellar solutions were prepared by injecting concentrated aliquots of BPh in ethanol into 0.1 M aqueous CTAB followed by addition of the electron acceptor. These solutions were thoroughly degassed by at least 10 freeze-thaw cycles on a high-vacuum line, and sealed. Fluorescence quenching studies were carried out on a Farrand MKI spectrofluorometer.

Sites of solubilization

Previous studies suggest that Chl-a is solubilized within the nonpolar inner core of micelle, the process being assisted by hydrophobic interactions between the hydrocarbon (phytyl) chain of Chl-a and the hydrocarbon chain of the surfactant molecules [15-18]. Based on the structural similarity between Chl-a and BPh, we believe that BPh is incorporated into the inner core of the micelle. The site of solubilization of BQ in CTAB micelles was determined by proton NMR spectroscopy to be on the average near the inner surface of the Stern layer [21]. As described below, the behavior of photoexcited BPh in the presence of BQ supports our views on the sites of solubilization of both molecules.

Excited singlet state quenching

Difference spectra for the formation of the BPh excited singlet state (BPh^*), the excited triplet state (BPh^T), and the cation radical (BPh^+)

in CTAB micelles are closely similar to those obtained in a number of organic solvents [8,21].

The lifetime of BPh* was obtained from the decay of excited state absorbance at 610 nm and from recovery of BPh ground state bleaching at 755 nm. Lifetimes measured at the two wavelengths were the same within experimental error. Figure 1 shows the first order decay plots for BPh* in CTAB at 755 nm. These measurements give lifetimes for BPh* of 2.2 ± 0.3 ns, 1.1 ± 0.2 and 0.6 ± 0.1 ns in the absence and in the presence of 30 or 70 mM BQ, respectively. The lifetime in the absence of quenchers is the same within experimental error as the value of 2.0 ± 0.2 ns obtained previously in acetone:methanol (7:3) solution [8].

The reduction in BPh* lifetime and the fluoresence quenching measurements (not shown) are in good agreement and are linear in BQ concentration up to about 30 mM BQ. These data give a quenching constant K_Q = 33 ± 2 M^{-1}. Together with a 2.2 ns lifetime in the absence of quencher, this yields a second order quenching rate of 1.5 ± 0.2 x 10^{10} $M^{-1}s^{-1}$ in CTAB micelles. Previously a value of 1.7 ± 0.2 x 10^{10} $M^{-1}s^{-1}$ was obtained in acetone:methanol (7:3) [8]. Thus, quenching rates of BPh* by BQ are about the same in CTAB micelles and in this homogeneous solution.

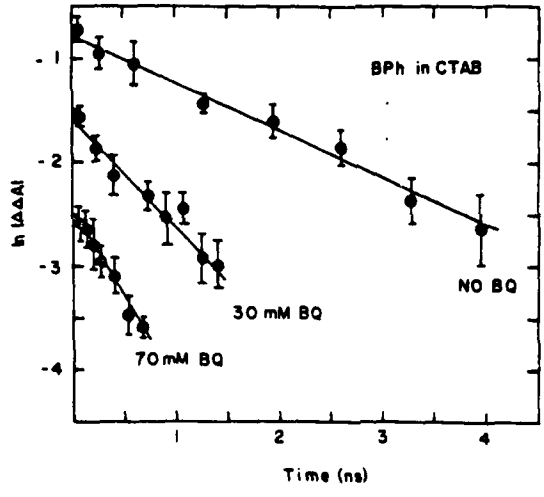

Fig.1 First order decay plots for 20 μM BPh following excitation with 8 ps 530 nm flashes, measured from recovery of ground state bleaching at 755 nm. The ordinate is the absorbance change at time, t, minus that at the asymptote of the decay curve, measured between 6 and 9 ns after excitation.

Above 30 mM the quenching becomes nonlinear in BQ concentration in both CTAB and in organic solvents, but is much more pronounced in CTAB

micelles. This does not appear to be due to ground state complexes involving BPh and BQ, because at the highest concentration of BQ used (70 mM) no new bands were observed in the absorption or fluorescence spectra. Such nonlinear quenching behavior has been attributed previously to static quenching and would involve "instantaneous" quenching of those BPh* molecules formed within an active quenching radius of an electron acceptor, and thus becomes increasingly important at higher quencher concentrations [22]. Enhanced static quenching in CTAB micelles at high BQ concentrations suggests that at these concentrations more BQ molecules lie within the effective quenching distance of BPh at the time of excitation than in nomogeneous solution. This result is in agreement with the contention that BQ molecules are preferentially solubilized at the inner surface of the Stern layer and that BPh molecules reside within the micellar inner core.

Formation of cation radicals

Irradiation with 200 ns 530 nm flashes of BPh in CTAB micelles in the absence of quenchers produces absorbance changes due to $BPh^{\dagger}$, that decay with a time constant of 48 μs. In the presence of BQ, these absorbance changes are replaced by the spectrum of the cation radical, BPh^{+}. Kinetics for the decay of BPh^{+} measured at 420 nm for 10 μM BPh and 10 mM BQ in CTAB were found to be essentially second order. With a value of 1.0 ± 0.3 x 10^{5} $M^{-1}cm^{-1}$ for the differential extinction coefficient at 420 nm [8,23], we obtain a second order rate constant for the recombination of the separated ions, BPh^{+} and BQ^{-}, of 2.3 ± 1.5 x 10^{10} $M^{-1}s^{-1}$ in CTAB micelles. A value of 1.8 ± 1.0 x 10^{10} $M^{-1}s^{-1}$ was obtained in acetone:methanol (7:3).

With the ps apparatus, no additional absorbance changes near 850 nm, where BPh^{+} is known to have weak absorption [8,23], were detectable for 40 μM BPh in CTAB micelles in the presence of 30 or 70 mM BQ. Since the detection limit for absorbance changes is 0.025 with our ps apparatus, the yield of BPh^{+} could be as much as 40% at the 40 μM BPh concentration used and still go unobserved at 850 nm. Thus, in the present study we were not able to determine whether BPh^{+} in CTAB micelles forms preferentially via BPh* or $BPh^{\dagger}$.

A better region for monitoring the formation of BPh^{+} would be at 400 nm where it absorbs strongly. Unfortunately, we could not make ps observations in this region because of strong sample absorbance and declining probe intensity. Efforts are currently underway to obtain enhanced probe intensity in the 400 nm region by using 530 nm light to generate the picosecond continuum and by improvements in the optics.

The fact that BPh is readily seen with 200 ns excitation flashes but goes undetected in the ps experiments is due to multiple recycling of the system during the much longer 200 ns flashes. Thus our observation of BPh^{+} in this case does not necessarily imply a high intrinsic quantum yield of formation [8].

Conclusions

Electron transfer from BPh* to BQ is more efficient in CTAB micelles than in acetone:methanol solution at high BQ concentrations. At low BQ concentrations the quenching rate is about the same in the two systems, as is the recombination rate of separated ions. Similar observations have

been reported on the chlorophyll sensitized reduction of methyl viologen in nonionic micelles [16], whereas other systems have shown more pronounced effects [17,18].

Additional studies with an expanded series of electron donors and acceptors are underway to elucidate this behavior and to further investigate the effects of various types of micelles on the rate of electron transfer quenching, the yield of ion separation and the rate of charge recombination. We also hope to resolve optically the formation of radical ions from excited singlet and triplet state reactions in micelles, as has been done in homogeneous solution [8], since this is crucial for devising efficient models for photosynthetic electron transfer.

Acknolwedgements

This work was supported by the U.S. Army Research Office under grant DAA629-76-9-0275 and by the NSF under grant PCM 79-02911.

References

1. D. Holten, C. Hoganson, M. W. Windsor, C. C. Schenk, W. W. Parson, A. Migus, R. L. Fork, and C. V. Shank, Biochim. Biophys. Acta
2. W. W. Parson, R. K. Clayton and R. J. Cogdell, Biochim. Biophys. Acta 416, 105 (1975).
3. Kaufmann, K. J., P. L. Dutton, T. L. Netzel, J. S. Leigh and P. M. Rentzepis, Science 188, 1301 (1975).
4. M. G. Rockley, M. W. Windsor, R. J. Cogdell and W. W. Parson, Proc. Natl. Acad. Sci. USA 72, 2251 (1975).
5. R. K. Clayton and T. Yamamoto, Photochem. Photobiol. 24, 67 (1976).
7. D. Huppert, P. M. Rentzepis and G. Tollin, Biochim. Biophys. Acta 440, 356 (1976).
8. D. Holten, M. Gouterman, W. W. Parson, M. W. Windsor and M. G. Rockley, Photochem. Photobiol. 23, 415 (1976).
9. A. A. Lamola, M. L. Manion, H. D. Roth and G. Tollin, Proc. Natl. Acad. Sci. USA 72, 3265 (1975).
10. N. E. Andreava, G. V. Zakharova, V. V. Shubin and A. K. Chibisov, Chem. Phys. Lett. 53, 317 (1978).
11. G. Tollin, F. Castelli, G. Cheddar and F. Rizzuto, Photochem. Photobiol. 29, 147, 153 (1978).
12. M. Gouterman, and D. Holten, Photochem. Photobiol. 25, 85 (1977).
13. D. Holten, and M. W. Windsor, Ann. Rev. Biophys. Bioeng. 7, 189 (1978).
14. D. Holten, M. Gouterman, W. W. Parson and M. W. Windsor, Photochem. Photobiol. 28, 951 (1978).
15. J. H. Fendler, and E. J. Fendler, Catalysis in Micellar and Macromolecular Systems, Academic Press, N.Y. (1975).
16. K. Kalyanasundaram, and G. Porter, Proc. Roy. Soc. A., (1978).
17. C. Wolf, and M. Gratzel, Chem. Phys. Lett. 52, 542 (1977).
18. G. R. Seely in Topics in Photosynthesis (J. Barber, ed.) pp. 36-37, Elsevier, Heidelberg (1977).
19. D. Magde, and M. W. Windsor, Chem. Phys. Lett. 27, 31 (1974).
20. J. Simplicio, Biochem. 11, 2525 (1972).
21. S. S. Shah, D. Holten and M. W. Windsor, Photobiol. Photobiophys., submitted.
22. J. B. Birks, Photophysics of Aromatic Molecules, Wiley, New York (1970).
23 J. Fajer, D. C. Borg, A. Forman, R. H. Felton, D. Dolphin and L. Vegh, Proc. Natl. Acad. Sci. USA, 71, 994 (1974).

(H)

Picosecond Phenomena II

Proceedings of the Second International Conference
on Picosecond Phenomena
Cape Cod, Massachusetts, USA
June 18–20, 1980

Editors
R. Hochstrasser W. Kaiser C.V. Shank

With 252 Figures

Springer-Verlag Berlin Heidelberg New York 1980

Picosecond Studies of Electronic Relaxation in Triphenylmethane Dyes by Fluorescence-Upconversion

G.S. Beddard, T. Doust, and M.W. Windsor[1]

Davy Faraday Research Laboratory, The Royal Institution,
21 Albemarle Street, London W1X 4BS, United Kingdom

INTRODUCTION

The electronic relaxation in solution of triphenylmethane dyes, TPM(Fig. 1), such as crystal violet (CV) and malachite green (MG), has been studied in several ways and is found to show a significant dependence on solvent viscosity. The fluorescence quantum yield, Q, is very small (<0.1) in fluid solvents, but increases to about 30 % in extremely viscous media [1-3]. Both fluorescence yield studies and picosecond spectroscopic kinetic measurements [4-8] of the decay of excited state absorption (ESA) and of the rates of ground state repopulation (GSR) show that increased

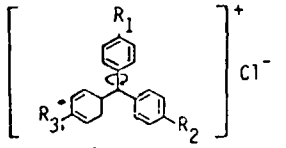

Fig. 1

Fig. 1 The triphenylmethane dyes crystal violet CV [$R_1 = R_2 = R_3 = N(CH_3)_2$] and malachite green MG [$R_1 = H$, $R_2 = R_3 = N(CH_3)_2$]

solvent viscosity leads to reduced rates of electronic relaxation. The cations of TPM dyes assume a 3-bladed propeller configuration in solution. The model proposed by Forster and Hoffmann (FH) [1] envisages that the excited molecule undergoes a conformational change involving synchronous rotation of the phenyl rings to new conformations that have enhanced rates of non-radiative decay. The ring rotation is driven by steric repulsion between ortho hydrogen atoms on adjacent phenyl rings and is hindered by solvent viscosity. Their model predicts a $Q \propto \eta^{2/3}$ dependence that is supported by some measurements [1,3,8], but the time dependence of excited state relaxation of exp $(-at^3)$, also predicted by the model, has not been observed. Picosecond GSR studies of CV by Magde and Windsor[4] indicated that internal conversion is the dominant mechanism, but their data did not distinguish between several possible functional descriptions of the recovery. Ippen et al. [6] studied GSR for MG and found a single exponential recovery for $\eta<1$ poise and a double exponential for $\eta>1$ poise. A single exponential decay of fluorescence for MG was reported by Yu et al. [7], but Hirsch and Mahr[8] observed a double exponential decay. However, the lifetimes of the faster decays of Hirsch and Mahr agree both with the lifetimes of Yu et al. and the slower component of GSR reported by Ippen et al. Very recently Cremers and

[1] Permanent address: Department of Chemistry, Washington State University, Pullman, WA 99164, USA

Windsor[9], in a detailed study by picosecond flash photolysis, found that a sum of many decaying exponentials was required to fit their GSR and ESA kinetic data. In their model excitation produces in the excited state a replica of the ground-state conformational distribution. In high viscosity solvents the conformations are fixed and each conformation exhibits an independent and different rate of decay, thus leading to an overall multi-exponential decay. In solvents of lower viscosity, conformational changes can occur on the time scale of the relaxation and reduced viscosity leads to a transfer of excited molecules into the faster non-radiative decay channels. This model reconciles the kinetic data of Hirsch and Mahr and of Ippen et al., but the disparity between the kinetic and quantum yield measurements remains to be explained. Although a large amount of kinetic data has now been accumulated on the viscosity-dependent relaxation of CV via studies of ESA and GSR, to date no time-resolved studies of CV fluorescence have yet been made. We present here a picosecond kinetic study of the solvent-dependent relaxation of both CV and MG studied by laser upconversion of the fluorescence emission.

EXPERIMENTAL

A synchronously-pumped jet-stream dye laser producing pulses of 4 ps duration at 595 nm was used to excite the fluorescence of solutions of CV and MG in various viscous solvent mixtures. Heating of the sample volume was avoided by the use of a jet stream for the more fluid solutions and a sample cell rotated eccentrically about an axis normal to the plane of the cell for the more viscous solutions. The fluorescence was upconverted to about 310 nm by mixing in a $LiIO_3$ crystal with a portion of the excitation beam obtained by use of a suitable beam splitter. By varying the time delay of this latter beam with a delay line controlled by a stepping motor, the fluorescence decay profile can be mapped out. The fluorescence signal was observed over the range 650-800 nm by angle tuning the $LiIO_3$ crystal. CV samples were purified samples provided by Cremers and Windsor. Commercial samples of CV not specially purified, gave results that did not differ from those for the purified material. The MG used was a biological stain sample of 98% purity. All experiments were performed at 21.5°C. Solution viscosities were also measured at this temperature with an Ostwald viscometer which was calibrated against oils of standard viscosity. Viscosity data were reproducible to ± 2%.

RESULTS

Our results are summarized in Figures 2-4. Fig. 2 is a logarithmic plot of the decay of CV fluorescence in a glycol/water solution of viscosity 11P. The time axis corresponds to 3 ps per channel. Note that the decay is very close to being exponential except at the earliest times. A computer fit to a double exponential decay gives a major component with a lifetime of 150 ps and a minor (15% amplitude) contribution from a faster decaying component with a lifetime of 41 ps.

We studied the fluorescence decay of CV in solutions ranging in viscosity from 0.8 P to 50 P. The results for both the long and short decay components are summarized in a log-log plot in Fig. 3. Within experimental error both fit quite well to a dependence of the lifetime on the 2/3 power of the viscosity in agreement with the FH model.

Similar data were obtained for MG, but the dual exponential character of the decay was more pronounced than for CV even in the more fluid solvents. Figure 4 shows the kinetics in a glycerol/water mixture of viscosity 11.5 P together with a dual exponential fit to the data. There is a long component of 153 ps and a shorter component (45% amplitude) of 58 ps. The viscosity dependence of the MG fluorescence shows an

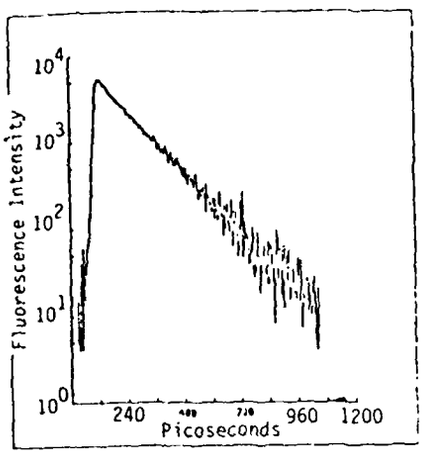

Fig. 2 Decay of crystal violet fluorescence in glycerol/water solution of viscosity 11 poise t 21.5°C

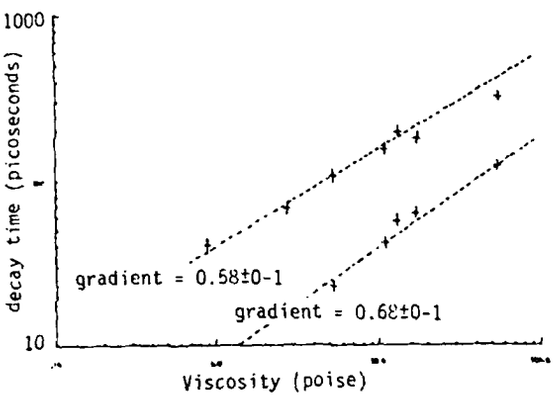

Fig. 3 Log-log plot of fluorescence decay times of crystal violet versus solvent viscosity

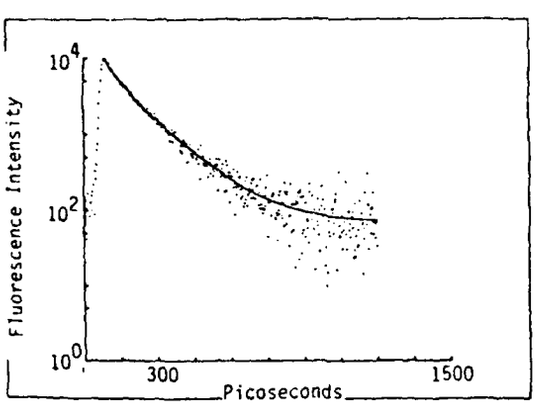

Fig. 4 Decay of malachite green fluorescence in glycerol/water solution of viscosity.11.5 poise at 21.5°C. The solid line is a dual exponential fit to the experimental data

approximately 1/3 power dependence of both lifetimes on viscosity in agreement with the data of Hirsch and Mahr.

We also studied the wavelength dependence of the fluorescence decay of CV over the range 650-800 nm. To within 1% we were unable to observe any variation in the decay times over this range.

DISCUSSION

Our results can be understood in terms of the model of Cremers and Windsor [9]. Excitation produces in the excited state, a replica of the ground-state population distributed over various angular conformations of the phenyl rings. In high viscosity solvents ring twisting is very slow and this distribution does not change on the time scale of fluorescence emission. The fluorescence decay is multi-exponential because, owing to the convergence of the upper and ground state potential energy surfaces with increasing ring angle, the rate of internal conversion also increases with increasing ring angle. Thus a different rate of fluorescence decay obtains for each angular conformation, determined by the internal conversion rate appropriate to each value of ring angle. In low viscosity solvents, the rate of twisting of the phenyl rings becomes rate controlling and the decay approximates to a single exponential. We do not at present understand the differences between the behavior of CV and that of MG. Probably these differences are connected with differences in the relative disposition of the upper and lower potential energy surfaces for the two molecules.

The weaker dependence of the decay time on viscosity for MG implies that ring rotation by the solvent is less hindered than in the case of CV. This is consistent with the presence in MG of one unsubstituted phenyl ring, i.e., one ring does not carry a $-N(CH_3)_2$ group in the para position, leading to a lower degree of π bonding to the central carbon atom and therefore less resistance to twisting.

ACKNOWLEDGEMENTS

This work was supported by the Science Research Council. GSB is grateful to the Royal Society for a Jaffe Research Fellowship and T. Doust for a SRC Studentship. M.W.W. acknowledges support from NSF grant PCM79-02911 and from the U.S. Army Research Office under grant DAA G29-76-9-0275.

References

1. Th. Forster and G. Hoffmann, Z. Physik. Chem. NF 75 (1971) 63.
2. C. J. Mastrangelo and H. W. Offen, Chem. Phys. Letters 46 (1977) 598.
3. L. A. Brey, G. B. Schuster and H. G. Drickamer, J. Chem. Phys. 67 (1977) 2648.
4. D. Magde and M. W. Windsor, Chem. Phys. Letters 24 (1974) 144.
5. B. A. Bushaw, Ph.D Thesis, Washington State University (1975).
6. E. P. Ippen, C. V. Shank and A. Bergman, Chem. Phys. Letters 38 (1976) 611.
7. W. Yu, F. Pellegrino, M. Grant and R. R. Alfano, J. Chem. Phys. 67 (1977) 588.
8. M. D. Hirsch and H. Mahr, Chem. Phys. Letters 60 (1979) 299.
9. D. A. Cremers and M. W. Windsor, Chem. Phys. Letters 71 (1980) 27.

Photobiochemistry and Photobiophysics, 1 (1980) 243–252
Elsevier/North-Holland Biomedical Press

AUTOMATED PICOSECOND SPECTROSCOPY WITH A STANDARD TWO-DIMENSIONAL OPTICAL MULTICHANNEL ANALYZER AND AN INEXPENSIVE MICROPROCESSOR

DEWEY HOLTEN and MAURICE W. WINDSOR

Department of Chemistry, Washington State University, Pullman, WA 99164, U.S.A.

Received May 9, 1980
Accepted May 10, 1980

SUMMARY

Picosecond kinetic spectroscopy has contributed greatly in the past five years to our understanding of primary photophysical and photochemical events in biological systems, notably photosynthesis. Such systems are chemically and spectrally complex and for progress to be made, broad-band transient difference spectra are essential. We describe the construction and use of a low-cost system for converting a single-pulse picosecond laser spectrometer to an automated instrument in which broad-band transient difference spectra with good resolution in both absorbance change and wavelength can be acquired in only a few laser shots. The detection system uses a standard vidicon-optical multichannel analyzer combination, present in most picosecond spectroscopy laboratories, interfaced to a reliable, home-assembled microcomputer. Detailed "how to" descriptions of the method and its implementation are given and representative spectra of an intermediary electron transfer state in bacterial photosynthetic reaction centers are used to demonstrate the advantages of the automated two-dimensional technique over the point-by-point single-shot approach.

INTRODUCTION

Picosecond flash photolysis and kinetic spectroscopy have been of great value in biology and biophysics during the past five years, notably in improving our understanding of the early stages of photosynthesis (see refs. 1–3 for recent reviews). Biological systems are often chemically and spectrally complex and kinetic studies at a single wavelength are of limited value. Not only fast time resolution, but also broad spectral coverage and the ability to detect small changes in absorbance, are needed to elucidate the primary photophysical and photochemical steps. Much of the work has been carried

AD-A107 733 WASHINGTON STATE UNIV PULLMAN PICOSECOND LASER LAB F/G 20/5
NANOSECOND AND PICOSECOND SPECTROSCOPY AND KINETICS OF DYNAMIC --ETC(U)
OCT 81 M W WINDSOR DAAG29-76-G-0275

UNCLASSIFIED ARO-14081.11-C NL

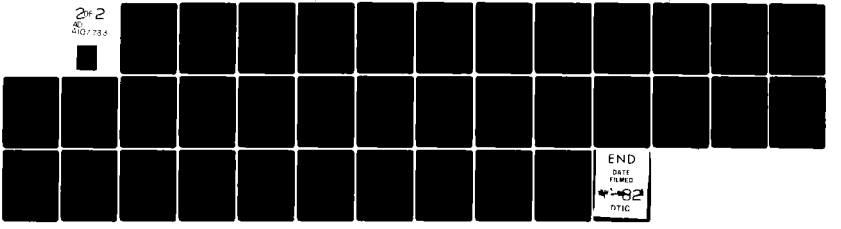

out with th aid of the single shot picosecond flash photolysis technique [4—7]. The OD of the sample is obtained at a given time delay, in the range from a few ps to a few ns following excitation by a 5—10 ps duration pump pulse, by means of a spectrally broad ("white light") picosecond continuum pulse generated via a process commonly called self-phase modulation (SPM) [4]. The probe pulse monitors both a region of the sample that is exposed to the pump pulse and also adjacent immediately contiguous regions that are not exposed. Comparison of the probe pulse intensity transmitted through the exposed region (I) and the unexposed regions (I_0) enables the change in optical density of the sample to be calculated (as $\Delta OD = \log I_0/I$) in a manner similar to that used in a conventional spectrophotometer. With this technique, to acquire an absorption spectrum over a range of several hundred nm, it is necessary to obtain the transient OD point-to-point at a multitude of wavelength settings. In addition, since 5 or more shots are often required at each setting to obtain a satisfactory signal-to-noise ratio, several hundred laser shots and a period of 4—8 h are usually needed to acquire the desired spectrum with adequate resolution in both absorbance and wavelength. Not only is the above process tedious, time-consuming and laborious, it is also quite unsatisfactory for the study of irreversible photolabile systems (e.g., rhodopsin) necessitating the use of a flow system and large sample volume to provide fresh sample for each laser shot. Finally, ambiguities in the interpretation of kinetic data arise at short delay times when measurements are made at a single wavelength, owing to possible spectral changes associated with energy relaxation on the time scale of the measurement [8]. Observations over a broad spectral band are advantageous in such situations.

In response to the above problems, automated 2-dimensional (optical density vs. wavelength) measurement techniques have been developed. These typically make use of commercially available vidicon detectors interfaced to a 2-d Optical Multichannel Analyzer (OMA) such as the Princeton Applied Research (PAR) 1215 OMA-2 and a dedicated minicomputer. Such detection systems have been used with a subpicosecond resolution dye laser apparatus [9] and with 7—10 ps resolution Nd/glass laser systems [9—11]. Huppert et al. have used a liquid N_2-cooled RCA 4532 vidicon and controller interfaced to a Nova minicomputer [12].

A major disadvantage of the above systems is that they may cost as much as US $ 50,000 over and above the cost of the basic laser apparatus. In our laboratory, we have developed, constructed and used an inexpensive system that is based on the commonly used standard PAR 1205A/B OMA-vidicon detection system (cost about $ 12,000). We have interfaced this to a microcomputer system built in our laboratory from kits obtained from several vendors (see below and ref. 13). Since the majority of picosecond spectroscopists using Nd/glass laser systems already possess the standard 1205 OMA-vidicon combination, the additional cost to make possible 2-dimensional recording of data is no more than $ 7200 ($ 3500 for the microprocessor and peripherals, $ 1500 for a low-dispersion monochromator, and $ 2200 for 1205-08 2-d option card).

METHODS AND MATERIALS

Description of system

A block diagram of the complete detection system is given in Fig. 1. The ground and excited state absorbance information is provided by our laser system [4,5]. A single 1060 nm pulse of ~8 ps duration is selected from the output train of a modelocked Nd/glass laser, amplified twice and frequency-doubled with about 15% efficiency to give a 3 mJ pulse at 530 nm. The 530 nm radiation is split off by a dichroic mirror and is focused to a 1.5 mm spot on a 1—5 mm path sample cuvette. Excitation pulses at 627 or 600 nm are obtained via the stimulated Raman process by focusing the 530 nm light into a 5 cm cell containing cyclohexane or its perdeuterated analogue. The 1060 nm pulse remaining after frequency doubling passes the dichroic mirror and is focused into a 10 cm long cell containing CCl_4 in which a broad-band (360 to beyond 1060 nm) continuum probe pulse, also of ~8 ps duration, is produced. Residual 1060 nm light is removed with another dichroic mirror. The probe pulse traverses an optical delay line, is elongated in the vertical direction with two cylindrical lenses, and passes a spherical lens to produce an essentially collimated beam about 1.5 cm in height which is directed to the sample position. [The system is aligned with a He-Ne laser beam traversing the same optical paths as the 8 ps pump and probe pulses.] As shown in Fig. 2A, the sample holder has a vertical slit 3 cm high and 5 mm wide behind the sample cuvette. Behind this we place a plate containing two horizontal slits whose centers are separated vertically by 1 cm. These slits are each 2 mm wide (vertical direction). The point midway between the two slits is at the same height above the optical table as the center of the vertically elongated probe beam and the center of the 1/4 m Jarrell—Ash monochromator entrance slit. The pump pulse is focused at the center of the sample cuvette and through the lower of the two slits, henceforth called the "excited region slit". The upper slit is called the "reference region slit". The

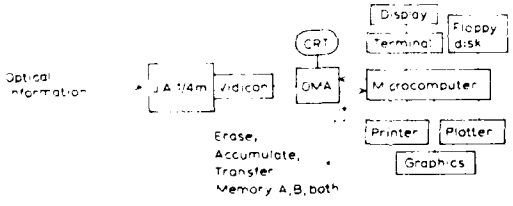

Fig. 1. Block diagram of the overall data acquisition, storage and analysis system of the picosecond absorption spectrometer. The monitoring pulse from the laser apparatus contains sample ground and excited state absorption information over a range of wavelengths. This is dispersed by the monochromator and detected by the vidicon coupled to an optical multichannel analyzer (OMA). Spectral information from the OMA is processed by the computer to yield a transient absorption spectrum for a single laser shot. This is displayed and then stored on a floppy disk.

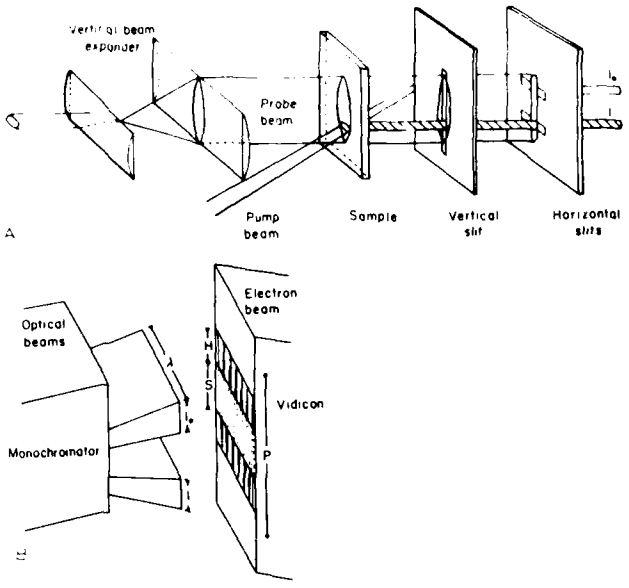

Fig. 2. A) Pump and probe beam geometry at the sample position. The sample holder and plates containing vertical and horizontal slits are actually sandwiched together. The pump beam is incident on the sample at an angle of about 10° with respect to the probe beam and passes through the vertical and lower horizontal slits. The light transmitted through unexcited (I_0) and excited (I) sample regions is then focused onto the entrance slit of a monochromator, as described in the text. B) Imaging of excited and reference region light dispersed by the monochromator onto the two 500 channel vidicon tracks. The electron beam actually does two 500 channel triangular scans. On the first scan the "selected" excited region track is read and data are stored in OMA memory A; the electron beam does not "read" off charge on the remainder of the vidicon during this scan. On the second scan, intensity information for the sample reference region is read from the second track and stored in memory B. The results of 5 such accumulations for each track are added in the corresponding memories, since a preset of 10 is used. The track settings used for trimpots on the 2-d option card are height (H) = minimum, separation (S) = maximum, and position (P) = centered. See text for more details.

probe light passes through both excited and reference region slits (Fig. 2A) and the two spots are focused by a 100 mm focal length, 35 mm diameter lens on to the 250 μm entrance slit of the monochromator. This lens is placed on an X-Y-Z translation stage in order that its position can be adjusted so that the two optical spots overlap two tracks on the face of the vidicon as described below. If desired, the cylindrical lenses could be replaced with a beam splitter and mirror to generate two probe beams that pass through excited and reference region slits.

We machined off the exit slit and holder from the monochromator so that the vidicon detector surface can be placed at the exit slit plane, and so that the vidicon can be rotated about the optical axis. For 2-d measurements the

vidicon is rotated so that the square preamp box is pointed down. Since the electron beam sweeps the vidicon channel by channel perpendicular to the preamp box, it will sweep perpendicular to the 500 channel track direction (Fig. 2B), reading one track at a time and placing the information in the appropriate OMA memory. The OMA circuitry is adjusted as follows:

1. Set switch on rear of OMA to 2-d.
2. Set ANSUB switch (S2) on the timing card to left-hand position to defeat automatic baseline subtract.
3. Set thumbwheel switches on 2-d card for two tracks, which should be seen on the display.
   Track Height, Separation and Position are adjusted with the aid of three trimpots on the 2-d circuit card, as follows:
4. Set track height (width) to minimum setting (fully CCW) while listening for trimpot clicking. This is done to avoid possible track overlap which could otherwise occur because of the reduced span of the vidicon employed when only two tracks are in use (see No. 5).
5. Set track separation to the maximum setting (full CW). Note that when only two tracks are used, only a fraction of the entire 0.5 inch dimension of the vidicon is employed. Thus, even at maximum track separation, there is no danger of spillover of either track off the active surface of the vidicon provided that the active region is properly centered (see No. 6).
6. Adjust track position to middle setting (about 6 turns from either extreme). This setting centers the two tracks along the y-axis of the vidicon surface. We find the settings given in 4—6 above work well with our light level (additional filters are required even at the minimum track width), optical spot spacing and size.
7. Set switch on 2-d circuit card to right hand position for "dual spectrum" mode. Use "track select" button to identify the excited region track as the "selected track" (the selected track is intensified on the display). Data from this track will then be stored in the A memory and data from the reference region track will be stored automatically in the B memory. This procedure ensures that the calculated optical density difference, ΔOD, will have the correct sign (our software assumes that excited state data are always stored in memory A).

Procedure for aligning optical spots with vidicon tracks

The focusing lens must be adjusted so that the two optical spots are in optical registration with the two tracks on the vidicon surface. This may be accomplished with the 632 nm line of the He-Ne laser and the OMA in the real time mode. Best alignment is achieved by obtaining the following sequence of signals on the vidicon as the focusing lens is moved vertically downward (see Fig. 3): (1) lower spot lines up with upper track, (2) both spots line up with the corresponding tracks, (3) upper spot lines up with lower track (not shown). No signal is obtained for the intermediate positions, ensuring that the tracks are not overlapped. If this sequence cannot be

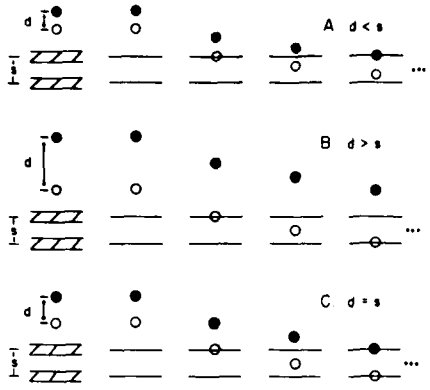

Fig. 3. Alignment of the two optical spots with the two vidicon tracks using the 632 nm line of the He-Ne laser and the OMA in the real time mode. The track separation (s) is set at the maximum value as discussed in the text. The distance (d) between optical spots is adjusted by changing the distance of the focusing lens from the entrance slit of the monochromator. The 632 nm peaks are obtained on the two track display for three possible combinations of d and s as the focusing lens is moved vertically downward. The distance of the vertical lens from the monochromator should be adjusted so that case C (d = c) is obtained and the vertical setting of the lens returned to the position where both optical spots are exactly aligned with the two tracks, as shown at the lower right of the figure.

obtained, the distance of the focusing lens from the entrance slit of the monochromator should be adjusted. After the proper patterns shown in Fig. 3 are obtained, the lens is finally reset to the position for which both spots (excited and reference region light) are aligned with the corresponding tracks. Some fine tuning can also be accomplished with the OMA track height and separation trimpots.

To ensure that no wavelength disparity exists between the two tracks, the monochromator setting is adjusted so that the peak of the 632 nm line of the He-Ne laser is near the center (channel 250) of both tracks. When the cursor is moved to the peak of the signal on one track, it should also lie within one channel of the peak of the signal on the second track. If this is not the case, the vidicon must be rotated about the optical axis until the two tracks are aligned properly with one another at this wavelength. The monochromator setting should be scanned in both directions to ensure that the heights of the peaks do not change as they approach either extreme (channels 0 or 499). If the intensities drop off before either extreme is reached, then the monochromator with vidicon attached must be rotated in the horizontal plane until the probe light enters the monochromator directly down the optical axis.

The microcomputer system

A complete description of the microcomputer, peripherals, and the simple OMA interface hardware and software is given elsewhere [13]. The system

is configured around the Motorola 6800 microprocessor, built into a Southwest Technical Products Corporation (SWTPC) mainframe. (SWTPC now offers a more powerful mainframe designed around the Motorola 6809 microprocessor; the same OMA interface circuitry can be used.) The entire microcomputer system, including 28K static RAM memory, 4K programmable EPROM, terminal, printer, plotter, A/D and D/A converters, 8-in. floppy disk drive with 350 Kbytes per disk, and software can be purchased for under $ 4000. Of these items, all except the plotter were purchased in kit form and assembled in our laboratory; all components can be purchased in assembled and tested form at additional cost.

Acquisition and presentation of spectral data

When the laser is fired, a trigger pulse from a flashlamp-light detection circuit in the main laser cavity is applied to the interface circuitry [13]. This in turn enables the OMA to accumulate excited and reference region data into the OMA A and B memories for the preset number of accumulation cycles. We use a preset of 10 to give an accumulation of 5 scans of each of the two tracks. Upon completion of the total accumulation, the OMA signals the computer that the experimental data are stored in the OMA memories and that data transfer from OMA to computer can take place. This transfer is completely controlled by the interface hardware and software [13], and the data are stored in the computer RAM memory. Immediately following this sequence, the results of a dark noise (laser not fired) accumulation are transferred to the computer and subtracted from the results of the data accumulation. For each of the 500 channels along the wavelength axis, the computer calculates $\Delta OD = \log$ (unexcited region data/excited region data) and stores the resultant spectrum on floppy disk. To correct the spectrum for inhomogeneities in the probe light falling on the two tracks a second spectrum is acquired and stored on disk according to the sequence just described, except that the excitation light is blocked. Several spectra with and without excitation are acquired and stored, the number depending on the magnitude and desired accuracy of ΔOD. A spectrum which is the average of those taken with no excitation present is subtracted point by point from the spectrum representing the average of those taken with excitation light present. The resultant is the final corrected spectrum of ΔOD vs. wavelength at the selected pump—probe delay time. We choose to store the spectrum obtained from each laser shot on floppy disk; however, spectra can be added and averaged within computer memory so that the system can be operated at a much higher repetition rate if necessary.

Wavelength resolution and total span of the spectrum are determined primarily by the dispersion of the monochromator grating (a 250 μm entrance slit is used). The active surface of the vidicon is 12.7 mm by 12.7 mm. For most studies we use a 147.5 grooves/mm grating having a dispersion of 26 nm/mm. Thus along the 500 channels of both vidicon tracks there is a $26 \times 12.7 = 330$ nm total wavelength span with $330/500 = 0.66$ nm/channel

resolution. Gratings of lower dispersion are used when higher resolution and lower total wavelength span are required. With large spectral spans and fast kinetics "chirping" of the probe beam must be considered. Chirping arises because different wavelengths of the continuum have different velocities in dispersive media and therefore arrive at the sample at different times. This effect can be measured and allowed for, but it is preferable to minimize chirping by reducing as much as possible the number of dispersive elements in the optical path [14].

For samples with both strong and weak regions of sample absorbance, colored glass and neutral density filters are used to keep the light intensity across the desired spectral range within the range of counts (100—700 counts per channel) that gives best reproducibility of ΔOD values.

RESULTS

Fig. 4 compares the near-infrared difference spectrum for the formation of state P^+Q^- in *Rhodopseudomonas spheroides* reaction centers obtained with the 2-d acquisition mode and the point-by-point 1-d method. Here, P is a bacteriochlorophyll dimer and Q is a ubiquinone [1]. The 1-d spectrum

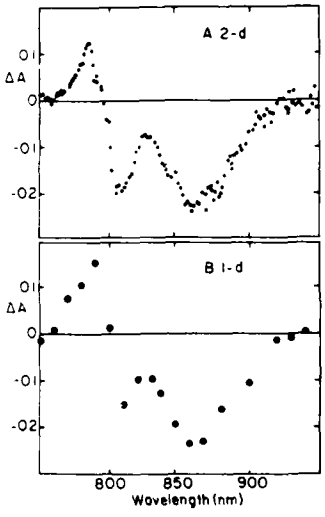

Fig. 4. Comparison of the transient difference spectrum for state P^+Q^- in *R. spheroides* R-26 reaction centers taken with 1-d and 2-d modes of operation. Both spectra were taken 500 ps after excitation with a 600 nm 8 ps pulse. The 1-d spectrum shown in B required about 90 laser shots and 4 h of work. The 2-d spectrum shown in A took only 7 laser shots with and 7 shots without excitation and required about 35 min to acquire and display. Each of the points on the 1-d spectrum is the average of 5 laser shots and typically has an S.D. of ±0.025. Because of the presence of both strong and weak regions of sample absorbance about 12 shots with and 12 without excitation in the 2-d mode will give ±0.025 accuracy across the entire region shown.

required 90 laser shots (5 at each wavelength) and took 4 h to obtain. The 2-d spectrum required 7 shots with and 7 shots without excitation, and was obtained in only 35 min. Thus, the acquisition time for 2-d operation is substantially less than for the 1-d method. Furthermore, points are obtained at intervals of 0.7 nm rather than 10 nm. The 2-d data give an essentially continuous spectrum and do not require guesses to be made as to how the appropriate curve through the points is to be drawn, as is necessary in the 1-d case. This advantage is particularly important for complex multicomponent systems such as the photosynthetic reaction centers, where transient difference spectra have many peaks and troughs over a relatively small wavelength range. For this reason the 2-d mode is extremely valuable for exploratory work on such biological systems, especially when prior information regarding highly featured spectra is absent.

CONCLUSIONS

The automated picosecond spectrometer we have described makes possible the acquisition, in a period of less than an hour using only one or two dozen laser shots, broad-band absorption spectra of transient intermediates over a range of up to 300 nm with excellent resolution in both absorbance (±0.025) and wavelength (0.7 nm). These features are especially useful for studying biological systems. Lower resolution spectra, suitable for exploratory study of new systems, are obtained in a matter of minutes with only a few laser shots — a great advantage in the case of samples susceptible to photodegradation. The system can be constructed at a modest incremental cost ($ 7200) over the cost of instrumentation present in most picosecond spectroscopy laboratories. In addition to controlling the detection system for the picosecond laser apparatus, the microcomputer system we have described is also very useful for acquisition and analysis of data from other laboratory instruments.

REFERENCES

1 Holten, D. and M.W. Windsor (1978) Ann. Rev. Biophys. Bioeng. *7*, 189–227.
2 Campillo, A.J. and S.L. Shapiro (1977) *in:* Ultra Short Light Pulses (Shapiro, S.L., ed.), pp. 317–376. Springer, Heidelberg.
3 Rentzepis, P.M. (1978) Biophys. J. *23*, 272–284.
4 Magde, D. and M.W. Windsor (1974) Chem. Phys. Lett. *27*, 31–36.
5 Pyke, S.C. and M.W. Windsor (1980) *in:* Chemical Experimentation Under Extreme Conditions (Rossiter, B.V., ed.), pp. 205–276. Interscience, New York
6 Eisenthal, K.B. (1977) see ref. 2, pp. 275–315.
7 Lauberau, A. and K. Kaiser (1975) Ann. Rev. Phys. Chem. *26*, 83–99.
8 Green, B.I., R.B. Weisman and R.M. Hochstrasser (1979) Chem. Phys. Lett. *62*, 427–430.
9 Ippen, E.P. and C.V. Shank (1978) *in:* Picosecond Phenomena (Shank, C.V., Ippen, E.P. and Shapiro, S.L., eds.), pp. 103–107. Springer, Heidelberg.
10 Green, S.I., R.M. Hochstrasser, R.B. Weisman and W.A. Eaton (1978) Proc. Nat. Acad. Sci. U.S.A. *75*, 5255–5259.

11 Netzel, T.L., P. Kroger, C.K. Chang, I. Fujita and J. Fajer (1979) *Chem. Phys. Lett.* *67*, 223–228.
12 Huppert, D., K.D. Straub and P.M. Rentzepis (1977) *Proc. Nat. Acad. Sci. U.S.A.* *74*, 4139–4143.
13 Holten, D., D.A. Cremers, S.C. Pyke, R. Selensky, S.S. Shah, D.W. Warner and M.W. Windsor (1979) Rev. Sci. Instrum. *50*, 1653–1655.
14 Holten, D., C. Hoganson, M.W. Windsor, C.D. Schenck, W.W. Parson, R.L. Fork, A. Migus and C.V. Shank (1980) Biochim. Biophys. Acta (in press).

Photobiochemistry and Photobiophysics, 1 (1980) 361–373

MODELS FOR PHOTOSYNTHETIC CHARGE SEPARATION: EXCITED STATE ELECTRON TRANSFER REACTIONS OF BACTERIOPHEOPHYTIN IN MICELLES

S. SADIQ SHAH, DEWEY HOLTEN * and MAURICE W. WINDSOR

Department of Chemistry, Washington State University, Pullman, WA 99164, U.S.A.

Received July 4, 1980
Accepted July 6, 1980

INTRODUCTION

Photoinitiated charge separation in bacterial reaction centers involves at least two electron transfer steps: an initial step from the excited singlet state (P^*) of a bacteriochlorophyll dimer (P) to a bacteriopheophytin (BPh) within 4 ps of excitation [1] followed by transfer of the electron from BPh^- to a quinone in about 200 ps [1–4]. Both steps have quantum yields of 100% [5,6], indicating that the forward reaction is much faster than the reverse electron transfer within the intermediate radical pair state [P^+BPh^-].

In homogeneous solution the situation is quite different. Although the excited singlet states of BPh and chlorophyll (Chl) are effectively quenched by *p*-benzoquinone (BQ) and other electron acceptors in polar organic solvents, this reaction does not lead to detectable yields of charge separated ions [7–10]. In contrast, electron transfer from the lowest excited triplet states of BPh and Chl to BQ yields easily detectable amounts of the radical cations [8–11]. The reason adduced is that reverse electron transfer within the intermediate triplet radical pairs to give the ground singlet state is spin-forbidden, giving the ions more time to diffuse apart [12,13]. Under specially favorable conditions in solution radical ions have been detected from excited singlet state electron transfer. For example, in the case of BPh^* quenched by methyl viologen (MV^{++}), the radical pair state [BPh^+MV^+] is repulsive and the ions fly apart. But, even under these extreme conditions, 75% of the singlet radical pairs deactivate to the ground state by reverse electron transfer [14].

It is not at present understood why the singlet pathway is so effective in the reaction center, whereas only the triplet route operates effectively in homogeneous solution, although several reasons for this difference in behav-

* Present address: Department of Chemistry, Washington University, St. Louis, MO 63130, U.S.A.

ior have been considered. These include the effect of vibrational changes (Franck–Condon factors) on reverse electron transfer rates and the possibility that different orbitals may be involved in the forward and reverse electron transfer steps [13,14]. The possible importance of the microscopic environment in assisting charge separation and hindering reverse electron transfer in reaction centers has not explicitly been considered in these discussions. To explore its role, we have studied reactions of photoexcited BPh in aqueous micellar solutions with picosecond and slower spectroscopic techniques.

Surfactant (detergent) molecules possess a polar headgroup and a nonpolar hydrocarbon tail. In a narrow concentration range the surfactant molecules self-aggregate in aqueous solution to form colloidal complexes of high molecular weight, called micelles [15]. These are roughly spherical structures with a nonpolar inner core comprising the hydrocarbon tails and a charged surface region made up of the headgroups, called the Stern layer, surrounded by the counterions and the bulk aqueous phase. The micellar surface is positively charged (cationic) in cetyltrimethylammonium bromide (CTAB) micelles and negatively charged (anionic) in sodium dodecylsulfate (SDS) micelles. The hydrophobic interactions responsible for micellar stability are similar to those which stabilize biological membranes and globular proteins [15]. Micelles provide a means for imposing structure on the microscopic environment and for controlling the distance between the reactants.

Our purpose in undertaking the studies presented here was to find out if micelles could affect the rate of electron transfer between the reactants, the rate of reverse electron transfer within the radical pair state, and the recombination rate of separated ions. Previous studies in micelles of electron transfer from photosynthetic pigments and other porphyrins to various electron acceptors have had some success in this regard [16–19]. We chose the systems BPh + BQ and BPh + MV^{++} for our initial investigations in micelles because the excited state photophysics and electron transfer behavior of BPh with these electron acceptors in homogeneous solution are well characterized [8,12–14]. By comparing results obtained in micelles, homogeneous solutions, and reaction centers, we hope to explore the effect of the environment on charge separation in a systematic way.

METHODS AND MATERIALS

The picosecond apparatus has been described previously [20]. For the present study, 8 ps 530 nm flashes were used to excite sample solutions of 40 μM BPh in 2 or 5 mm path cells. Microsecond flash photolysis studies made use of 200 ns 530 nm excitation flashes from a flashlamp-pumped coumarin 7 dye laser. The detection system was similar in design to that used previously [8]. It consisted of a 0.25 m monochromator, RCA 7151W photomultiplier tube, op-amp circuit, and Tektronix 549 storage oscilloscope. The total detection system had a response time of approximately 1 μs.

BPh was prepared as described previously [8]. Micellar solutions were prepared by injecting concentrated aliquots of BPh in ethanol into 0.1 M aqueous CTAB or SDS, followed by addition of the electron acceptor. These solutions were thoroughly degassed by at least 10 freeze–thaw cycles on a high-vacuum line, and sealed. Fluorescence quenching studies were carried out on a Farrand MKI spectrofluorometer. Proton NMR spectra were recorded on a JEOL-100 spectrometer.

RESULTS

Electron transfer from photoexcited BPh to BQ in CTAB micelles and in a number of organic solvents was investigated in detail. Less detailed studies were made of BPh + MV^{++} in CTAB and BPh in SDS micelles.

Sites of solubilization

Previous studies suggest that Chl*a* and other metalloporphyrins reside in the nonpolar inner core of micelles. In the case of Chl*a* and related pigments, it has been suggested that hydrophobic interactions between the hydrocarbon (phytyl) chain of the substrate and the hydrocarbon chain of the surfactant molecules assist in the incorporation of the substrate molecules into the micelles [17,21,22]. Based on the structural similarity between Chl*a* and BPh we believe that BPh is incorporated into the inner core of the micelle. Furthermore, solid BPh is insoluble in water, while an ethanolic stock solution of BPh is very soluble in aqueous surfactant solutions. Alcohols are known to be solubilized in micelles, rather than in the bulk aqueous phase [15].

The sites of solubilization of BQ and MV^{++} in CTAB and SDS micelles were determined by proton NMR spectroscopy. In all cases but MV^{++} in CTAB, we observed shifts in the α-CH_2 resonance of the surfactant molecule hydrocarbon chain, suggesting that these electron acceptors are solubilized on the average near the inner surface of the Stern layer. In the case of MV^{++} in CTAB, repulsive interactions force the ion away from the positively charged surface of the micelle into the bulk aqueous phase. As described below, the behavior of photoexcited BPh in the presence of BQ or MV^{++} supports our views on the sites of solubilization of all three molecules.

Excited state spectra and lifetimes in the absence of quenchers

Difference spectra for the formation of $BPh^{\bullet}$ and BPh^{T} in CTAB micelles are shown in Fig. 1. These spectra are closely similar to those obtained in ethanol, in cyclohexane, and previously in acetone : methanol (7 : 3) solution [8,14]. The spectrum for the formation of $BPh^{\bullet}$ (crosses in Fig. 1) is also shown and will be discussed below.

The lifetime of $BPh^{\bullet}$ was obtained from the decay of excited state absorbance at 610 nm (an isosbestic wavelength in the spectrum of $BPh^{\bullet}$, Fig. 1)

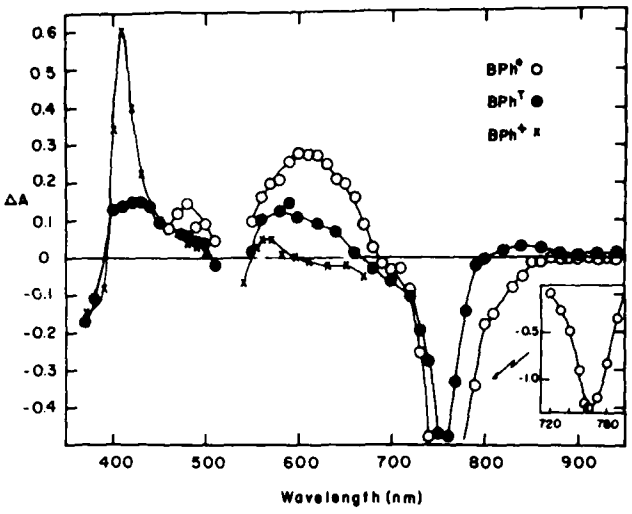

Fig. 1. Difference spectra for the formation of BPh^* (○), BPh^T (●), and BPh^+ (×) in CTAB micelles. The BPh^* spectrum was measured 50 ps after excitation of 40 μM BPh with 8 ps 530 nm flashes. Absorbance changes between 720 and 800 nm were measured in a 2 mm path cell and then scaled for the 5 mm path cell used for the remainder of the spectrum. The spectrum of BPh^T was measured from 450 to 950 nm with the ps apparatus 5 ns after excitation of 40 μM BPh in a 5 mm path cell and with the μs apparatus from 360 to 650 nm. The latter measurements employed 200 ns 530 nm flashes with 20 μM BPh in a 1 cm cell. The two portions were normalized at 600 nm and plotted together. The spectrum of BPh^+ (×) was obtained from the initial absorbance changes on the μs apparatus following excitation of 20 μM BPh + 20 mM BQ in CTAB in a 1 cm cell. These absorbance changes were scaled by the same amount as the BPh^T spectrum; the measured absorbance change at 410 nm was 0.1. Each point from the ps measurements is the average of at least 5 laser shots, while those from the μs apparatus are the average of 2 laser shots.

and from recovery of BPh ground state bleaching at 755 nm. Lifetimes measured at the two wavelengths were the same within experimental error. Fig. 2 shows the first order decay plot for BPh^* in CTAB at 755 nm. Measurements at this wavelength and at 610 nm give lifetimes for BPh^* of 2.2 ± 0.3 ns in CTAB, 2.0 ± 0.2 ns in ethanol and 2.1 ± 0.2 ns in cyclohexane. These figures are the same within experimental error as the value of 2.0 ± 0.2 ns obtained previously in acetone : methanol (7 : 3) solution [8]. The agreement suggests that there is no significant heavy atom effect of the Br^- counter ions on the decay of BPh^* in CTAB micelles, and supports the view expressed above that BPh resides in the inner core of the micelles with no access to the aqueous phase where the Br^- ions are located. The BPh^* lifetime also appears to be insensitive to the presence of O_2, since the same lifetime was obtained whether or not samples were degassed. Henceforth, we will use a value of 2 ns for the BPh^* lifetime in the absence of quencher in CTAB micelles or in the organic solvents used in this study.

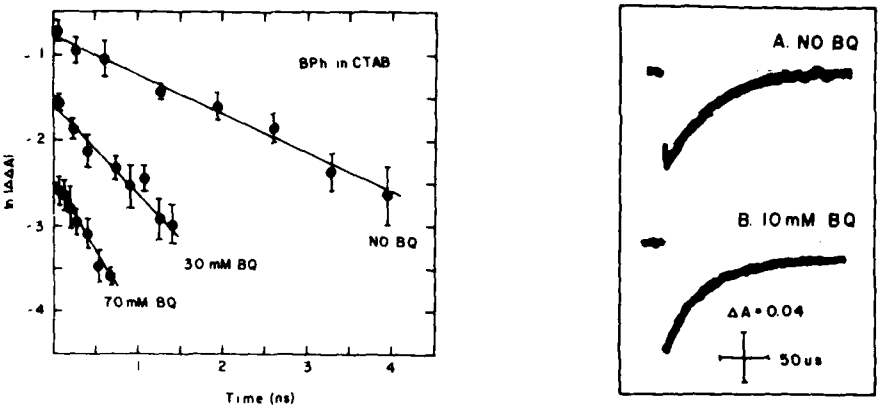

Fig. 2. First order BPh* decay plots measured from recovery of ground state bleaching at 755 nm following excitation of 40 μM BPh in CTAB micelles in the presence or absence of BQ with 8 ps 530 nm flashes. The quantity $\ln|\Delta\Delta A|$ plotted on the ordinate is the absorbance change measured at time, t, minus the value measured at the asymptote of the decay curve, measured between 5 and 9 ns after excitation. The absorbance change at each time is the average of the results from at least 5 laser shots. The lifetimes obtained from a series of measurements such as those shown, at both 755 and 610 nm, are listed in Table I.

Fig. 3. Absorbance changes at 420 nm following excitation of 20 μM BPh in CTAB micelles in the presence or absence of BQ with 200 ns 530 nm flashes.

By contrast, the lifetime of the triplet state, BPh^T, is extremely sensitive to the presence of O_2 and its lifetime was measured with the μs apparatus in thoroughly degassed samples at several wavelengths between 400 and 650 nm. The decays in CTAB micelles (Fig. 3A) in ethanol and in cyclohexane were found to be first order, with a time constant of 46 ± 4 μs. A value of 16 ± 2 μs was reported previously in acetone : methanol (7 : 3) [8].

Excited state quenching by BQ

The lifetime of BPh* in CTAB is reduced from 2 ns to 1.1 or to 0.6 ns upon addition of 30 or 70 mM BQ (Fig. 2). Addition of the same concentrations of BQ to samples of BPh in ethanol decreases the lifetime of BPh* to 1.3 or to 0.9 ns, respectively. The results of the BPh* lifetime measurements are gathered in Table I.

Fig. 4 shows the Stern—Volmer plot for quenching of BPh* fluorescence by BQ in CTAB micelles. Quenching appears to be linear up to about 30 mM BQ, giving a quenching constant $K_Q = 33 \pm 2\ M^{-1}$. Together with the lifetime in the absence of quencher, $\tau_s^0 = 2.2$ ns, this yields a second order quenching rate constant $k_q = K_Q/\tau_s^0 = 1.5 \pm 0.2 \times 10^{10}\ M^{-1} \cdot s^{-1}$ in CTAB.

Above 30 mM the quenching becomes nonlinear in BQ concentration

TABLE I

EXCITED SINGLET LIFETIMES AND TRIPLET YIELDS

Medium	BQ (mM)	τ_s (ns)	ϕ_T
CTAB micelles	0	2.2 ± 0.3	0.46 [a]
	30	1.1 ± 0.2	0.25 [b]
	70	0.6 ± 0.1	0.14 [b]
Ethanol	0	2.0 ± 0.2	0.46 [a]
	30	1.2 ± 0.1	0.28 [b]
	70	0.9 ± 0.1	0.21 [b]
SDS micelles	0	0.8 [c]	
Cyclohexane	0	2.1 ± 0.2	

[a] Measured in acetone : methanol (7 : 3) [8,14].
[b] Calculated from $\phi_T = k_{isc}\tau_s$ with $k_{isc} = 2.3 \pm 0.4 \times 10^8\ M^{-1} \cdot s^{-1}$ [14].
[c] Biphasic (see text).

(closed circles in Fig. 4). However, this does not appear to be due to ground state complexes involving BPh and BQ, because at the highest concentration of BQ used (80 mM) no new bands were observed in the absorption or fluorescence spectra. Such nonlinear quenching behavior has been attributed to static quenching [23]. This is thought to involve "instantaneous" quenching of those BPh* molecules formed within an active quenching radius of an electron acceptor, and thus becomes increasingly important at higher quenching concentrations.

The results of BPh* lifetime reduction by BQ in CTAB micelles (Fig. 2 and Table I) are also plotted in Fig. 4 (open circles) and give the same value of K_Q within experimental error as the fluorescence quenching data. However, the lifetime quenching appears to be linear up to the highest concentration of BQ used (70 mM). This quantity would not be expected to be affected by static quenching as severely as is the fluoresence yield [23].

Fluorescence quenching and BPh* lifetime reduction data in ethanol are also presented in Fig. 4 and Table I. Fluorescence quenching (closed triangles) is linear up to about 30 mM BQ with $K_Q = 22 \pm 2\ M^{-1}$. Given the BPh* lifetime of 2 ns in the absence of quencher, we obtain $k_q = 1.1 \pm 0.1 \times 10^{10}\ M^{-1} \cdot s^{-1}$ in ethanol. As in the case of CTAB micelles, fluorescence quenching but not BPh* lifetime reduction (open triangles) becomes nonlinear at high BQ concentrations. From similar measurements, we obtained the second order quenching rate constants in acetone : methanol (7 : 3) and in acetone listed in Table II. The results indicate that quenching of BPh* by BQ in CTAB micelles is about the same as that observed in a number of organic solvents and slightly faster than in ethanol.

Previous studies of BPh in acetone : methanol (7 : 3) in the absence of quenchers gave a quantum yield for BPh^T of 0.46 ± 0.08 and a rate constant for intersystem crossing, $k_{isc} = 2.3 \pm 0.4 \times 10^8\ M^{-1} \cdot s^{-1}$ [14]. It is reasonable to assume the same values in CTAB micelles in view of the absence of a

TABLE II

SECOND ORDER RATE CONSTANTS ($\times 10^{10}$ $M^{-1} \cdot s^{-1}$)

Solvent	$BPh^* + BQ$	$BPh^* + BQ^-$
CTAB micelles	1.5 ± 0.2	2.3 ± 1.5
Ethanol	1.1 ± 0.1	1.4 ± 1.0
Acetone · methanol	1.7 ± 0.2	1.8 ± 1.0 [a]
Acetone	1.6 ± 0.2	2.8 ± 1.1
Cyclohexane	—	[b]

[a] Measured in this study and in ref. 8.
[b] No ions detected (see text).

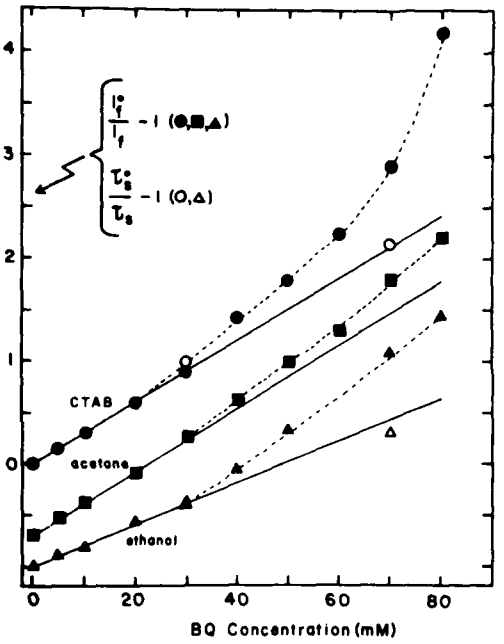

Fig. 4. Fluorescence quenching (closed symbols) and BPh^* lifetime reduction (open symbols) for BPh in CTAB micelles, in acetone and in ethanol as a function of BQ concentration. Fluorescence from samples of 20 μM BPh was detected at 770 nm and excited at 735 nm to avoid corrections for absorption of the excitation light by BQ. BPh^* lifetimes were measured as in Fig. 2. For the ordinate of the plots, I_f and τ_s are the fluorescence intensity and BPh^* lifetime while the superscript (^{0}) refers to the value in the absence of quencher. For the purpose of presenting the data, the results in acetone and in ethanol have been shifted down vertically by 0.6 and 1.0 units along the ordinate respectively. From the linear portions of the curves quenching constants of 33 ± 2, 32 ± 2 and 22 ± 2 M^{-1} are obtained for CTAB micelles, acetone, and ethanol. These values and those obtained in other solvents were used together with the BPh^* lifetime in the absence of quencher to attain the second order quenching rate constants listed in Table II.

heavy atom effect of the BPh^* lifetime (see above). In the presence of quenchers, the triplet yield is given by $\varphi_T = k_{isc}\tau_s$ where τ_s is the BPh^* lifetime with quencher present. With this expression, we obtain the values of ϕ_T shown in Table I for BPh in CTAB micelles and in ethanol with 30 or 70 mM BQ present.

Formation of cation radicals

Irradiation of BPh in CTAB micelles or in ethanol in the presence of BQ with 200 ns 530 nm flashes produces absorption changes attributable to the formation of the cation radical, BPh^+ (Fig. 1). We also see this spectrum following excitation of BPh and BQ in ethanol, and the same spectrum has been reported previously in acetone : methanol (7 : 3) solution [8], and following electrochemical production of BPh^+ in CH_2Cl_2 [24].

Kinetics for the decay of BPh^+ measured at 420 nm for 10 μM BPh and 10 mM BQ in CTAB (Fig. 3B) or in organic solvents were computer fit with an iterative least squares program for mixed first and second order kinetics [25]. The decay of BPh^+ was found to be essentially second order in CTAB and in all organic solvents used. With a value of $1.0 \pm 0.3 \times 10^5\ M^{-1} \cdot cm^{-1}$ for the differential extinction coefficient at 420 nm (an average of values obtained in acetone : methanol [14] and CH_2Cl_2 [24]), we obtain the second order rate constants for the recombination of the separated ions, BPh^+ and BQ^-, listed in Table II.

Addition of 10 mM BQ to 20 mM BPh in cyclohexane quenches all detectable absorbance changes on the μs apparatus, indicating that the intermediate radical pairs deactivate completely to the ground state by reverse electron transfer before the ions can separate. This behavior is consistent with the results obtained on a variety of systems, in which charge separation is inhibited in nonpolar solvents [23].

With the ps apparatus, no additional absorbance changes near 850 nm, where BPh^+ is known to have weak absorption [8,24], were detectable for 40 μM BPh in CTAB micelles in the presence of 30 or 70 mM BQ. At 30 mM BQ, the expected yield is about 50% (Fig. 4) if every BPh^* that is quenched leads to the production of separated ions, or about 25% (Table I) if every BPh^T that is formed reacts with a BQ to give a BPh^+. Since the detection limit for absorbance changes is 0.025 with our ps apparatus, the yield of BPh^+ could be as much as 40% at the 40 μM BPh concentration used and still go unobserved at 850 nm. Thus we could not determine the relative efficiencies of BPh^* and BPh^T in producing radical ions.

A better region for monitoring the formation of BPh^+ would be at 400 nm where it absorbs strongly (Fig. 1). Unfortunately, we could not make ps observations in this region because of strong sample absorbance and declining probe intensity. Efforts are currently underway to obtain enhanced probe intensity in the 400 nm region by using 530 nm light to generate the picosecond continuum and by improvements in the optics.

The fact that BPh is readily seen with 200 ns excitation flashes (Fig. 1)

but goes undetected in the ps experiments is explained by multiple recycling of the system during the much longer 200 ns flashes. Thus our observation of BPh^* in this case (Fig. 1) does not necessarily imply a high intrinsic quantum yield of formation [8].

Quenching by methyl viologen

Addition of up to 80 mM MV^{++} to samples of BPh in CTAB causes no detectable changes either in the lifetime of BPh^* or in the fluorescence yield. This observation is consistent with the NMR results presented earlier which indicate that MV^{++} is forced into the bulk aqueous phase by repulsive interaction with the positively charged micellar surface. It also supports the contention that BPh is located in the micellar inner core, with no access to the aqueous phase.

Aggregation of BPh in SDS micelles

In SDS micelles a distinct shoulder near 840 nm appears on the long-wavelength side of the BPh absorption band centered at 760 nm, and a corresponding shoulder, although weak, appears in the appropriate region of the fluorescence spectrum. Such a shoulder is usually taken as evidence for aggregation [18]. Additional evidence comes from the observed reduction of the BPh^* lifetime. For 20 μM BPh in SDS micelles, in the absence of quencher, the decay of BPh^* is biphasic with an 800 ps major component and a smaller amplitude component of several nanoseconds. The latter value is in the same range as that obtained above for unaggregated BPh in other solvents (Table I), and probably corresponds to the lifetime for unaggregated BPh. The faster component undoubtedly reflects the lifetime of aggregated BPh, since a reduction in excited singlet state lifetime usually accompanies aggregation [23].

A possible explanation for aggregation of BPh in SDS but not in CTAB is that SDS micelles have a larger inner core [15] that could accommodate more than one BPh. However, at the concentrations used (20 μM BPh and 1—3 mM micelles) the probability of there being more than one BPh per micelle is extremely low. The observed aggregation in SDS implies additional specific interactions involving BPh and SDS that do not occur in the case of CTAB micelles.

In addition to the problem of aggregation of BPh, some thermal chemistry involving BQ also occurs in SDS micelles. This appears to include conversion of some BQ to the semiquinone; it could be facilitated by water molecules that penetrate to a certain extent into the SDS micelles [15]. We did not observe such degradation of BQ in CTAB micelles over the period of the measurements.

DISCUSSION

The incentive for undertaking the present study was to see if micelles could be used to enhance or retard the rates of the electron transfer reactions involving BPh and BQ or MV^{++} compared to those found in homogeneous solution. We hoped by using micelles to accomplish three important objectives. First, to increase the effectiveness of quenching BPh^{*} and BPh^{T} by electron acceptors by reason of the forced proximity of the partners within the micelle. Second, to increase the rate of separation of the radical ions by means of specific charge interactions present in the micelle, thus reducing the adverse effect of fast reverse electron transfer within the radical pair states. And third, to reduce the rate of recombination of the radical ions, once they had separated, because one ion would be outside the micelle while the other would be retained within the inner core.

BPh^{*} is readily quenched by BQ in CTAB micelles, but with a second order rate constant not appreciably different from those measured in a number of organic solvents (Table II). At relatively low BQ concentrations (Fig. 4), CTAB micelles do not provide an environment that gives more efficient quenching of BPh^{*} than do organic solvents. Quenching is somewhat less effective in ethanol. Alcohols are known to affect the redox potential of Chl, possibly through complexing to the ring-keto oxygen [26]. Similar interactions could occur between BPh and ethanol, making BPh a weaker electron donor in ethanol than in the other solvents. We did not explore this possibility in detail.

Electron transfer quenching occurs after the acceptor has approached to within an effective quenching distance of the donor and after the molecules have reoriented to a position giving the good orbital overlap on which electron transfer strongly depends [27]. In the region of linear quenching (below about 30 mM BQ in Fig. 4), diffusion of the reactants to within the critical quenching distance is generally believed to be the rate-limiting step in homogeneous solution. The finding of similar quenching rates in CTAB micelles and in a number of organic solvents (Table II) would be explained if the surface region of the CTAB micelle does not restrict movement of BQ toward or away from the BPh within the micelle. Alternatively there might be compensating effects arising from restricted outward diffusion of BQs preferentially solubilized within the Stern layer, and from inhibition of the necessary molecular reorientation by the semi-structured micellar environment.

At high BQ concentrations, the fluorescence quenching becomes nonlinear in all solvent systems studied. As shown by the closed circles in Fig. 4, this nonlinearity is especially pronounced in CTAB micelles. As stated above, this effect does not appear to involve the formation of ground state complexes between BPh and BQ. It does suggest that at high quencher concentrations more BQ molecules lie within the effective quenching radius of the BPhs at the time of excitation. The effect would be greater in CTAB micelles because BQs are preferentially solubilized at the inner surface of the Stern layer (see above), whereas in homogeneous solution BQs undergo random diffusion.

These BPh^* molecules are "instantaneously" quenched upon excitation, while the remaining ones are quenched by those BQs that must diffuse before electron transfer can occur. Both types of quenching behavior affect the fluorescence yield, while only the latter will affect the BPh^* lifetime. These arguments explain the fluorescence quenching and BPh^* lifetime reduction measurements shown in Fig. 4, and are consistent with previous studies on a number of systems [23]. Our results show that only at high quencher concentrations is electron transfer from BPh^* to BQ more efficient in CTAB micelles than in homogeneous solution.

The observed yield of BPh^* in CTAB micelles is about a factor of two lower than that found in acetone, acetone : methanol (7 : 3), or in ethanol, judging from the amplitude of the initial absorbance changes at 420 nm following excitation of 20 μM BPh in the presence of 20 mM BQ with 200 ns flashes (cf. Fig. 3B). Apparently, attractive interaction between BQ^- and the positively charged micellar surface hinders, to some extent, ejection of BQ^- into the aqueous phase. In contrast, just the opposite behavior is observed for the quenching of Chl by duroquinone in SDS micelles, where the duroquinone anion appears to be forced into the bulk aqueous phase by repulsive interactions with the negatively charged micellar surface [17]. One might expect a similar enhancement of charge separation with MV^{++} as an electron acceptor in CTAB micelles, but, in fact, such an enhancement is not observed. The explanation probably lies in repulsive interactions between MV^{++} and the similarly charged micellar surface that prevent MV^{++} from getting close enough to BPh for effective quenching. This finding supports our view that BPh is solubilized within the micelle and that the quencher must penetrate into the micelle or at least into the Stern layer for electron transfer to occur. In nonpolar organic solvents such as cyclohexane, charge separation appears not to occur at all due to poor solubilization of the radical ions (Table II).

The rate of recombination of BPh^* and BQ^- is also about the same or possibly slightly faster in CTAB micelles than in a number of polar organic solvents (Table II). Our observation that the BPh^* decay is second order indicates that a BPh^* is reduced by a BQ^- different from the one formed in a particular forward electron transfer reaction. This could occur if the electron is transferred between BQ^- and other BQs at the inner surface of the micelle before being returned back to a BPh^*. It is also possible that BQ^- escapes from one micelle and reduces a BPh^* in another micelle, but this possibility is not very attractive in view of the site of solubilization of BQ and the attractive interaction between BQ^- and the positively charged micellar surface. Experiments using a third molecule solubilized in the bulk aqueous phase which could reoxidize the BQ^- will be necessary to distinguish between these possibilities.

Consistent with our results for BPh + BQ in CTAB micelles, it has been found previously that the rate of recombination of Chl^* and MV^* in nonionic micelles is about the same as in ethanol [16]. Thus, only under favorable conditions is the recombination rate of separated ions reduced by the

micellar environment. We expected the rate of recombination of $BPh^{\cdot}$ and BQ^{-} to be reduced in SDS (anionic) micelles, because of the possibility that BQ^{-} would be ejected into the bulk aqueous phase by repulsive interactions. As mentioned above this has indeed been observed in the case of quenching of Chl^{*} by duroquinone in SDS micelles [17]. However, in the present study, aggregation of BPh and additional chemistry involving BQ in SDS micelles prevented us from testing this hypothesis. We plan to explore this matter further in our future investigations of electron transfer in micelles.

CONCLUSIONS

BPh is preferentially solubilized within the inner core of the micelle. Electron transfer from BPh^{*} to BQ is more efficient in CTAB micelles than in homogeneous solutions at high BQ concentrations. At low BQ concentrations the quenching rate is about the same in the two systems, and the yield of charge separated ions is slightly lower in CTAB micelles than in homogeneous solution. The recombination rate of the ions that do separate is about the same or slightly faster in CTAB micelles than in a number of organic solvents.

Quenching of BPh^{*} by MV^{++} in CTAB micelles is inhibited by repulsive interactions between the electron acceptor and the surface region of the micelle. Aggregation of BPh in SDS micelles is important even at low concentrations, indicating that there are some special interactions, involving BPh and SDS micelles, that do not occur in CTAB. Some thermal chemistry, involving BQ, also takes place in SDS micelles.

Additional studies with an expanded series of electron donors and acceptors are underway to investigate further the effects of various types of micelles on electron transfer quenching, the yields of ion separation, and the rates of charge recombination. We also plan to explore further the difference in reactivity of excited singlet and triplet state electron donors in micelles, since this difference is important for devising efficient model systems based on photosynthetic energy conversion.

ACKNOWLEDGEMENTS

This work was supported by the U.S. Army Research Office under grant DAAG29-76-9-0275, and by the NSF under grant PCM79-02911.

REFERENCES

1 Holten, D., C. Hoganson, M.W. Windsor, C.C. Schenk, W.W. Parson, A. Migus, R.L. Fork and C.V. Shank (1980) Biochim. Biophys. Acta in press.
2 Kaufmann, K.J., P.L. Dutton, T.L. Netzel, J.S. Leigh and P.M. Rentzepis (1975) Science *188*, 1301.
3 Rockley, M.G., M.W. Windsor, R.J. Cogdell and W.W. Parson (1975) Proc. Natl. Acad. Sci. U.S.A. *72*, 2251.

4 Holten, D., M.W. Windsor, W.W. Parson and J.P. Thornber (1978) Biochim. Biophys. Acta *501*, 112.
5 Wraight, C.A. (1977) Biochim. Biophys. Acta *459*, 525.
6 Parson, W.W., R.K. Clayton and R.J. Cogdell (1975) Biochim. Biophys. Acta *416*, 105.
7 Huppert, D., P.M. Rentzepis and G. Tollin (1976) Biochim. Biochim. Acta *440*, 356.
8 Holten, D., M. Gouterman, W.W. Parson, M.W. Windsor and M.G. Rockley (1976) Photochem. Photobiol. *23*, 415.
9 Lamola, A.A., M.L. Manion, H.D. Roth and G. Tollin (1975) Proc. Natl. Acad. Sci. U.S.A. *72*, 3265.
10 Andreava, N.E., G.V. Zakharova, V.V. Shubin and A.K. Chibisov (1978) Chem. Phys. Lett. *53*, 317.
11 Tollin, G., F. Castelli, G. Cheddar and F. Rizzuto (1978) Photochem. Photobiol. *29*, 147, 153.
12 Gouterman, M. and D. Holten (1977) Photochem. Photobiol. *25*, 85.
13 Holten, D. and M.W. Windsor (1978) Ann. Rev. Biophys. Bioeng. *7*, 189.
14 Holten, D., M. Gouterman, W.W. Parson and M.W. Windsor (1978) Photochem. Photobiol. *28*, 951.
15 Fendler, J.H. and E.J. Fendler (1975) Catalysis in Micellar and Macromolecular Systems. Academic Press, New York.
16 Kalyanasundaram, K. and G. Porter (1978) Proc. R. Soc. London A.
17 Wolf, C. and M. Grätzel (1977) Chem. Phys. Lett. *52*, 542.
18 Seely, G.R. (1977) *in*: Topics in Photosynthesis (Barber, J., ed.) pp. 36–37. Elsevier, Amsterdam.
19 Kano, K., K. Takuma, T. Ikeda, D. Nakajima, Y. Tsutsui and M. Matsuo (1978) Photochem. Photobiol. *27*, 695.
20 Magde, D. and M.W. Windsor (1974) Chem. Phys. Lett. *27*, 31.
21 Simplicio, J. (1972) Biochemistry *11*, 2525.
22 Minch, M.J. and S.S. Shah (1979) J. Org. Chem. *44*, 3252.
23 Birks, J.B. (1970) Photophysics of Aromatic Molecules. Wiley, New York.
24 Fajer, J., D.C. Borg, A. Forman, R.H. Felton, D. Dolphin and L. Vegh (1974) Proc. Natl. Acad. Sci. U.S.A. *71*, 994.
25 Gorman, D.S. and J.S. Connolly (1973) Int. J. Chem. Kinet. *5*, 977.
26 Diehn, B. and G.R. Seely (1968) Biochim. Biophys. Acta *153*, 862.
27 Kestner, N.R., J. Logan and J. Jorther (1974) J. Phys. Chem. *78*, 2148.

Chemical Physics 60 (1981) 33–46
North-Holland Publishing Company

EXCITONIC INTERACTIONS IN COVALENTLY-LINKED PORPHYRIN DIMERS

Ron SELENSKY, Dewey HOLTEN*, Maurice W. WINDSOR
Department of Chemistry, Washington State University, Pullman, WA 99164, USA

John B. PAINE III, David DOLPHIN
Department of Chemistry, University of British Columbia, Vancouver, BC, V6T 1Y6, Canada

and

Martin GOUTERMAN and John C. THOMAS‡
Department of Chemistry, University of Washington, Seattle, WA 98195, USA

Received 14 February 1981

We have studied the absorption spectra, emission spectra, and fluorescence excitation polarization spectra of a series of free base and diprotonated etioporphyrin-I dimers covalently linked through $(CH_2)_n$ bridges, $n = 0$–8. The absorption spectra of the $n = 0$ and $n = 1$ dimers show red shifts, which are largest (≈15 mm) for the Soret band of the $n = 0$ dimer. The Soret bands of the diprotonated dimers $n = 0$–3 show splitting (≈500–1000 cm^{-1}) which can be interpreted by an exciton model assuming a reasonable geometry. The fluorescence spectra and quantum yields are similar to that of the monomer, except for the same red shift seen in absorption; however, the $n = 0$ diprotonated dimer shows an anomalous vibronic structure. The fluorescence excitation polarization spectra for the $n = 0$ and the $n = 1$ dimers differ substantially from the monomer; the dimers $n \geq 3$ have fluorescence excitation polarization spectra that suggest that some of the excitation stays localized in one moiety while the rest hops to the dimer partner.

1. Introduction

(Bacterio)chlorophyll and related pigment molecules serve several important functions in the photosynthetic process. Antenna (bacterio)-chlorophylls absorb the incident light and transfer the excitation energy to photochemically active pigment–protein complexes, called reaction centers, where the initial charge separation process takes place. In the reaction center, the harvested energy promotes a primary electron donor to an excited state, which then transfers an electron to the primary electron acceptor via one or more intermediary electron carriers. In reaction centers isolated from photosynthetic bacteria, the primary donor appears to be a special pair or dimer of bacteriochlorophyll molecules [1–4]. It is believed that special electronic properties resulting from the excitonic interactions within this dimer contribute to its important role in the charge separation process. For example, exciton splitting in the excited singlet state gives the dimer two absorption bands, one of which is lower and the other higher in energy than the corresponding monomer. The low energy component makes the dimer an effective trap for the energy harvested by the antenna pigments. Once the

* Present address: Department of Chemistry, Washington University, St. Louis, MO 63130, USA.
‡ Present address: Department of Physics, University of Waikato, Private Box, Hamilton, New Zealand.

0301-0104/81/0000-0000/$02.50

electron is transferred from the dimer to the subsequent electron acceptor, a molecule of bacteriopheophytin in bacterial reaction centers [5, 6], the unpaired electron is delocalized over the large π systems of both molecules of bacteriochlorophyll [1–3, 7]. Such delocalization may be important for the fast rate of the forward reaction and for hindering unwanted reverse electron transfer that would otherwise reduce the overall yield of the charge separation process [5, 8]. Similarly, chlorophyll dimers have been proposed as electron donors in plant reaction centers [6]. Thus, it is important for devising useful model systems based on photosynthetic energy conversion that we understand the effects of dimer formation and exciton interactions on the electronic properties of porphyrin complexes.

Several models have been proposed for the chlorophyll special pair [9–14], and theoretical calculations based on exciton interactions have been given to account for its observed spectral features [15–18]. General theories of exciton interactions [19–24] and applications for porphyrins [25–31] and a variety of pigment complexes [32–34] in both solution and the solid phase are given elsewhere.

In the context of understanding the photophysics of the special pair, model systems of simpler porphyrin dimers are attractive for spectroscopic and kinetic studies, because of the flexibility of incorporating specifically desired structural features during the synthesis [35–40]. These complexes, and particularly mixed metal dimers, offer the possibility of isolating the factors affecting the rates of energy and electron transfer from one porphyrin ring to another [41–44]. We hope to carry out such studies in the future. However, before the photophysics of more complex dimers can be understood, it is useful to have results on the simplest type of dimers. In this paper we present studies on the absorption, fluorescence, and fluorescence polarization of a series of free base porphyrin dimers joined by a single hydrocarbon chain of variable length. We also give some idealized exciton calculations to account for the observed spectra.

2. Experimental

Etioporphyrin I (2,7,12,17-tetraethyl-3,8,13,18-tetramethyl porphyrin) dimers (fig. 1) were synthesized as previously described [35]. These were further purified by thin-layer chromatography on silica gel with CH_2Cl_2 as eluent.

Fluorescence, fluorescence excitation, and fluorescence excitation polarization spectra were measured on a Farrand MKI spectrofluorometer interfaced to a Southwest Technical Products Corporation 6800 microcomputer. Intensity readings were taken via an eight bit A/D converter interface, with stepping-motor driven wavelength scans controlled by the microcomputer. Spectra were not corrected for variations of the excitation intensity or the detection sensitivity with wavelength; these variations were not very large and were not important for our study. Further details of the construction and operation of this apparatus are given elsewhere [45]. Absorption spectra were taken on a Varian Superscan II spectrometer.

Room temperature fluorescence and excitation spectra were measured in CH_2Cl_2 in 1 cm square cells using 2.5 nm bandpass slits in the fluorescence or excitation path depending on the spectrum being taken, and 5 nm bandpass slits in the alternate path. Optical densities were adjusted to 0.1 at 500 nm for excitation in the visible region and to 0.1 at 400 nm for spectra in the Soret band to avoid front-face effects. Scattered light was negligible.

Liquid nitrogen temperature spectra were measured in a Dewar assembly with samples in

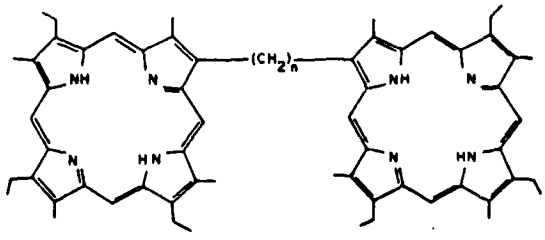

Fig. 1. Basic structure for etioporphyrin based covalently linked dimers with $n = 0$–8. The $n = 0$ dimer contains a direct link between the rings.

EPA (ethyl ether : pentane : ethnol = 5 : 5 : 2 by volume) in 4 mm i.d. round tubes adjusted to the optical densities given above. Excitation polarization spectra were taken under these conditions and at 5 nm intervals with rotatable quartz disk polarizers in the excitation and emission beams, which were at 90° to one another.

The degree of fluorescence polarization was calculated from the formula

$$p = \frac{I_{vv} - I_{vh}(I_{hv}/I_{hh})}{I_{vv} + I_{vh}(I_{hv}/I_{hh})},$$

where I_{vh} is the relative fluorescence intensity measured on the spectrofluorometer with vertically polarized excitation light and horizontally polarized emission light. The intensity readings with other combinations of excitation and emission polarizers are similarly defined. The quantity (I_{hv}/I_{hh}) corrects for the instrumentally induced contribution to the observed degree of polarization as previously described [46]. All fluorescence excitation polarization spectra represent the average of the results for two or three measurements.

Fluorescense lifetimes were measured by exciting the samples with a picosecond dye laser and determining the fluorescence response using time-correlated single photon counting. A detailed description of the apparatus and the deconvolution and data analysis procedures has appeared elsewhere [47].

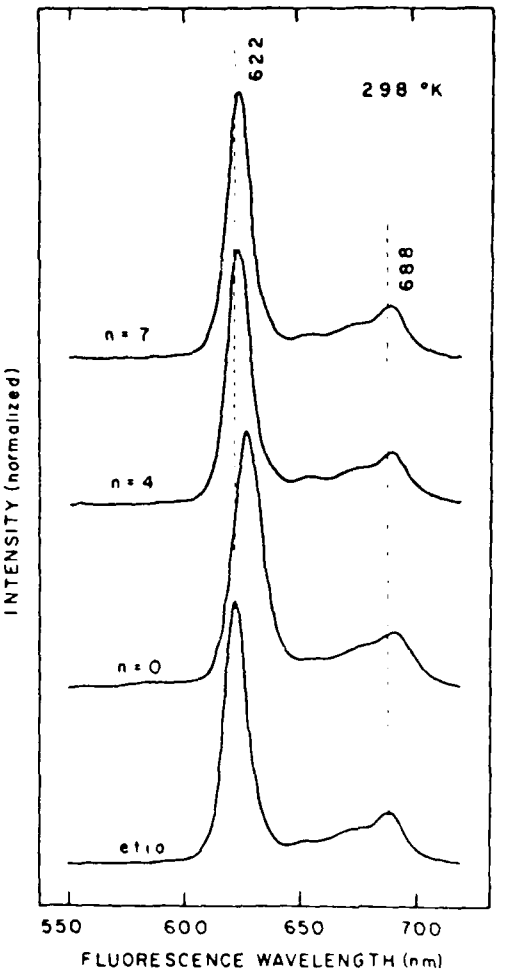

Fig. 2. Room temperature fluorescence spectra for the etioporphyrin monomer and for the $n = 0$, $n = 4$ and $n = 7$ dimers. Molecules were excited at the $Q_Y(1, 0)$ absorbance maximum. Peak wavelengths for all free base spectra are listed in table 1.

3. Results

3.1. Fluorescence and excitation spectra of free base compounds

Room temperature fluorescence spectra in CH_2Cl_2 with excitation in the $Q_Y(1, 0)$ band at 500 nm (OD = 0.1) are shown in fig. 2. The peak of the major fluorescence band, $Q_X(0, 0)$, in the $n = 0$ dimer is shifted by 5 nm to the red of the position in the monomer. The $n = 1$–8 dimers are red shifted by progressively less amounts (last column of table 1). The same fluorescence spectra are obtained upon exciting in the other visible (Q) bands or in the Soret (B) band

Room temperature excitation spectra obtained by monitoring at the peak of the $Q_X(0, 0)$ fluorescence band are shown in fig. 3. The same spectra are obtained by monitoring the $Q_X(0, 1)$ band at 688 nm and all excitation spectra are found to be identical within error to the absorption spectra (table 1 and ref. [30]).

Table 1
Peak wavelengths for free base compounds [a]

Compound	Temp. (K)	Absorption or excitation					
		B(0, 0)	$Q_Y(1,0)$	$Q_Y(0,0)$	$Q_X(1,0)$	$Q_X(0,0)$	$Q_X(0,0)$ [b]
etio monomer	298	401	500	533	568	622	622
	77	401	496	529	567		619
dimers							
$n = 0$	298	416	505	539	570	625	627
	77	414	504	542	570		626
$n = 1$	298	410	503	536	570	624	625
	77	407	498	532	568		622
$n = 3$	298	402	501	534	568	624	624
	77	404	497	529	566		621
$n = 4$	298	402	501	534	569	623	624
	77	402	496	529	566		620
$n = 5$	298	402	501	534	569	623	624
	77	402	496	529	566		620
$n = 6$	298	401	500	533	568	623	623
	77	401	497	531	567		620
$n = 7$	298	401	500	533	568	623	623
	77	401	496	529	566		620
$n = 8$	298	401	500	533	569	622	623
	77	401	496	529	567		619

[a] 298 K spectra in CH_2Cl_2, 77 K spectra in EPA; wavelengths in nm.
[b] Fluorescence.

As in the fluorescence spectra, the maximum red shifts in the excitation spectra are observed for the $n = 0$ dimer. This is particularly noticeable in the $Q_Y(1,0)$ band at 500 nm and in the Soret (B) band which was shifted from 401 nm in the monomer to 416 nm in the $n = 0$ dimer.

Liquid nitrogen temperature fluorescence and excitation spectra are closely similar to those obtained at room temperature, except for some narrowing and a small blue shift of the bands (table 1, see also fig. 6B). The peak wavelengths of the Soret bands are not shifted significantly from the monomer except for the $n = 0$ and $n = 1$ dimers. For the $n = 0$ dimer, the peak of the Soret band is shifted to 414 nm from 401 nm in the monomer at 77 K. The liquid nitrogen temperature fluorescence and excitation spectra show the same trends found in the room temperature spectra: maximum deviation from the monomer is observed for the $n = 0$ dimer (direct link) and when the separation of the rings is progressively increased to eight carbon atoms the spectra look more and more similar to the etioporphyrin monomer. (The $n = 2$ dimer was the least soluble of all members of the series and will not be discussed in detail here. However, all of our measurements indicate that spectral shifts from the monomer were less for the $n = 2$ than for $n = 0$ or $n = 1$ dimers.)

We had difficulty in determining accurately the relative fluorescence yields of the monomer versus the dimers. There appeared to be a small variable amount of a nonfluorescing or a very weakly fluorescing impurity that was difficult to remove completely by column or thin-layer chromatography. The relative fluorescence yields along the series changed upon each purification step, but the maximum quenching

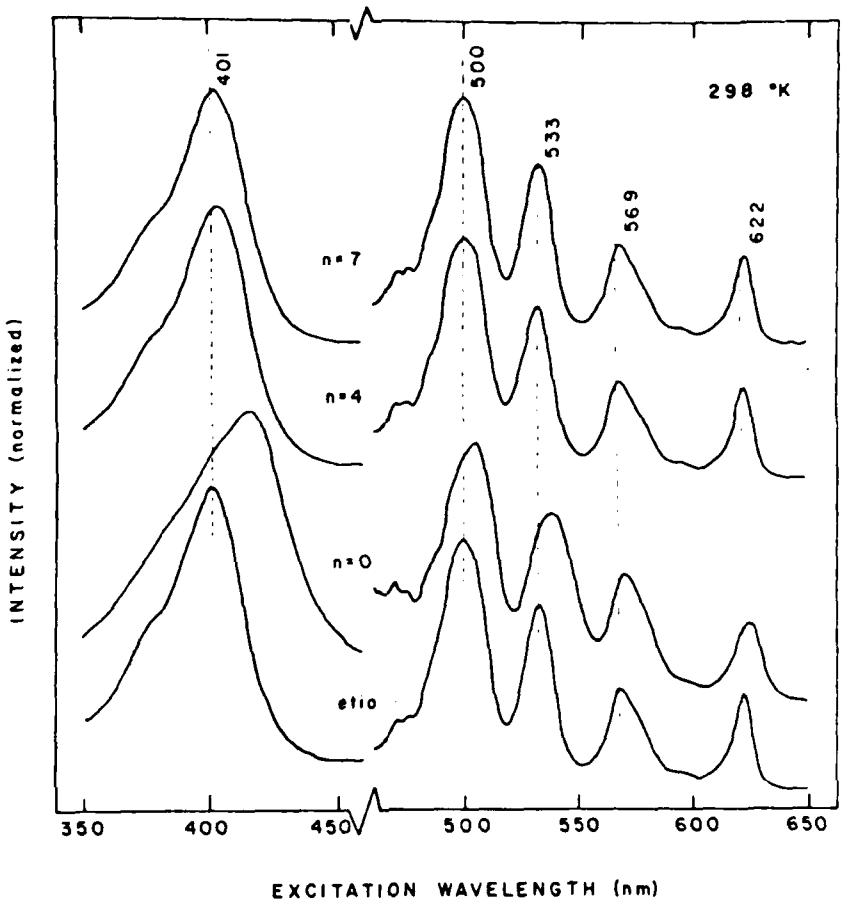

Fig. 3. Room temperature excitation spectra in CH_2Cl_2 for fluorescence detected in the $Q_X(0,0)$ emission band. Scattered light was negligible.

always occurred in the $n = 4$ dimer. For the purest samples we obtained, this corresponds to a reduction in fluorescence of about 30% for the $n = 4$ dimer versus the monomer. Although variations occur along the series, the other dimers exhibit a reduction in fluorescence compared to the monomer that is less than this value.

A second estimate for the quenching of the lowest excited singlet state of the dimers was obtained by measuring the fluorescence lifetimes. To minimize the effects of impurities, excitation was in the moderatly strong $Q_X(1,0)$ band at 575 nm (the shortest wavelength to which the laser could be tuned), and the emission was detected at 625 nm, the strong $Q_X(0,0)$ fluorescence band. The fluorescence decay curves were consistently monoexponential yielding a single fluorescence lifetime. The results of these measurements are summarized in table 2. Note that each value is the mean of several measurements. The trend in the fluorescence lifetime is in general similar to that observed in the fluorescence quenching measurements, with a 15% shortening in the lifetime for the $n = 4$ dimer, and much less for the other

Table 2
Fluorescence lifetimes in CH_2Cl_2 at room temperature

Compound	Lifetime (ns)	Reduction (%)
etio monomer	10.75 ± 0.23	[0]
dimers		
$n = 0$	9.89 ± 0.11	8
$n = 1$	10.41 ± 0.11	3
$n = 3$	9.89 ± 0.05	8
$n = 4$	9.14 ± 0.09	15
$n = 5$	10.14 ± 0.02	6
$n = 6$	10.41 ± 0.05	3
$n = 7$	10.44 ± 0.03	3
$n = 8$	10.47 ± 0.03	3

dimers. The difference between the 15% reduction in fluorescence lifetime and the 30% reduction in fluorescence yield we tend to ascribe to impurities.

These results indicate that excited state quenching is not very pronounced in the dimers compared to the monomers. Similar observations were made on several cofacial μ-oxo bridged scandium porphyrin dimers, where within experimental error no fluorescence quenching compared to the monomer was found [31].

3.2. Fluorescence and excitation spectra of diprotonated compounds

Addition of a small amount of trifluoroacetic acid (TFA) to a CH_2Cl_2 solution of the free base etioporphyrin monomer results in the protonation of the remaining two nitrogen atoms in the center of the porphyrin macrocycle. This effectively changes the symmetry of the molecule from D_{2h} to D_{4h}. In the visible region, the spectrum collapses from a four-banded to a two-banded spectrum, as occurs when the free base porphyrin is converted to a metal complex [48]. This effect is clearly seen in the excitation spectra of the etioporphyrin monomer and dimers in a 1% TFA solution in CH_2Cl_2 (fig. 4), and also in the absorption spectra [30]. As in the free base case, red shifts from the monomer are observed in the diprotonated dimer excitation spectra (fig. 4) and fluorescence spectra (fig. 5). In the excitation spectra, the Q(1, 0) absorption band is red-shifted 8 nm in going from the monomer to the $n = 0$ dimer. The Q(0, 0) band is red shifted by 12 nm both in absorption and in fluorescence. These spectral shifts are roughly twice as large as those described for the free base $n = 0$ dimer (no TFA added). The vibrational structure in the fluorescence spectrum of the diprotonated $n = 0$ dimer is also different from the monomer and the other dimers shown in fig. 5, having an anomalous reduction in the intensity of the Q(0, 1) band relative to Q(0, 0). However, for the dimers other than $n = 0$ and $n = 1$ only minimal spectral shifts from the monomer are observed (table 3).

The most dramatic effect in the spectra of the diprotonated series is the split Soret band observed in the $n = 0$–3 dimers [30]. In the $n = 0$ dimer these occur at 409 and 425 nm (fig. 4).

3.3. Fluorescence excitation polarization of free base compounds

Fluorescence polarization spectra can be useful for measuring the angle of the emission oscillator with respect to the excitation oscillator and in determining the importance of energy transfer between rings in a dimer. Such spectra permitted resolution of the two exciton components in the Soret region of several μ-oxo Sc-porphyrin dimers [31].

Therefore, we measured the polarization ratio for excitation in the Soret and visible bands of the free base monomer and dimers with fluorescence detected in the Q(0, 0) band at 625 nm. These spectra were taken in EPA glasses at 77 K. The results for the monomer and $n = 0$ and $n = 1$ dimers are shown in fig. 6A, and for the $n = 3$ and $n = 7$ dimers in fig. 7A. Maxima and minima in these spectra should be compared with the peak wavelengths in the 77 K excitation spectra shown in figs. 6B and 7B and listed in table 1.

All spectra of figs. 6A and 7A exhibit a low positive polarization ratio at the peak of the Soret B(0, 0) band near 400 nm. In the monomer spectrum the polarization ratio increases to a value of 0.3 at 435 nm on the

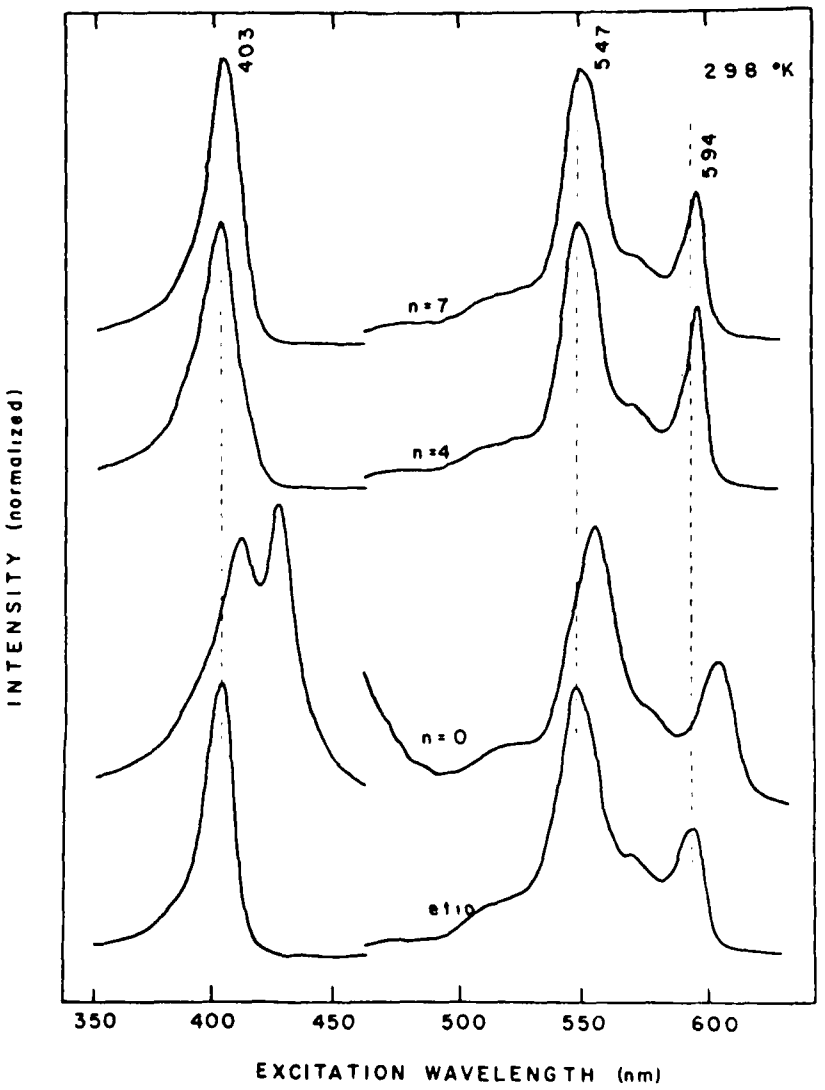

Fig. 4. Room temperature excitation spectra in CH_2Cl_2 + 1 drop TFA, the fluorescence detected in the Q(0, 0) emission band. TFA causes diprotonation of the remaining two nitrogen atoms in the center of the porphyrin rings. Peak wavelengths for all diprotonated compounds are listed in table 3.

long wavelength side of the Soret and then decreases to 0.1 at 475 nm, the trough between the B(0, 0) and $Q_Y(1, 0)$ bands. The monomer spectrum progresses to a large positive polarization ratio of 0.33 on the long wavelength side of the $Q_Y(1, 0)$ band and then dips to a negative value of −0.18 near the maximum of the $Q_Y(0, 0)$ band. The polarization ratio approaches a positive value of 0.4 or greater in the $Q_X(0, 0)$ band from which the fluorescence is monitored, broken by a series of small positive changes through the $Q_X(1, 0)$ region.

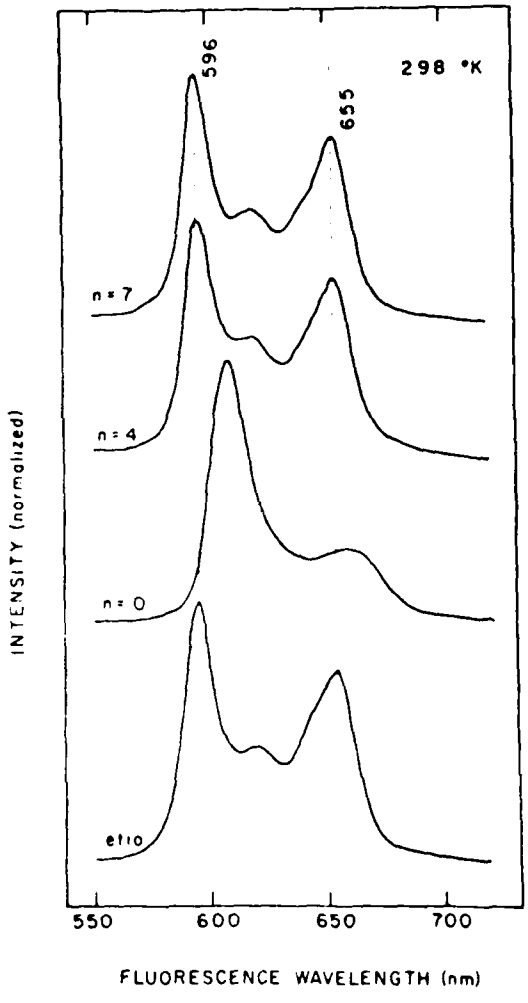

Fig. 5. Room temperature fluorescence spectra for diprotonated compounds excited in the Q(1, 0) absorption band.

The polarization spectra of the $n = 3$ and $n = 7$ dimers (fig. 7) are similar to the etioporphyrin monomer except for a general "collapse" of the polarization ratios. Polarization spectra for the $n = 4$–6 dimers lie between the spectrum of the $n = 3$ dimer and that of the $n = 7$ and $n = 8$ dimers, whose spectra are essentially the same.

The situation is somewhat different for the $n = 0$ and $n = 1$ dimers. In the case of the $n = 0$ dimer shown in fig. 6, the polarization ratio on the long wavelength side of the Soret band reaches the same positive value of 0.3 as for the monomer, but at a wavelength 15 nm to the red, at 450 nm. The peak of the B(0, 0) absorption band is shifted to longer wavelengths by about the same amount (fig. 6B and table 1). The polarization ratio remains more positive across the remainder of the spectrum with some minor maxima and minima occurring near the peaks of the visible bands. However, the polarization ratio is almost zero in the region of the B(1, 0) band near 370 nm, being lower than that observed for the other members of the series.

The polarization spectrum of the $n = 1$ dimer (fig. 6A) is more similar to the spectra of the $n = 3$ and $n = 7$ dimers than it is to that of the $n = 0$ dimer; there is a general collapse of the polarization ratios across the spectrum from those observed in the monomer. However, the polarization maximum on the long wavelength

Table 3
Peak wavelengths for diprotonated compounds [a]

Compound	Absorption or excitation			Fluorescence
	B(0, 0)	Q(1, 0)	Q(0, 0)	Q(0, 0)
etio monomer	401	547	594	596
dimers				
$n = 0$	409 425[b]	555	606	608
$n = 1$	402 422[b,c]	553	600	601
$n = 3$	402 411[b,c]	549	596	598
$n = 4$	401	547	596	596
$n = 5$	402	548	596	597
$n = 6$	402	548	596	596
$n = 7$	402	548	596	596
$n = 8$	402	549	595	596

[a] 298 K spectra in CH_2Cl_2 + 1% trifluoroacetic acid (TFA), wavelengths in nm.
[b] Doublet.
[c] Definite shoulder near 395 nm not present in monomer, see also fig. 2 of ref. [30].

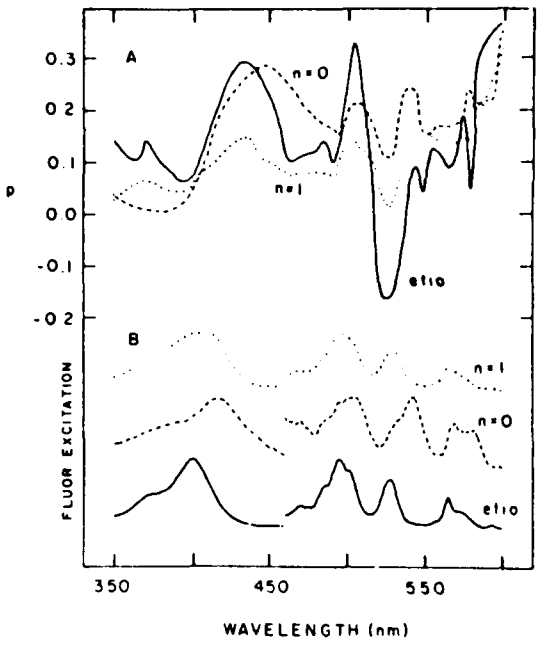

Fig. 6. (A) Low temperature fluorescence excitation polarization spectra in EPA glasses with emission detected in the $Q_X(0,0)$ band (≈620 nm). (B) Low temperature excitation spectra in EPA glass detected in the $Q_X(0,0)$ fluorescence band. Data for monomer and dimers $n = 0, 1$. [Scattered light prevented study of the $Q_X(0,0)$ band in the excitation spectra.]

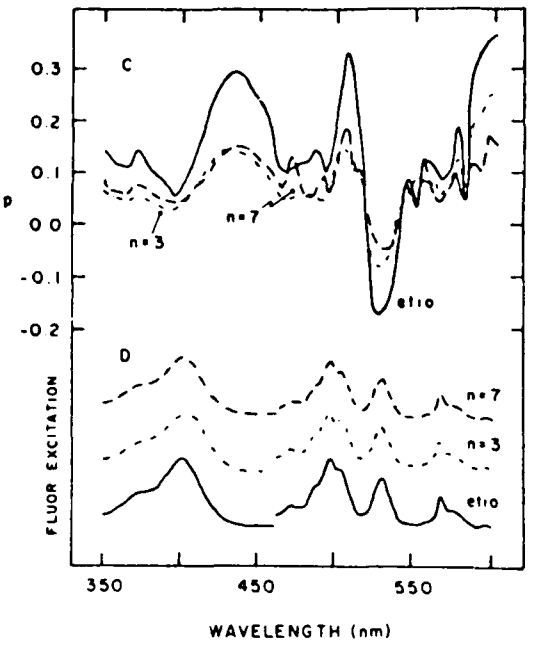

Fig. 7. (A) Low temperature fluorescence excitation polarization spectra in EPA glasses with emission detected in $Q_X(0,0)$ band (≈620 nm). (B) Low temperature excitation spectra in EPA glass detected in $Q_X(0,0)$ fluorescence band. Data for monomer and dimers $n = 3, 7$.

side of the Soret band in the $n = 1$ dimer is slightly red shifted from the corresponding peak in the monomer spectrum, but to a lesser degree than observed in the case of the $n = 0$ dimer (fig. 6A). This probably reflects the red shift of the Soret band maxima in the excitation spectra of the $n = 0$ and $n = 1$ dimers, as seen in fig. 6B. These results suggest that ring interactions are significantly less in the $n = 1$ dimer than in the $n = 0$ dimer.

The fluorescence polarization spectra of fig. 6A are in agreement with our other spectral observations that maximum deviation from the monomer occurs in the $n = 0$ and $n = 1$ dimers. This clearly suggests that maximum ring interaction occurs in these members of the series. More detailed interpretations of the polarization data are given in section 4.

4. Discussion

4.1. Theory

A general theory for exciton interactions in porphyrin dimers was presented previously and used to discuss spectral observations on several μ-oxo scandium porphyrin dimers [31]. The interaction between two transition dipoles μ_A and μ_B on moieties A and B separated by a distance, R, can be expressed as follows [15, 17, 19, 31]:

$$V = [\mu_A \cdot \mu_B - 3(\mu_A \cdot \hat{R}_{AB})(\mu_A \cdot \hat{R}_{AB})]/R^3, \quad (1a)$$

$$V = Fe^2M^2/R^3. \quad (1b)$$

Here $\hat{R}_{AB}$ is the unit vector from the center of porphyrin A to the center of porphyrin B. The dipoles have magnitude $|\mu| = eM$, where M is

the transition moment and e is the electronic charge. (We assume both moieties are identical in setting $|\mu_A| = |\mu_B|$.) All of the geometrical factors have been lumped into the factor F in eq. (1b). Thus, the exciton interaction is proportional to the square of the monomer transition moment M. It should be noted that eq. (1) is based on the dipole–dipole approximation which may fail at very small R.

The effect of this dipolar coupling is to produce symmetric and antisymmetric combinations of the individual monomer excited states, $[\psi_A \pm \psi_B]/\sqrt{2}$. The detailed geometry of the dimer will determine the magnitude and direction of the transition dipoles $[\mu_A + \mu_B]/\sqrt{2}$ as well as the energy splitting between the states, $2V$. The intensities of the absorption bands corresponding to the two transitions can be expressed as:

$$I^* = M^2[1 \pm f(\beta)]/2, \qquad (2)$$

where $f(\beta)$ is a function of the relative orientations of the interacting dipoles. For coplanar interacting dipoles tilted from one another by an angle 2θ, $f(\beta) = \cos(2\theta)$.

Cofacial porphyrin dimers: The simple exciton theory just presented is more complicated in porphyrins because with square symmetry the (π, π^*) allowed excited states are doubly degenerate. Thus dimer formation leads to a four-fold degeneracy in zeroth order. This problem was considered for the μ-oxo bridged scandium porphyrin dimer [31]. It was shown that for geometries where the porphyrin units are close to face-to-face (cofacial), the interaction among the four-fold degenerate states factors into two pairs of interacting states. The resulting exciton states are then $(X_A \pm X_B)/\sqrt{2}$ and $(Y_A \pm Y_B)/\sqrt{2}$, with I^+_X and I^+_Y strongly allowed and I^-_X and I^-_Y weak or forbidden. If the dimer lacks full square symmetry the X and Y polarized states will have somewhat different energies and intensities. Furthermore, since the exciton interaction depends on the square of the transition moment M [eq. (1)], generally only the strong Soret (B) band is affected by exciton interaction in porphyrin dimers. For the weak visible (Q) bands, the result of ring interaction is smaller than other effects such as inhomogeneous solvent broadening. Thus, for $[Sc(OEP)]_2O$ the peak of the Soret band is blue shifted by 11 nm (strong symmetric component) with a red tail out to 480 nm (weak antisymmetric component), while the Q bands are only slightly red shifted and broadened [31]. Similar spectral features have been observed for other cofacial porphyrin dimers [37–39].

4.2. *Edge-on porphyrin dimers (Soret bands)*

The relative geometry of the two porphyrin rings for the dimers studied here is not constrained as in the μ-oxo dimers [31]. Probably the only constraint is that for the shorter dimers ($n \leq 4$) a cofacial geometry is impossible. Since the largest deviations from the monomer occur in the $n = 0$ dimer and since it has the most constrained geometry, we shall treat that case first and then go on to the others in the series.

At the top of fig. 8 we present the Soret bands observed in the room temperature excitation spectra of the monomer, the free base (H_2) $n = 0$ dimer, and the diprotonated (H_4) $n = 0$ dimers. Fig. 8 also shows three idealized geometries for the $n = 0$ dimer. These are based on structures assumed by LaPine space filling models. For cases 1 and 3 the models show that the two rings are not strictly coplanar with the Y, Y' and X, X' axes strictly parallel as idealized in fig. 8. For case 2 the models show that the rings are not quite aligned with axes Y and Y' mutually perpendicular with both perpendicular to X parallel to X'. However, with the idealized geometries of fig. 8 the exciton coupling factors into interactions between X, X' and Y, Y' pairs except for case 2, where Y and Y' are non-interacting. Thus these structures are a useful starting point for our discussion.

For the free base case the exciton coupling of the Soret states is extremely complicated as the states B_x and B_y defined with regard to the proton axes are not degenerate [48–50]. Furthermore, there is no reason to believe that the proton axes are oriented with regard to the ring–ring link. Thus there are several tautomeric structures each with different exciton coupling among the four monomer Soret states. It is then

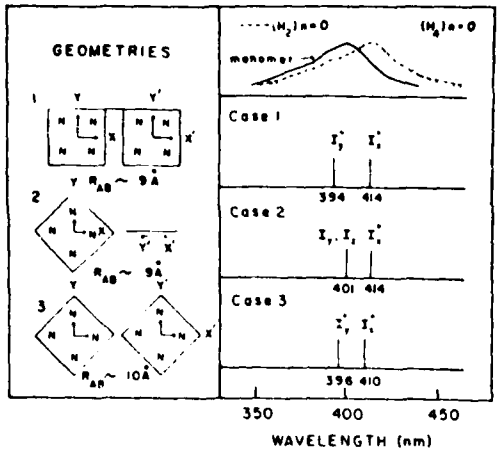

Fig. 8. Geometries and corresponding stick absorption spectra calculated for the diprotonated cation from exciton theory for the idealized geometries shown on the left. Cases 1 and 3 have the rings coplanar; for case 2 the right hand ring is perpendicular to the page. The stick spectra do not include any "solvent shift" term. See text. The observed room temperature excitation spectra of the monomer and of the free base (H_2) and diprotonated (H_4) $n = 0$ dimers are presented at the top.

not surprising that the $n = 0$ free base dimer Soret band looks much like that of the monomer with an extra skewed broadness (figs. 3 and 8). That the dimer peak shows a red shift of 15 nm (table 1) from the monomer is attributable to the "solvent effect" of the dimer environment; i.e., the D term in eq. (23) of ref. [31].

The diprotonated $n = 0$ dimer is easier to treat than the free base dimer since the X and Y directions are equivalent in each ring. Hence we can choose these directions as defined by the dimer structure, as was done for the μ-oxo dimer [31] and as shown in fig. 8. The stick spectra show the pattern of absorption intensity calculated by eqs. (1) and (2), neglecting any "solvent shift term" from the monomer peak at 401 nm. All three cases show a split Soret band with the two bands having equal intensity. Using the space filling models we estimate $R_{AB} \approx 9$ Å for cases 1 and 2 and $R_{AB} \approx 10$ Å for case 3. The result is a calculated splitting between allowed Soret bands of 20, 13, and 14 nm for cases 1, 2, and 3, respectively. The observed peaks at 409 and 425 nm (table 3) are most consistent with case 3 if the exciton coupling is calculated with respect to the shifted free base dimer at 416 nm. Case 2 would also fit the data if a somewhat smaller solvent shift than the free base is assumed. However, the exciton splitting calculated for case 1 is too large.

The diprotonated dimers $n = 1$ and $n = 3$ continue to show Soret splitting. In addition, spectra for the diprotonated $n = 1$ and $n = 3$ dimers show a definite shoulder of reasonable intensity near 395 nm not present in the monomer nor in dimers with $n > 3$. The splitting of the Soret bands for the $n = 0$, 1, and 3 dimers is 920, 1180, and 545 cm^{-1}, respectively. Molecular models suggest that the $n = 1$ dimer is more constrained than the $n = 0$ dimer, and the observed exciton splitting suggests that R_{AB} is shorter. The models suggest that a distorted geometry resembling case 2 is the most likely for $n = 1$ dimers. For $n = 3$ dimers, molecular models allow case 3 with $R_{AB} = 12$ Å. This leads to a calculated exciton splitting of 520 cm^{-1}, which is quite consistent with the data. For $n = 4$ dimers, molecular models allow case 3 with $R_{AB} = 14$ Å, and the exciton calculation gives a Soret splitting of 309 cm^{-1}. At this size the splitting is comparable to the monomer linewidth, and so the Soret band becomes single again. It would seem from the data that the solvent shift term also declines quickly as R_{AB} gets large, so that the optical spectra look like independent units in the Soret band for $n > 4$.

4.3. *Edge-on porphyrin dimers (visible bands)*

The exciton splitting in the visible bands is substantially less than in the Soret bands because M^2 is substantially lower. It should be noted that M^2 for the strongest band, $Q_x(1, 0)$, is divided among several vibronic bands so that a weak coupling case is expected [22]. The M^2 values for $Q_x(0, 0)$ and $Q_y(0, 0)$ are, respectively, about 20 and 80 times smaller than for the B band [48]. Thus exciton splittings of 60 cm^{-1} or less are expected even in the largest case [$Q_y(0, 0)$ for case 1 of $n = 0$]. The main

observed effect of dimer formation is the solvent shift term apparent for the $n = 0$, 1, and 3 dimers. For the diprotonated dimers the visible solvent shift is roughly half that of the Soret band. For the free base dimers the solvent shift of the Q_y bands is about one-third, and that of the Q_x bands about one-fifth that of the Soret bands. Qualitatively it would appear that the solvent shift follows the size of the exciton coupling. A theory of the solvent shift term is, however, not yet developed.

4.4. *Fluorescence spectra and quantum yields*

We observe in these dimers essentially the same amount of fluorescence as in the monomer; i.e., there is no extra quenching. The fact that the lowest energy visible exciton states are allowed with edge-on geometries may play a role here. This is to be contrasted with the case of cofacial dimers where the lower energy exciton state is forbidden, so that a decrease in fluorescence yield is expected especially at lower temperatures. The question of fluorescence quenching in the dimer is an interesting one; quenching is sometimes observed [38, 39] and sometimes is not [31, 38], even though the apparent exciton splittings are about the same.

Another interesting effect is the anomalous vibrational structure of the fluorescence spectrum of the diprotonated $n = 0$ dimer (fig. 5). The underlying structure centered near 620 nm is absent and the intensity of the Q(0, 1) emission band is about half that observed in the other molecules. The effect does not occur in the diprotonated $n = 1$ dimer nor in the fluorescence spectrum of any of the free base complexes. The reason for this effect is unclear at present.

4.5. *Fluorescence polarization spectra*

Theoretical groundwork for discussing porphyrin fluorescence excitation polarization spectra has been given previously [49, 50]. The lowest energy porphyrin visible absorption band, and thus the emission arising from this state, is expected to be polarized parallel the proton axis, which is called the X axis [48–50]. To obtain the polarized excitation spectra, we monitored the $Q_X(0, 0)$ emission at 619 nm in low temperature EPA glass (fig. 6). A polarization ratio approaching +0.4 or greater is observed in the monomer as the excitation is scanned into the $Q_X(0, 0)$ absorption band. Scattered light prevented us from determining the maximum polarization ratio in this region and from resolving the low temperature $Q_X(0, 0)$ absorption band (fig. 6B). As expected [49], the monomer polarization spectrum reaches its most negative value near the peak of the $Q_Y(0, 0)$ absorption band. The $Q_Y(1, 0)$ absorption band centered at 496 nm is predominantly X polarized, judging from the +0.33 polarization ratio observed at this wavelength, and the $Q_X(1, 0)$ is predominantly Y polarized, judging from the polarization ratio below 0.14 (fig. 6A). Perrin et al. [51] considered vibronic borrowing in porphyrins using a cyclic polyene model. They noted: "Since there are two vibronically active b_{1g} modes and only one a_g mode, it follows that there should be more Y than X polarization in $Q_X(1, 0)$ . . ." Similarly, there should be more X than Y polarization in $Q_Y(1, 0)$, particularly since the lower energy Soret band, from which it borrows intensity, is X polarized. The X polarization of the lower energy Soret band is expected theoretically [50] and is evidenced experimentally in the +0.3 polarization ratio observed near 425 nm in the monomer (fig. 6A). A dip in the polarization spectrum at the peak of the monomer Soret band at 401 nm indicates significant Y polarization in this region.

The $n = 1$–8 dimer polarization spectra, when compared to that of the monomer (figs. 6A and 7A) suggest a general collapse to a value of $p_0 < 0.15$. In an attempt to quantify this collapse, we related the dimer polarization spectrum $p_n(\lambda)$ to the monomer polarization spectrum $p_m(\lambda)$ by the equation

$$p_n(\lambda) = f_n p_m(\lambda) + (1 - f_n) p_{0n}. \quad (3)$$

In eq. (3) we assume that a fraction f_n of the light comes out polarized as in the monomer, and a fraction $(1 - f_n)$ comes out with constant

polarization p_{0n}. A least-squares fit was carried out using 26 wavelengths taken at 10 nm intervals from 350 to 600 nm. The result of these fits is given in table 4. As can be seen by the magnitude of the standard error, the poorest fit is for the $n = 0$ dimer; the fits are otherwise fairly good. The data may then be interpreted as follows, using the $n = 7$ dimer as an example: 33% of the photons are emitted as in the monomer, while the remainder come out with an average angle α between absorption and emission such that [49]

$$p_{07} = (3\langle\cos^2\alpha\rangle - 1)/(\langle\cos^2\alpha\rangle + 3) = 0.057, \qquad (4)$$

giving $\langle\cos^2\alpha\rangle = 0.40$, the average cosine between absorption and emission dipoles. If the excitation hopped between monomer units oriented as in case 3 (fig. 8) and the proton axes were randomly distributed in each moiety, the hopped excitons would be randomly emitting in a plane, giving $\langle\cos^2\alpha\rangle = \frac{1}{2}$ and $p_0 = 0.143$. The same assumption assuming random emission from the dipoles oriented as in case 2 (fig. 8) gives $\langle\cos^2\alpha\rangle = \frac{1}{4}$ and $p_0 = -0.077$. Thus for dimers $n = 1$–8 we can interpret the polarization spectra as indicating that between $\frac{1}{2}$ and $\frac{3}{4}$ of the absorbed photons are hopping between units that are oriented somewhere between cases 2 and 3.

The $n = 0$ polarization data is less structured than the monomer and is relatively more different from the monomer than the polarization data for the $n = 1$–8 dimers. Qualitatively this is consistent with greater interaction between the monomer moieties. The $n = 0$ polarization data tends to center around $p = 0.14$, a value more consistent with the coplanar dimers of case 3 than with the perpendicular dimers of case 2. It would be helpful to have fluorescence polarization spectra of the $n = 0$ and $n = 1$ diprotonated dimers because of the splittings observed (fig. 4), but we could not obtain good low temperature glasses due to the added TFA. We tried to take spectra in glycerol, since rotational depolarization is minimal in this solvent even at room temperature, but broad absorption spectra were obtained in this case.

Table 4
Least-squares fit of polarization data [a]

Dimer (n)	f	$(1-f)p_{0n}$	p_{0n}
0	0.379 ± 0.150	0.117 ± 0.028	0.188
1	0.390 ± 0.078	0.056 ± 0.015	0.092
3	0.527 ± 0.041	0.004 ± 0.008	0.008
4	0.333 ± 0.044	0.069 ± 0.008	0.103
5	0.487 ± 0.049	0.043 ± 0.009	0.084
6	0.485 ± 0.092	0.079 ± 0.017	0.153
7	0.329 ± 0.039	0.038 ± 0.007	0.057
8	0.478 ± 0.063	0.064 ± 0.011	0.123

[a] See eq. (3). The standard error is indicated.

5. Conclusions

We have studied the electronic spectra of a series of etioporphyrin dimers bridged by a single hydrocarbon chain of variable length. The experimental results show (i) very little quenching of fluorescence; (ii) a red shift of the spectra that, for a given band, decreases with increased length of the bridge and, for a given dimer, decreases with decreased absorption strength of the band [i.e. $B(0,0) \gg Q_x(0,0) > Q_y(0,0)$]; (iii) a splitting of the Soret band in the case of the diprotonated species, which can be explained by an exciton coupling model assuming a reasonable geometry for the rings; (iv) a substantial change in the fluorescence excitation polarization spectra of the various dimers from that of the monomer. The fluorescence polarization data for the $n = 0$ free base dimer show substantial interaction between the rings. For the chains with $n \geq 1$ the data can be qualitatively explained by assuming $\frac{1}{4}$ to $\frac{1}{2}$ of the excitation stays localized in each moiety, while the remaining excitation hops between the covalently linked moieties.

We are planning to extend these studies to doubly-linked and mixed-metal porphyrin dimers, specifically designed to have large exciton splittings. We hope to study increasingly complex systems that more closely resemble those known to be so important in photosynthesis and in other biological processes.

Acknowledgement

This work was supported by the US Army Research Office under grant DAAG29-76-9-0275 and by the NSF under grants PCM79-0211 and DMR-7823958, and by NIH grant AM-17989 (DD). Dr. Rachel Wang helped with the least-squares fit of the polarization data.

References

[1] G. Feher, A.J. Hoff, R.A. Isaacson and L.C. Ackerson, Ann. N.Y. Acad. Sci. 244 (1975) 239.
[2] J.R. Norris, R.A. Uphaus, H.L. Crespi and J.J. Katz, Proc. Nat. Acad. Sci. USA 68 (1971) 625.
[3] J. Fajer, M.S. Davis, D.C. Brune, L.D. Spaulding, D.C. Borg and A. Forman, Brookhaven Symp. Biol. Chlorophyll-Proteins, Reaction Centers and Photosynthetic Membranes (1977) p. 74.
[4] J.J. Katz, J.R. Norris, L.L. Shipman, M.C. Thurnauer and M.R. Wasielewski, Ann. Rev. Biophys. Bioeng. 7 (1978) 393.
[5] D. Holten and M.W. Windsor, Ann. Rev. Biophys. Bioeng. 7 (1978) 189.
[6] R.E. Blankenship and W.W. Parson, Ann. Rev. Biochem. 47 (1978) 635.
[7] J. Fajer, D.C. Brune, M.S. Davis, A. Forman and L.D. Spaulding, Proc. Nat. Acad. Sci. USA 72 (1975) 4956.
[8] D. Holten, M.W. Windsor, W.W. Parson and M. Gouterman, Photochem. Photobiol. 28 (1978) 951.
[9] C.E. Strouse, Proc. Nat. Acad. Sci. USA 71 (1974) 325.
[10] F.K. Fong, Proc. Nat. Acad. Sci. USA 71 (1974) 3692.
[11] L.L. Shipman, T.M. Cotton, J.R. Norris and J.J. Katz, Proc. Nat. Acad. Sci. USA 73 (1976) 1791.
[12] M.R. Wasielewski, M.H. Studier and J.J. Katz, Proc. Nat. Acad. Sci. USA 73 (1976) 4282.
[13] S.G. Boxer and R.R. Bucks, J. Am. Chem. Soc. 101 (1979) 1883.
[14] S.G. Boxer and G.L. Closs, J. Am. Chem. Soc. 98 (1976) 5406.
[15] L.L. Shipman and J.J. Katz, J. Phys. Chem. 81 (1977) 577.
[16] L.L. Shipman, J.R. Norris and J.J. Katz, J. Phys. Chem. 80 (1976) 877.
[17] V.J. Koester and F.K. Fong, J. Phys. Chem. 80 (1976) 2310.
[18] K. Sauer, in: Bioenergetics of photosynthesis, ed. Govindgee (Academic Press, New York, 1974) pp. 115–181.
[19] E.C. McRae and M. Kasha, J. Chem. Phys. 28 (1958) 721.
[20] R.P. Hemenger, J. Chem. Phys. 66 (1977) 1795.
[21] M.Z. Zgierski, Chem. Phys. Letters 21 (1973) 525.
[22] W.T. Simpson and D.L. Peterson, J. Chem. Phys. 26 (1957) 588.
[23] M.R. Philpott, J. Chem. Phys. 53 (1970) 968.
[24] R.L. Fulton and M. Gouterman, J. Chem. Phys. 41 (1964) 2280.
[25] N.S. Hush and L.S. Woolsey, Mol. Phys. 21 (1970) 465.
[26] K.A. Zachariasse and D.G. Whitten, Chem. Phys. Letters 22 (1973) 527.
[27] M.P. Tsvirko and K.N. Solov'ev, Z. Prikl. Speckt. 20 (1974) 115.
[28] C.W. Tang and A.C. Albrecht, J. Chem. Phys. 62 (1975) 2139.
[29] F.J. Kampas and M. Gouterman, J. Lumin. 14 (1976) 121.
[30] J.B. Paine III, D. Dolphin and M. Gouterman, Can. J. Chem. 56 (1978) 1712.
[31] M. Gouterman, D. Holten and E. Lieberman, Chem. Phys. 25 (1977) 139.
[32] T. Kajiwara, R.W. Chambers and D.R. Kearns, Chem. Phys. Letters 22 (1973) 37.
[33] D.J. Bears and S.S. Danyluk, J. Am. Chem. Soc. 87 (1967) 21.
[34] M. Nastansi, R.W. Yip, V.L. Seligy, A.G. Szabo and R.E. Williams, Nature 249 (1974) 248.
[35] J.B. Paine III and D. Dolphin, Can. J. Chem. 56 (1978) 1710.
[36] J.A. Anton, J. Kwong and P.A. Loach, J. Heterocycl. Chem. 13 (1976) 717.
[37] J.P. Collman, C.M. Elliot, T.R. Halbert and B.J. Tovrog, Proc. Nat. Acad. Sci. 74 (1977) 18.
[38] C.K. Chang, J. Am. Chem Soc. 99 (1977) 2819.
[39] N.E. Kagan, D. Mauzerall and R.B. Merrifield, J. Am. Chem. Soc. 99 (1977) 5484.
[40] H. Ogoshi, H. Sugimoto and Z. Yoshida, Tet. Letters 169 (1977).
[41] F.P. Schwarz, M. Gouterman, Z. Muljiani and D. Dolphin, Bionorg. Chem. 2 (1972) 1.
[42] J.A. Anton, P.A. Loach and Govindgee, Photochem. Photobiol. 28 (1978) 235.
[43] N. Periasany, H. Linschitz, G.L. Closs and S.G. Boxer, Proc. Nat. Acad. Sci. USA 75 (1978) 2563.
[44] T.L. Netzel, P. Kroger, C.K. Chang, I. Fujito and J. Fajer, Chem. Phys. Letters 67 (1979) 223.
[45] R. Selensky, M.S. Thesis, Washington State University (1980).
[46] T. Azumi and S.P. McGlynn, J. Chem. Phys. 37 (1962) 2413.
[47] J.C. Thomas, S.A. Allison, C.J. Appelof and J.M. Schurr, Biophys. Chem. 12 (1980) 177.
[48] M. Gouterman, J. Chem. Phys. 30 (1959) 30; in: The porphyrins, Vol. 3, ed. D. Dolphin (Academic Press, New York, 1978) ch. 1, p. 1.
[49] M. Gouterman and L. Stryer, J. Chem. Phys. 37 (1962) 2260.
[50] A.J. McHugh, M. Gouterman and C. Weiss Jr., Theoret. Chim. Acta 24 (1972) 346.
[51] M.H. Perrin, M. Gouterman and C.L. Perrin, J. Chem. Phys. 50 (1969) 4137.
[52] A. Albrecht, J. Mol. Spectry. 6 (1961) 84.

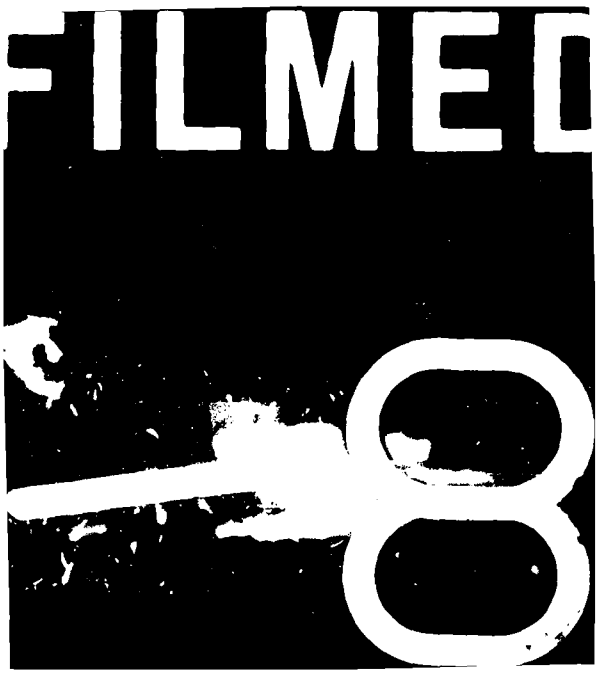
FILME